Design, Synthesis and Characterization of Photoactivable Cyclodextrin-Based Nanoparticles for Multimodal Anticancer Therapy

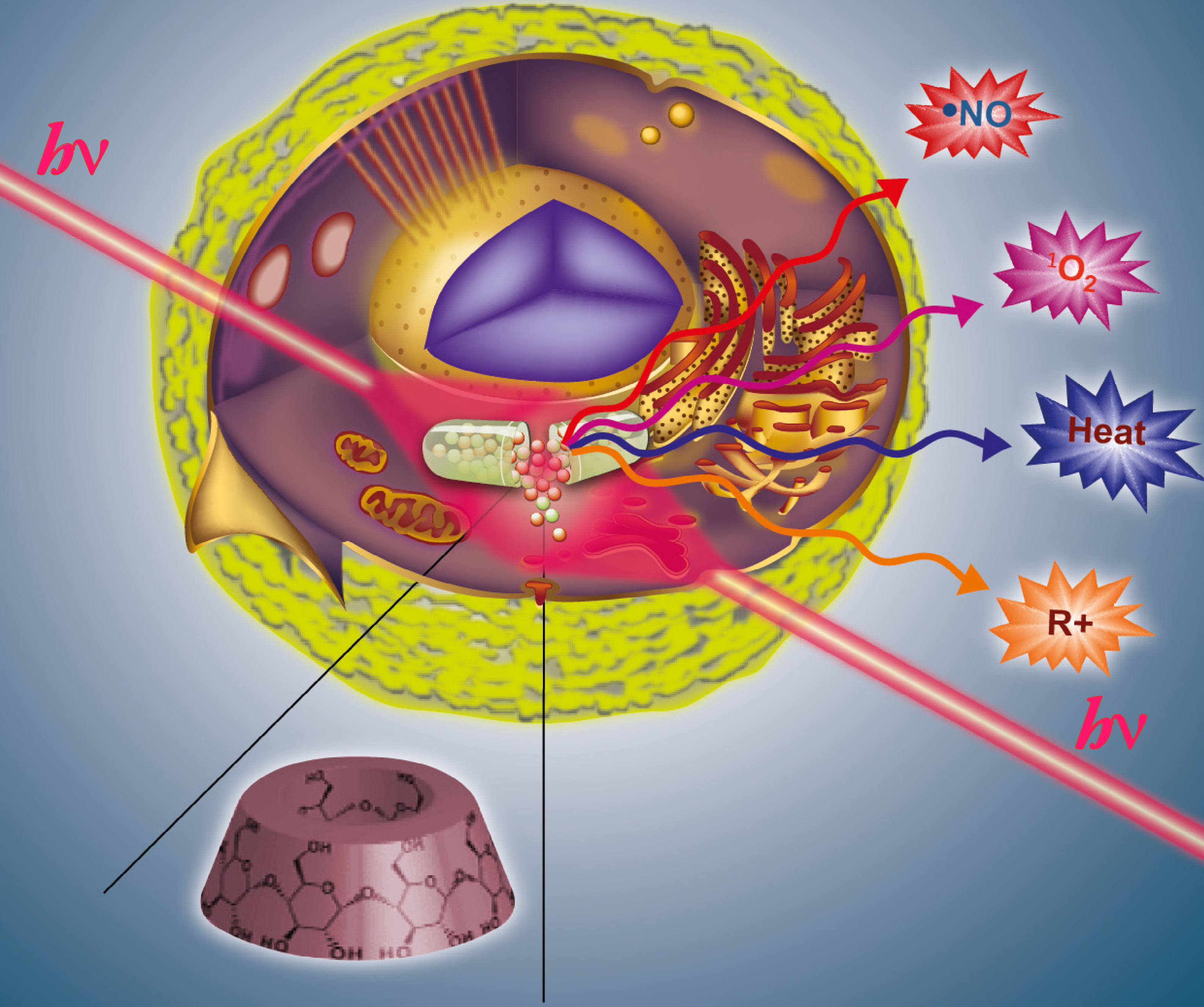

Noufal Kandoth

UNIVERSITY OF CATANIA

International PhD in Chemical Sciences (XXV Cycle)

Noufal KANDOTH

Design, Synthesis and Characterization of Photoactivable Cyclodextrin-Based Nanoparticles For Multimodal Anticancer Therapy

DEPARTMENT OF CHEMICAL SCIENCES,
UNIVERSITY OF CATANIA, ITALY

Coordinator:
Prof. G. Musumarra

Supervisor:
Prof. S. Sortino

2010-2013

Signature of Author:..................

Department of Chemical Sciences

Certified by:................................

Thesis supervisor
Department of Drug Sciences
Chemistry Division
University of Catania

Evaluated and accepted by,

1. Prof. G. Musumarra

   Coordinator,
   XXVth International PhD
   in Chemical Sciences,
   University of Catania.

I prostrate myself in front of
God almighty, the most merciful.

Design, Synthesis and Characterization of Photoactivable Cyclodextrin-Based Nanoparticles for Multimodal Anticancer Therapy

By

Noufal KANDOTH

PhD dissertation Submitted to Department of Chemical Sciences,
University of Catania, Italy, on 10 December 2012.

Abstract

The general goal of this thesis is the development of new generation photoactivable smart nanomaterials that can be modulated into tremendous way to achieve multimodal anticancer and antimicrobial therapeutic actions. Here the cyclodextrins act as the building block for the development of the nanocarrier in order to convey the therapeutic payload to the desired site. With this goal in mind, we have developed several kinds of nanosystems and are discussed in each chapter. The entire dissertation is divided into four sections based on the types of materials and the sections are further divided into twelve chapters based on the functional behavior of each nanosystems. The content of each chapter is shortly described below.

Chapter 1. Chapter 1 give the introduction and brief discussion of scientific concepts generally encountered through out the thesis.

Chapter 2. Chapter 2 explains the formulation of hybrid rotaxane like nanostructures in which supramolecular complex of a suitable host and a photoactivable guest of tailored nitric oxide donor is self-assembled on the surface of Gold nanoparticles. The self-assembly exhibit photoregulated release of NO and localized hyperthermia in tandem.

Chapter 3. Chapter 3 explains the design and developement of a supramolecular system based on a tailored NO photodonor and a fluorophore-labeled β-cyclodextrin conjugate. This nanoassembly is able to image the site and release therapeutic active species simultaneously.

Chapter 4. Chapter 4 explains a nanoensemble formed by the Host-Guest interaction of a fluorophore labeled CD oligomer and nitric oxide photodonor. The design allows on-site biological imaging and higher uptake of therapeutic payload by tumor tissues.

Chapter 5. Chapter 5 explains a nanoassembly in which a fluorescent, singlet oxygen photosensitizer and a tailored nitric oxide photodonor are incorporated on cationic amphiphilic cyclodextrin based nanoparticles. This nanoassembly is able to photogenerate both of nitric oxide and singlet oxygen simultaneously.

Chapter 6. Chapter 6 explains synthesis and formulations of a polymer based bichromophoric cyclodextrin nanoensemble where two photoactive units such as singlet oxygen photosensitizer and nitric oxide photodonor were partitioned at the appropriate region of the carrier.

Chapter 7. Chapter 7 explains design and development of a polymer-based nanoparticles loaded with two fluorescent and two therapeutically relevant moieties. This multimodal system is able to release singlet oxygen and nitric oxide plus the biological imaging with green and red fluorescence.

Chapter 8. Chapter 8 explains design and synthesis of polymer-based nanoparticles assembled with a fluorophore-photochrome dyad and nitric oxide photodonor. This assembly is potent for super-resolution imaging at sub-nanolevel and releasing nitric oxide at the desired bio-site.

Chapter 9. Chapter 9 explains a supramolecular nanoassembly in which a photocage based on the covalent conjugate of fluorophore and nitric oxide photodonor is included. The design lets the quantitative detection of the amount of active species delivered to the bio-site from the variation of fluorescence intensity of the uncaged fluorophore.

Chapter 10. Chapter 10 explains CD-based supramolecular hydrogel where the nitric oxide photodonor is encompassed within the suparamolecular container. This nanogel assembly is effective to decimate antibiotic resistant bacterial colonies.

Chapter 11. Chapter 11 explains CD-based supramolecular hydrogel where both Silver nanoparticles and nitric oxide photodonor is entangled with out compromising their photochemical features. The nanogel structure is expected to facilitate bimodal bactericidal actions.

Chapter 12. Chapter 12 explains the same CD-based supramolecular hydrogel in which a covalent conjugate of fluorophore labelled nitric oxide photodonor and fluorescent photosensitizer is logically encompassed to achieve multimodal imaging and therapy.

Table of contents

SECTION I: Metal based CD-Nanoparticles

SECTION II: Nanoconstructs Based on CD Conjugates

SECTION III: Nanoparticles based on CD polymers

SECTION IV: Photoactivable polymeric nanogel

Glossary of acronym

AgNPs	silver nanoparticles
α-CD	alpha cyclodexrin
ATP	adenosine try-phosphate
AuNPs	gold nanoparticles
Au-CD-1	supramolecular complex assembled on gold surface
β-CD	beta cyclodextrin
CFU	colony forming unit
CW	continuous wave
DNA	deoxyribonucleic acid
DAPI	4',6-diamidino-2-phenylindole
DMF	dimethyl formamide
DMSO	dimethyl sulphoxide
DMEM	dulbecco's modified eagle medium
DLS	dynamic light scattering
DTGS	deuterated triglycine sulphate
eNOS	epithelial nitric oxide synthase
E. Coli	escherichia coli
FTIR-ATR	fourier transform infrared-attenuated total reflectance
γ- CD	gama cyclodextrin
HCl	hydrochloric acid
Hz	hertz
iNOS	inducible nitric oxide synthase
isc	inter system crossing
IPTG	isopropyl-β-D-thiogalactoside

KBr	potassium bromide
NaH	sodium hydride
μm	micrometer
λ_{em}	emission wavelength
λ_{ex}	excitation wavelength
MTT	((3-(4,5-Dimethylthiazol-2-yl)-2,5-diphenyltetrazolium bromide
MEM	minimum essential medium eagle
mM	millimolar
mW	millli watts
MPC	monolayer protected clustures
Mb	myoglobin
nm	nanometer
NIR	near infra red
nNOS	neuronal nitric oxide synthase
NO	nitric oxide
NOS	nitric oxide synthase
NBF	nitro benzofurazan
NLO	non linear optics
OD	optical density
Pgp	para glycoprotein
PBS	phosphate buffer saline
PDT	photodynamic therapy
PTT	phototghermal therapy
PCs	phthalocyanines
PEG	polyethylene glycol
ROI	region of interest

SPR	surface plasmon resonance
$^1O_2$	singlet oxygen
thiol-1	thiol terminated NO photodonor
$^3O_2$	triplet oxygen
TPA	two-photon excitation
X-gal	5-bromo-4-chloro-3-indolyl-β-D-galactopyranoside

1

Introduction to the PhD dissertation

Everything existing in the Universe is the fruit of chance and necessity

- Democritus of Abdera, Greek philosopher

The scientific community was on continuous quest in pursuit of unraveling the multi faceted therapeutic ailments of the global society from the beginning of the human civilization. Common challenges and problems related with the life threatening diseases set the global community necessitate of unifying each other and to find quick remedies. In fact, the evolution of science witness unprecedented achievement on alleviating the social trauma of chronic diseases and consequent socio-economical issues time to time. Although these comprehensive efforts bring the issues of therapies in to the limelight, scientific community awfully failed to eradicate and implement strategies for treating one of the most challenging diseases of the present century, malignant neoplasm or simply cancer. Simply speaking, the cancer arises when cells in part of body divide in an uncontrollable manner. Usually the cancer occurs either oncogenes become stuck in their course of action or tumor suppressor genes fails in slowing down the mitosis and in repairing the DNA mistakes. The DNA mistakes and abnormalities are continuously replicating to the new cells and finally leading to tumor metastasis.

Unfortunately clinically approved current treatment modalities pose serious limitations over the treatment of cancer, as they would only end up in hiking the antitumor agents through out the body. They heavily relies on high efficacy drugs and the lack of selectivity for tumor cells over normal cells can cause severe drawbacks and consequent side effects on its application, which certainly diverge from its therapeutic action. In addition, cancer cells impart cross resistance towards the multitude of anticancer chemo drugs through the over expression of membrane bound protein effluxers, known by the term multi drug resistance, first proposed by Biedler et.al,[1] which prevents the optimum accumulation of the chemo drug and cuts the pharmacological pathway of the latter towards tumor targets.

1.1 Multi Drug Resistance (MDR)

The MDR imparted by the conventional chemo drugs is found to be related with ATP-binding cassette transporters (ABC transporters).[2,3] Commonly, these effluxers function in transporting various types of compounds through the cell membrane exploiting ATP hydrolysis as the energy source. One of the main member of ABC effluxers among various types of ABC tranporters is ABCB1, called P-Glycoprotein abbreviated as Pgp.[2,4] The principal physiological funtion of Pgp is to detoxify the cells from the intake of potentially toxic components present in the environment and consequently the effluxers regulate the membrane transport either through decreased drug uptake or increased drug efflux pump[5]. The cancer cells mimic this function of Pgp to resist anticancer drugs and to self protect themselves from therapeutic action of the latter by over expressing Pgp efflux pump,[6] which in turn reduce the bioavailability of the chemodrugs and impede the therapeutic efficacy. Unfortunately the current methodological treatments are inefficient to evade Pgp efflux pump successfully. Indeed, the different modulation of chemotherapeutic drugs which potentially modify the tumor resistance are being under continuous investigation and several *in-vitro* studies were done to modulate Pgp binding surfaces.[7,8] Though the lack of selectivity and inefficiency of uptaking chemodrugs by both normal and tumor tissues limits its clinical application of the latter. Tumor resistance and recurrence surmounts the problem of effective application of cancer drugs. In this scenario, the new treatment methodologies have to be formulated over the epitome of all the current treatment methods to combat against these diseases.

The limited bioavailability and solubility of current antitumor therapeutic drugs have been greatly addressed by the multitude of the *in situ* drug delivery strategies in recent time.[9,10,11] The innovative approaches spanned from engineering to biology have paved tremendous opportunity to confer biologically active entities to the desired bio site. Now the effort is to brief various kinds of prevailing drug delivery strategies intended for antitumor therapy and those are as follows.

1.2 Nanoparticle mediated drug delivery

The introduction of nanotechnology in the pharmaceutical field and with the emerging trend and recent advances in developing nanoscale delivery vehicles gave a new direction to the drug delivery strategies, which causes the evolution of new branch of science; nanomedicine.[12,13,14] Various types of drug delivery vehicles, which change the pharmacokinetic and pharmacodynamic properties of the delivering molecules, have been emerged in recent years by making use of enormous possibilities of nanotechnology[12]. Nanoparticles (NPs) are versatile candidate being able to modify into *ad-hoc* nanostructure and to target the drug payload at the specific site with accurate dosage. In addition, NPs offer longer circulation time, enhanced solubility, reduced degradation and resistance of the drug cargo. The possibilities of modifying the NP surface by virtue of its enormous surface area along with bio-inertness make them a smart candidate in biomedical field.[15,16,17] The simple targeting of nanostructure occurs passively through the porous and leaky inflamed vasculature characteristic to the tumor tissues by enhanced permeability and retention effects of the tumor vasculature (EPR effect), known as passive targeting, whereas the receptor mediated targeting is made possible by exploiting the overexpression of particular receptor on the tumor tissues (active targeting). Most often the size of the particles are the key factor in determining the therapeutic efficacy, as sub-100 nm nanostructure is found to extravasate easily through the tumor vasculature mediated by passive targeting.[18]

The modified NP self assembly release its payload to desired bio-site with the respective trigger, for instance, change in chemical stimuli[19], temperature[20], pH[21], light,[13] electromagnetic field,[17] ultrasounds[22] etc. Among these, light is definitely the most appealing because of its peculiar features as "biofriendly" and as an easily manipulated reactant.

1.3 Light based strategies for anticancer therapy

Fate of the anticancer therapeutic delivery is generally determined by i) site, ii) dose, iii) timing of the delivered species.[14] The light is a highly orthogonal trigger, which address all these issues. Targeting of specific generation of cytotoxic species is achieved simply by controlling the timing and site of light illumination. The dose dependent delayed or burst release of therapeutic payload is resulted by using light of continuous or pulsed light sources respectively. In addition to providing fast/slow reaction rates, light is a finely tunable external input for the non-invasive introduction of therapeutic agents in a desired bio-environment, mimicking an "optical syringe" with an exquisite spatio-temporal control.[13,23] Moreover, light triggering offers the additional advantage of not affecting physiological parameters, such as temperature, pH and ionic strength, which is a fundamental requisite for biomedical applications. On these directions, several light activated anticancer therapies have been garnered an upsurge of interest in recent years.[24,25,26] The frontline arsenals among plethora of light based therapies evolved out during past decade were based on photodynamic therapy

(PDT), photothermal therapy (PTT) and recently explored nitric oxide (NO) based phototherapy, which aim at selectively killing the neoplastic lesions by the combined action of a photosensitizer (PS) and visible light and they have shown to be innovative modalities for the treatment of localized tumors as an alternative or adjuvant to chemotherapy.[27]

1.3.1 Photodynamic therapy (PDT)

The use of light as therapeutic healing agent has been known since ancient ages as Greeks, Egyptians and Roman people generally exploited the light for therapy,[28] though application of PDT in anticancer therapy have been relatively new.[29,30,31] The treatment modality relies on the retention of the photosensitizer (PS) at the diseased tissue and photoactivation of the former with the visible or near-infra red (NIR) light. The local sensitization of the PS release out cytotoxic active species; which triggers cascade of irreversible photochemical and photobiological events in cells and finally leading to cell mortality.[32,33] The key ingredient for the PDT is the presence of molecular oxygen since it is needed to be excited to generate cytotoxic species at the tumor target and could be summarised as follows. This emerging and promising treatment modality takes advantage of the effects originated by the appropriate combination of light with a photosensitizer in the presence of molecular oxygen.[34,35] The excited singlet state of the PS (S1) generated upon light absorption is not directly involved in reactions with cells and tissues. In contrast, the lowest excited triplet state of the PS (T1) formed upon intersystem crossing (isc) transfers its energy to nearby molecular oxygen in its ground triplet state ($^3O_2$). This energy transfer process (Type II mechanism) results, in general, in the *in situ* production of singlet oxygen ($^1O_2$) which is a powerful oxidizing agent able to cause irreversible damage to lipids, proteins and nucleic acids in the cellular environment leading to cell death (Figure 1.1).

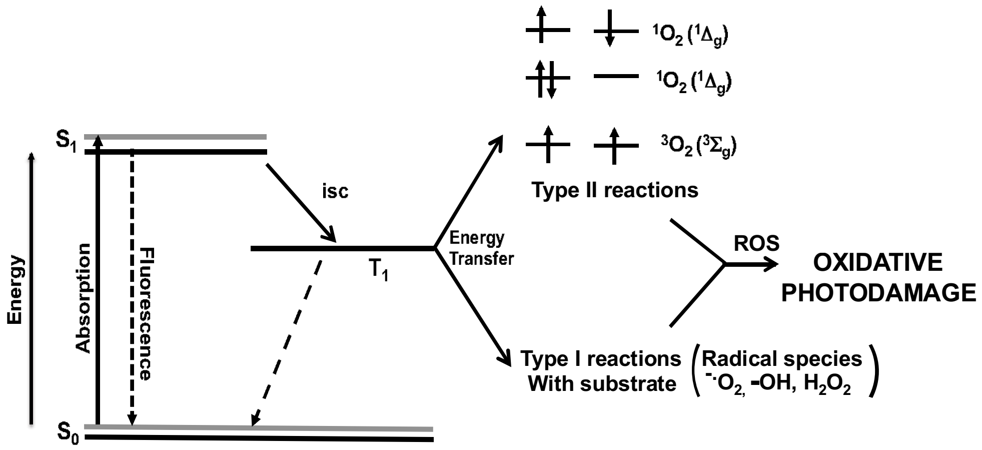

Figure 1.1. Mechanism of photodynamic action of PS explained by a simplified Jabalonsky diagram. Electronic transition involving singlet oxygen is shown on the right.

Although other reactive intermediates harmful to cells, such as superoxide and hydroxyl radicals, may also be photogenerated through electron transfer between the triplet state and molecular oxygen (Type I mechanism), $^1O_2$ is nowadays accepted as the foremost mediator of cytotoxic reactions in the cells in PDT. Unlike other reactive oxygen species, i.e. hydrogen peroxide and superoxide radical, $^1O_2$ is not consumed by enzymes produced by cancer cells such as catalase and superoxide dismutase.[36] Furthermore, PDT is not affected by MDR, overcoming the major problems faced in chemotherapy.[37] Porphyrins and phthalocyanines play a central role as PSs in PDT by virtue of their high triplet quantum yields, very long triplet lifetimes, and strong absorption in the visible region, which are all key parameters for effective photoproduction of $^1O_2$.[38] For deep-seated tumors, second generation PSs which have NIR absorption, such as core modified porphyrin and phthalocyanines, have been introduced. The cellular internalization of the PS and the capacity to effectively photogenerate $^1O_2$ nearby are two crucial prerequisites in PDT. This is due to the short lifetime of $^1O_2$ (several μs) and its short range of action inside the cells (up to about 150 nm).

This issue has inspired intense research activity devoted to integrating the PSs in biocompatible materials, which merge delivery characteristics and preservation of the photodynamic activity of the PS.[39]

1.3.2 Photostimulated NO cytotoxicity.

Nitric oxide is one of the most appealing and studied molecules in the fascinating realm of the biomedical sciences[40,41] after the path-breaking discovery of multiple roles of NO in physiological and pathophysiological processes by the Nobel laureates; R. F. Furchgott, L. J. Ignarro, F. Murad.[42,43,44] Besides its pivotal role in the maintenance and bioregulation of vital functions including neurotransmission, hormone secretion, and vasodilatation in living bodies, this ephemeral free radical has recently stimulated an upsurge of interest because of its promising antioxidant, antibacterial, and anticancer activity.[45,46,47] These exciting discoveries have made the development of new strategies and methods for NO delivery a hot topic[48,49] with the intriguing prospect to tackle important diseases, especially cancer.[50,51]

NO is a free radical gaseous molecule, ubiquitous in cellular events by virtue of its involvement in key physiological processes. Actually the cellular NO is produced internally from the electron oxidation of L-arginine to citrulline catalyzed by Nitric Oxide Synthase (NOS). The key physiological activity of NO in the cell is resulted from the binding of NO with soluble guanylate cyclase (sGC) to transform into cyclic guanosine monophosphate (cGMP). [52] Three different isoforms of NOS are found to be catalyzing the NO generation- iNOS (inducible NOS), eNOS (epithelial NOS), nNOS (neuronal NOS). Among these, the role of iNOS in tumor suppression has been mostly studied and commonly observed the upregulation of the iNOS expression in tumor tissues. The iNOS overexpression results large production of NO which in turn leads to macrophage assisted cytotoxicity towards tumor cells.[53] Interestingly, some scattered literatures show the overexpression of both nNOS and eNOS in tumor tissues demonstrating the NO mediated multidirectional modulation in cancer cells. However, the biological effects of NO have been shown to be highly site, concentration, and dosage dependent, creating a complex role for this molecule in opposing beneficial and deleterious events.[54,55] This dichotomy has made the light-controlled NO donors much more appealing than those based on spontaneous thermolysis for potential use in nanomedicine.[56,57]

Due to its half-life of approximately 5 seconds in tissues and several others key features such as, very small size, lack of charge, lipophilic character etc., NO is capable to diffuse some micrometers (40–200 μm) in the cellular environment. Therefore, this radical species offers the advantage to confine its reactivity in the restricted region of space where it has been photogenerated. Furthermore, the NO radical is able to attack biological substrates of different nature like the plasma membrane[58] the mitochondria[59] and the cell nucleus,[60] thus representing a multitarget cytotoxic agent and avoiding problems of MDR encountered with several conventional anticancer drugs. Finally, since the NO release from NO photodonors is independent from O_2 availability, the photostimulated NO therapy can potentially very well complement the photodynamic therapy, in which the phototoxicity mechanism is entirely dependent on the presence of oxygen[61] at the onset of hypoxic conditions.

1.3.3 Photothermal therapy (PTT)

Heat has become one of the major cytotoxic species for tumor therapy. Hyperthermia, commonly defined as heating tissue in the range 41-47°C for tens of minutes,[62] causes irreversible cell damage by loosening cell membranes, denaturating proteins and leading eventually to tumor destruction. However, the application of conventional heating sources for hyperthermia is strongly limited because of their damage to surrounding healthy tissues. Use of light and a suited

PS to produce heat are at the basis of the photothermal therapy (PTT), which offers the great advantage of overcoming the above limitation. The basic principle is quite simple and consists in the relaxation of the excitation energy absorbed by the PS through nonradiative decay pathways. This results in the overheating of the region of space around the chromophore produce selective tissue damage. [63,64] In this case, the choice of the PS is based on its absorption cross section and the capacity to convert almost all the absorbed light into heat. Exogenous dyes, such as naphthalocyanines and metal porphyrins, have been some of the most commonly used PSs[65,66] but they suffer photobleaching under laser irradiation, which is a serious drawback. The impressive breakthrough of material science has had a tremendous impact in PTT, providing a variety of nanostructures possessing a combination of unique properties for this application.[67]

1.4 Metal-based nanoparticles

1.4.1 Gold Nanoparticle (AuNPs)

PTTs based on the localized hyperthermia from the various nanostructures such as Au based nanostructures, semiconductor quantum dots, magnetic NPs, carbon based nanostructures etc. have recently attained momentum towards biomedical field.[68,69,70] Among these gold nanostructures are more fascinating owing to their peculiar features key to the anticancer therapies and enormous photostability at strong illumination condition with high intensity laser sources. AuNPs are characterised by large absorption cross section several order of magnitude higher than any of the strongly absorbing organic dye making them allowing a large number of photons per AuNPs to be absorbed.[71] The innate biocompatibility and biosafety related with AuNP make them highly interesting to use in biological environment.[70] The coherent oscillation between metal free conduction band electrons on AuNP surface with the alternating incident light magnetic field, a phenomenon called Surface Plasmon Resonance (SPR)[71], is the hallmark of all its desirable features. The plasmon frequency band of AuNPs and the respective scattering cross section are exactly matching with the size, shape, composition and environment of the particle, facilitating an additional tool to tune its optical properties and contrast application,[72,73] often above-mentioned surface parameters of AuNPs is the key for better contrast biomedical imaging.[74] The interesting feature of the AuNP is the tremendous freedom of synthetic versatility to modify particle surface with various conjugates tailored by thiol, disulphides, amines etc., unleashing possibilities to personal imagination.[75,76]

AuNPs re-emit strongly absorbed SPR band nonradiatively in terms of heat owing to the high scattering cross section of the particle, featuring as powerful arsenal for photothermal anticancer agent.[77,78] In fact, AuNP based PTT and localized hyperthermia is more selective towards malignant tumor cells than benign cells, validating the logic of using AuNP as photothermal antitumoral agent[78, 79]. The plasmonic absorption properties of these nanoparticle could be finely tuned to near-infrared region by varying their aspect ratio,[68,80] as the bio-analytes are maximum sensitive to the light in the near-infra region, called "biological NIR window".[68]

1.4.2 Silver Nanoparticles (AgNPs)

The therapeutic implication of silver has been well known in past and dates to ancient Greek civilization.[81] Nowadays AgNP has gained increased attention for their excellent antimicrobial properties against antibiotic resistant bacteria[82,83], viruses including HIV[84] and Hepatitis B,[85] antitumor actions[86,87] etc. They are able to inhibit cell division event during cytokinesis and preferentially bind to DNA through electrovalent interaction leading to structural damage on DNA replication and finally directing cell mortality.[58] The fast oxidation of AgNP into cations render the particle to be able to attack on oppositely charged lipid bilayer of cells through lipid peroxidation, though the fast oxidation make the processing the Ag nanostructure little tricky.

Analogous to the AuNPs, AgNP shows peculiar physicochemical properties, mainly attributed by large scattering cross section and enhanced SPR band at visible region, which enable molecular labelling and biological imaging at sub cellular level.[88] As the scattering coefficient of AgNPs, somewhat similar to Au nanostructures, is in accordance with the size, shape and composition of the particle,[89] allows the possibility to tune the optical properties anywhere in the visible region.

Several other metal-based nanostructures have been burst out in recent years with intention for the application from electronic devices to medicinal instruments, but those are out of current topic of interest.

1.5 Nonmetal-based NPs

Past decade have envisaged remarkable evolution of various nonmetal nanostructures able to release the confined therapeutic cargo to the biological target. Majority of the nanomaterials on this direction were centered on macrocyclic host structures- mainly involving Calixarene[90], Cyclodextrin[91,92] and Cucurbituril,[93] mesoporous silica based NP, denderimeric or polymeric materials, amphiphilic ensembles etc. and a detailed review on this aspects is already been published from our group.[13] Among these, Cyclodextrin (CD) based nanaostructures have been studied immensely because of their peculiar property to alter the pharamacodynamic properties of poorly absorbing hydrophobic drug therapeutics and in consequence, several clinical trials based CD nanocarriers are being under continuous investigation by various groups around the world.[94]

1.5.1 CD based nanocarrier

Among the different kinds of available host molecules, cyclodextrins (CDs) have been the most extensively investigated host structure due to their higher solubility in aqueous medium and related impact on processing the drug delivery application. CDs are cyclic oligosaccharides composed of D-glucopyranose units joined by ether linkages.[95,96] Depending upon the number of monomer units, CD homologues of different sizes are obtained, the most common members of this family being α-, β-, and γ-CDs, which are made up of six, seven and eight D-glucopyranose units, respectively (Figure 1.2).

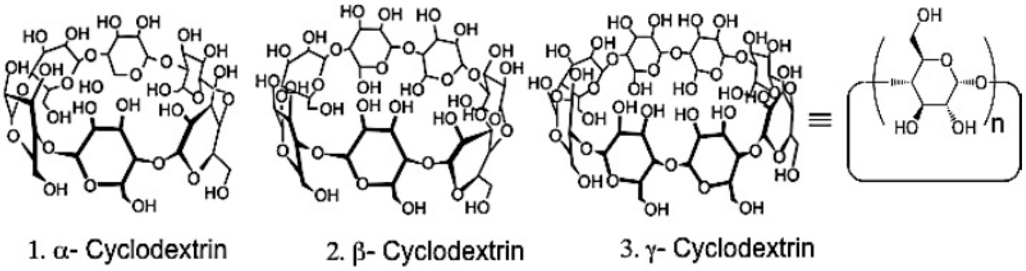

1. α- Cyclodextrin 2. β- Cyclodextrin 3. γ- Cyclodextrin

Figure 1.2. Pictorial representation showing three different isomer of cyclodextrin,

The structure of the CD is that of a truncated cone, having an inner hydrophobic cavity and outer hydrophilic edges consisting of hydroxyl groups. Solute molecules of suitable dimensions can interact and bind to the CD cavity by inclusion complex formation.[97, 98] The reduced polarity and restricted microenvironment provided by the CD cavity can markedly and advantageously influence a number of properties of the included analyte.[99,100,101] Among CDs, β-CD has been studied and utilized more to understand the complexation events, though they are less aqueous soluble than other CDs, since the optimum cavity size for encapsulation and increased bioavailability favors the stability of aromatic lipophilic drug.[102] Poor aqueous solubility of β-CD is found to be resulted partly from the stronger binding affinity between the CD units in crystal state and increased intra molecular hydrogen bond between the secondary OH groups of CD units, making sluggish response on interacting with surrounding water molecules.[103] Random alkylation of the secondary OH groups is found to be viable strategy to break the intramolecular hydrogen bond and increase solubility parameters.[103] Actually the host-guest inclusion chemistry of natural CDs with various kinds of modal therapeutic drugs have been well known and dates back to 1970s. [104] Indeed, continuous efforts have been done to improve the physicochemical properties and the inclusion phenomenon by modifying both primary and secondary rim of CDs with hydrophilic and hydrophobic functionalities, and by exploiting tremendous opportunities spawned by the emerging trends in nanomedicine so far.[105,106] This new generation nanoscaled CD analogues are smart enough for facile encapsulation with phototherapeutic prodrugs and finally conveying the therapeutic active species to the tumor outreach.[92,107] Based on their logical designing, CD carriers self organize each other to micelles, vesicles, nanoparticles and polymeric ensemble etc. based on their topological environment, facilitating enhanced solubility, bioavailability and photodynamic stability of photoactive drugs.[108,109,110] The CDs can be modified both by the hydrophilic and the hydrophobic terminations at primary and secondary rim to accommodate various kinds of probe at the different region of CD networks[111]. In addition, the normal CDs are able to form aqueous soluble polymeric NPs with very high efficiency of drug loading in to their interior networks and the rapid introduction of the drug payload to the targeted bio-site[112,113]. The polymeric NPs are more affirmative towards increased local concentration of the drug payload and the enhanced binding affinities of the latter.[92,108,109,112, 114] The tailored CDs are capable of forming the colloidal dispersion and hydrogels by the inclusion process between hydrophobic guest molecules and apolar concavities of CD host units tailored on polymeric backbone. This hydrogel assemblies formed by the "lock and key" mechanism are highly feasible for differential entrapment of drug payload and for their topological applications.[115] Above all, nanoparticulate delivery of therapeutic drugs based on CD nanostructures circumvent the issues of MDR and they are known to evade efflux pump by accumulating passively at the leaky tumor vasculature through EPR effect.[116]

1.6 Multimodal therapy

The different types of methods demonstrated for antitumor treatment in the preceding sections leaves a space for logical extension of those methods in the form of utilizing the combination of multiple methods at the same time. The molecular complexity related with the cellular response of the tumor tissues on various anticancer drugs demands the use of ‘cocktail’ drugs for anticancer treatments.[117,118] Here the multimodal therapy definitely sees a bright future. In this direction, the new novel method of treatment such as light mediated multimodal therapy offers intriguing perspectives, which aim to exploit either additive or synergistic effects arising from the generation of two or more anticancer species in the same region of space with the final goal to maximize the therapeutic efficiency (Figure 1.3). The ability of combining the PDT or PTT along with the stimulatory effects NO based toxicity in tandem might sum up a remarkable avenue on light based anticancer therapies. The well versed synchronising and complimentary actions of these active transient species offers enhanced therapeutic efficacies. Though the key for the combined administration and therapeutic effectiveness is the prime understanding of the optimum dose of active agents to be delivered since different pharmacokinetics and physiological pathways related to different active agents generally determine the therapeutic fate. Here light based multimodal therapies have a leading edge over other modalities since light is an excellent ON/OFF trigger with exact control over dosage, timing and site of the delivered species.

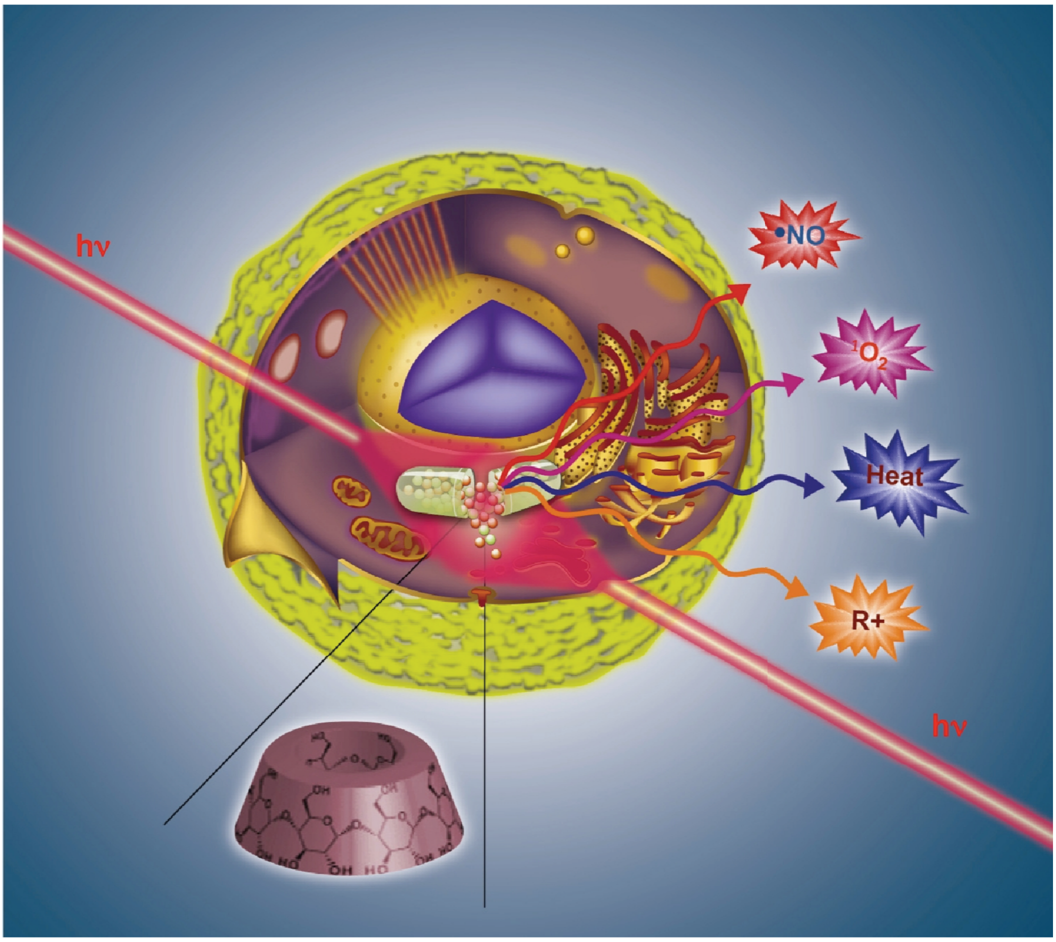

Figure 1.3. Schematic representation showing the multimodal therapy in cell.

Synergism of NO action with PDT or PTT is found to be highly promising towards new generation antitumor treatments owing to its multiple role in cellular processes. In case of oxygen deficient areas in tumor cells called hypoxic areas, which is responsible for the generation of acquired drug resistance, NO serves as a vasodilator by increasing the concentration of oxygen. The combined action of NO and molecular oxygen generates potential free radicals which trigger cell apoptosis.[119, 120] In addition, using NO in conjunction with radiotherapy or chemotherapy is also found to be highly desirable towards antitumor actions as the NO intervenes in hypoxia induced resistance mechanism and cancer cell cycle events.[121] In short all this revelation validate that multimodal therapies offer an intriguing alternative for current antitumor treatments.

1.7 Fluorescence Imaging

Optical microscopic techniques have revolutionized the understanding of bio-sites since it offers noninvasive imaging of living cells by fluorescent optical probe with high spatio-temporal resolution at microscopic level.[122] Optical microscopy imaging is characterized by the interaction of source light in Visible/IR region with the biological target where the biological analyte can absorb, scatter or emit light in terms of fluorescent signal. Among various optical microscopy techniques, fluorescent microscopy is far more popular, owing to their efficiency, less expensive instrumentation and easiness to track the emitted photon. Most of the fluorescent microscopes work in epifluorescence configuration where the excitation and emission signals pass through the same objective (Figure 1.4). Practically the technique is quite simple, where the source light incident on the analyte is reflected back to the detector.[123]

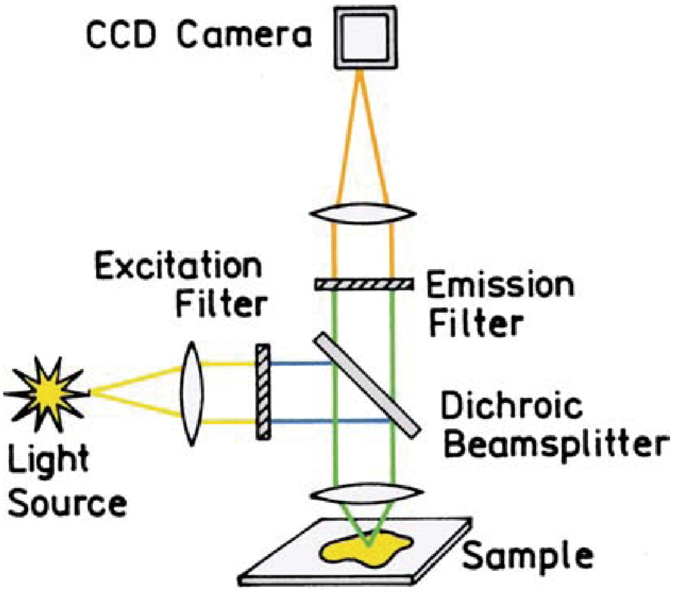

Figure 1.4. Pictorial representation of the commonly used epifluorescence microscope (©Springer Science+Business Media, LLC, 2006, 1999, 1983).

The beam light pass through an excitation filter, emission filter and a dichroic beam splitter on the way to the anlayte and back to the detector. The excitation filter selects range of wavelength light from the broad source to excite the sample analyte and emission filter transmit the emission light and rejects the excitation beam. The detector is usually a CCD (Charge-Coupled Device) camera detecting the emitted reflected light.

Among the perspectives of the multimodal therapy, the localization of PS at the target tumor tissues is of pivotal importance to achieve the efficacy of the therapy. This demands suitable methods to internalize the PS with matching carrier system and diagnose the former at tumor sites. Here the fluorescence imaging with non-invasive light has an immense role to image the PS at cellular interphase and to aid the therapy. Moreover the integration of the PS with a fluorophore or selection of fluorescent PS imparts a simple strategy with innumerous prospective. The wavelength of the incident light have great role to determine the contrast and resolution of imaging as the organelles at tissue surface can dent the deep imaging, where they show maximum absorption at UV/Visible region up to 650 nm. The imaging at NIR region is more promising where the tissue surface shows minimum absorption coefficient and minimum unwanted autofluorescence, making deep cell imaging at sub-cellular level[124]. However, optimizing the excitation of the fluorophore in to a fixed focal volume could drastically reduce all the noises and background fluorescence of biological imaging. This has been achieved by utilizing the tremendous possibilities laid out by advanced laser techniques, where high intensity laser sources with femtosecond pulse width excite the probe by two-photon absorption. Here the high intensity laser facilitates the fluorophore to absorb two long wavelength photons and to reach on its excited singlet state.[116] Advantage of this process is that the probe excited only at the focal volume and the fluorophore above and below the focal plane remain inactive, resulting remarkably sharp contrast images. The femtosecond pulse width laser source can simply connected with microscope to achieve aforementioned technique, which is known as Two Photon or Multiphoton confocal microscopy (TPM).[125,126]

Though the confocal imaging based on NIR light brought the optical imaging into new frontiers, the technique is seriously limited to achieve the image resolution at submicron or nanolevel of biological environment, attributed by the diffraction limit imposed by the light[127]. This inherent problem was studied by Ernst Abbe and Lord Rayleigh and proposed that resolution of the image is in direct consequence with the size of the focal spot and the size is nearly equal to the half of the incident light.[128] Hence the minimum resolution that can be achieved with the visible light of 400 nm is 180 nm at the focal plane and 500-800 nm along optic axes, provided all other instrumental parameters are fixed.[129] Though the light at near UV region could be detrimental for the cell application[130]. In short, diffraction barrier seriously pause the understanding cellular events as fundamental biological processes occurs through the macromolecular interaction at the nanometer regime.[131]

Recently, several technical methodologies have been proposed to unravel detailed in-depth information of cell organelles with the advent of many sophisticated laser optical techniques and most of these techniques relies on the selectivity of the fluorophore.[132,133,134,135,136] Among these, reversibly switching the fluorophore between continuous ON-OFF cycles is speculated to be more elegant strategy as the single fluorescent emitters allows high accuracy localization at nanometer precision with the aid of easy laser techniques rather using high intensity laser sources. Actually the aberration and the diffraction dependent blurring of the image originate from the multiple excitation of the fluorophore from the same focal volume.[137] The reversible switching of the fluorophore eliminates this problem and the single emission profile from each individual fluorophore can be reconstructed through stochastic algorithm to yield super-resolution imaging at nanometer level precision.

1.8 Scope of the PhD dissertation

The goal of this project is to design and develop a new generation of multifunctional photoactivable nanoparticles based on a family of water soluble and biocompatible oligosaccharides, the CDs. The nanocarriers will be thoroughly studied and evaluated as delivery vehicles of photoactive anticancer drugs addressed to multimodal treatment. The CD-based nanocarriers, composed of a few or many CD molecules in a single formulation will be designed to have high drug loading capacity, protect the drugs against in vivo degradation/metabolism, have long circulation times, light tunable drug release properties, possibility to evade resistance mechanisms, and ability to transport drugs inside cells. CD-based metal and nonmetal nanoparticles will be taken into account.

The dissertation work, carried out at University of Catania, Italy, University of Gothenburg, Sweden and in collaboration with several other institutes and industrial company as the part of CYCLON community network program, Marie Curie collaboration, was intended to formulate various kinds of nanostructures and evaluation of the latter at biological environment. To this end we developed several kinds of nanofabrications and those are detailed and categorized in each chapters. Actually the entire dissertation is divided in to four sections based on the functional behavior of formulations towards anticancer therapy, which in turn divided in to twelve chapters addressing each nanofabrications and their photochemical and biological behaviour. Though two chapters are devoted to antibacterial therapy. Considerable attention was taken to bridge the interdisciplinary subjects in harmony that is commonly encountered in all the present research works.

1.9 References

1. J. L. Biedler, H. Riehm, *Cancer Res.*, 1970, **30**, 1174.

2. A. P. Talice, J. M. Arau´jo, C. Torres, J. M. P. Victoria, F. Gamarro, S. Castanys, *Biochim. Biophys. Acta*, 2003, **1612**, 95–207.

3. I. B. Holland, M. A. Blight, *J. Mol. Biol.*, 1999, **293**, 381–399.

4. G. Bradley, P. F. Juranka, V. Ling, *Biochim. Biophys. Acta*, 1988, **948**, 87-128.

5 M. Dietel, *Pathol. Res. Pract.*, 1991, **187**, 892–905.

6. J. Robert, *Eur. J. Clin. Invest.*, 1999, **29**, 6, 536–545.

7. E. Teodori, S. Dei, S. Scapecchi, F. Gualtieri, *Il Farmaco*, 2002, **57**, 385–415.

8. J. Robert, C. Jarry, *J. Med. Chem.*, 2003, **46**, 23, 4805.

9. D. S. Kohane, M. Lipp, R. C. Kinney, D. C. Anthony, D. N. Louis, N. Lotan, R. Langer, *J. Biomed. Mater. Res.*, Part A, 2002, **59**, 3, 450–459.

10. J. P. Shofner, N. A. Peppas, *In Biodrug Delivery Systems: Fundamentals, Applications and Clinical Development*, M. Morishita, K. Park, Eds.; Informa Healthcare, New York, NY, 2010, 1-12.

11 . N. A. Peppas, *Adv. Drug Deliv.*, 2012, DOI: http://dx.doi.org/10.1016/j.addr.2012.09.040.

12. J. Shi, A. R. Votruba, O. C. Farokhzad, R. Langer, *Nano Lett.*, 2010, **10**, 3223.

13. S. Sortino, *J. Mater. Chem.*, 2012, **22**, 301.

14. O. C. Farokhzad, R. Langer, *ACS Nano*, 2009, **3**, 120.

15. R. Gref, Y. Minamitake, M. T. Peracchia, V. Trubetskoy, V. Torchilin, R. Langer, *Science*, 1994, **263**, 1600.

16. P. T. Hammond, *ACS Nano*, 2011, 5, **2**, 681–684.

17. M. De, P. S. Ghosh, V. M. Rotello, *Adv. Mater.*, 2008, **20**, 4225.

18. S. D. Perrault, C. Walkey, T. Jennings, H. C. Fischer, W. C. W. Chan, *Nano Lett.*, 2009, **9**, 5.

19. C. Park, H. Youn, H. Kim, T. Noh, Y. H. Kook, E. T. Oh, H. J. Park, C. Kim, *J. Mater. Chem.*, 2009, **19**, 2310–2315.

---

20. D. E. Owens III, J. K. Eby, Y. Jian, N. A. Peppas, *J. Biomed. Mat. Res. Part A*, 83A, 2007, **3**, 692–695.

21. K. Raemdonck, J. Demeester, S. D. Smedt, *Soft Matter*, 2009, **5**, 707–715.

22. V. Frenkel, *Adv. Drug Del. Rev.*, 2008, **60**, 1193–1208.

23. S. Sortino, *Photochem. Photobiol.Sci.*, 2008, **7**, 911-924.

24. C. A. Lorenzo, L. Bromberg, A. Concheiro, *Photochem.Photobiol.*, 2009, **85**, 848.

25. M. J. Manyak, A. Russo, P. D. Smith, E. Glatstein, *Clin. Oncol.*, 1988, **6**, 2, 380.

26. A. G. Skirtach, A. M. Javier, O. Kreft, K. Köhler, A. P. Alberola, H. Möhwald, W. J. Parak, G. B. Sukhorukov, *Angew.Chem. Int. Ed.*, 2006, **45**, 28, 4612–4617.

27. R. Pandey, G. Zheng, *In The Porphyrin Handbook*; K. M. Smith, K. Kadish, R. Guilard, Eds.; Academic Press: San Diego, 2000; **Vol. 6.**, pp. 157-230.

28. J. D. Spikes, *In Primary Photoprocesses in Biology and Medicine* (Edited by R. V. Bergasson, G. Jori, E. J. Land and T. G. Truscott), pp. 209– 227, Plenum Press, New York, 1985.

29. T. J. Dougherty, J. E. Kaufman, A. Goldfarb, K. R. Weishaupt, D. Boyle, A. Mittleman, *Cancer Res.*, 1976, **38**, 2628–2635.

30. J. F. Kelly, M. E. Snell, *J. Urol.,* 1976, **115**, 150.

31. J. G. Levy, M. Obochi, *Photochem. Photobiol.,* 1996, **64**, 5, 737–739.

32. M. C. DeRosa, R. J. Crutchley, *Coord. Chem. Rev.,* 2002, **233-234**, 351-371.

33. Y. N. Konan, R. Gurny, E. Alle´mann, *J. Photochem. Photobiol. B: Biol.*, 2002, **66**, 89.

34. I. J. McDonald, T. J. Doughery, *J. Porphyrins Phthalocyanines*, 2001, **5**, 105.

35. T. Hasan, A. C. E. Moor, B. Ortel, *Photodynamic therapy of cancer, In: Cancer Medicine*, R. C. Bast, D. W. Kufe, R. E. Pollock et al. Eds., 5th ed., BC Decker Inc., Hamilton, 2000.

36. R. Cai, Y. Kubota, T. Shuin, H. Sakai, K. Hashimoto, K. Fujishima, *Cancer Res.,* 1992, **52**, 2346-2348.

37. K. J. Reeves, M. W. R. Reed, N. J. Brown, *J. Photochem. Photobiol. B: Biol.*, 2009, **95**, 141-147.

---

38. M. Ethirajan, Y. Chen, P. Joshi, R. K. Pandey, *Chem. Soc. Rev.*, 2011, **40**, 340-362.
39. S. Wang, R. Gao, F. Zhou, M. Selke, *J. Mater. Chem.*, 2004, **14**, 487-493.
40. *Nitric Oxide: Biology and Pathobiology (Ed.: L. J. Ignarro)*, Elsevier Inc., 2010.
41. *Journal Issue on Nitric Oxide Chemistry and Biology* (Ed.: L. J. Ignarro), Arch. Pharmacal Res. 2009.
42. L. J. Ignarro, *Angew. Chem. Int. Ed.,* 1999, **38**, 1882.
43. F. Murad, *Angew. Chem. Int. Ed.*, 1999, **38**, 1856.
44. R. F. Furchgott, *Angew. Chem. Int. Ed.,* 1999, **38**, 18870.
45. *Methods in Enzymology*, **Vol. 301**: Nitric Oxide, Part C: Biological and Antioxidant Activities (Ed.: Packer, Lester), Academic Press, San Diego, 1999.
46. S. Carlsson, E. Weitzberg, P. Wiklund, J. O. Lundberg, *Antimicrob. Agents Chemother.*, 2005, **49**, 2352.
47. D. Fukumura, S. Kashiwagi, R. K. Jain, *Nat. Rev. Cancer,* 2006, **6**, 521.
48. D. A. Riccio, M. H. Schoenfisch, *Chem. Soc. Rev.,* 2012, **41**, 3731.
49. P. G. Wang, M. Xian, X. Tang, X. Wu, Z. Wen, T. Cai, A. J. Janczuk, *Chem. Rev.,* 2002, **102**, 1091.
50. A. W. Carpenter, M. H. Schoenfisch, *Chem. Soc. Rev.,* 2012, **41**, 3742.
51. *Nitric Oxide Donors for Pharmaceutical and Biological Applications* (Eds.: P. G. Wang, T. B. Cai, N. Taniguchi), Wiley-VCH, Weinheim, Germany, 2005.
52. J. W. Denninger, M. A. Marletta, *Biochim. Biophys. Acta*, 1999, **1411**, 334.
53. W. Xu, L. Z. Liu, M. Loizidou, M. Ahmed, I. G Charles, *Cell Res.*, 2002, **12**, 311-320.
54. A. Bishop, J. E. Anderson, *Toxicology*, 2005, **208**, 193.
55. S. Pervin, R. Singh, E. Hernandez, G. Wu, G. Chaudhuri, *Cancer Res.*, 2007, **67**, 289.
56. S. Sortino, *Chem. Soc. Rev.,* 2010, **39**, 2903.
57. M. J. Rose, N. L. Fry, R. Marlow, L. Hinck, P. K. Mascharak, *J. Am. Chem. Soc.*, 2008, **130**, 8834.
58. S. Gupta, C. McArthur, C. Grady, N. B. Ruderman, *Am. J. Physiol.,* 1994, **266**,

2146.

59. M. Nishikawa, E. F. Sato, K. Utsumi, M. Inoue, *Cancer Res.,* 1996, **56**, 4535.
60. M. N. Routledge, D. A. Wink, L. K. Keefer, A. Dipple, *Chem. Res. Toxicol.*, 1994, **7**, 628.
61. I. J. McDonald, T. J. Doughery, *J. Porphyrins Phthalocyanines*, 2001, **5**, 105.
62. L. O. Svaasand, C. J. Gomer, E. Morinelli, *Laser Med. Sci.*, 1990, **5**, 121-128.
63. G. Jori, J. D. Spikes, *J. Photochem. Photobiol. B Biol.*, 1990, **6**, 93-101.
64. M. Camerin, S. Rello, A. Villanueva, X. Ping, M. E. Kenney, M. A. J. Rodgers, G. Jori, *Eur. J. Cancer*, 2005, **41**, 1203-1212.
65. G. Jori, L. Schindl, P. L. Schindl, *J. Photochem. Photobiol. A Chem.*, 1996, 102, 101.
66. G. Jori, J. D. Spikes, *J. Photochem. Photobiol. B Biol*, 1990, **6**, 93, 101.
67. P. K. Jain, X. Huang, I. H. El-Sayed, M. A. El-Sayed, *Acc. Chem. Res.*, 2008, **41**, 1578-1586.
68. P. K. Jain, I. H. El-Sayed, M. A. El-Sayed, *nanotoday*, 2007, **2**, 1.
69. A. Sperling, P. R. Gil, F. Zhang, M. Zanella, W. J. Parak, *Chem. Soc. Rev.*, 2008, **37**, 1896.
70. X. Huang, P. K. Jain, I. H. El-Sayed, M. A. El-Sayed, *Nanomedicine*, 2007, **2**, 5, 681–693.
71. K. L. Kelly, E. Coronado, L. L. Zhao, G. C. Schatz, *J. Phys. Chem. B*, 2003, **107**, 668.
72. C. J. Orendorff, T. K. Sau, C. J. Murphy, *Small*, 2006, **2**, 5, 636.
73. C. F. Bohren, D. R. Huffman, *Absorption and scattering of light by small particles*, John Wiley & Sons, New York, 1983.
74. I. H. El-Sayed, X. Huang, M. A. El-Sayed, *Nano Lett.*, 2005, **5**, 5.
75. E. Katz, I. Willner, *Angew. Chem. Int. Ed.*, 2004, **43**, 6042.
76. L. M. Liz-Marzán, *Mater. today*, 2004, **7**, 2, 26-31.

77. X. Huang, P. K. Jain, I. H. El Sayed, M. A. El Sayed, *Lasers Med. Sci.*, 2008, **23**,

217.

78. I. H. El-Sayed, X. Huang, M. A. El-Sayed, *Cancer Lett.*, 2006, **239**, 129.
79. X. Huang, P. K. Jain, I. H. El-Sayed, M. A. El Sayed, *Photochem. Photobiol.*, 2006, **82**, 412.
80. M. Hu, J. Chen, Z. Y. Li, L. Au, G. V. Hartland, X. Li, M. Marquez, Y. Xia, *Chem. Soc. Rev.*, 2006, **35**, 1084.
81. A. Wadhera, M. Fung, *Dermatol. Online. J.,* 2005, **11**, 12.
82. A. Coates, Y. Hu, R. Bax, C. Page, *Nat. Rev. Drug Discov.*, 2002, **1**, 895-910.
83. K. Page, M. Wilson, I. P. Parkin, *J. Mater. Chem.,* 2009, **19**, 3819–3831.
84. R. W. Y. Sun, R. Chen, N. P. Y. Chung, C. M. Ho, C. L. S. Lin, C. M. Che, *Chem. Commun.*, 2005, 5059–5061.
85. L. Lu, R. W. Sun, R. Chen, C. K. Hui, C. M. Ho, J. M. Luk, G. K. Lau, C. M. Che, *Antivir Ther.,* 2008, **13**, 253.
86. P. D. Nallathamby, X. H. N. Xu, *Nanoscale*, 2010, **2**, 942–952.
87. M. I. Sriram, S. B. M. Kanth, K. Kalishwaralal, S. Gurunathan, *Int. J. Nanomedicine*, 2010, **5**, 753–762.
88. S. Schultz, D. R. Smith, J. J. Mock, D. A. Schultz, *Proc. Natl. Acad. Sci. USA*, 2000, **97**, 3, 996–1001.
89. J. Yguerabide, E. E. Yguerabide, *Anal. Biochem.*, 1998, **262**, 137–156.
90. R. V. Rodik, A. S. Klymchenko, N. Jain, S. I. Miroshnichenko, L. Richert, V. I. Kalchenko, Y. Mely, *Chem. Eur. J.*, 2011, **17**, 5526–5538.
91. D. Duchene, G. Ponchel, D. Wouessidjewe, *Adv Drug Deliv Rev.,* 1999, **36**, 1, 29.
92. A. Mazzaglia, M. T. Sciortino, N. Kandoth, S. Sortino, *J. Drug Del. Sci. Tech.*, 2012, **22**, 3, 235-242.
93. K. M. Park, K. Suh, H. Jung, D. W. Lee, Y. Ahn, J. Kim, K. Baeka, K. Kim, *Chem. Commun.*, 2009, 71–73.
94. T. Loftsson, M. E. Brewster, *J. Pharmaceutical Sci.*, 1996, **85**, 10, 1017.
95. J. Szejtly, *Chem. Rev.*, 1998, **98**, 1743.
96. M. V. Rekharsky, Y. Inoue, *Chem. Rev.*, 1998, **98**, 1875–1917.

---

97. T. Loftsson, D. Duchêne, *Int. J. Pharm.*, 2007, **329**, 1-11.

98. K. A. Connors, *Chem. Rev.*, 1997, **97**, 1325–1357.

99. K. Kalyanasundaram, *Photochemistry in Microheterogeneous Systems*, Academic Press, Orlando, FL, 1987.

100. S. Monti, S. Sortino, *Chem. Soc. Rev.*, 2002, **31**, 287–300.

101. K. Uekama, F. Hirayama, T. Irie, *Chem. Rev.,* 1998, **98**, 2045.

102. T. Loftsson, M. E. Brewster, *J. Pharmacy and Pharmacology*, 2010, **62**, 1607–1621.

103. J. Szejtli, *Cyclodextrin Technology*, Kluwer Acad. Publ.: Dordrecht, 1988.

104. E. Davis, M. E. Brewster, *Nature Rev.*, 2004, **3**, 1023.

105. J. Pitha, L. Szente, J. Szejtli, In Controlled Drug Delivery; Bruck, S. D., Ed.; CRC: Boca Raton, FL, 1983; p 125.

106. *New Trends in Cyclodextrins and Derivatives*; D. Duchêne, Ed.; Editions de Sante´: Paris, 1991.

107. N. C. Bellocq, D. W. Kang, X. H. Wang, G. S. Jensen, S. H. Pun, T. Schluep, M. L. Zepeda, M. E. Davis, *Bioconjugate Chem.*, 2004, **15**, 6, 1201.

108. B. J. Ravoo, R. Darcy, *Angew. Chem. Int. Ed.*, 2000, **39**, 23.

109. R. Donohue, A. Mazzaglia, B. J. Ravoo, R. Darcy, *Chem. Commun.*, 2002, 2864.

110. F. V. de Manakker, T. Vermonden, C. F. van Nostrum, W. E. Hennink, *Biomacromolecules*, 2009, **10**, 12.

111. N. Kandoth, E. Vittorino, M. T. Sciortino, T. Parisi, I. Colao, A. Mazzaglia, S. Sortino, *Chem. Eur. J.,* 2012, **18**, 1684.

112. J. Zhou, H. Ritter, *Polym. Chem.*, 2010, **1**, 1552.

113. E. Renard, A. Deratani, G. Volet, B. Sebille, *Eur. Polym. J.*, 1997, **33**, 1, 4957.

114. E. Renard, A. Deratan, Z. Fu̇lop, S. V. Kurkov, T. T. Nielsen, K. L. Larsen, T. Loftsson, *J. Drug Del. Sci. Tech.*, 2012, **22**, 3, 215.

115. S. D. Mahammed, C. R. Lefebvre, N. Razzouq, V. Rosilio, B. Gillet, P. Couvreur, C. Amiel, R. Gref, *J. Coll. Interf. Sci.*, 2007, **307**, 83.

116. S. W. Kamau, S. D. Kramer, M. Gunthert, H. W- Allenspach, *In Vitro Cell Dev Biol Anim.*, 2005, **4**, 207.

---

117. F. Greco, M. J. Vicent, *Adv. Drug Del. Rev.*, 2009, **61**, 1203–1213.

118. M. J. Vicent, F. Greco, R. I. Nicholson, A. Paul, P. C. Griffiths, R. Duncan, *Angew. Chem. Int. Ed.*, 2005, **44**, 4061–4066.

119. D. G. Hirst, T. Robson, *Front. Biosci.*, 2007, **12**, 3406-3418.

120. A. D. Ostrowski. P. C. Ford, *Dalton Trans.*, 2009, 10660–10669.

121. B. Bonavida, S. Khineche, S. H- Yepez, H. Garban, *Drug Resist. Updates*, 2006, **9**, 157–173.

122. R. Weissleder, V. Ntziachristos, *Nat. Med.,* 2003, **9**, 1.

123. J. R. Lakowitz, *Principles of Fluorescence Spectroscopy*, 3rd ed.; Springer: New York, 2006.

124. K. Licha, C. Olbrich, *Adv. Drug Del. Rev.*, 2005, **57**, 1087.

125. M. G- Mayer, *Ann. Phys.,* 1931, **9**, 273–295.

126. W. Kaiser, C. G. B. Garrett, *Phys. Rev. Lett.,* 1961, **7**, 229–231.

127. S. W. Hell, *Nat. Biotechnol.*, 2003, **21**, 11.

128. E. Abbe, *Archiv für mikroskopische Anatomie*, 1873, **9**, 413–418.

129. M. Dyba, S. W. Hell, *Phys. Rev. Lett.,* 2002, **88**, 16, 163901.

130. K. König, Y. Tadir, P. Patrizio, M. W. Berns, B. J. Tromberg, *Hum. Reprod.*, 1996, **11**, 2162–2164.

131. L. Schermelleh, R. Heintzmann, H. Leonhardt, *J. Cell Biol.,* 2010, **190**, 2, 165.

132. S. W. Hell, *Nat. Biotechnol.*, 2003, **21**, 1347–1355.

133. S. W. Hell, *Science,* 2007, **316**, 1153–1158.

134. S. W. Hell, *Nat. Methods*, 2009, **6**, 24–32.

135. S. T. Hess, T. P. K. Girirajan, M. D. Mason, *Biophys. J.*, 2006, **91**, 4258–4272.

136. M. J. Rust, M. Bates, X. Zhuang, *Nat. Methods*, 2006, **3**, 10, 793.

137. P. Dedecker, C. Flors, J. Hotta, H. Uji-i, J. Hofkens, *Angew. Chem. Int. Ed.*, 2007, **46**, 8330–8332.

SECTION I

Metal Based CD-Nanoparticles

There is Plenty of room at the bottom
- Richard P Feynman, Renowned Physicist

2

Gold nanoparticle based molecular rotaxane for bimodal anticancer therapy

2.1 Introduction

From the evolution of several NO releasing strategies in line to the antitumor therapy, light based NO therapy is more affirmative as the fast response of the photochemical reactions associated to their instantaneous initiation/stopping depending on the presence or not of the illumination, represents a powerful tool for the rapid introduction of bioactive species in the desired bio-environment with accurate control in space and time.[1,2,3,4] In this direction, several NO releasing molecules came to prominence in biomedical science with the NO releasing capabilities, for instance organic nitrites, metal nitrosyls, glyceryl nitrates, S-nitrosothiols etc.[5] Generally the key factors, which determine the therapeutic efficacies of NO actions, are concentration of NO release, duration and rate of NO release at the bio-site. However most of the NO donors drastically fail on this concern either because they deliver lower concentration of NO, making the tumor proliferating, or associated with serious adverse side effects induced by the side products after NO release.[5,6] It is perceived by the fact that the micromolar concentration NO is optimal for antitumor actions and picomolar concentration is responsible for angiogenic effects, which lead to the tumorigenesis.[7] On these circumstances, our group have devised a new chromogenic moiety, a commercial nitroaniline derivative (Figure 2.1) to be able to release NO upon light irradiation in nanomolar level with the additional advantage of satisfying several biological prerequisites for photocages.[8]

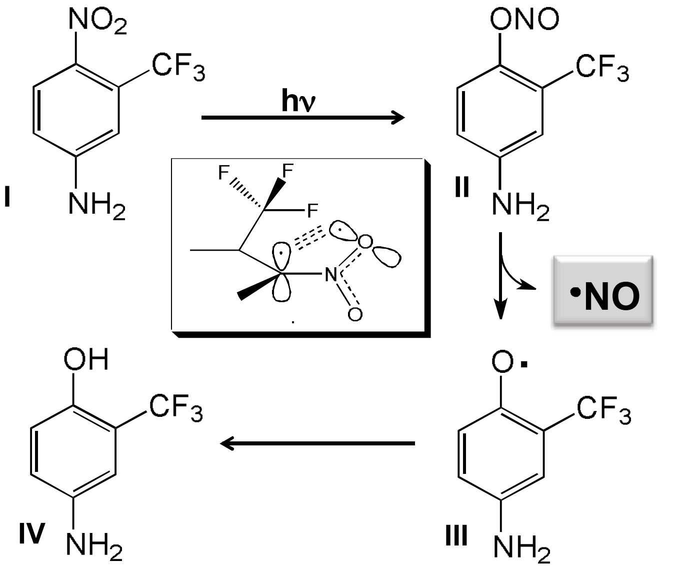

Figure 2.1. Schematic representation of light induced NO release from nitroaniline chromophore.

In fact it combines long term dark stability, adequate absorption coefficient at wavelengths longer than 350 nm, release of NO under the exclusive control of light input and generation of non-toxic and non-absorbing photoproducts in the visible region. In particular, the NO photorelease takes place through a nitro to nitrite photorearrangement followed by the rupture of the O-NO bond with formation of NO and a phenoxyradical.[9] The concentration dependent cytocidal actions of NO necessitate multifunctional delivery of NO by assembling several NO donors in to a macromolecular vehicle. In fact the combinatorial approach of designing NO delivery in conjunction with other PDT or PTT modalities is found to highly favorable since NO set drug resistant tumor sites susceptible to other treatment methods.[10]

Tunable optoelectronic properties of AuNPs by optimizing the synthetic protocol favors worthwhile objective to achieve a hybrid self-assembly in which photoactive ligand self-assemble on the particle surface in to a rotaxane nanostructure. In this direction, thiol-stabilized AuNPs, commonly referred to as monolayer protected clusters (MPC), provide a fascinating synthetic scaffold for the creation of drug delivery systems due to their versatility, superior biocompatibility and low toxicity.[11,12,13] Facile surface features of AuNPs allows simple modification or replacement of the ligand with desired functionalities through phase transfer reaction and the entire system can repeatedly dispersed and dissolved in common organic solvents with no sign of irreversible aggregation or decomposition.[14] Above all localized hyperthermia and SPR characteristics harnessed by AuNP by the selective excitation of the core could be instrumental in determining the therapeutic efficacies and site of action. Moreover the integration of NO delivering moiety onto the AuNP surface which able to deliver anticancer species on demand may represent a viable strategy for fabricating intriguing nanoarchitectures with great potential in the emerging field of "bimodal" anticancer therapies. With this goal in mind, the present effort is to show that aqueous soluble NO photoreleasing AuNPs can be achieved through a simple approach by self-assembling a host/guest complex between the thiol derivative NO photodonor and α-cyclodextrin (α-CD) on the surface of colloidal AuNPs (**Au-CD-1**, Scheme 2.1). In principle, such a system may combine a dense Au core for imaging and photothermia with a photoactivable shell for controlled release of NO. Here the NO releasing moiety, the nitroaniline derivative have been logically incorporated on thiol termination (thiol-**1**) in order to exploit the novel and easy surface chemistry between thiol group and AuNP.

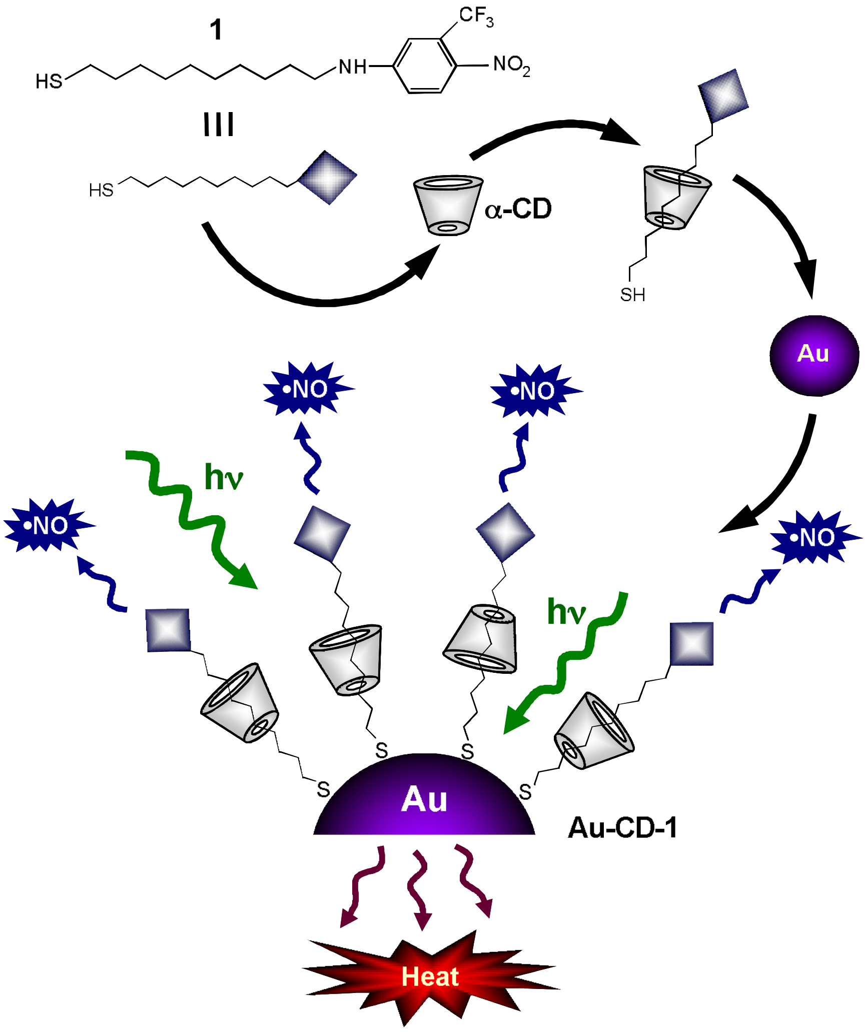

Scheme 2.1. Pictorial depiction of AuNP based self-assembling monolayers and light activated release of both NO and heat.

2.2 Experimental

2.2.1 Synthesis of the tailored NO photodonor

Thiol-1. [10-[3-(trifluoromethyl)-4-nitrophenylamino]decan-1-thiol] was synthesized in a three step synthesis according to the procedure shown in Figure 2.2 and described in the following. Syntheses were carried out under a low intensity level of visible light.

3-(trifluoromethyl)-N-(10-iododecyl)-4-nitrobenzenamine (A). Compound 2 (1.088 g, 5.2 mmol) and 1-10-diiododecane (8.3 g, 20 mmol) were refluxed in 40 mL of acetonitrile for 5 days. The organic solution was concentrated under reduced pressure and purified by column chromatography (dichloromethane:cyclohexane, 70:30) to give A (yield 65 %) as a brown-yellow oil. Anal. Calcd (%) for $C_{17}H_{24}F_3IN_2O_2$ (472.28): C, 43.23; H, 5.12; N, 5.93; found: C, 44.05; H, 5.53; N, 6.60;. ESI-MS m/z: $[M+H]^+$ 473.1. ^{1}H-NMR $CDCl_3$-d_1 (200 MHz) δ = 7.98 (1H, d, J =9.2 Hz), 6.84 (1H, d, J =2.2 Hz), 6.60 (1H, dd, J_1 =9.2 Hz, J_2 =2.2 Hz), 4.65 (1H, s, broad), 3.28 (2H, t, J =7.0 Hz), 3.17 (2H, t, J =7.3), 1.73-1.26 (16H, m).

S-10-[3-(trifluoromethyl)-4-nitrophenylamino]decylthanethioate (B). A mixture of A (0.47 g, 1 mmol) and MeCOSK (0.60 g, 5 mmol) in acetonitrile (500 mL) was heated for 6 h under reflux and N_2. After cooling down to ambient temperature, the solvent was distilled off under reduced pressure. The residue was suspended in CH_2Cl_2 and filtered. The organic solution was concentrated under reduced pressure and purified by column chromatography (dichloromethane:cyclohexane, 70:30) to give B (yield 85 %) as a yellow powder. Anal. Calcd (%) for $C_{19}H_{27}F_3N_2O_3S$ (420.49): C, 54.27; H, 6.47; N, 6.66; S, 7.63; found: C, 54.98; H, 7.11; N, 7.15; S, 8.12. ESI-MS m/z: $[M+H]^+$ 421.5.

^{1}H-NMR CDCl$_3$-d$_1$ (200 MHz) δ = 7.98 (1H, d, J =9.2 Hz), 6.84 (1H, d, J =2.2 Hz), 6.60 (1H, dd, J$_1$ =9.2 Hz, J$_2$ =2.2 Hz), 4.65 (1H, s, broad), 3.17 (2H, t, J =7.0), 2.82 (2H, t, J =7.0 Hz), 2.29 (3H, s), 1.73-1.26 (16H, m).

10-[3-(trifluoromethyl)-4-nitrophenylamino]decan-1-thiol (thiol-1). Acetyl chloride (100 ml, 1.4 mmol) was added drop wise to a solution of B (42 mg, 0.1 mmol) in methanol (50 mL) maintained at –78°C under N_2. After 15 min, the mixture was allowed to warm up to ambient temperature about 3 h. The solvent was distilled off under reduced pressure to afford 1 as a yellow powder. Anal. Calcd (%) for $C_{17}H_{25}F_3N_2O_2S$ (378.45): C, 53.95; H, 6.66; N, 7.40; S, 8.47; found: C, 54.63; H, 7.21; N, 8.13; S, 9.25. ESI-MS m/z: $[M+H]^+$ 379.3; ^{1}H-NMR CDCl$_3$-d$_1$ (200 MHz) δ = 7.87 (1H, d, J =8.9 Hz), 7.10 (1H, d, J =2.4 Hz), 6.68 (1H, dd, J$_1$ =8.9 Hz, J$_2$ =2.4 Hz), 4.45 (1H, s, broad), 3.25 (2H, t, J =6.8), 2.62 (2H t, J =7.1), 1.73-1.26 (16H, m).

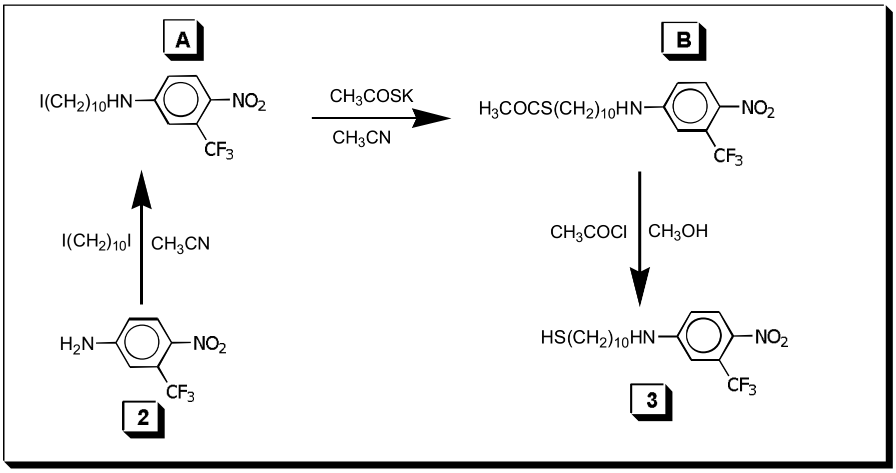

Figure 2.2. Scheme showing the steps to synthesize the thiol-1.

2.2.2 Synthesis of the "naked" gold nanoparticles

Preparation of gold nanoparticles abounds on several methods depending on the size required, in the literature.[15,16,17] One of the most popular protocol was proposed by Turkevitch in 1951 well known as "Turkevitch method".[18] This method was based on the reduction of $AuCl_4^-$ by citrate in water.

$$6\ AuCl_4^- + C_6H_8O_7 + 5H_2O \rightarrow 6CO_2 + 24\ Cl^- + 6\ Au^0 + 18\ H^+$$

Here citrate serves both as reducing agent and the capping agent, which protects the colloidal nanoparticle from undesirable modification. We have followed this way of preparing the Au nanoparticle with slight modification. In the preparative way, aqueous $HAuCl_4$ (5×10^{-3} mass %, solution 1) were reduced by citric acid (0.15 mass %, solution 2).[19] Solution 1 (750 mL) was heated at 100°C for 12 min, and then solution 2 (37.5 mL) added. After *ca*. 2 min the boiling solution turned blue, and after 3 minute became reddish purple. The mean size of the particle was found to be 30 nm in diameter at this stage by the DLS measurement. These AuNPs were filtered with a 0.8 μM membrane filter, before assembling with thiol-**1**/α-CD. The absence of α-CD and free thiol-**1** after washing the precipitate was verified by TLC and spectrophotometric analysis.

2.2.3 Synthesis of Au-CD-1

1 mg of thiol-**1** was added to 50 mL of the gold colloidal water solution containing 20 mM α-CD (purchased from the Sigma and used without further purification) and the resulting mixture was stirred for 3 days at room temperature while a dark-red precipitate was formed. The solid obtained was collected by centrifugation and washed several times with water first, and acetonitrile then, in order to remove the large excess of α-CD and the unreacted thiol-**1**, respectively. The dried precipitate was insoluble in nonpolar solvents such as chloroform and dichloromethane but fairly soluble in water and dimethyl formamide.

2.3 Instrumentation

Absorption spectra were recorded with a Jasco V 560 spectrophotometer. Nanoparticle sizes were measured by a dynamic light scattering performed with a Horiba LS 550 apparatus equipped with a diode laser with a wavelength of 650 nm. FTIR-ATR spectra were recorded at room temperature using a Bomem DA8 Fourier transformer Spectrometer, operating with a Globar Source in combination with a KBr beamsplitter and a DTGS/KBr detector. The powders were contained in a Golden Gate diamond ATR system, based on the attenuated total reflectance (ATR) technique and covering a wavelength range from 600 to 4000 cm^{-1}. In this configuration the evanescent wave will be attenuated in region of the IR spectrum where the sample absorbs energy. The spectra were recorded with a resolution of 2 cm^{-1}, averaging 100 scans to achieve a good signal-to-noise ratio and highly reproducible spectra. No smoothing was applied and spectroscopic manipulation such as baseline adjustment and normalization was performed using the Spectracalc software package GRAMS (Galactic Industries).

2.3.1 Photochemical experiments

Steady state and pulsed laser irradiation was performed in a thermostated quartz cell (1 cm pathlength, 3 mL capacity) by using a Rayonet photochemical reactor equipped with 8 RPR lamps with an emission in the 380-480 nm range with a maximum at 420 nm in the presence of a 400 nm cut-off filter, and the second harmonic of a Nd-YAG Continuum Surelite II-10 laser system (pulse width 6 ns FWHM, at λ = 532 nm, E_{532} ~ 1 mJ/pulse), respectively (Figure 2.3).

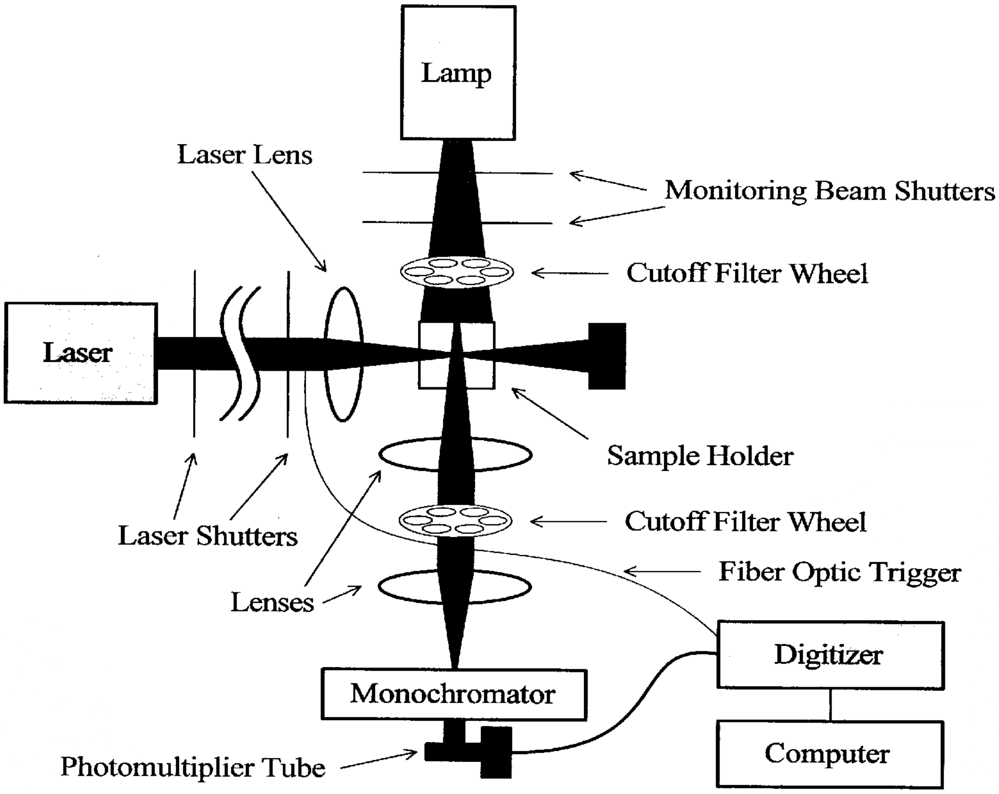

Figure 2.3. Schematic diagram of laser flash photolysis instrument used for the experiments.

The NO photorelease experiments were performed by irradiating the samples in the same cell as above using the monochromatic radiation (λ_{exc}= 400 nm) of a fluorimeter Fluorolog-2 (model F-111), under continuous stirring.

2.3.2 NO detection

NO release was measured with a World Precision Instrument, ISO-NO meter, equipped with a data acquisition system, and based on direct amperometric detection of NO with short response time (< 5 s) and sensitivity range 1 nM – 20 μM. The analog signal was digitalized with a four-channel recording system and transferred to a computer. The sensor was accurately calibrated by mixing standard solutions of $NaNO_2$ with 0.1 M H_2SO_4 and 0.1 M KI according to the reaction:

$$4H^+ + 2I^- + 2NO_2^- \rightarrow 2H_2O + 2NO + I_2$$

NO measurements were carried out with the electrode positioned outside the light path in order to avoid false NO signal due to photoelectric interference on the ISO-NO electrode.

2.4 Results and Discussion

Thiol-**1** was not soluble in water but it is clearly aqueous soluble when included inside the host cavity of α-CD forming a host guest inclusion complex as evident from the characteristic absorption spectra of thiol-**1**/ α-CD, which shows the absorption maxima at *ca*. 400 nm (a in Figure 2.4).

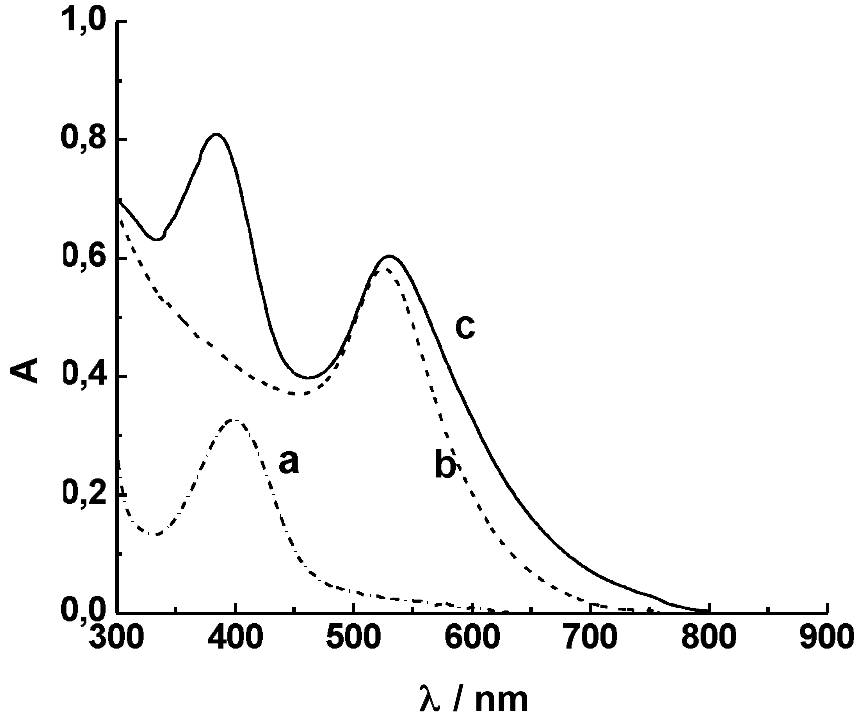

Figure 2.4. Absorption spectra of (a) Thiol **1** in the presence of aqueous 20 mM α-CD, (b) unfunctionalized AuNPs and (c) **Au-CD-1** in water solution. Spectrum b is reported in arbitrary absorbance, for sake of comparison.

It is generally accepted that host complexation is primarily determined by the size fit concept between the guest and the CD cavity. The diameter of the α-CD cavity is similar to the lateral size of the photoactive centre of thiol-**1** (*ca.* 0.57 nm) so that the host should accommodates preferentially a part of the hydrophobic alkyl chain of thiol-**1** most snugly (Scheme 2.1), analogously to what reported for alkanethiols with chain length comparable to thiol-**1**.[20] This hypothesis is corroborated by the absence of any significant induced circular dichroism signal in correspondence of the absorption bands of the nitroaniline chromophore which, in contrast, is observed when it is encapsulated within the larger β-CD cavity.[21]

The Au nanoparticle shows characteristic visible plasmon absorption band at 524 nm (b in the Figure 2.4) in consequence with their size, shape, composition,[22] whereas the typical synthetic protocol mentioned above gives small particle with the mean diameter of *ca.* 30 nm (Figure 2.5), particularly attractive for our objective. The host guest complex of thiol-**1** and α-CD were self-assembled on the surface of the AuNPs to form rotaxane nanostructure in which supramolecular assembly is chemisorbed on the particle surface through the thiol binder (Scheme 2.1) in aqueous phase. The absorption spectra of the nanohybrid structure (c in the Figure 2.4) shows slightly broadened absorption spectra with two peak positions at 540 and 385 nm followed by a red shift beyond 550 nm in comparison to AuNPs alone. Whereas the peak at 385 nm is little blue shifted from the thiol-**1** alone. Primary inspection of the steady state absorption spectra of the **Au-CD-1** reveals the formation of rotaxane nanostructure as the peak at 385 nm corresponds to the thiol-**1**/ α-CD self-assembly and band at 540 nm refers to the plasmon band of AuNP (c in Figure 2.4). In particular, the red shift and consequent broadening of Au plasmon absorption band of the nanostructure as compared to that of the unfunctionalized AuNPs is consistent with the modification of the gold surface upon covalent binding of the thiol group[23]. Interestingly, decoration of the AuNPs surface does not alter the mean diameter significantly since it changes from *ca.* 30 to *ca.* 33 nm. Nevertheless, the size distribution is larger (Figure 2.5) probably due to minor inter-particles interactions. This view is also in agreement with the slight blue shift of the absorption maximum of the NO photodonor when compared with the unbound host-guest complex (spectra a and c in Figure 2.4).

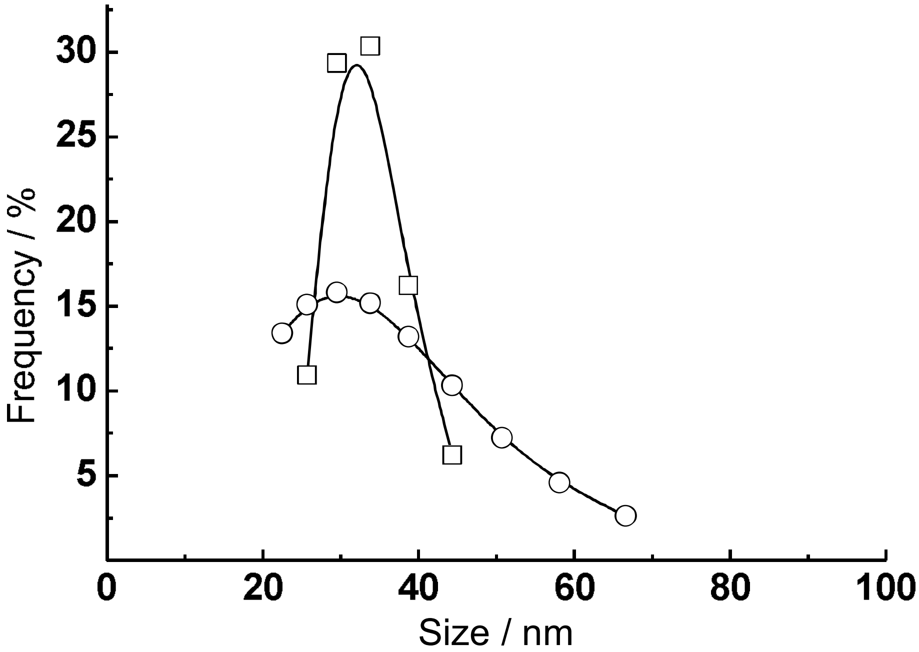

Figure 2.5. The size distribution of (□) AuNPs and (O) **Au-CD-1** samples, obtained by dynamic light scattering measurement.

In order to demonstrate the presence of the "rotaxane like" nanostructure of AuNP and NO donor, the FTIR-ATR analysis have been carried out on freeze-dried sample of the **Au-CD-1**, and for comparison on α-CD (Figure 2.6).

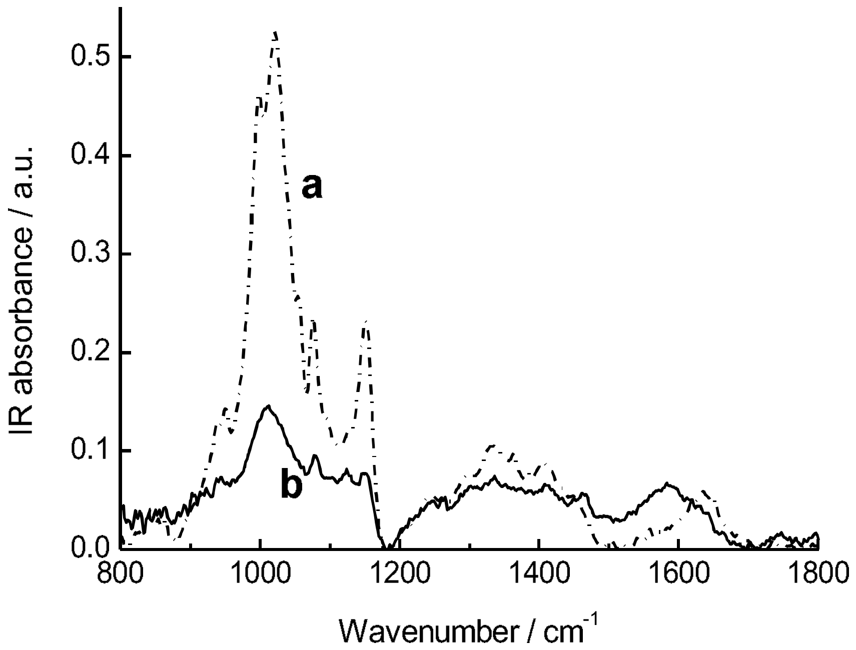

Figure 2.6. FTIR-ATR spectra on dried samples of (a) α-CD and (b) **Au-CD-1.**

As shown in Figure 2.6, the modified AuNPs shows the typical C-O stretching pattern of α-CD in the range 1000-1200 cm^{-1}. The band at *ca.* 1640 cm^{-1} corresponds to the HOH bending band, due to crystallization water molecules of α-CD. This band shifts to lower frequency, at the same time, increases in relative intensity in the case of **Au-CD-1**. This occurrence confirms that the chromophore thiol-**1** gets encapsulated in side the hydrophobic region of the α-CD cavities and forming an inclusion complex between them. According to recent literature data,[24] the observed spectral changes are indicative of a loss of a bulk-like structural arrangement for water molecules with a corresponding establishment of H-bonded networks of increasing co-operativity. This can be ascribed to the release of intra-cavity bulk-like water molecules upon complexation, in conjunction with their substitution with less polar "guest" molecules, and their following rearrangement in interstitial H-bonded environments.

In order to understand the photoregulated NO release in a controlled way, the modified AuNP were irradiated with light of 400 nm. We could observe that the aqueous solution of **Au-CD-1** is very sensitive to photolysis and the absorption peak at 400 nm undergo continuous photobleaching, whereas the plasmon absorption band of Au remain unaffected (Figure 2.7). The result propounds selective photochemical action of assembly with out altering the chemical identity of Au core.

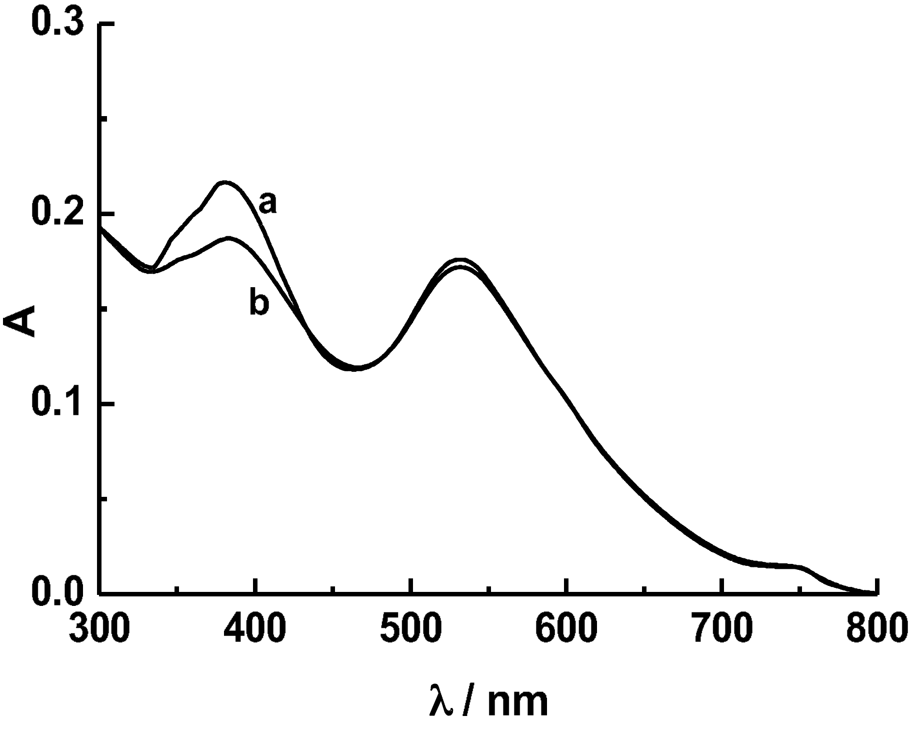

Figure 2.7. Absorption spectra of **Au-CD-1** in water solution at 25°C before (a) and after (b) 40 min of 400 nm light irradiation.

The most convenient methodology to demonstrate the photochemical decomposition is due to the NO release from **Au-CD-1** is the direct and in real-time monitoring of this radical species. To this end, we have used an ultrasensitive NO electrode (see experimental), which directly detects NO, with nanomolar concentration resolution, by an amperometric technique.

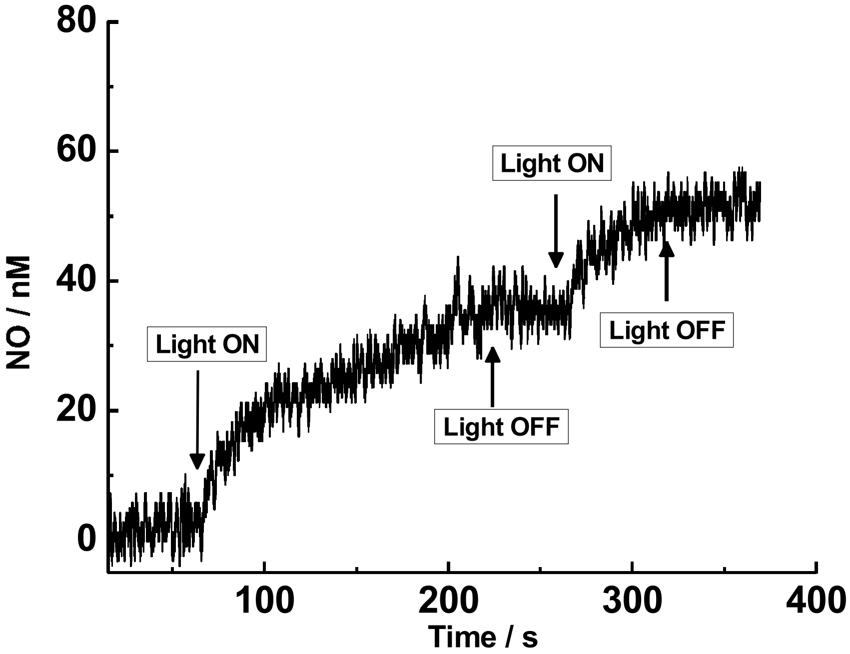

Figure 2.8. NO release from N_2-purged water solution of Au-CD-1 upon alternate periods of light (ON) and dark (OFF) at 25°C.

The results shown above (Figure 2.8) provide unambiguous evidence that the modified AuNPs are stable in the dark but supply NO upon illumination when irradiated with light of 400 nm. The release process is strictly dependent on the external light inputs, as confirmed by the linear NO photodelivery, which promptly stops as the light is turned off and restarts as the illumination is turned on again. Furthermore, no NO release was detected when the excitation energy was longer than 450 nm, in according to the negligible absorption of the NO photodonor unit at these wavelengths.

In order to prove the suitability of Au-CD-1 for photothermal treatments we tested both the thermal stability and photochemical stability towards visible excitation centred in the plasmon absorption band of the Au core. An aqueous sample of **Au-CD-1** was heated for 30 min at 70°C and irradiated for 20 min with a 532 nm laser excitation (see experimental). After these treatment the absorption spectrum remained basically unaffected (data not shown) revealing that the decorated AuNPs tolerates photochemical and thermal stress.

2.5 Conclusion

The present work based on the self-assembly of supramolecular complex and AuNPs encompass several art of design inspired from engineering to molecular biology. Actually it involves rational synthesis, preparation and characterization of a CD-based metal nanoassembly that, to the best of our knowledge, represents the first example of AuNPs exhibiting photoregulated release of NO. This system has been achieved by the appropriate self-assembling of three basic components. The role of the host cavity is manifold. In fact, it conveys the photoactive unit, insoluble in water, to the metal surface, allows the solubilization of the resulting modified AuNPs in polar aqueous solvents and, in view of its extensive use in biocompatible materials, is also envisaged to improve the biocompatibility of the resulting AuNPs. **Au-CD-1** exhibits a combination of indispensable properties in view of bio-applications, such as small sizes, water solubility, thermal stability and photoactivation with low energy light. In this latter concern, a further, remarkable advantage arising from the logical design of our systems is that the distinct absorption spectral region of the Au center and the NO photodonor units, allows in principle the selective excitation of the core (triggering photothermia), the shell (triggering NO release) or both (triggering bimodal effects) by the appropriate tuning of the visible light energy. These features make **Au-CD-1** a multifunctional, eligible candidate for light-mediated experiments in biomedical research.

2.6 References

1. P. P. Liccioli, J. Wirz, *Photochem. Photobiol. Sci.*, 2002, **1**, 441.
2. P. Neveu, I. Aujard, C. Benbrahim, T. Le Saux, J. -F. Allemand, S. Vriz, D. Bensimon, L. Jullien, *Angew. Chem. Int. Ed.*, 2006, **45**, 4099.
3. G. Cosa, M. Lukeman, J. C. Scaiano, *Acc. Chem. Res.*, 2009, **42**, 599.
4. N. K. Mal, M. Fujiwara, Y. Tanaka, *Nature*, 2003, **421**, 350.
5. P. G. Wang, M. Xian, X. Tang, X. Wu, Z. Wen, T. Cai, A. J. Janczuk, *Chem. Rev.*, 2002, **102**, 1091.
6. M. R. Miller, I. L. Megson, *Br. J. Pharmacol.*, 2007, **151**, 305–321.
7. S. Mocellein, V. Bronte, D. Nitti, *Med. Res. Rev.*, 2007, **27**, 317–352.
8. S. Conoci, S. Petralia, S. Sortino, U.S. Pat. Appl. Publ., 2009, 20 pp., Appl. No. PCT/IT2006/000575.
9. E. B. Caruso, S. Petralia, S. Conoci, S. Giuffrida, S. Sortino, *J. Am. Chem. Soc.*, 2007, **129**, 480.
10. A. W. Carpenter, M. H. Schoenfisch, *Chem. Soc. Rev.*, 2012, **41**, 3742–3752.
11. M. De, P. S. Ghosh, V. M. Rotello, *Adv. Mater.*, 2008, **20**, 4225.
12. S. S. Agasti, A. Chompoosor, C. -C. You, P. Ghosh, C. K. Kim, V. M. Rotello, *J. Am. Chem. Soc.*, 2009, **131**, 5728.
13. R. Bhattacharya, P. Mukherjee, *Adv. Drug Delivery Rev.*, 2008, **60**, 1289.
14. A. C. Templeton, W. P. Wuelfing, R. W. Murray, *Acc. Chem. Res.*, 2000, **33**, 27-36.
15. D. I. Gittins, F. Caruso, *Angew. Chem. Int. Ed.*, 2001, **40**, 16.
16. M. A. Hayat, *Colloidal Gold: Principles, Methods and Applications*, Academic Press, San Diego, 1989.
17. A. Henglein, D. Meisel, *Langmuir*, 1998, **14**, 7392.
18. J. Turkevitch, P. C. Stevenson, H. Hiller, Discuss. *Faraday Soc.*, 1951, **11**, 55.
19. G. Frens, *Nature*, 1973, **241**, 20.
20. J. Yan, S. Dong, *J. Electroanal. Chem.*, 1997, **440**, 229.

---

21. S. Sortino, S. Giuffrida, G. De Guidi, R. Chillemi, S. Petralia, G. Marconi, G. Condorelli, S. Sciuto, *Photochem. Photobiol.*, 2001, **73**, 6.

22. P. K. Jain, I. H. El-Sayed, M. A. El-Sayed, *nanotoday*, 2007, **2**, 1.

23. J. Zhang, J. K. Whitesell, M. A. Fox, *Chem. Mater.*, 2001, **13**, 2323.

24. F. Mallamace, M. Broccio, C. Corsaro, A. Faraone, D. Majolino, V. Venuti, L. Liu, C. Y. Mou, S. H. Chen, *Proc. Natl. Acad. Sci. U.S.A.*, 2007, **104**, 424.

SECTION II

Nanoconstructs Based on CD Conjugates

"If one way be better than another, you may be sure it is nature's way"- Aristotle, Greek philosopher

3

CD-based supramolecular nanoconstructs for simultaneous imaging and therapy

3.1 Introduction

There is high need for the diagnosis and imaging of tumor site where the action of cancer therapeutics is said to occur. The diagnosis of the bio-site with the non-invasive optical imaging technique adds an additional tool for in-depth understanding of tumor sites with increased tissue specificity, sensitivity and efficacy. The ideal fluorescent probe for the biological imaging should be effectively internalized in stringent acidic subcellular environment with high contrast as compared to the background.[1] To this end, rhodamine based fluorophores are proposed extensively for the biological subcellular imaging owing to their high quantum efficiency and increased penetration depth.[2,3,4] Rhodamine generally belongs to the Xanthene class of dyes, which is well versed as fluorescence standard.[5] Structurally, rhodamine exist in several isoforms, for example rhodamine B, rhodamine isothiocyanate, rhodamine 6G, rhodamine 101 etc., depending on the substitution and protonated groups which make them highly soluble in water. These isoforms are characterized by the non-centrosymmetric structure leading them one of the good probe for two-photon absorption ('Rho' in Scheme 3.1).[6] The amble two-photon absorption cross section (TPA) of the rhodamine is highly favorable for biological imaging at NIR window. In addition, rhodamine is capable to sensitize molecular oxygen into singlet oxygen and there by triggering PDT based cytotoxicity.[7]

Prospective of merging photoinduced NO cytotoxicity and non-invasive optical imaging by utilizing the emissive properties of rhoadamine in single nanoconstructs could be highly viable strategy towards bimodal antitumor therapy. However the independent cell penetrating abilities of both NO photodonor and rhodamine greatly determine the efficacy of this strategy. Indeed the logical designing of CD nanostructure meet this requirement as they incorporate suitable rhodamine moiety and NO photodonor at two different regions. This has been achieved by integrating fluorescent rhodamine moiety attached covalently on to the CD network and a phototherapeutic NO donor at the interior of CD pockets. Here the chromogenic centers should be able to absorb the light of desirable wavelength and release the active species on demand. However the poor binding of the unmodified CD pockets with the guest probe preclude the final goal to achieve increased local concentration of the therapeutic species[8]. Indeed, the logical synthetic designing allows possibility of modifying the primary and secondary rim of the of CD units with a plethora of substituents which can i) elongate the cavity or make it flexible, thus modifying its binding capacity, ii) alter the hydrophilic characteristics, iii) introduce charged groups that will enable cell penetration, iv) enable them to form conjugates with other functional molecules[9,10] (Scheme 3.1).

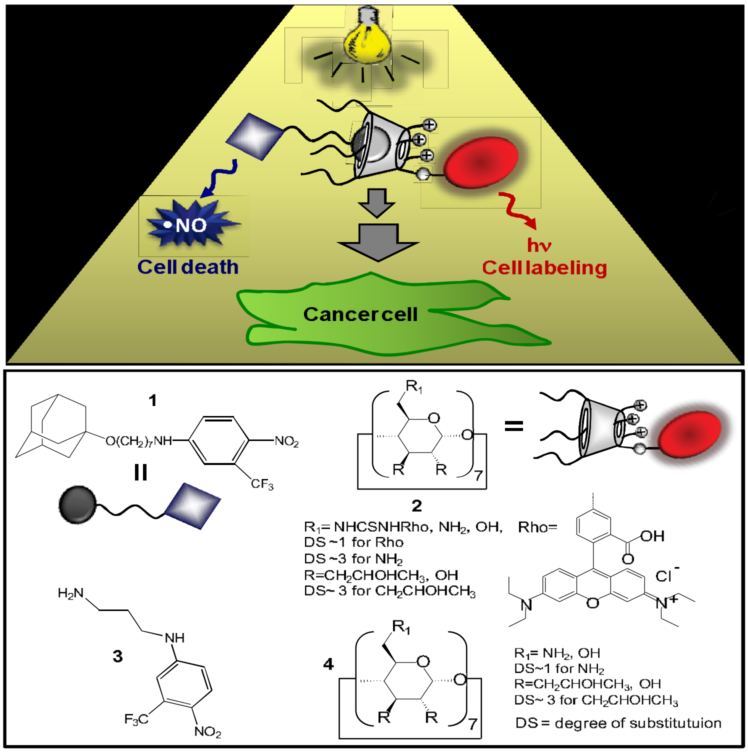

Scheme 3.1. Schematic representation of the photoresponsive host-guest supramolecular complex and molecular structures of the components.

Here the modification of CD units by amphiphilic tail is expected to increase the veheculation of the drug cargo and thereby increase the circulation time of the drug. Above all the fluorophore, rhodamine, attached to CD units enable local mapping of the entire system in cancer cells.

The considerable efforts have been done so far by various research groups to develop several kinds of NO delivering functionalities which delivers NO at the tumor site and various reviews detail all the emerging NO releasing molecules.[11,12,13] It is worthy to point out again that the generation of NO could be deleterious in action, since the therapeutic efficacy is largely depend on the site and dosage of NO release.[13] This narrow window related to the effective delivery and cytotoxicity imparted by the NO stimulated us to develop a nitroaniline based NO photodonor which meet all the requirement needed for the effective photoactivated NO delivery as it is able to release NO upon light irradiation in nanomolar level[14] and satisfies several biological prerequisites for efficient therapeutic efficacies.[15] The respective nitroaniline moiety is covalently attached to adamantanyloxy moeity by an alkyl spacer, enabling entire molecule to be anchored in apolar CD pockets (Scheme 3.1). Tailoring NO photodonor with adamantane appendage through the alkyl spacer facilitate the binding of the probe in CD pockets as hydrophobic cooperative interaction have major role in host-guest binding interactions.

3.2 Experimental

3.2.1 Materials

All the cyclodextrin intermediates were synthesized by CycloLab, Hungary. All other reagents were of the highest commercial grade available and used without further purification. All solvent used (from Carlo Erba) were analytical grade and were dried by conventional methods and distilled immediately prior to use. Phosphate buffer (10 mM, pH 7.4) was prepared with biological grade reagents and all solutions were prepared with nanopure water (grade 18 MΩ).

3.2.2 Syntheses

A Synthesis of tailored NO photodonor

[7-(Adamantan-1-yloxy)-heptyl]-(4-nitro-3-trifluoromethyl-phenyl)-amine (A)

The compound A was synthesized in two steps. Syntheses were carried out under a low intensity level of light.

1-(7-Bromo-heptyloxy)-adamantane (B). A THF solution of adamantanol (1 g, 6.56 mmol) was added to a suspension of sodium hydride (377 mg, 9.84 mmol) in 10 mL of dry THF at 0°C under argon atmosphere. After leaving at room temperature for 2 h, the mixture was added with 1,7 dibromoheptane (3.92 mL, 22.96 mmol). The reaction mixture was stirred overnight at room temperature and afterwards the excess of NaH was quenched by addition of water. The mixture was concentrated under reduced pressure and the aqueous phase was extracted with Et_2O (3 x 10 mL). The organic phases were then collected, washed, anhydried with Na_2SO_4, filtered, concentrated under reduced pressure and purified by column chromatography (dichloromethane:cyclohexane 30:70) to give **3a** (yield 90 %).^{1}H-NMR ($CDCl_3$, 500 MHz): δ 3.56 (2H, d, J= 6.50 Hz), 3.26 (2H, t, J = 6.68 Hz), 1.90-1.84 (3H, m), 1.72-1.35 (24H, m).

[7-(Adamantan-1-yloxy)-heptyl]-(4-nitro-3-trifluoromethyl-phenyl)-amine (**A**). A mixture of **B** (1 g, 3.03 mmol) and 4-nitro-3-(trifluoromethyl) aniline (200 mg, 1.01 mmol) were refluxed in acetonitrile for 5 days. The organic mixture was dried under vacuum and purified by column chromatography (dichloromethane:cyclohexane 70:30) compound **A** as a yellowish powder (yield 60 %, Figure 3.1). ^{1}H-NMR ($CDCl_3$, 500 MHz): δ 7.95 (1H, d, J= 9.2 Hz), 6.80 (1H, d, J= 2.4 Hz), 6.56 (1H, dd, J_1= 9.2 Hz, J_2= 2.4 Hz), 4.47 (1H, broad), 3.34 (2H, dd, J_1= 9.5 Hz, J_2= 6.5 Hz), 3.15 (2H, dd, J_1= 9.8 Hz, J_2= 6.9 Hz s), 1.83-1.77 (3H, m,), 1.63-1.57 (6H, m) 1.44-1.18 (16H, m).

B. Synthesis of rhodamine modified CD units

The rhodamine labeled CD units have been synthesized from CycloLab Ltd., Hungary[16] in collaboration with the Marie Curie Program and used as such with out further purification.

3.3 Instrumentation

UV/Vis absorption and fluorescence spectra were recorded with a Jasco V-560 spectrophotometer and a Fluorolog-2 (mod. F-111) spectrofluorimeter, respectively. Two-photon fluorescence images were recorded using LSM 710 NLO microscope (Carl Zeiss, Jena, Germany) equipped with mode-locked femtosecond pulsed *Mai Tai Deep See* laser. Microscope was equipped with a Plan-Apochromat 20x water immersion objective (NA 1.0) (Carl Zeiss, Jena, Germany). Laser light intensity at the sample, was approximately 15 mW. Fluorescence images were taken with a Biomed fluorescence microscope (Leitz, Wetzlar, Germany). The ESI–MS experiments were performed using a Waters Q-TOF Premier (Waters Corporation, 34 Maple St, Milford, MA, USA). Melting points were determined by a Buchi OP545 and are uncorrected. ^{1}H- and ^{13}C-NMR spectra were recorded on a Varian VXR-600 at 400 or 600 MHz. IR spectra were recorded in KBr disk on a Nicolet 205 FTIR. Photolysis experiments were performed in a thermostated quartz cell (1 cm pathlength, 3 mL capacity) by using a Rayonet photochemical reactor equipped with 8 RPR lamps with an emission in the 380-480 nm ranges with a maximum at 420 nm in the presence of a 400 nm cut-off filter. The incident photon flux on quartz cuvettes was *ca*. 0.8×10^{15} quanta sec^{-1}.

3.3.1 NO detection

NO release was measured with a World Precision Instrument, ISO-NO meter, equipped with a data acquisition system, and based on direct amperometric detection of NO with short response time (< 5 s) and sensitivity range 1 nM– 20 µM. The procedure is exactly same as used in chapter 2.

3.4 Samples preparation

Compound **1** was dissolved in methanol and slowly evaporated to form a thin film. This film was then hydrated with an aqueous solution of either **2** or the model compound **4**, in phosphate buffer at pH 7.4. The mixtures were stirred for 1 hour at 50°C and then the final solutions were left to equilibrate at room temperature.

3.4.1 Experiments with cells

HeLa cells were obtained from American Type Culture Collection and propagated at 1:6 ratio using Dulbecco's modification of Eagle's Minimal Essential Medium supplemented with 10% FBS (Fetal Bovine Serum). The samples of cells treated with the different samples of either **2** or its complex with **1**, trypsinized, placed separately in spectrophotometric cuvettes and either kept in the dark or irradiated with visible light in the photoreactor as described above. Before and after irradiation 8x10^4 cells were placed in 96-well plates with 100 µl of RPMI-1640 medium and incubated in presence of tetrazolium compound [3-(4,5-dimethylthiazol-2-yl)-5-(3-carboxymethoxyphenyl)-2-(4-sulfophenyl)-2H tetrazolium, inner salt; MTS, Promega] and an electron coupling reagent (phenazine methosulfate) PMS dye (MTS 20 µl/well). After further incubation of 1 h, the absorbance was read at 490 nm in a microplate reader (Labsystems Multiskan Bichromatic). The cell viability (%) was calculated according to the following equation:

Cell viability (%)= (A (before Lamp)-(A (after Lamp)/-A (before Lamp)) x 100

Where, A (sample before Lamp) represents measurement from the wells treated with samples before the light exposure to and A (sample after Lamp) represents measurement from the wells treated with samples after the light exposure.

A431 epidermal carcinoma cells were used for the two-photon imaging. Firstly the cells were seeded on the glass bottom of 3 cm diameter petridish for 24 hours prior to experiment. The medium was substituted with photactive components in PBS(10 mM) diluted 3 times and 4 hours prior to imaging. The experimental solution was removed before imaging and cells are gently rinsed with PBS. Afterwards, 2 mL of protein free MEM medium was added to the cell culture to keep cells allive and allow imaging with water imersion objective.

3.5 Results and Discussion

The steady state absorption and emssion spectrum of **2** is mainly contributed by the rhodamine and shows absorption peak position at 558 nm and emission maxima at 586 nm respectively (a and b in Figure 3.1). Analysis of spectroscopic features of Rhodamine B isothiocyanate[17] reveals that covalent binding of rhodamine to CD units does not compromise the photophysical features of the former, enable fluorescent tagging on CD units and respective imaging of the site where the putative therapeutic actions start to play. In fact the fluorescence quantum yield of **2** was calculated as $\Phi_f = 0.21$, which is closed to the reported value of the quantum yield of Rhodamine B isothiocyanate ($\Phi_f = 0.28 \pm 0.03$).[18]

The photoactive host **2** consists of β-CD units modified at both rims. The substitution of hydroxypropyl group at the secondary rim is expected to facilitate co-operative hydrophobic inter chain binding interaction with the alkyl spacer of guest **1** and there by increasing the binding constant. Whereas the alkyl ammonium salts attached on the CD rim is responsible for tracking the entire ensemble through the aqueous environment as peripheral amino groups are expected to be protonated at physiological pH, should assist in cell penetration owing to their positive charges, and ensure an excellent solubility in aqueous media. Since the rhodamine is attached to the primary rim of β-CD units, secondary rim of CD networks are free to host **2** non-covalently and the rhodamine can track the entire ensemble in living cells by the optical microscopic techniques.

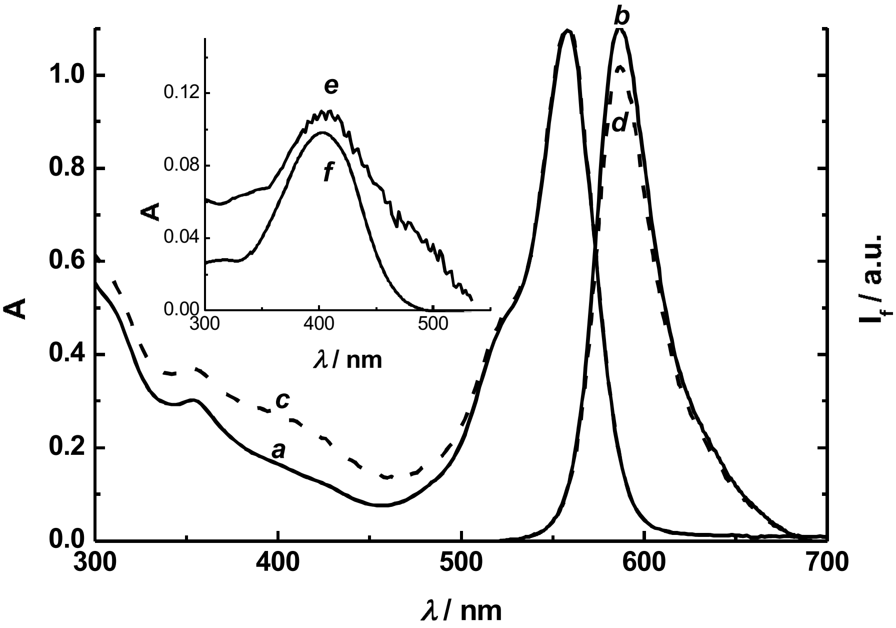

Figure 3.1. Absorption and fluorescence emission spectra (λ_{exc}= 525 nm, isosbestic point) in phosphate buffer (10 mM, pH 7.4) of **2** in the absence (**a** and **b**) and in the presence (**c** and **d** of **1**. The inset shows the difference absorption spectrum between sample **c** and **a** (**e**), and absorption spectrum of the model compound **3** (**f**). [1]= 10 μM, [2]= 10.8 μM, T= 25°C, cell path= 1 cm.

The compound **1** as such is not soluble in water, but become aqueous soluble as a result of supramolecular complex formation with the host **2**. Compound **1** is designed in a way that adamantane appendage encapsulate in to the CD pockets allowing the nitroaniline moiety to be exposed on the aqueous phase. The encapsulation phenomenon is much evident from the appearance of additional band below 500 nm of the host **2** (curve c in Figure 3.1). The similarity between differences in the absorption spectrum (c and a in Figure 3.1) of host **2** with the absorption spectrum of the aqueous soluble modal compound **3** (Inset Figure 3.1) demonstrates that the additional contribution of the absorption below 500 nm in the absorption spectrum of host is due to the nitroaniline chromophore resulting from efficient inclusion phenomenon between the guest and host. It has been shown that isomerization process of the nitro group of the nitroaniline is very sensitive to microenvironment and solvent polarities.[19] In this compound, the twisted conformation of the nitro group with respect to the aromatic plane is crucial for efficient isomerization of nitro group and followed NO photorelease. In addition, the incorporation of NO releasing moiety in constrained environment could be nocuous towards the effective NO release.[19] Here the adamantane moiety serves an important role for the NO photorelease as they occupy the empty CD pockets and thereby directing the nitroaniline moiety to water pool (*vide supra*) exposed on aqueous phase. This view is corroborated by the absorption spectra where the absence of any shift in the absorption maximum of **1** with respect to **3** suggests a binding mode in which the NO photodonor is mainly exposed to a water pool while the adamantane unit occupies the CD cavity, as illustrated in Scheme 3.1.

The absorption spectra give some insights to the mode of binding between components **1** and **2**. Based on the absorbance values of the NO photodonor at 403 nm and of the rhodamine label at 558 nm, and the related extinction coefficients at the same wavelengths (*ca.* 10,000 $M^{-1}cm^{-1}$ and 100,000 $M^{-1}cm^{-1}$, respectively), a nearly complete complexation between **1** and **2** with a 1:1 stoichiometry can be estimated. In view of the low concentrations of the components (*ca.* 10 μm), this finding accounts for a high binding constant (K_a $>10^5$ M^{-1}). Taking into account that the Ka values for adamantane and unfunctionalized β-CD are on the order of 10^4 M^{-1} [20,21] we believe that the effective binding process might stem from cooperative intra-cavity interactions involving the adamantane moiety and hydrophobic inter chain interactions involving the alkyl spacer of **1** and the isopropyl termini of **2**. Such an efficient complexation of the active guest is a fundamental requisite for its intracellular delivery.

The emission profile and consequent photochemical properties of rhodamine attached to host **2** are remaining unaltered during the complexation between host **2** and guest **1** (b and d in Figure 3.1). This could be conceived by the fact that guest **1** encapsulate at lower rim of the CD units. As the two chromophores are wide each other, the intramolecular quenching by photoinduced electron transfer between two chromophores are not trivial, whereas photoinduced energy transfer from rhodamine and NO photodonor **1** is highly endergonic in nature.

Encapsulated NO photodonor **1** undergo photdynamic action by releasing out NO upon irradiation with prompt light. This is much clear in the absorption spectra of supramolecular complex (Figure 3.2), where the absorption band corresponding to the NO photodonor undergo bleaching from a to e with out changing the absorption band of host **1** beyond 500 nm. This extend of bleaching is exclusively depend on the photochemical reactions occurs on NO photodonor **1** on its way to nitro-nitrite isomerism.[15] Moreover, the emissive property of rhodamine is independent of the photobleaching as the steady state fluorescence spectrum of rhodamine is remain preserved even after the NO photorelease (f and g in Figure 3.2).

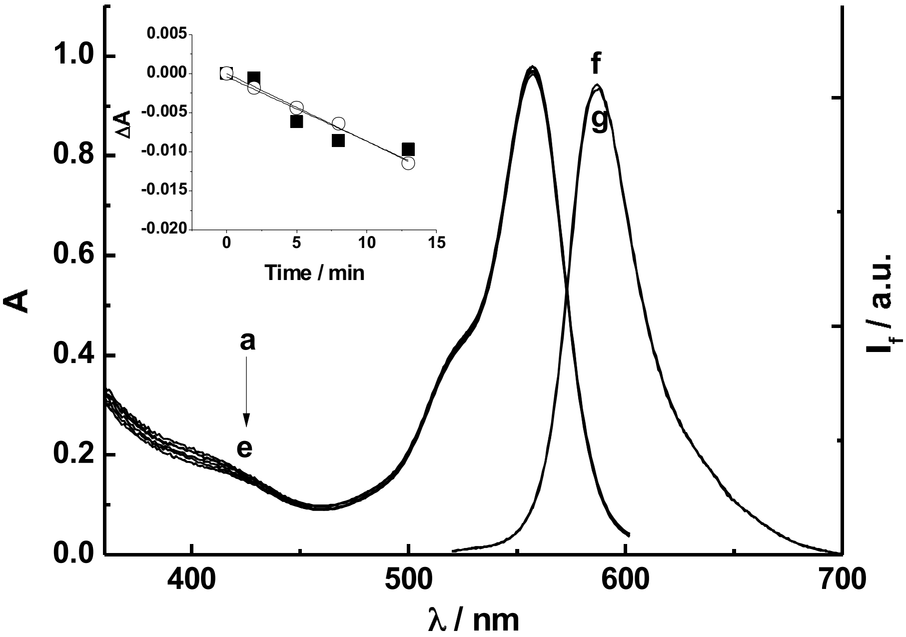

Figure 3.2. Absorption spectral changes (from **a** to **e**) observed upon 420 nm light irradiation of the complex **1**/**2** in phosphate buffer (10 mM, pH 7.4). Fluorescence emission spectra of the supramolecular complex before (**f**) and after (**g**) photolysis (λ_{exc}= 525 nm). The inset shows the kinetic profiles, monitored at 400 nm, and the related linear fitting, observed in the case of the complex of **1** with **2** (○) and the model compound 4 (■). [1]= 10 μM, [2]= 10.8 μM, T= 25°C, cell path= 1 cm.

Though most convenient methodology to analyze NO photorelease from the supramolecular ensemble is the direct and real time measurement of NO free radical. To this end, we used an ultra sensitive NO electrode, which detect NO at nM resolution by an amperometeric technique.[22] The linear generation of amperogram which promptly stops when the light is turned off and regenerate again upon illumination with light of λ_{exc}= 420 nm, gives an unambiguous evidence of NO release from the ensemble (Figure 3.3). The respective amperogram confirms that the NO release process strictly depend on the external light inputs and ineffective towards other external parameters.

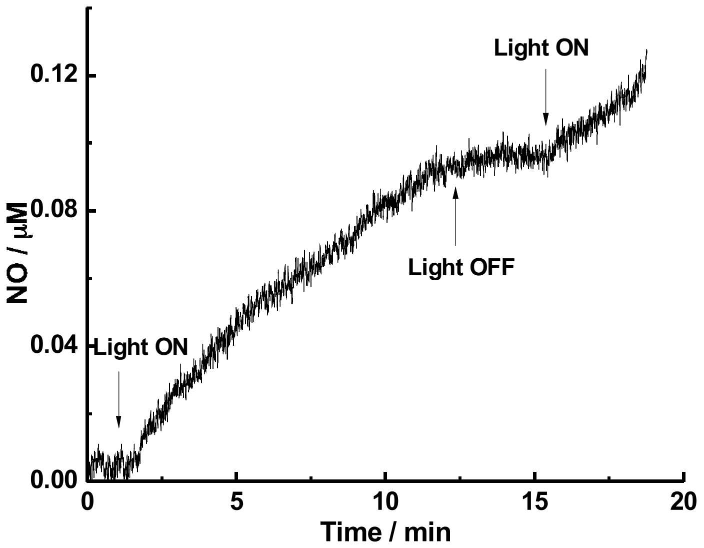

Figure 3.3. NO release profile observed upon 420 nm light irradiation of the complex in the same conditions as Figure 3.2.

In addition, it was found that NO photorelease process is practically same when NO photodonor **1** is included in CD units devoid of rhodamine (modal compound **4** in Scheme 3.1) discarding the notion that rhodamine may interfere with the NO release from the NO photodonor (data not shown). The similar kinetic profile with the same slopes obtained for the photobleaching of NO photodonor **1** in both rhodamine attached CD **2** and free CD units **4** (Inset Figure 3.2), excludes any effect of the rhodamine fluorophore on the photoreactivity of the former.

Normal fluorescence microscopy imaging studies were done to understand the site of NO photodelivery and consequent NO actions. In this regard, the HeLa cells used for the cell mortality experiments were incubated with the supramolecular ensemble for three hours and imaging was done after that (Figure 3.4). The presence of the CD derivative inside the cells can be easily revealed by the red fluorescence emission typical of the rhodamine label, while the location of the nuclear compartment is accomplished by staining the cells with the fluorescent DNA binding dye Hoechst 33342. Figure 3.4A shows a well detectable level of intracellular red fluorescence within HeLa cells as observed in case of epidermal cancer cell line confirms the ability of the CD conjugate to penetrate the cells. Figure 3.4B evidences nuclear staining of the same cells with Hoechst 33342, as revealed by the blue fluorescence emission of this dye. Figure 3.4C shows the corresponding merged image obtained by double fluorescence analysis.

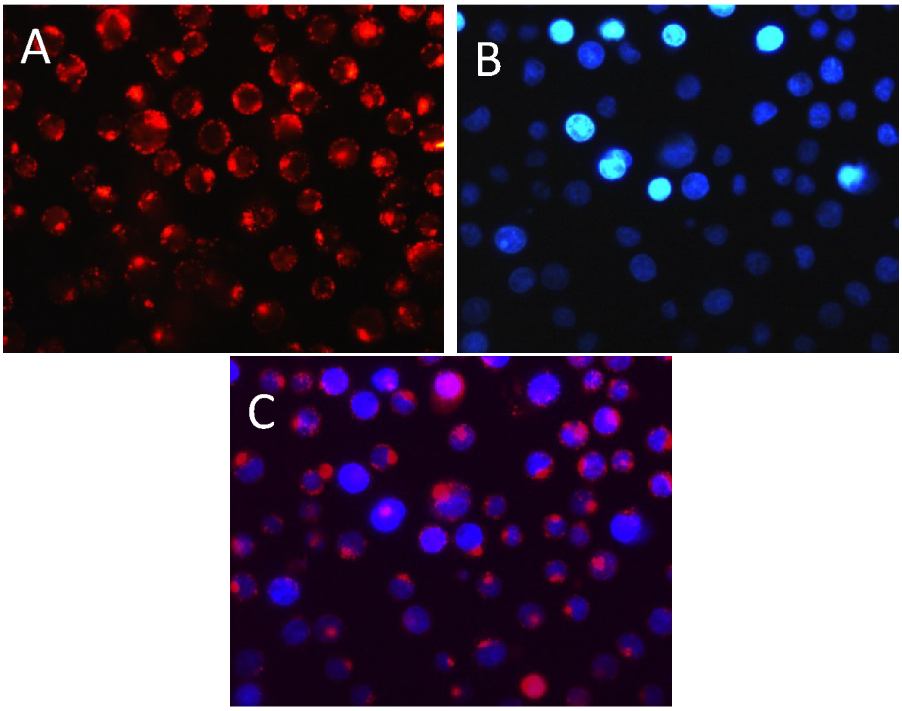

Figure 3.4. Fluorescence microscopy analysis of HeLa cells treated with the complex **1/2** (*ca.* 10 µM) and stained with HOECHST 33342 dye in phosphate buffer solution (10 mM, pH 7.4). The cells were analyzed by fluorescence microscopy (40×) with a rhodamine filter (**A**), a Hoechst emission filter (**B**) or by merging images A and B (**C**), respectively.

A close inspection of this image excludes the confinement of the CD derivative in the nuclear compartment of the HeLa cells, accounting for localization mainly in the cytoplasm or a possible colocalization with mitochondria, in agreement with typical observations for rhodamine derivatives.[23]

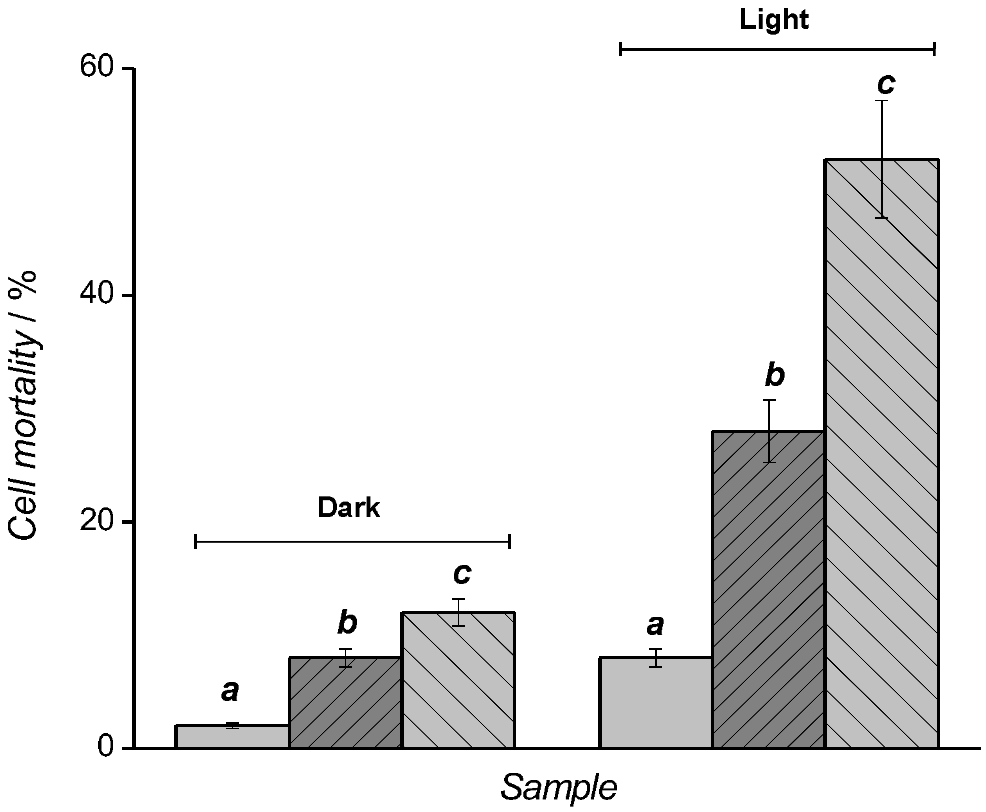

Figure 3.5. Dark and photoinduced mortality of HeLa cells without the photoactive components (**a**) and incubated with **2** (10 μM) (**b**) and its complex with **1** (**c**).

To evaluate the effectiveness of this system to induce antitumor effects upon light irradiation, the cell cultures were treated for 3 hours with the complex and, for comparison, with the host **2** alone, and the samples were either kept in the dark or irradiated with visible light for 30 minutes. The results (Figure 3.5) show that both **2** and its complex with **1** exhibit a low level of cytotoxicity in the dark. By contrast, considerable cell mortality is observed under light excitation. It can be seen that the extent of cellular death observed for the complex is greater than that noted in the case of the host alone. This result provides clear-cut evidence for the capability of **2** to deliver **1** to the cell compartment, although we cannot exclude the possibility that the complex dissociates after cell internalization.

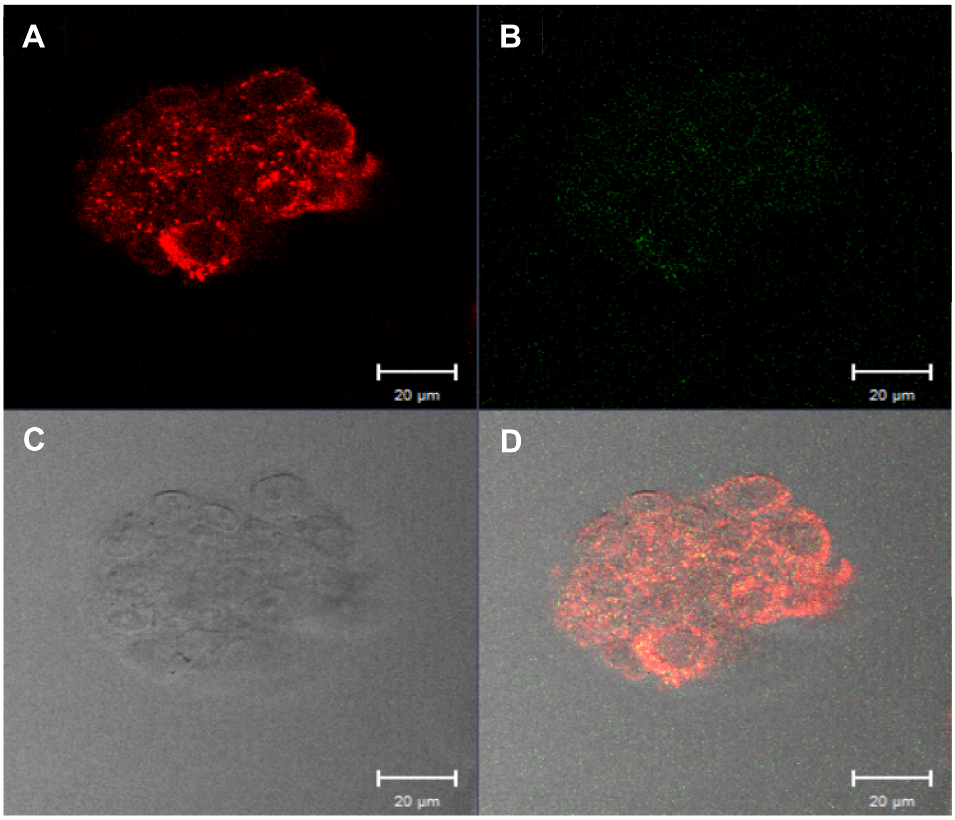

Figure 3.6. The two-photon fluorescence microscopy image of epidermal cancer cell lines (Model No. A431) incubated with the complex **1/2** (*ca.* 10 μM) in 10 mM phosphate buffer (pH 7.4). The assembly mapped as A) Ex. at 840 nm and detection: Green channel at 435-555 nm; band passfilters is at 435-555 nm. B) The same excitation and band pass filter with detection at red channel (620-710 nm) C) transmission image D) overlay of all images.

The photoinduced cell mortality induced by **2** alone can be reasonably ascribed to the generation of ROS by the rhodamine dye, which has been reported to act as a photosensitizer although with low efficiency[24].

The supramolecular dispersion is tracked in A431 cancer cell lines by two photon imaging technique exploiting the amble two-photon cross section of the rhodamine[25] (Figure 3.6), which allows the excitation of the fluorophore with non-invasive far red light making biological imaging a highly desirable tool for tumor diagnosis. The respective image shows that the supramolecular assemblies are well internalized at the cytoplasmic level. Well detectable red fluorescence of rhodamine augments the idea that majority of the supramolecular complex intake in to cell cytoplasm and nuclear organelles excluding the nucleus (Figure 3.6).

3.6 Conclusion

A novel multifunctional, photoresponsive supramolecular "Lego system" was devised here based on the effective formation of an inclusion complex between a tailor-made NO photodonor and an *ad hoc* devised CD conjugate carrying a rhodamine fluorophore. Both the guest and the host behave as independent photoactive centers in the supramolecular complex, as proven by the excellent preservation of their photochemical and photophysical properties. As a result, this nanoassembly exhibits the convergence of photoregulated release of NO and fluorescence imaging in one single nanostructure. We would like to highlight that, in contrast to non-photoresponsive compounds, the preservation of the photobehavior of independent components after their assembly is not a "trivial result". In most cases, the response to light of single or multiple photoactive units located in a confined space can be, in fact, considerably influenced, in both nature and efficiency, by the occurrence of competitive photoprocesses (i.e., photoinduced energy and/or electron transfer, hydrogen abstraction, nonradiative deactivation, etc.,[26,27,28] which preclude the final goal.

The host–guest complex internalizes in cancer cells, probably assisted by its cationic nature at physiological pH, can be easily mapped therein in view of its satisfactory fluorescence emission, and is able to induce about 50% cell photomortality. In this regard, it appears that the extent of the cellular death is not exclusively due to the light-triggered generation of NO but also to the involvement of ROS photogenerated by the rhodamine unit. Studies addressed to clarify this point deserve certainly attention.

3.7 References

1. Y. Hama, Y. Urano, Y. Koyama, M. Bernardo, P. L. Choyke, H. Kobayashi, *Bioconjugate Chem*., 2006, **17**, 1426–1431.
2. R. N. Dsouza, U. Pischel, W. M. Nau, *Chem. Rev*., 2011, **111**, 7941.
3. M. R. Longmire, M. Ogawa, Y. Hama, N. Kosaka, C. A. S. Regino, P. L. Choyke, H. Kobayashi, *Bioconjugate Chem.,* 2008, **19**, 1735–1742.
4. M. Fontaine, W. F. Elmquist, D. W. Miller, *Life Sci.*, 1996, **59**, 18, 1521-1531.
5. T. Karstens, K. Kobs, *J. Phys. Chem.,* 1980, **84**, 1871-1872.
6. A. Nag, D. Goswami, *J. Photochem. Photobiol. A: Che*m., 2009, **206**, 188–197.
7. F. Stracke, Ma. Heupel, E. Thiel, *J. Photochem. Photobiol. A. Chem*., 1999, **126**, 51–58.
8. A. Mazzaglia, N. Micali, L. M. Scolaro, *Cyclodextrin Materials Photochemistry-Photophysics and Photobiology*, Elsevier, 2006, pp. 203-222.
9. P. Falvey, C. W. Lim, R. Darcy, T. Revermann, U. Karst, M. Giesbers, A. T. M. Marcelis, A. Lazar, A. W. Coleman, D. N. Reinhoudt, B. J. Ravoo, *Chem. Eur. J*., 2005, **11**, 1171.
10. R. Donohue, A. Mazzaglia, B. J. Ravoo, R. Darcy, *Chem. Commun*., 2002, 2864.
11. S. Sortino, *Chem. Soc. Rev*., 2010, **39**, 2903.
12. P. G. Wang, M. Xian, X. Tang, X. Wu, Z. Wen, T. Cai, A. J. Janczuk, *Chem. Rev*., 2002, **102**, 109.
13. D. A. Riccio, M. H. Schoenfisch, *Chem. Soc. Rev*., 2012, **41**, 3731.
14. S. Conoci, S. Petralia, S. Sortino, U.S. Pat. Appl. Publ., 2009, 20 pp., Appl. No. PCT/IT2006/000575.
15. E. B. Caruso, S. Petralia, S. Conoci, S. Giuffrida, S. Sortino, *J. Am. Chem. Soc*., 2007, **129**, 480.
16. N. Kandoth, M. Malanga, A. Fraix, L. Jicsinszky, E. Fenyvesi, T. Parisi, I. Colao, M. T. Sciortino, S. Sortino, *Chem. Asian J*., DOI:10.1002/asia.201200640.
17. S. A. Soper, H. L. Nutter, R. A. Keller, L. M. Davis, E. B. Shera, *Photochem. Photobiol.*, 1993, **57**, 972–977.

---

18. H. S. Nalwa, *Advances in Surface Science*, Eds.; R. Celota, T. Lucatorto, In Experimental Methods in the Physical Sciences, Academic Press, San Diego, 2001, **Vol. 38,** pp. 327-329.

19. S. Sortino, G. Marconi, G. Condorelli, *Chem. Commun.*, 2001, 1226.

20. J. Carrazana, A. Jover, F. Meijide, V. H. Soto, J. V. Tato, *J. Phys. Chem.,* 2005, **109**, 9719.

21. M. Rekharsky, Y. Inoue, *Chem. Rev.,* 1998, **98**, 1875.

22. P. N. Coneski, M. H. Schoenfisch, *Chem. Soc. Rev.*, 2012, **41**, 3753.

23. A. Sasnauskiene, J. Kadziauskas, D. Labeikyte, V. Kirveliene, *Biologija*, 2009, **55**, 51.

24. F. Stracke, M. Heupel, E. Thiel, *J. Photochem. Photobiol. A*, 1999, **126**, 51.

25. M. A. Albota, C. Xu, W. W. Webb, *Applied Optics*, 1998, **37**, 31.

26. P. Bortolus, S. Monti, *Adv. Photochem.*, 1996, **21**, 1.

27. V. Ramamurthy, *Photochemistry in Organized and Constrained Media*, VCH Publisher, New York, 1991.

28. S. Monti, S. Sortino, *Chem. Soc. Rev.*, 2002, **31**, 287.

4

CD-oligomer based nanoconstructs for simulatneous imaging and therapy

4.1 Introduction

Non-invasive optical imaging by fluorescent tagging on the nanocarrier is one of the novel strategies to understand the site of therapeutic action in cell environment.[1,2,3] The covalent modification of the carrier by a suitable fluorophore allows real time localization of the entire system at the cellular environment in which the aqueous insoluble drug payload is incorporated. Several methods have been proposed to tag the fluorophore on the carrier cyclodextrin with the interest ranging from drug delivery system to chemo sensors.[4,5] Actually tagging the fluorophore on primary or secondary side of CD structures can in principle act like a light harvesting antenna and the excited fluorophore can simply transfer the energy to the included analyte either through the energy transfer or electron transfer, adding interesting features to the physicochemical properties of the included analyte.[6,7] Conversely the same approach could be extended into an assembly where two chromogenic moieties incorporate in the CD interior with out any energy or electronic communication each other.[8,9]

Similar to the strategy of probing tailored NO photodonor in rhodamine attached single CD pockets explained in the previous chapter, the former could be utilized to encompass with extended CD networks. Specifically, several CD units could interconnect covalently each other to form the oligomer or polymer. Interconnecting several CD units into oligomer is highly favorable for drug delivery applications as i) several *ad hoc* modified CD units is able to interact with higher concentration of the probe and thereby increasing the local concentration of therapeutic payload,[10] ii) increased number of functional substituents attached to the multiple CD units can simply interact with various structural sites of the analyte with increased cooperative binding[11] iii) enable the construction of supramolecular CD scaffolds in nanometer regime and there by increasing bioavailability and biocompatibility of the whole system.[12]

With the goal to achieve photoactivated NO release accompanied by the biological imaging, NO photodonor is being incorporated in CD based oligomer attached with rhodamine (Scheme 4.1). The CD units are interconnected by epichlorohydrin polymer to form the oligomeric structure with hydrophilic glyceryl cross-links. The modification of the secondary rim of the CD unit with carboxylic group favors excellent aqueous stability and additional binding features. The rhodamine is attached on the primary side of the CD, precluding any detrimental interaction of rhodamine with the including probe on account of the steric reasons. In addition, it may facilitate the entire assembly to be tracked at the biological interphase. Moreover the facile two-photon cross section of the rhodamine permits optical imaging at NIR region.[13]

The tailor made NO photodonor, where nitroaniline derivative is connected to adamantane appendage by an alkyl spacer (**2** in Scheme 4.1) is anchored in the extended CD network enabling NO release exclusively controlled by the light photons.[14,15] The adamantane is perfect encapsulator inside the β-CD cavity owing to it matching size fit with the CD cavity.[16] In fact, both chromogenic centers can be activated independently for their respective photoactions since the photochemical features of both probe are at distinctive spectral window. Above all, the intriguing strategy of encompassing two probe, namely tailored NO donor and the fluorophore rhodamine unit, both attached covalently and noncovalently to the biocompatible CD nanostructure favors ongoing interest of developing smart nanoconstructs addressed to photoactivated bimodal therapy.

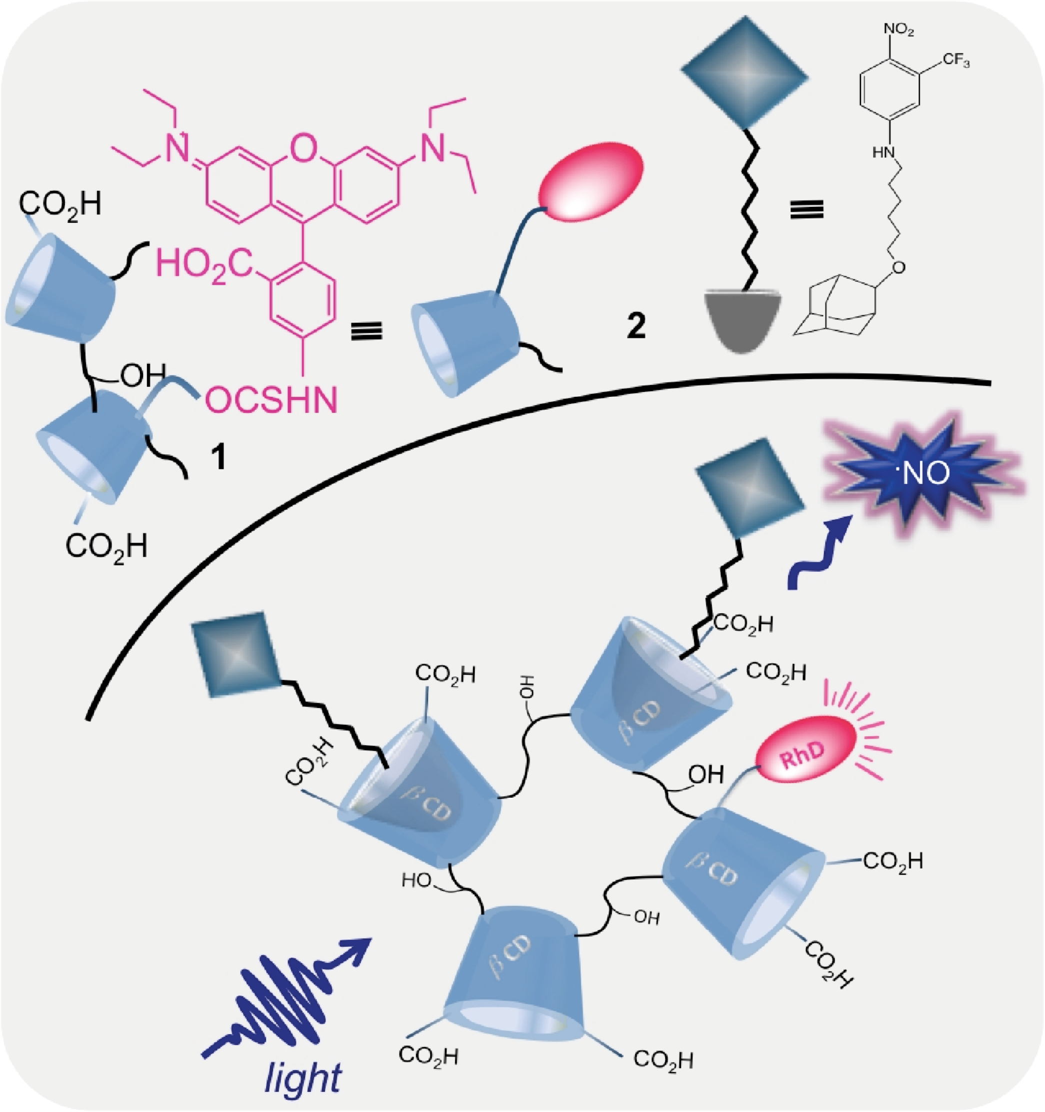

Scheme 4.1. Pictorial representation of the supramolecular assembly formed between rhodamine attached carboxymethyl CD units (**1**) and adamantane terminated NO photodonor (**2**) and their respective photoactions. The CO$_2$H groups are connected to the secondary side of CD while the rhodamine is attached mainly at the primary side.

4.2 Experimental

4.2.1 Materials

All cyclodextrin intermediates for preparing CD-based oligomer was obtained from CycloLab Ltd., Hungary. All other reagents and the conditions used for the experiments is exactly same as that used in the previous chapter.

4.2.2 Syntheses

A Synthesis of tailored NO photodonor

The synthetic procedure is same as described in the previous chapter (Chapter 3, Section 3.2.2 A).

B Synthesis of rhodamince modified CD oligomer

The rhodamine attached CD oligomer have been synthesized from CycloLab Ltd., Hungary, as the part of Marie Curie Program and used as such with out further purification. All other experimental procedures are exactly replicated as in the previous chapter (see Chapter 3, Section 3.3).

4.3 Instrumentation

All the instruments used for the experiment is same as that used in the previous chapter (Chapter 3).

4.4 Results and Discussion

Steady state absorption spectra of the aqueous dispersion of CD oligomer (**1**) with NO photodonor (**2**) reveals that **1** is clearly able to encapsulate the aqueous insoluble **2** in the CD cavities (Figure 4.1). Moreover the absorption features are similar to the complexation observed in case of NO photodonor included in rhodamine attached single CD unit (Section 3.4, Chapter 3). Though in the present case, the additional band of the host-guest complex below 500 nm is higher than the band where the compound **1** absorbs alone (h and j respectively, in Figure 4.2) resulting possibility of loading high local concentration of NO photodonor in the CD pockets of oligomer than in the case of single CD unit. This is trivial as more free CD units are free to undergo encapsulation and in consequence, leading to NO release with greater quantum yield. In fact, the difference in the absorption spectra of free **1** and supramolecular complex (Inset Figure 4.2) validates this point, as it shows the amble absorption of compound **2** at 400 nm similar to the observation of the absorption spectra of model compound (data is shown in Chapter 3).

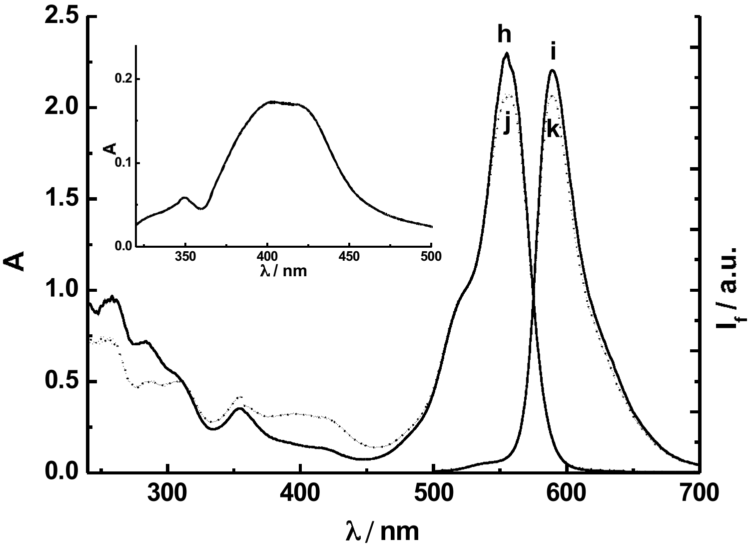

Figure 4.1. Normalized steady state absorption and emission (λ_{exc} = 490 nm) spectra of **1** in phosphate buffer (10 mM, pH 7.4) in the absence (h and i) and in the presence (j and k) of **2**. The inset shows the difference of absorption spectrum between sample j and h. [**1**] = 20 μM, [**2**] = 15 μM, T = 25°C, cell path = 1 cm.

Interestingly the complexation event does not influence much on the emissive properties of rhodamine attached to CD units. Though little change over the fluorescence intensity could be attributed by the fact that the presence of NO photodonor at the closed vicinity may change the local environment and orientation of fluorophore.[17]

Figure 4.2 shows the bleaching of the absorption spectra of **2** in the supramolecular complex upon irradiation with light of 420 nm. Here the band corresponding to the absorption of NO photodonor undergoes bleaching followed by the release of NO.

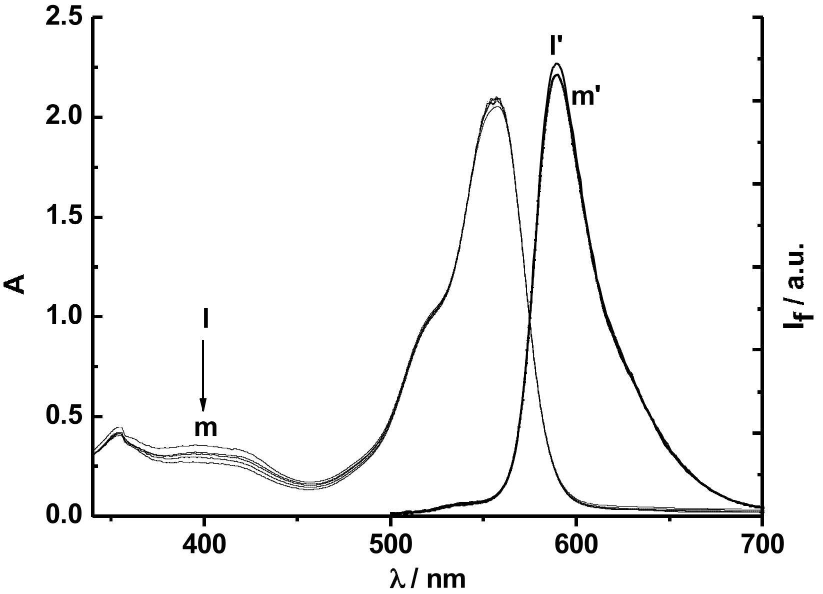

Figure 4.2. Absorption spectral changes observed upon 420 nm light irradiation of the complex **2**/**1** in phosphate buffer (10 mM, pH 7.4) at 25°C. Fluorescence emission spectra of the supramolecular complex before (l') and after (m') photolysis (λ_{exc} = 490 nm). [**1**]= 20 μM, [**2**]= 15 μM, T= 25°C, cell path length =1 cm.

Moreover, the similar appearance of the fluorescence spectra of **1** in the absence and presence (l' and m' respectively in Figure 4.2) of NO photodonor **2** accounts the idea of using rhodamine as a tracker for the entire assembly.

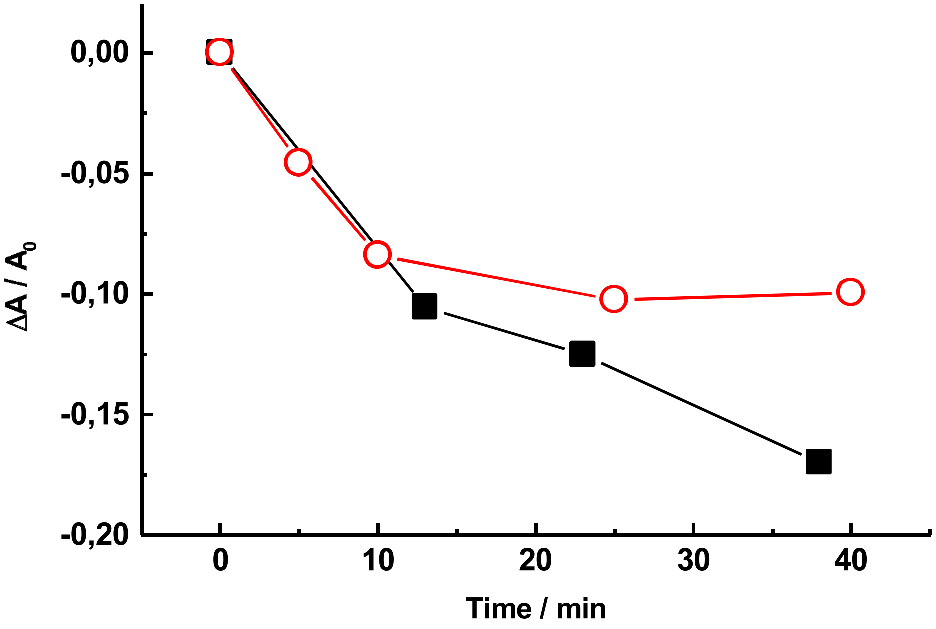

Figure 4.3. Comparison of extend of photobleaching between **2** included in rhodamine attached single CD (O) and (■) rhodamine attached CD oligomer.

Figure 4.3 explains that the extend of potobleaching of NO photodonor **2** in **1**, is much more pronounced than that in case of rhodamine attached single CD units. It can be seen from the figure that the extend of photolysis of **2** in rhodamine attached single CD unit become stagnant after 10 minutes of photolysis while the same photolytic profile prolong even after 40 minutes in case of rhodamine attached CD oligomer with higher value of slope than in rhodamine attached single CD unit (Figure 4.3). The results validate the inclusion of higher concentration of **1** in apolar CD cavities with enhanced binding features, eventhough the binding calculation become complex in this case.

The supramolecular ensemble **2/1** was mapped in the epidermal cancer cell lines (Figure 4.4). The respective image shows the marginal internalization of the ensemble into the cell cytoplasm. Though the accumulation of assembly at the cell membrane could be accounted by the net opposite negative charge of the ensemble, which compete with the internalization. Nevertheless, the NO release at the membrane is also promising for the antitumor actions.[18]

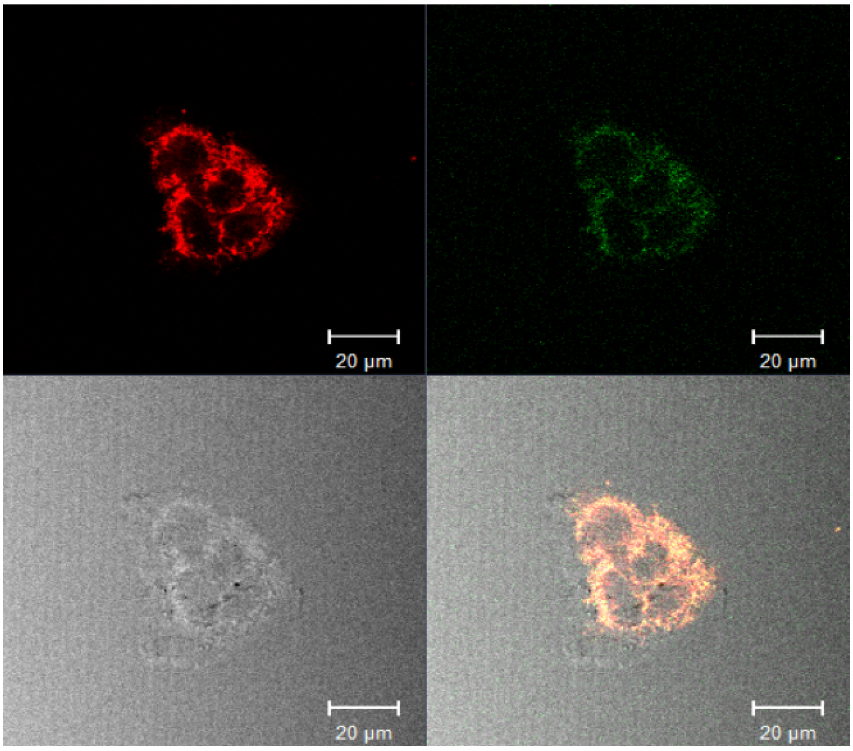

Figure 4.4. The two-photon fluorescence microscopy image of epidermal cancer cell lines (Model No. A431) incubated with the complex **2/1** (*ca.* 10 µM) in 10 mM phosphate buffer (pH 7.4). The assembly mapped at the excitation of 840 nm and the detection A) Red channel; band pass filter at 620-710 nm, B) Green channel at the band passfilters of 435-555 nm, C) transmission image D) Overlay of all images.

Cell mortality experiments performed on epidermal cancer cell-line gives the clear information on the tumor cell mortality. In this regard, the supramolecular ensemble has been incubated for 5 hours with the NO photodonor in cultural cells prior to photoirradiation. The mortality results plotted in the form of histograms shows the significant light mortality induced by the NO photodonor (Figure 4.5), whereas the rhodamine attached oligomer does not have any influence on the tumor mortality (II in Figure 4.5).

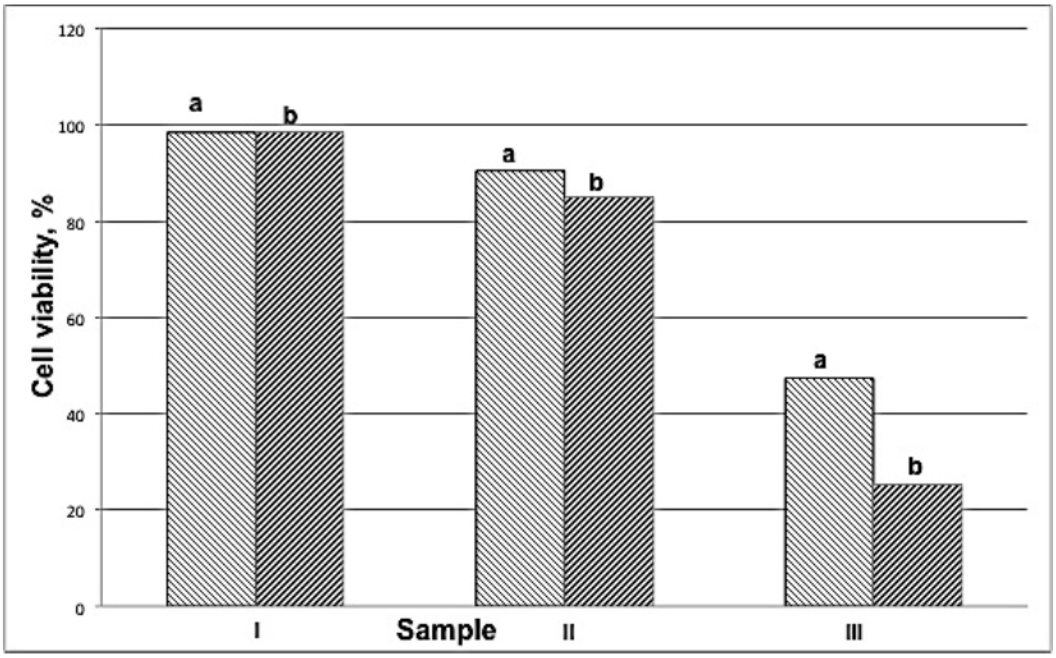

Figure 4.5. Dark and photoinduced mortality of A431 epidermal cancer cell lines. I) The control of CD oligomer devoid of rhodamine, II) rhodamine attached CD oligomer (5 mM interms of CD unit) III) supramolecular dispersion of **1** with the photoactive component **2**. All the experiments are performed and compared in the absence (a) and presence (b) of light. [**1**]= 20 μM, [**2**]= 15 μM, T= 25°C.

In addition, the control experiment where the oligomer devoid of rhodamine unit is also incubated and photoirradiated in the cells and the results does not show much difference from the above results of rhodamine attached CD oligomer. The supramolecular dispersion of the NO photodonor contribute significantly to the tumor cell mortality, *ca.* 75 %, owing to the diverse biological function of photoreleased NO. Though the dark cytotoxicity resulted by the ensemble have to be taken in to serious consideration. This could be conceived by the fact the concentration of the carrier used for the experiments were remarkably high and sort of optimization on the incubation time[19] and concentration of the carrier[20] could lead to more appealing results. At this point the experiment have to be repeated and studied in great details to understand noxious dark cytotoxicity.

4.5 Conclusion

Multifunctional photoactive CD-based supramolecular assemblies have been formulated through the logical designing and novel synthetic routes. Here the fluorophore rhodamine was covalently bound to CD networks and apolar concavities of CD units are prone to encapsulate NO photodonor to achieve a bichromophoric assembly. The novel design allows the modulation of several parameters key to the fate of therapeutic actions. Both the fluorophore and NO photodonor behave independently on its action as their photochemical features are preserved in the single nanostructure.

The entire system is capable to internalize in the cells, deliver the NO and image the close vicinity of the cells where all the photochemical action is said to occur and finally able to induce satisfactory rate of cell mortality. On the light of these results we would like to point out the following key features associated with this ensemble; i) the carrier conveys greater concentration of the NO to the target with increased efficacy as compared to single CD analogues, ii) tailoring the CD units with hydrophilic cross-links enable polymeric character with long circulation time iii) possibility of desired modulation of the physico-chemical properties of both chromogenic centers by exactly tuning with matching light trigger. Finally, the convergence of the undisputed cytotoxicity bestowed by the NO actions and the possibility of non-invasive, inexpensive and real time imaging at the same site where the NO actions occurs in single nanoensemble imparts the unparalleled opportunity to address the current issues related to the conventional anticancer treatments.

4.6 References

1. X. He, J. Chen, K. Wang, D. Qin, W. Tan, *Talanta*, 2007, **72**, 1519–1526.
2. Z. Liu, M. Liu, W. Song, K. Pan, J. Li, Y. Bai, T. Li, *Mater. Lett.*, 2006, **60**, 1629–1633.
3. H. Shi, X. He, K. Wang, Y. Yuan, K. Deng, J. Chen, W. Tan, *Nanomed-Nanotechnol.,* 2007, **3**, 266–272.
4. M. Malanga, L. Jicsinszky, E. Fenvesy, *J. Drug Del. Sci. Tech.*, 2012, **22**, 3, 260-265.
5. H. F. M. Nelissen, F. Venema, R. M. Uittenbogaard, M. C. Feiters, R. J. M. Nolte, *J. Chem. Soc., Perkin Trans.*, 1997, **2**, 2045.
6. L. Jullien, J. Canceill, B. Valeur, E. Bardez, J. -P. Lefevre, J. -M. Lehn, V. Marchi-Artzner, R. Pansu, *J. Am. Chem. Soc.*, 1996, **118**, 5432, 5442.
7. P. Choppinet, L. Jullien, B. Valeur, *Chem. Eur. J.*, 1999, **5**, 12.
8. N. Kandoth, M. Malanga, A. Fraix, L. Jicsinszky, É. Fenyvesi, T. Parisi, I. Colao, M. T. Sciortino, S. Sortino, *Chem. –Asian J.*, 2012, **7**, 11.
9. J. Kralova, Z. Kejik, T. Briza, P. Pouckova, A. Kral, P. Martasek, V. Kral, *J. Med. Chem.*, 2010, **53**, 128–138.
10. Z. Fülop, S. V. Kurkov, T. T. Nielsen, K. L. Larsen, T. Loftsson, *J. Drug Del. Sci. Tech.*, 2012, **22**, 3, 215.
11. Y. Chen, Y. Liu, *Chem. Soc. Rev.*, 2010, **39**, 495–505.
12. A. Mazzaglia, M. T. Sciortino, N. Kandoth, S. Sortino, *J. Drug Del. Sci. Tech.*, 2012, **22**, 3, 235-242.
13. F. Bestvater, E. Spiess, G. Stobrawa, M. Hacker, T. Feurer, T. Porwol, U. B-Pfannschmidt, C. Wotzlaw, H. Acker, *J. Microsc.*, 2002, **208**, 2, 108–115.
14. S. Conoci, S. Petralia, S. Sortino, U.S. Pat. Appl. Publ., 2009, 20 pp., Appl. No. PCT/IT2006/000575.
15. S. Sortino, *Chem. Soc. Rev.*, 2010, **39**, 2903.
16. K. A. Connors, *Chem. Rev.*, 1997, **97**, 1325.
17. R. N. Dsouza, U. Pischel, W. M. Nau, *Chem. Rev.*, 2011, **111**, 7941.

18. A. W. Carpenter, M. H. Schoenfisch, *Chem. Soc. Rev.*, 2012, **41**, 3742.
19. D. J. Smith, D. Chakravarthy, S. Pulfer, M. L. Simmons, J. A. Hrabie, M. L. Citro, J. E. Saavedra, K. M. Davies, T. C. Hutsell, D. L. Mooradian, S. R. Hanson, L. K. Keefer, *J. Med. Chem.*, 1996, **39**, 1148-1156.
20. R. Challa, A. Ahuja, J. Ali, R. K. Khar, *AAPS PharmSciTech.*, 2005, **6**, 2, 43, E329-E357.

5 Amphiphilic CD-based nanoassemblies for bimodal photodynamicactions

5.1 Introduction

Modification of CDs into several *ad hoc* nanostructures at which they can self-assemble and modify based on the requirement of phototherapeutic agents draws the utmost attentions towards novel drug delivery strategies.[1,2,3] The ability to modify the natural CDs into heterotopic colloids of different charge enables versatile functionality to entrap probes of different nature. The domains of independent microenvironment resulted from charge localization are excellent to induce the partition of the phototherapeutic agents into their different region. This partitioning of the probe is found to be dependent on the surface charge of the ensemble, polarity, pH of the media[4] etc. In this direction CDs are modified to form amphiphilic micelle structures by grafting hydrophilic and hydrophobic tail on each side of the CD unit. Exact charge and structural balance between the additional tails determines the colloidal stability of the micelles in aqueous environment and consequent entrapment of the probe. Here, primary side of the CD is modified with thioalkyl chains while the secondary side with ammonium terminated ethylene glycol oligomers[5] (Figure 5.1). Grafting polyethylene glycol (PEG) is desirable for the increased biocompatibility and bioavailability of the system. In fact, synthetic versatility related to this CD unit allows bimodal entrapment of both $^1O_2$ photogenerator and NO releasing photoactive molecule addressed to multimodal anticancer therapy.

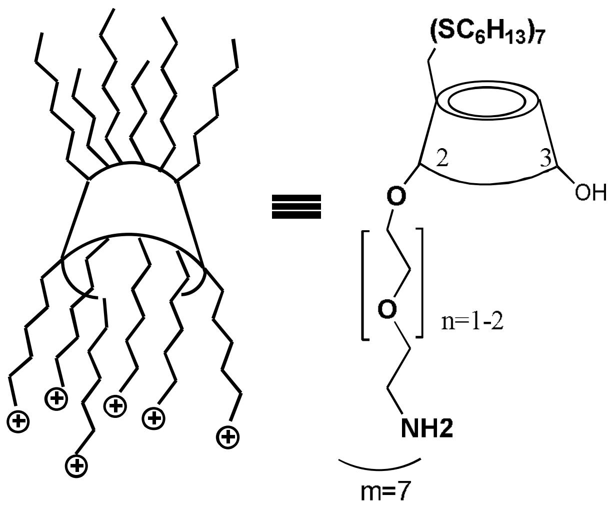

Figure 5.1. Schemtaic representation of modified CD unit forming micelles.

Specifically the photoactive anionic molecule can simply integrate with positively charged CD surface through strong electrovalent interaction, whereas the apolar CD pockets is utilized for encapsulating molecules of desired interest. Among the multitude of the photosensitizers able to generate $^1O_2$ from the molecular oxygen, porphyrins or porphyrinoid structures serves an important role.[6,7] The photodynamic actions of the porphyrin is largely explored because of their relatively high isc rate and long triplet state lifetime, of the order of milliseconds in fluid media, as compared to other PDT agents. Though the porphyrin is prone to self-aggregation at aqueous phase making their direct application at *in situ* tumor site practically impossible. The aggregated porphyrin are photochemically mute as all monomers form highly ordered molecular structure, where all the transition dipole get strongly aligned parallel (*J*-aggregate) or vertical (*H*-aggregate) precluding the excitation of the molecule accompanied by the change in transition dipole moments.[8,9,10] The hallmark of the aggregated structure is very short triplet state lifetime, creating difficulties to diffuse out to molecular oxygen for type II or to induce type I reactions. Considerable efforts have been employed to reduce the aggregation profile of native porphyrin macrocyclic ring for the efficient photodynamic actions. The substitution of sulfate group on the macrocyclic skeleton is found to be a viable strategy to reduce the aggregation pathway.[4] The anionic porphyrin sulfonate can simply interact with cationic CD micelles with the hydrodynamic radius ranging from ≈ 140 to ≈ 1000 nm, depending on the porphyrin loading[11]. The long-lived triplet state of modified porphyrin units allows higher quantum yield of singlet oxygen production. In addition, both soret band and Q band of the porphyrin can be excited with visible light. Here anionic 5,10,15,20-tetrakis(4-sulphonatophenyl)-21H,23H-porphyrin (porphyrin **2**), functioning as $^1O_2$ photosensitizer, interact with cationic surface of CD derivatives (Scheme 5.1).

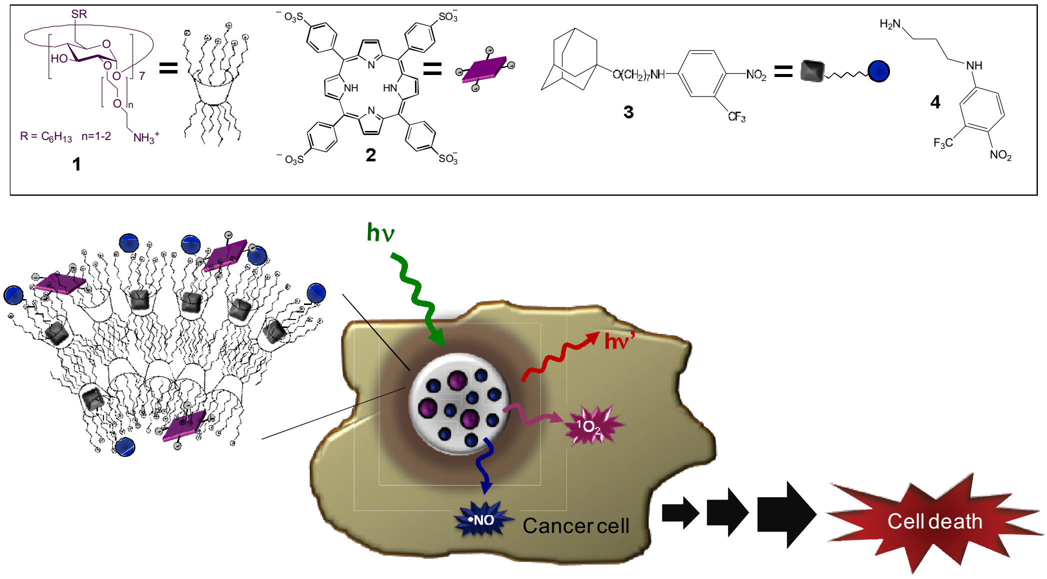

Scheme 5.1. Pictorial view of the photoactive CD-based bichromophoric nanoassembly and their respective therapeutic actions.

In line to the ongoing interest of assembling the NO photodonor with various supramolecular architects, the same tailored nitroaniline derivative that is used for previous experiments have been utilized to encapsulate inside the hydrophobic pockets of CD NPs in view of NO stimulated cancer cytotoxicity. On the wake of this interest, the present attempt is to design and formulate a supramolecular nanoassembly in which two probe *viz.*, Porphyrin **2** and NO photodonor **3** get entrapped at the cationic surface and in native cavities of CD respectively (Scheme 5.2). This multifunctional nanoassembly is able to photorelease two anticancer species, both $^1O_2$ and NO, simultaneously along with the imaging capabilities in cancer cells.

5.2 Experimental

5.2.1 Materials

A) The amphiphilic CD derivatives

The amphiphilic cyclodextrin (CD **1**) is obtained from Dr. Antonino Mazzaglia's group, University of Messina, Italy, and used as such with out further purification.

B) Porphyrin

The macrocyclic porphyrin derivative was directly purchased from Sigma Aldrich and used as such. All other reagents were of highest commercial grade available and used without further purification. All solvent used (from Carlo Erba) were analytical grade.

5.2.2 Synthesis of tailored NO photodonor

The protocol followed to synthesize the NO photodonor is exactly same as the synthetic procedure reported before (Chapter 3).

5.3 Instrumentation

UV/Vis absorption and fluorescence spectra were recorded with a JascoV-560 spectrophotometer and Fluorolog-2 (Model, F-111) spectrofluorimeter respectively. Nanoparticle sizes were measured by a dynamic light scattering Horiba LS 550 apparatus equipped with a diode laser with a wavelength of 650 nm. Fluorescence images were taken with a Biomed fluorescence microscope (Leitz, Wetzlar), Germany.

5.3.1 Laser flash photolysis

All of the samples were excited with the second harmonic of Nd–YAG Continuum Surelite II–10 laser (532 nm, 6 ns FWHM), using quartz cells with a path length of 1.0 cm. The excited solutions were analyzed with a Luzchem Research mLFP–111 apparatus with an orthogonal pump/probe configuration. The probe source was a ceramic xenon lamp coupled to quartz fiber-optic cables. The laser pulse and the mLFP–111 system were synchronized by a Tektronix TDS 3032 digitizer, operating in pre-trigger mode. The signals from a compact Hamamatsu photomultiplier were initially captured by the digitizer and then transferred to a personal computer, controlled by Luzchem Research software operating in the National Instruments LabView 5.1 environment. The solutions were deoxygenated by bubbling with a vigorous and constant flux of pure argon (previously saturated with solvent). In all of these experiments, the solutions were renewed after each laser shot (in a flow cell of 1 cm optical path), to prevent probable auto-oxidation processes. The sample temperature was 295 ± 2 K. The energy of the laser pulse was measured at each shot with a SPHD25 Scientech pyroelectric meter.

5.3.2 Singlet oxygen detection

Photogeneration of $^1O_2$ upon laser excitation of the photosensitizer was monitored by luminescence measurements in oxygen-saturated solutions. The near-IR luminescence of singlet oxygen at 1.27 μm resulting from the forbidden transition $^3\Sigma_g^- \leftarrow {}^1\Delta_g$; this was probed orthogonally to the exciting beam with a pre-amplified (low impedance) Ge-photodiode (Hamamatsu EI-P, 300 ns resolution) maintained at –196°C and coupled to a long-pass silicon filter (>1.1 μm) and an interference filter (1.27 μm). Pure signal of $^1O_2$ were obtained as difference between signals in air- and Ar-saturated solutions. The temporal profile of the luminescence was fitted to a single-exponential decay function with the exclusion of the initial portion of the plot, which was affected by scattered excitation light, fluorescence, and the formation profile of singlet oxygen itself.

5.3.3 NO detection

NO release was measured based on the protocol reported in previous chapter (Chapter 3).

5.4 Samples preparation

CD **1** NPs were prepared from stock solutions (180 μM) in $CHCl_3$, which were slowly evaporated to form a thin film. The films were hydrated, sonicated for 20 min at 50°C and equilibrated overnight. An aqueous solution of the porphyrin **2** was then added and each the sample was adjusted to a final volume of 2 mL with Phosphate buffer. Compound **3** was dissolved in acetonitrile and slowly evaporated to form a thin film. This film was then hydrated with the colloidal solutions of CD **1** either with or without the porphyrin **2**. All the final solutions were equilibrated overnight at 4°C, sonicated for 15 min and equilibrated at room temperature for 20 min. All the final stock solutions were prepared in phosphate buffer (10 mM).

5.4.1 Experiments with cells

The photobiological studies were done in collaboration with Dr. Maria Teresa Sciortino's group, University of Messina, Italy. HeLa cells were obtained from American Type Culture Collection and propagated at 1:6 ratio using Dulbecco's modification of Eagle's Minimal Essential Medium supplemented with 10 % FBS (Fetal Bovine Serum). The samples of cells treated with the different samples of CD **1** NPs, were placed separately in a cuvette and irradiated by a halogen lamp (Osram) for 30 min. The irradiating beam was filtered through an UV filter (Hoya glass type UV-34, cut-off: 340 nm) in order to cut the UV component and through a 1 cm cell filled with water, to remove the IR-component. Before and after irradiation, 8x10^4 cells were placed in 96-well plates with 100 ml of RPMI-1640 medium and incubated in presence of tetrazolium compound [3-(4,5-dimethylthiazol-2-yl)-5-(3-carboxymethoxyphenyl)-2-(4-sulfophenyl)-2H tetrazolium, inner salt; MTS, Promega] and an electron coupling reagent (phenazinemethosulfate) PMS dye (MTS 20 ml/well). After further incubation of 1 h, the absorbance was read at 490 nm in a microplate reader (Labsystems Multiskan Bichromatic). The cell viability (%) was calculated according to the following equation:

Cell viability =(OD (before Lamp)-(OD (after Lamp)/-OD (before Lamp)) x100

Where, OD (sample before Lamp) represents measurement from the wells treated with samples before the exposure to the halogen lamp and OD (sample after Lamp) represents measurement from the wells treated with samples after the exposure to the halogen lamp.

5.5 Results and Discussion

The porphyrin **2** is soluble in phosphate buffer and show the absorption spectra with the characteristic soret band and Q band at 414 nm and 532 nm respectively. As porphyrin form *J*- and *H*-type aggregate structures in aqueous media and photochemically mute in action (*vide supra*), one of the worthwhile objectives of designing the present nanoassembly is to disaggregate porphyrin **2** into its monomeric form. It was previously studied that when the porphyrin **2** is mixed with CD **1** in 1:50 ratio, the spontaneous formation of nanoparticles is resulted[6] owing to the entanglement on the surface of CD **1** through the electrovalent interaction between the anionic nature of the former and cationic CD **1** surface, which results red shift of its soret band (a and b in Figure 5.2)

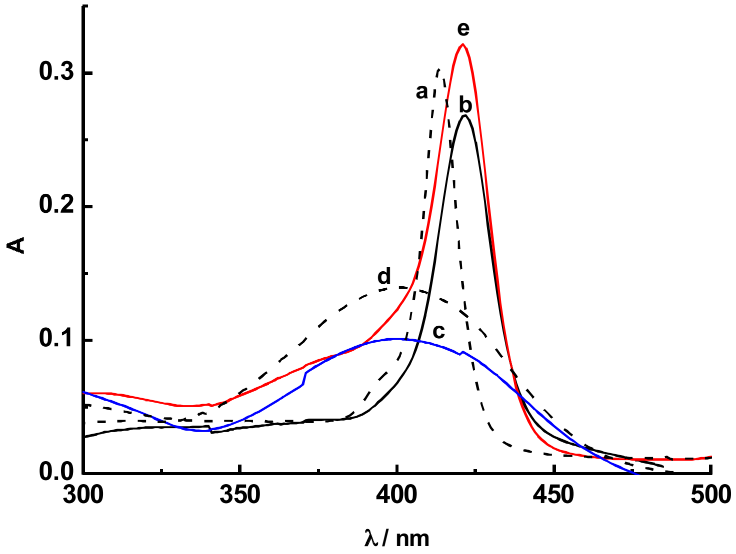

Figure 5.2. Absorption spectra (in phosphate buffer, 10 mM, pH 7.4) of **2** in the absence (a) and in the presence (b) of CD **1**, **3** in the presence of CD **1** (c), the model compound **4** (d), **2** + **3** in the presence of CD **1** (e). [**1**]= 40 μM, [**2**]= 0.8 μM, [**3**]= 10 μM, T= 25°C, cell path length= 1 cm.

According to the various literatures, this refers to the monomerization of porphyrin **2** and is responsible for the photosensitization and consequent $^1O_2$ generation.[6,12] The entanglement of porphyrin **2** only at the surface CD **1** leaves native cavities to be included with an additional guest molecule, leading to the formation of bichromophoric nanoassembly. In this scenario, the NO photodonor, a nitroaniline moeity is tailored with an adamantane moiety by an alkyl spacer with three-step synthetic method, is devised to encapsulate in CD cavities (see experimental part, Chapter 3). Certain key features make adamantane a suitable guest encapsulator such as- it is transparent in UV-Visible absorption spectral region and binding constant is very high to be included inside the CD pocket.[13] In addition, the co-operative and hydrophobic inter-chain interaction of alkyl spacer with the alkyl tails of CD units encourage the binding of the entire unit of **3** with CD **1** which enables nitroaniline moiety to get exposed on aqueous phase preserving the out of plane geometry of nitro group. In addition, the binding of **3** in the constrained environment of CD cavities encourage the partial non planarization of the nitro group and respective NO photorelease,[14] since the NO photorelease from nitroaniline moiety is solely based on the non planarization of the nitro group as mentioned before. The compound **3** is insoluble in aqueous phase, but clearly soluble once introduced into the CD assemblies. The steady state absorption spectra clearly validate this, as seen in the above spectra (c in Figure 5.2). The resemblance of the characteristic absorption peak of compound **3** with that of the aqueous soluble model compound **4** in the absence of CD nanoassemblies clearly demonstrate that the photochemical properties of NO photodonor is remain unhampered in the microenvironment of CD assemblies (c and d in Figure 5.2). Since the spectral change of the absorption band is prone to the polarity of the microenvironment of CD networks and changes in the geometry of nitro group,[15] the absence any significant spectral change well accounts that the nitro group is well exposed on water pool.

On the grounds to have a bichromophoric nanoassemblies, both the chromophore- porphyrin **2** and **3** were introduced simultaneously each other. The characteristic absorption band of bichromophoric assembly (e in Figure 5.2) clearly demonstrates that the absorption features of both chromophores are preserved once they self-assemble each other. The existence of two chromophores in close proximity is not common as they interact each other and results the concomitant loss of desired photoactions. It is noteworthy to point out that maximum peak position of chromophores, porphyrin **2** and **3**, were remaining unaltered when they are independent or entrapped together. The matching spectral characteristics observed by summing up of two individual spectra of both porphyrin **2** and **3** (b and c in Figure 5.2) with that of bichromophoric assembly (e in Figure 5.2) validates the absence of relevant interchromophoric interaction between two chromophores in the ground state.

The pharmacodynamic and pharmacokinetic profile of nanostructures heavily depends on the size of structures. The size of delivery system should be in sub-nano level for the effective bioavailability of the system and long circulation time through the reticuloendothelial system.[16] In the present case, the size of the nanoassembly is mainly attributed by the charge neutralization between the opposite charges of porphyrin **2** and CD networks and marginal variation in the order of mixing of the component porphyrin **2** with CD **1** is found to have remarkable influence on their total size.[6] Dynamic light Scattering measurement (DLS) of the bichromophoric nanoassembly shows the mean diameter of 300 nm (Figure 5.3), similar to the result obtained when the compound porphyrin **2** is mixed with the CD **1**.[6] The conjoint results confirm that the size of the bichromophoric nanoassembly is mainly attributed by the recombination of opposite charges of porphyrin **2** and CD **1** and the compound **3** does not have any influence on determining the size of the nanostructures (bichromophoric nanoassembly, Scheme 5.1).

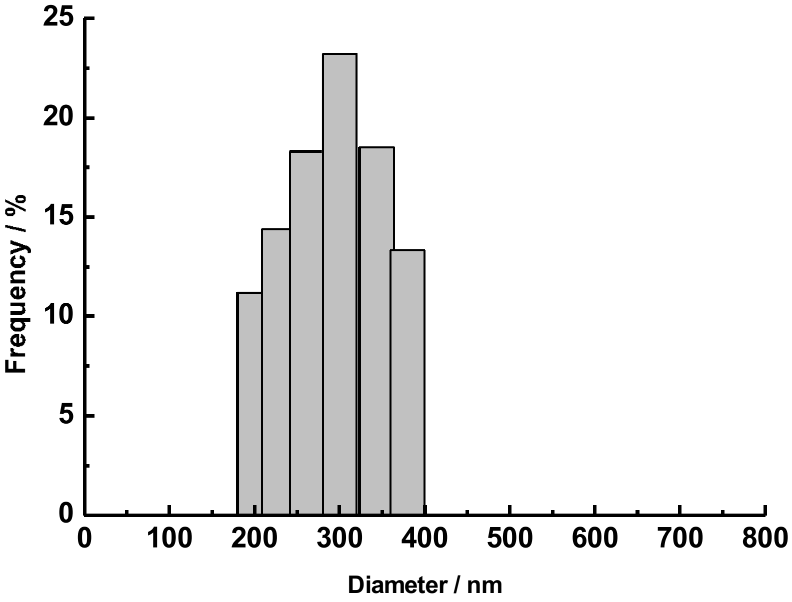

Figure 5.3. The size distribution of the bichromophoric nanoassembly obtained by dynamic light scattering measurements.

The objectives of selecting the porphyrin units were two fold- utilization of fluorescence to map the nanoassembly and $^1O_2$ generation from the compound **2**. The steady state fluorescent spectra of compound **2** show a dual band fluorescence emission with the emission maxima at 640 nm (a in Figure 5.4). When porphyrin **2** get entangled in the CD networks, the emission maxima undergoes red shift to 648 nm with the negligible changes on its fluorescence quantum yield (b in Figure 5.4).

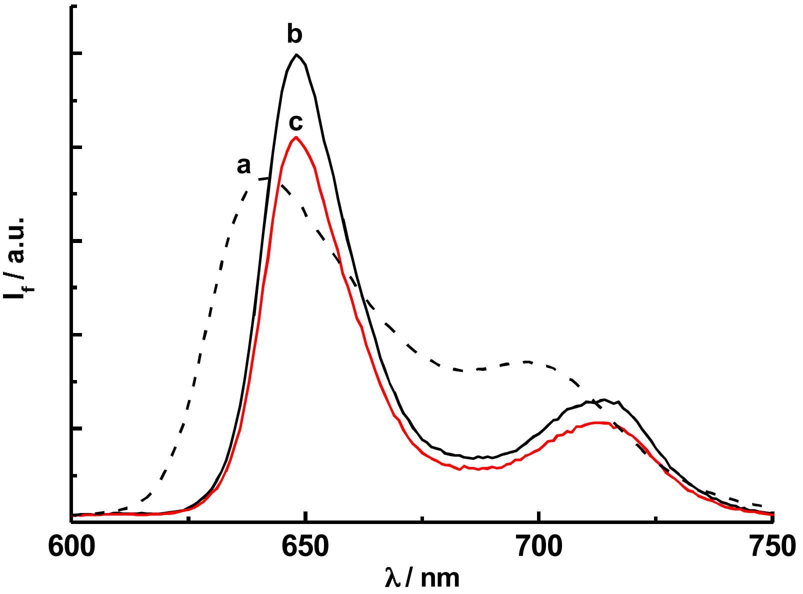

Figure 5.4. Fluorescence emission spectra (λ_{exc}= 440 nm) of **2** in the absence (**a**) and in the presence (**b**) of CD **1**, **2** + **3** in the presence of CD **1** (**c**). [**1**] = 40 μM, [**2**] = 0.8 μM, [**3**] = 10 μM, T = 25°C, cell path = 1 cm.

This confirms, as mentioned before, the disaggregation of compound porphyrin **2** with increased monomer population, which is responsible for the fluorescence enhancement and respective photodynamic action. The position of emission peaks were remain intact even after the excitation at different wavelength, which accounts that the fluorescence contribution is mainly from single population of the fluorophore in the assembly. Finally the fluorescence emission feature of porphyrin **2** is preserved in the bichromophoric nanoassemblies (c in Figure 5.4) with little changes in fluorescence intensity. In fact, it is clear from the steady state absorption spectra (Figure 5.2) that both chromophore absorb at the excitation wavelength of fluorophore and the intensity change is attributed by the different percentage of photon absorption of compound porphyrin **2** in the presence of compound **3** while entangled in nanoassembly.

The bichromophoric nanoassembly is utilized for mapping inside the cancer cells, since they can be traced in the cell environment by the fluorescence emission of porphyrin **2**.

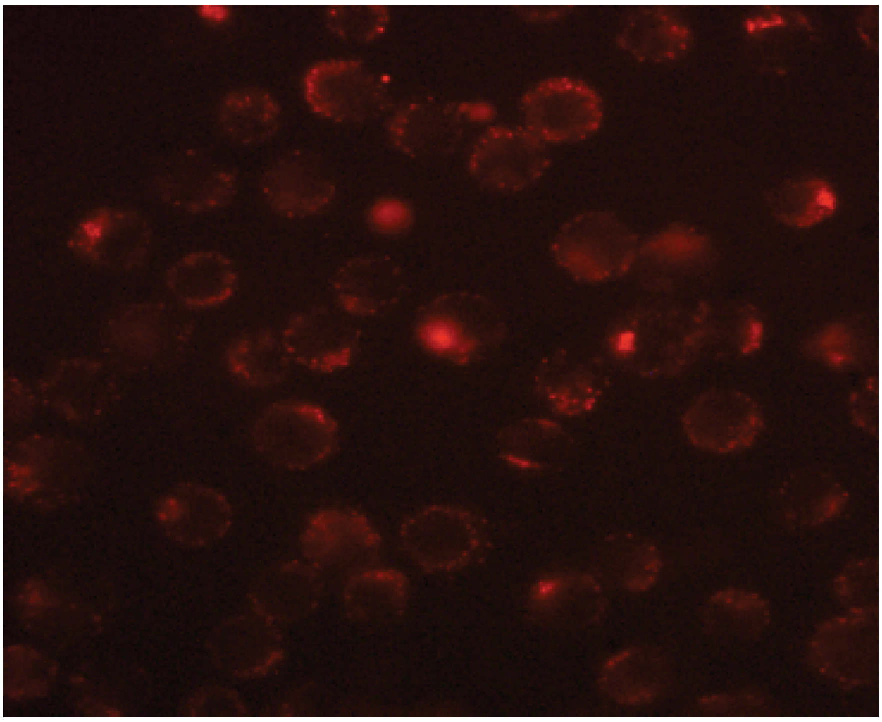

Figure 5.5. Microscopy images of HeLa cancer cells incubated with the bichromophoric nanoassembly for 1 h at 37°C.

The mapped image (Figure 5.5) demonstrates that the supramolecualr assembly is internalized well inside the cell and localization mainly occurs at the cytoplasmic level. Here the cationic surface of CD **1** imparts a great influence on the penetration of nanoassembly through the negatively charged membrane surface.

The significant action of photosensitization of porphyrin **2** in the bichromophoric nanoassembly is directly related to its excited triplet state and photoinduced energy transfer to nearby oxygen.[17] The excited triplet state of the porphyrin **2** entangled with CD **1** in the absence and in the presence of compound **3** has been studied with the laser flash photolysis.

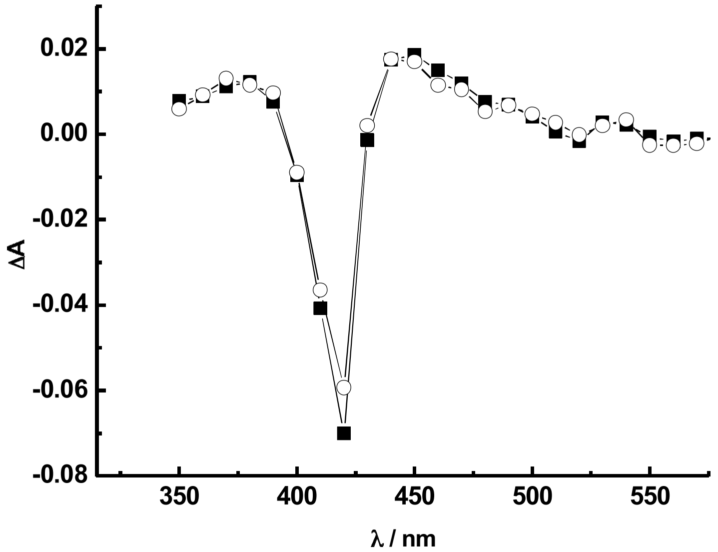

Figure 5.6. Transient absorption spectra observed upon 532 nm laser excitation of Ar-saturated solution of CD **1** loaded with **2** (■) and **2**+**3** (○), recorded 1 μs, after the laser pulse. Each point was obtained by signal average of 10 traces. E_{532} ~ 12 mJ/pulse, phosphate buffer (10 mM, pH 7.4), [**1**]= 40 μM, [**2**]= 0.8 μM, [**3**]= 10 μM, T= 25°C.

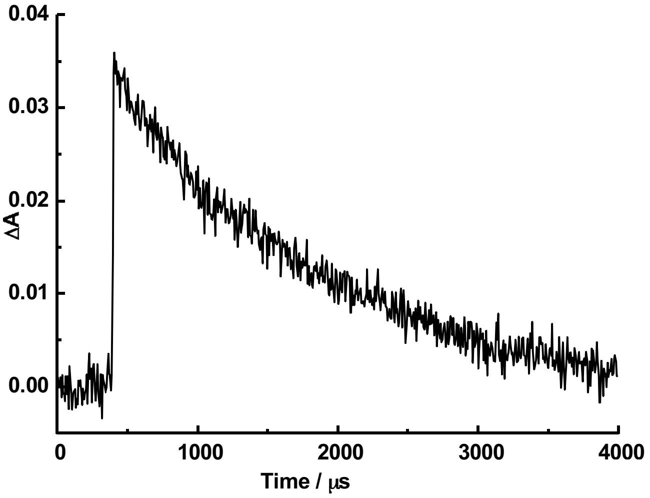

Figure 5.7. Kinetic decay trace of excited triplet state of **2** monitored at 450 nm. E_{532}~ 12 mJ /pulse. Phosphate buffer (10 mM, pH 7.4), [**1**] = 40 μM, [**2**] = 0.8 μM, [**3**] = 10 μM, T= 25°C.

The transient absorption spectra of compound porphyrin **2** shows the significant population at the excited triplet state (Figure 5.6). Since the two samples were optically matched at the excitation wavelength, the intensity of the transient absorption is the direct consequence of the triplet quantum yield. Here the similar transient spectra of porphyrin **2** (Figure 5.6) in both bichromophoric assembly and in presence of CD **1** alone well accounts the fact that the compound **3** does not influence its excited triplet lifetime. Moreover the mono exponential decay of the triplet with a lifetime of *ca.* 1500 μs (Figure 5.7), the same to that observed in the absence of **3**, indicates that no quenching by the NO photodonor occurs. Note that, the observed lifetime is much longer than that of free porphyrin in water medium in the absence of NPs (*ca.* 200 μs), excluding any exit dynamics of the porphyrin **2** triplet from the nanoassembly.[11] Here the lifetime component of porphyrin **2** at excited triplet state is also long enough to be quenched by the triplet oxygen and which enable consequent photosensitization action.

The bichromophoric nanoassembly releases the active species such as NO and $^1O_2$ upon irradiation. Indeed, the most convenient method for testing the suitability of the nanoassembly to photogenerate NO and $^1O_2$ is the direct and in real-time monitoring of these transient species. To this end, we have used an ultrasensitive NO electrode, which directly sense the NO release in nanomolar concentration level (see experimental part) by an amperometric technique.

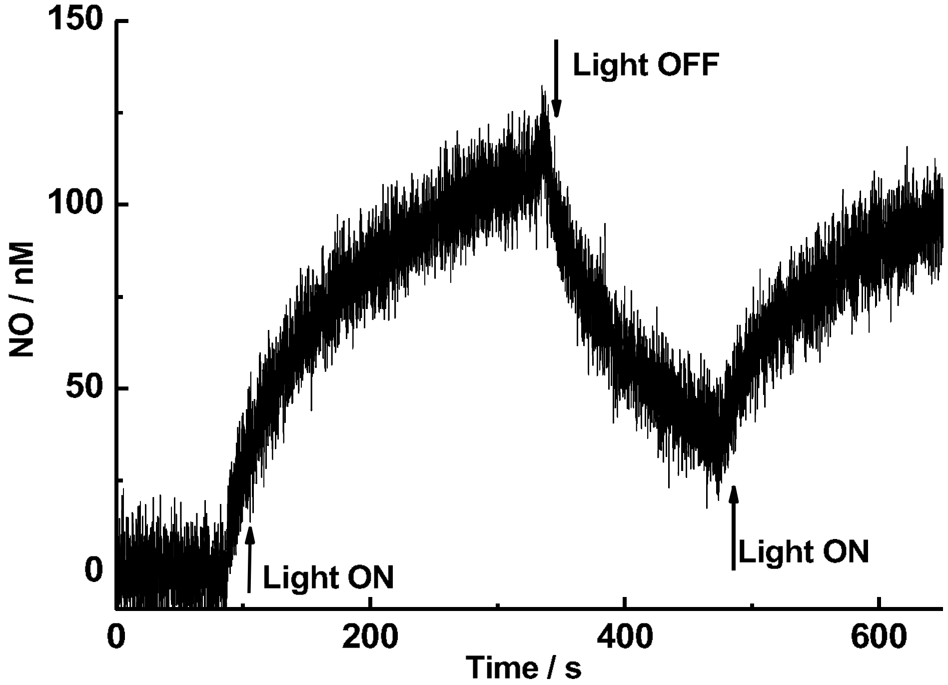

Figure 5.8. Amperogram showing the release of NO upon 400 nm light irradiation. Phosphate buffer (10 mM, pH 7.4), [1]= 40 μM, [2]= 0.8 μM, [3]= 10 μM, T= 25°C.

The linear generation of amperogram that promptly stops when the light is turned off and regenerate again when the light turned on clearly demonstrate light controlled release of NO (Figure 5.8).

It is worthy to point out that the release of NO is highly selective towards the wavelength of excitation light and rate of NO release in the nanoassembly is comparable to that obtained for the NO photodonor within the nanoassembly in the absence of porphyrins, indicating that the porphyrin units do not quench the excited NO photodonor. The typical phosphorescence of $^1O_2$ is analyzed to detect $^1O_2$ generation from the nanoassembly with the help of a time-resolved luminescence technique at 1270 nm[18] (Figure 5.9).

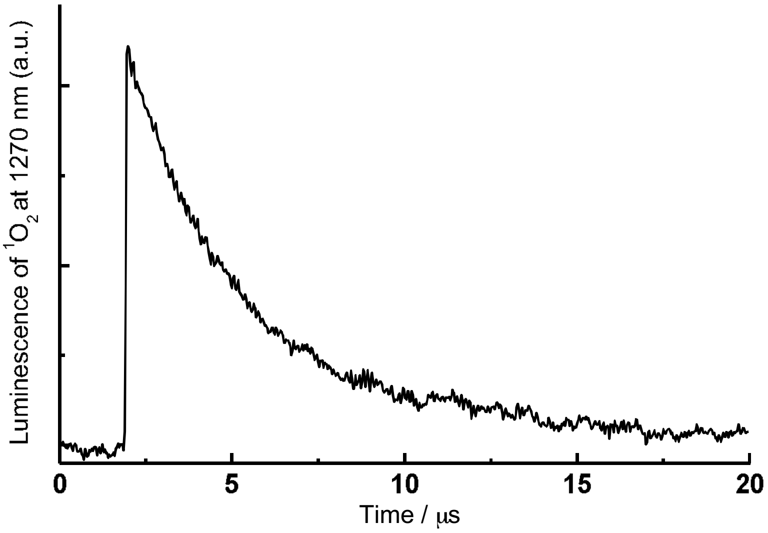

Figure 5.9. Kinetic trace of $^1O_2$ generated upon 532 nm laser excitation of the bichromophoric CD-based nanoassembly. Phosphate buffer (10 mM, pH 7.4), [**1**]= 40 μM, [**2**]= 0.8 μM, [**3**]= 10 μM, T= 25°C.

The infrared luminescence decay kinetics demonstrate that the excited triplet state is populated enough and the $^1O_2$ decay with first order kinetics in *ca.* 4 μs (Figure 5.9). Here the features of $^1O_2$ luminescence decay is solely depends on the excited triplet state of porphyrin **2** and NO photodonor does not have any influence on **2**.

The nanoassemblies are used for photobiological cell mortality studies to understand their bimodal therapeutic impacts at biological interface. The different formulations of CD **1** assembly entangled with porphyrin **2**, compound **3**, or with both chromophores have been applied into HeLa tumor cells and incubated 1 hour under different experimental conditions and either kept in the dark or irradiated with visible light for 30 min.

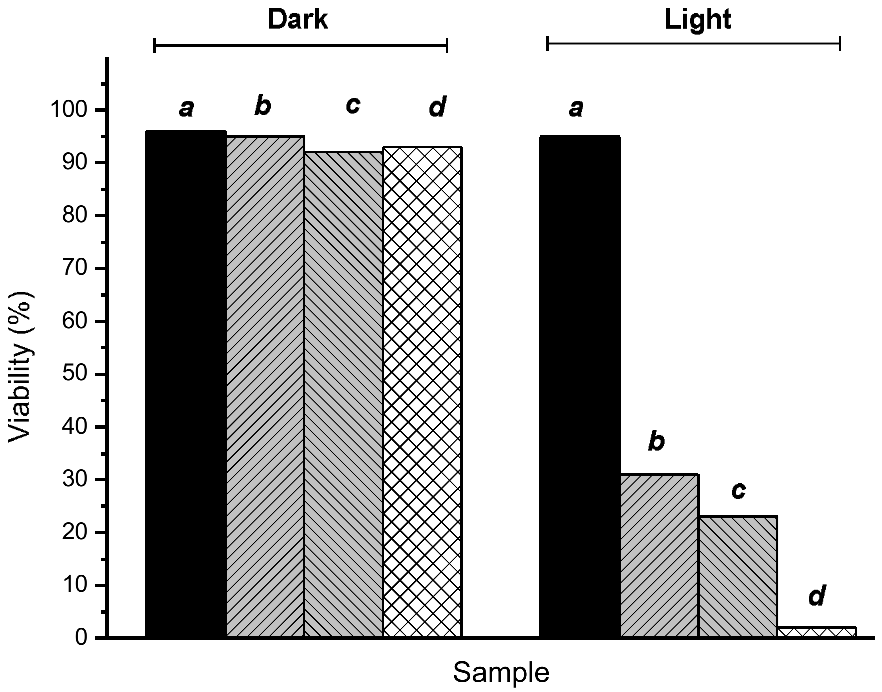

Figure 5.10. The Cell viability of HeLa cells incubated with CD **1** NPs= 40 μM (**a**) without the photoactive components and loaded with (**b**) **2** (0.8 μM), (**c**) **3** = 10 μM, (**d**) **2** + **3**.

The results show that the cells applied with different kinds of formulations are stable in dark and therapeutic action arise only after the concomitant irradiation of light and which accounts the good biocompatibility of the assemblies in dark (Figure 5.10). In addition, no effects observed in the cells incubated with only CD **1** in the absence of photoactive units. The significant rate of cell mortality after the continuous irradiation of light validates the photodynamic actions of nanoassemblies. The almost complete photodynamic inactivation induced by the bichromophoric nanoassembly, *ca.* 98 %, compared to the value observed with the NPs loaded with the single components either porphyrin **2** or **3** provides clear-cut evidence for the involvement of a double action photo-inactivation mechanism in the cell death, in which NO and $^1O_2$ are envisaged to play a key role.

5.6 Conclusion

We have designed, synthesized and characterized a supramolcular bichromophoric nanoassembly in which two chromophores, NO photodonor and $^1O_2$ photosensitizer, get embedded at the two different compartments of assembly made from amphiphilic CD nanoconstructs. The assembly was characterized with the steady state and time-resolved spectroscopic techniques. The steady state absorption spectra and fluorescence emission profile demonstrates that the photochemical and photodynamical features of both chromophores are preserved when entangled in CD **1** and no interaction between each chromophore at the excited singlet states. While the interaction of porphyrin **2** with CD **1** facilitates the photosensitization towards the near by oxygen upon excitation with matching light inputs and the NO photodonor release NO on irradiation with corresponding light trigger. In addition, the relevant fluorescence emission from the photosensitizer make possible to map the fate of nanoassembly inside the cancer cells. The bimodal photoactions arise from the cumulative and amplified release of both NO and $^1O_2$ in a concordant way. Above all, the light has immense control over the generation of these active species. We would like to stress that, in contrast to non-photoresponsive compounds, this finding is not obvious. In most cases, the photoresponse of single or multiple photoactive units located in a confined space can be in fact considerably affected by the occurrence of competitive photoprocesses (i.e., photoinduced energy and/or electron transfer, hydrogen abstraction, nonradiative deactivation, etc.),[19,20] which preclude the final goal.

Finally we would like to point out that the convergence of the dual photodynamic action and the imaging capacities in one single nanostructure, together with its biocompatibility, make this supramolecular architecture an appealing candidate for applications in biomedical research. To our knowledge this is the first report in which cancer cellular death due to the combined action of two above-mentioned transient species which are generated in a photocontrolled way is shown.

5.7 References

1. P. Falvey, C. W. Lim, R. Darcy, T. Revermann, U. Karst, M. Giesbers, A. T. M. Marcelis, A. Lazar, A. W. Coleman, D. N. Reinhoudt, B. J. Ravoo, *Chem Eur. J.*, 2005, **11**, 1171.
2. O. Bourdon, V. Mosqueira, P. Legrand, J. Blais, *J. Photochem.Photobiol. B Biol.*, 2000, **55**, 164–171.
3. R. Donohue, A. Mazzaglia, B. J. Ravoo, R. Darcy, *Chem. Commun.*, 2002, 2864.
4. A. Mazzaglia, N. Micali, L. M. Scolaro, M. T. Sciortino, S. Sortino, V. Villari, *J. Porphyrins Phthalocyanines*, 2010, **14**, 661.
5. A. Mazzaglia, R. Donohue, B. J. Ravoo, R. Darcy, *Eur. J. Org. Chem.*, 2001, 1715-1721.
6. A. Mazzaglia, N. Angelini, R. Darcy, R. Donohue, D. Lombardo, N. Micali, M. T. Sciortino, V. Villari, L. M. Scolaro, *Chem. Eur. J.*, 2003, **9**, 5762.
7. A. Mazzaglia, N. Angelini, D. Lombardo, N. Micali, S. Patanè, V. Villari, L. M. Scolaro, *J. Phys. Chem. B.*, 2005, **109**, 7258.
8. N. C. Maiti, S. Mazumdar, N. Periasamy, *J. Phys. Chem.B.*, 1998, **102**, 1528–1538.
9. M. Kasha, *Radiat. Res.*, 1963, **20**, 55.
10. D. L. Akins, H. R. Zhu, C. Guo, *J. Phys. Chem.*, 1996, **100**, 5420-5425.
11. S. Sortino, A. Mazzaglia, L. M. Scolaro, F. M. Merlo, V. Valveri, M. T. Sciortino, *Biomaterials,* 2006, **27**, 4256.
12. A. Mazzaglia, N. Angelini, D. Lombardo, N. Micali, S. Patane, V. Villari, L. M. Scolaro, *J. Phys. Chem. B*, 2005, **109**, 7258.
13. M. Rekharsky, Y. Inoue, *Chem. Rev.,* 1998, **98**, 1875.
14. S. Sortino, S. Giuffrida, G. De Guidi, R. Chillemi, S. Petralia, G. Marconi, G. Condorelli, S. Sciuto, *Photochem. Photobiol.,* 2001, **73**, 6.
15. S. Sortino, G. Marconi, G. Condorelli, *Chem. Commun.*, 2001, 1226.
16. K. Cho, X. Wang, S. Nie, Z. G. Chen, D. M. Shin, *Clin. Cancer Res.*, 2008, **14**, 5.
17. D. K. Chatterjee, L. S. Fong, Y. Zhang, *Adv. Drug Delivery Rev.*, 2008, **60**, 1627.

---

18. F. Wilkinson, W. P. Helman, A. B. Ross, *J. Phys. Chem. Ref. Data*, 1993, **22**, 113.
19. S. Monti, S. Sortino, *Chem. Soc. Rev.,* 2002, **31**, 287.
20. V. Ramamurthy, *Photochemistry in Organized and Constrained Media*, Wiley, New York, 1991.

SECTION III

Nanoparticles based on CD polymers

"Science arises from the discovery of Identity amid Diversity"
-William Stanley Jevons

6

Phthalocyanine based bichromophoric NPs for bimodal imaging and therapy

6.1 Introduction

After the inception of being as a stable blue-green pigment for dyeing purposes, phthalocyanine (PC) is one of the most studied organic functional molecule as its applications diverse from optoelectronics to anticancer therapy.[1,2,3,4,5] Phthalocycanine structure is similar to the endogenous hematoporphyrin, instead of four pyrrole unit interconnected by the methane linker in pophyrin, the phathlocyanine is a ring of four isoindole group which is interconnected by the nitrogen atoms (compound **2** in Scheme 6.1). Some key functionals associated with the phthalocyanine, such as i) strong absorption cross section with high decadic molar extinction coefficient (of the order > 10^5 Lmol^{-1}cm^{-1}) in visible range from 600-750 nm of absorption spectra,[6,7] ii) strong Q band absorption at the red side of the visible region with the maximum possibility to excite the molecule in distinctive spectral window suited to PDT,[8,9] iii) greater quantum efficiency for imaging application and higher triplet state quantum yield for excited triplet state dynamics and photosensitization mechanism[10] etc. make them as one of most attractive PDT agents. Actually the PC is an effective second-generation photosensitizer owing to the features of its fast clearance from reticuloendothelial system and long wavelength absorption characteristics.[11] Though the PC is proven to be effective for photodynamic action, its insolubility in aqueous phase practically spoils all its novelties.[12,13] The strong aggregation and aqueous insolubility results from the strong planar π-π interaction of the macrocyclic ring. Indeed the factors, which can avert the stacking interaction potentially increase the aqueous solubility of the system.[14,15] The modification of planar ring structure with the axial ligand or substitution of non-peripheral hydrophilic bulky group is desirable to break the stacking behaviour as the bulky substituent distorts the in planar geometry of PC units.[16,17,18] From the perspective of PDT it drives two interesting feature, substitution of the bulky group remarkably increase the triplet state characteristics essential for the photodynamic actions through 'heavy atom effect' and insertion of the diamagnetic metals, for instance Zn, Al, Si etc. is found to increase the triplet state quantum yield and lifetime[16]. Above all, strategy of incorporating the substituted phthalocyanine with the suitable carrier is more advantageous for the greater extend of disaggregation and consequent photoactivity.[19]

Numerous efforts have been reported to achieve monomeric PCs by integrating with the suitable carriers. In fact, utilization of nanocarrier to convey the photosensitizer at the desired target is found to prevent the self-aggregation process of the photosensitizer in incorporated state.[20,21] The CDs have a significant role here to encompass the weakly soluble PCs. The fervent modification on natural CDs leads to polymeric NPs for incorporating photosensitizer at nanometer regime and able to convey the payload at tumor on-site.[22,23] The natural CD units can be interconnected each other with epichlorohydrin to form glyceryl cross-linked β-CD polymer with size varies in 10-100 nm regime.[24,25] The modification of CD enable enhanced stability constant and as a consequence, increased payload concentration. In addition, this method allows the partitioning of the lipophilic drug at its different microdomain. Based on the features explained above, our current effort is to formulate a nanosytem by incorporating two chromogenic centers, namely Zinc phthalocyaninetetrasulfonate and NO releasing photodonor at two different compartment of CD-based polymer. The incorporation of two probes and independent photorelease of multiple active species from the incorporated probe confer a system addressed to multimodal anticancer therapy (Scheme 6.1).

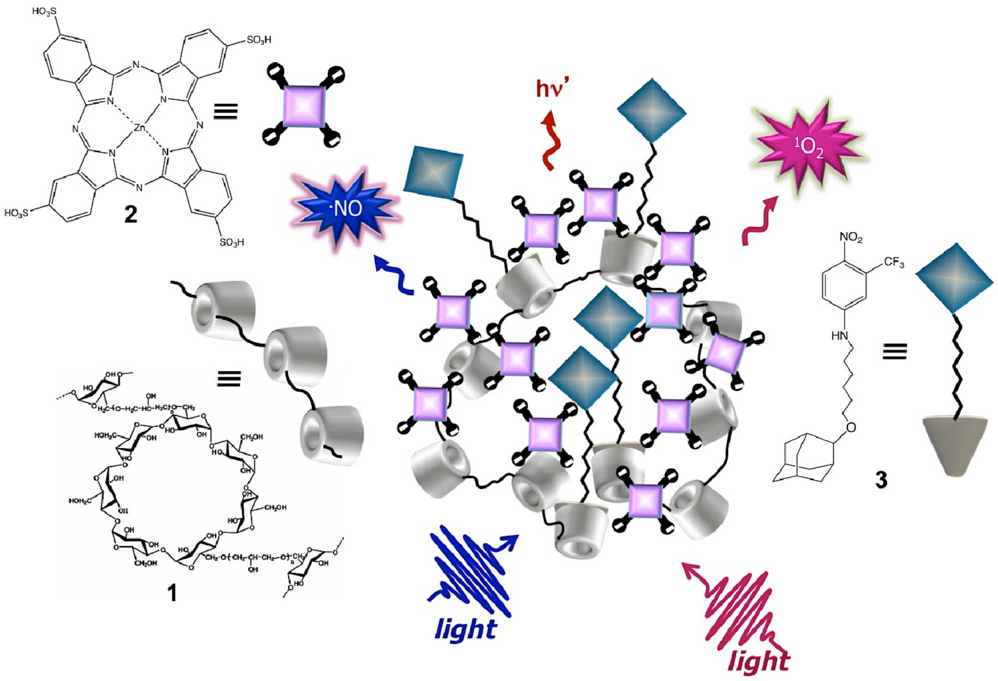

Scheme 6.1. Schematic representation of the multimodal photoactions from CD-based polymer nanoassemblies. **1**) CD polymer, **2**) Zn phthalocyanine tetrasulfonate, **3**) adamantane terminated NO photodonor.

The polymer ensemble is designed to envisage the controlled and independent release of active species exclusively tuned by the light sources. The multimodal actions such as the merging of $^1O_2$ and NO stimulated cytotoxicity with the non-invasive imaging capabilities in red region of the visible spectra in single nanostructure empower this multifunctional nanosystem for therapeutic applications.

6.2 Experimental

6.2.1 Materials

A) CD-based polymer

The CD-based polymer (**1**) is obtained from Dr. Ruxandra Gref, Faculty of Pharmcay, CNRS, University of South-Paris, France, and used as such with out further purification.

B) Zinc phthalocyaninetetrasulfonate

The macrocyclic Zinc phthalocyanine tetrasulfonate was directly purchased from Porphyrin Pdts. and used as such with out further purification. All other reagents were highest commercial grade available and used without further purification. All solvent used (from Carlo Erba) were analytical grade.

6.2.2 Synthesis of tailored NO photodonor

The protocol followed to synthesize the NO photodonor is exactly same as synthetic procedure reported before (Chapter 3).

6.3 Instrumentation

UV/Vis absorption and fluorescence spectra were recorded with a HP-8452 diode array spectrophotometer and Fluorolog-2 (Model, F-111) spectrofluorimeter respectively. Nanoparticle sizes were measured by a dynamic light scattering Horiba LS 550 apparatus equipped with a diode laser with a wavelength of 650 nm. Fluorescence images were taken with a Biomed fluorescence microscope (Leitz, Wetzlar, Germany). Photolysis experiments were performed in a thermostated quartz cell (1 cm path length, 3 mL capacity) by using a Rayonet photochemical reactor equipped with 8 RPR lamps with an emission in the 380-480 nm range with a maximum at 420 nm in the presence of a 400 nm cut-off filter. The incident photon flux on quartz cuvettes was ca. 0.8 x 10^{15} quanta sec^{-1}.

6.3.1 Laser flash photolysis

All of the samples were excited with the second harmonic of Nd–YAG Continuum Surelite II–10 laser (532 nm, 6 ns FWHM), using quartz cells with a path length of 1.0 cm. The excited solutions were analyzed with a Luzchem Research mLFP–111 apparatus with an orthogonal pump/probe configuration. The probe source was a ceramic xenon lamp coupled to quartz fiber-optic cables. The laser pulse and the mLFP–111 system were synchronized by a Tektronix TDS 3032 digitizer, operating in pre-trigger mode. The signals from a compact Hamamatsu photomultiplier were initially captured by the digitizer and then transferred to a personal computer, controlled by Luzchem Research software operating in the National Instruments LabView 5.1 environment. The solutions were deoxygenated by bubbling with a vigorous and constant flux of pure argon (previously saturated with solvent). In all of these experiments, the solutions were renewed after each laser shot (in a flow cell of 1 cm optical path), to prevent probable auto-oxidation processes. The sample temperature was 295 ± 2 K. The energy of the laser pulse was measured at each shot with a SPHD25 Scientech pyroelectric meter.

6.3.2 Singlet oxygen detection

Photogeneration of $^1O_2$ upon laser excitation of the photosensitizer was monitored by luminescence measurements in oxygen-saturated solutions. The near-IR luminescence of singlet oxygen at 1.27 μm resulting from the forbidden transition $^3\Sigma_g^- \leftarrow {}^1\Delta_g$; this was probed orthogonally to the exciting beam with a pre-amplified (low impedance) Ge-photodiode (Hamamatsu EI-P, 300 ns resolution) maintained at –196°C and coupled to a long-pass silicon filter (>1.1 μm) and an interference filter (1.27 μm). Pure signal of $^1O_2$ were obtained as difference between signals in air- and Ar-saturated solutions. The temporal profile of the luminescence was fitted to a single-exponential decay function with the exclusion of the initial portion of the plot, which was affected by scattered excitation light, fluorescence, and the formation profile of singlet oxygen itself.

6.3.3 NO detection

NO release was measured based on the protocol reported in previous chapter (Chapter 3).

6.3.4 Two-photon fluorescence spectroscopy and microscopy

Two-photon fluorescence spectra were recorded using LSM 710 NLO microscope (Carl Zeiss, Jena, Germany) equipped with mode-locked femtosecond pulsed *Mai Tai DeepSee* laser. TPM images and comparing mean gray values were analyzed to understand the fluorescence intensity. Two-photon fluorescence images were obtained using the same equipment described above. Microscope was equipped with a Plan-Apochromat 20x water immersion objective (NA 1.0) (Carl Zeiss, Jena, Germany). The excitation wavelength was set to 720 nm in case of epidermal cancer cell suspension and 840 nm in case of skin samples. Laser light intensity at the cell sample, was approximately 500 mW and the same for the skin samples were approximately 15 mW. Fluorescence was registered with descanned (internal) detectors with a fully opened pinhole. Band pass filters A) 577-700 nm in case of cellular suspension, B) 600-760 nm to record signals of bichromophoric assembly incubated in skin samples and 470-570 nm to detect skin autofluorescence. Images were acquired with a pixel dwell time of 1.58 μs. The image frame size was 1024 x 1024 pixels, which corresponds to a surface area of 425 x 425 μm. 3D imaging was performed by acquiring z-stacks of images at different sample depths. Image processing was performed with Carl Zeiss ZEN 2011 Black and Blue versions.

6.3.5 Binding calculation

This application was performed using the commercial SPECFIT/32 program, as reported.[26,27] Multi wavelength spectroscopic data sets (absorbances, fluorescence intensities) are arranged in matrix form **Y**, where a number Nw of wavelengths and a number Nm of corresponding measured spectroscopic signals are ordered in columns, whereas ligand and receptor concentrations are inserted in rows. Thus each element of the data matrix Y_{ij} corresponds to a wavelength j and an experimental quantity (absorbance, circular dichroism, fluorescence intensity) for a given couple of concentrations i of ligand and receptor (typically in our experiments one of them is kept constant). A least square best estimator **Y'** of the original data **Y** is reconstructed as the eigenvector representation **Y'** = **U×S×V**, where **S** is a vector that contains the relative weights of the significant eigenvectors (Ne, number of significant eigenvectors), **U** is a matrix (Nm × Ne) of concentration eigenvectors ($U^T \times U=1$, orthonormal) and **V** (Ne × Nw) is a matrix of spectroscopic eigenvectors ($V \times V^T$, orthonormal). This **Y'** matrix contains less noise than **Y** because the SVD procedure can factor random noise from the principal components. This reconstructed data matrix **Y'** is utilized in the global fitting instead of the original data matrix **Y**. Complexation equilibria are solved assuming a complexation model (i.e. contemporary presence of a number of complexes of given stoichiometries in equilibrium with free species in solution) and optimizing the numeric combination of all the spectroscopic contributions to best reproduce the **Y'** signals. The analysis relies mainly to absorption data but also fluorescence data may be analysed, provided they are relevant to optically thin samples (linear dependence of fluorescence signal on concentration for all the species involved). Given the direct linearity between absorbance or CD and concentration and the relation that must exist between the concentrations of the various species in the postulated simultaneous equilibria, the program calculates the conditional association constants and the spectra of the complexes based on a non linear least square fit, using the Levenberg-Marquardt algorithm, to best reproduce the experimental data for all the explored wavelengths and ligand-receptor concentration couples. The quality of the fits was evaluated on the basis of their Durbin-Watson (D. W.) factor and the relative error of fit. The D. W. test is very useful to check for the presence of auto-correlation in the residuals. This method is recommended for systematic misfit errors that can arise in titration experiments. It examines the tendency of successive residual errors to be correlated. The Durbin-Watson statistics ranges from 0.0 to 4.0, with an optimal mid-point value of 2.0 for uncorrelated residuals (i.e. no systematic misfit). In contrast to the χ^2 (Chi-squared) statistics, which requires the noise in the experimental data is random and normally distributed, the D. W. factor is meaningful even when the noise level in the data set is low. Since the factorized data usually have a significantly lower noise level than the original data, D. W. test is ideal for the present type of data.

6.4 Sample preparation

6.4.1 Photochemical experiments

An aqueous solution of compound **2** was prepared at micromolar concentration. The inclusion behavior of **2** with carrier **1** was studied by adding different weighed amounts of the corresponding polymer to the aqueous solution of **2**. The compound **3** was slowly evaporated in acetonitrile and stirred overnight with the saturated polymeric dispersion of **2** to obtain bichromphoric ensemble.

6.4.2 Experiments with cells

A) Cancer cell sample preparation

A431 epidermal carcinoma cells were used for the two photon imaging. Firstly the cells were seeded on the glass bottom of 3 cm diameter petridish for 24 hours prior to experiment. The medium was substituted with photoactive components in PBS(10 mM) diluted 3 times and 4 hours prior to imaging. The experimental solution was removed before imaging and cells are gently rinsed with PBS. Afterwards, 2 mL of protein free MEM medium was added to the cell culture to keep cells alive and allow imaging with water imersion objective.

B) Skin sample preparation

Human skin specimens from caucasian females, collected as leftovers from breast reduction surgery were used in experiments. The specimens were cut into 1 x 1 cm pieces, stored in -70°C and used within six months. The samples were thawed in room temperature before use. A major part of sub cutis was removed mechanically, using a scalpel. Afterwards, full-thickness skin samples were mounted in flow-through diffusion chambers, for exposure to the different test solutions. The receptor compartment was filled with PBS solution and the experimental solutions were added to the donor compartment. Diffusion chambers were covered with parafilm and aluminium foil and kept at 30°C temperature. Passive diffusion was allowed for 20 hours under constant stirring of donor compartment. After exposure, samples were taken out of the diffusion chamber, thoroughly rinsed with PBS solution and mounted on the microscopy slides using custom made imaging chambers consisting of a No. 1.5 cover slip (0.18 mm, Menzel-Gläser) and a double-sided sticky tape.

6.5 Results and Discussion

The compound **2** is soluble in water with the characteristic soret band at 335 nm, Q band at 630 nm and a shoulder at 658 nm (a in Figure 6.1).

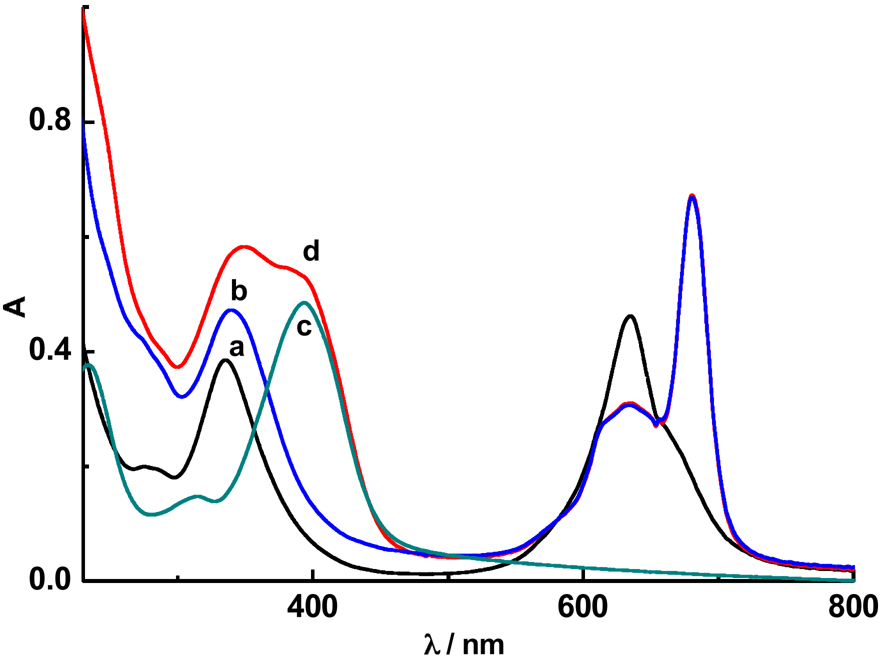

Figure 6.1. The steady state absorption spectra of **2** (in phosphate buffer, 10 mM, pH 7.4) in the absence (a) and in the presence (b) of **1**, **3** in the presence of **1** (c), **2** + **3** in the presence of **1** (d). [**1**]= 11 µM, [**2**]= 5 µM, [**3**]= 40 µM, T= 25°C, cell path length= 1 cm.

Though the water-soluble form of **2** as such is photodynamically mute (*vide supra*) as the protic solvents facilitate irreversible aggregated structures. While interaction of compound **2** with polymeric NPs of **1** leads to disaggregated structures as the new band appears at red side of the absorption spectrum (b in Figure 6.1) of **2**. Appearance of new absorption peak at 680 nm with relatively high peak intensity as compared to the band at 635 nm signify the monomerization of the **2** which is dependent on the concentration of the **1**.[28,29]

It is perceived from the ratio of absorbance that extend of monomerization of **2** is much far extend than the aggregated structure to have the effective photodynamic action.

The NO photodonor (**3**) is also used at the same token to encapsulate inside hydrophobic pockets of CD units, exploited by the efficient binding of the adamantane appendage with CD cavities with the binding constant of the order of 10^5 M^{-1}. Practically the compound **3** is insoluble in water, but shows characteristic absorption in presence of **1** with the peak maxima around 400 nm (c in Figure 6.1). The absorption band reveals the clear solubility of **3** in aqueous polymeric dispersion where adamantane appendage brings the compound to be encapsulated in CD networks. Above all, the absorption peak positions were remaining unaltered when both **2** and **3** encompassed together in polymer interiors (d in Figure 6.1). In fact, the arithmetic addition of both b and c were exactly matching with the absorption spectra of bichromophoric assembly revealing the absence any detrimental interchromophoric interactions at the ground state.

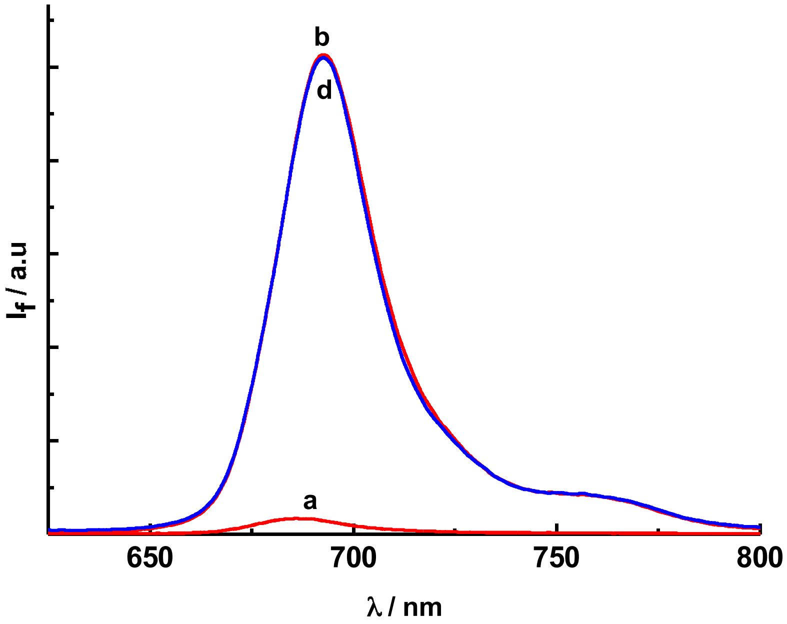

Figure 6.2. Fluorescence emission spectra (λ_{exc}= 575 nm) of **2** (a) in the absence and (b) in the presence of **1**, (d) of **2**+**3** in the presence of **1**.

In addition, the fluorescence spectrum of fluorophore **2** remain unaltered in the presence and in the absence of NO photodonor **3** (Figure 6.2), nullifying the sort of possibility that the intramolecular quenching (i.e., photoinduced electron-transfer) of the excited fluorphore **2** by the NO photodonor **3**. This would be understand on the point that the presence of NO photodonor does not 'reorganize' loaded fluorophore **2** owing to their compartmentalized orientation in different region of the polymer (Scheme 6.1). Compound **2** is barely fluorescent in phosphate buffer due to aggregation and follows very fast non-radiative decay pathway due to the vibrational relaxation.[12]

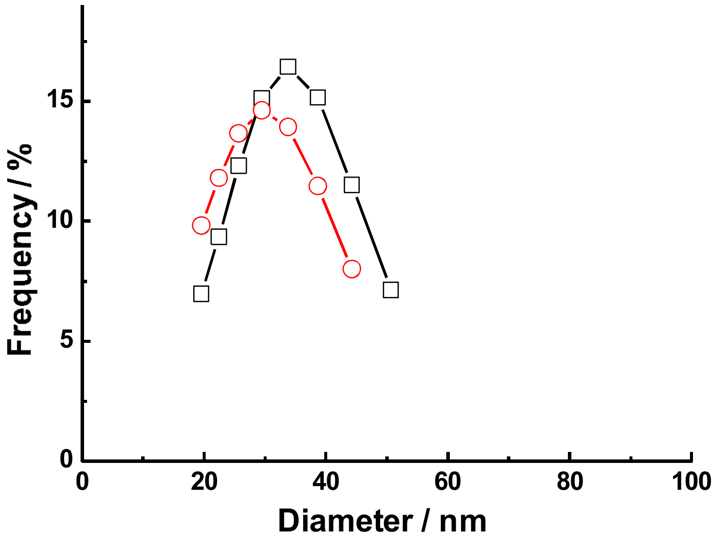

Figure 6.3. Dynamic light scattering measurement showing the size distribution of **2** in presence of **1** (O) and the size of bichromophoric assembly (**2+3/1**) in phosphate buffer (□).

In the direction to understand the size depenedent features of the ensemble, the present supramolecular assembly is studied by DLS (Figure 6.3). The hydrodynamic diameter of the ensemble is slightly varied by 15 nm (from ca. 30 nm to 45 nm) validating the entire assembling process to be able to penetrate in to the tissues.

Concentration dependent disaggregation profile of **2** in presence of **1** prompted us to do the titration experiment. In this regard constant weight of **1** was continuously added in to the aqueous solution of **2.** The change in the absorption spectral features of **2** is displayed below (Figure 6.4).

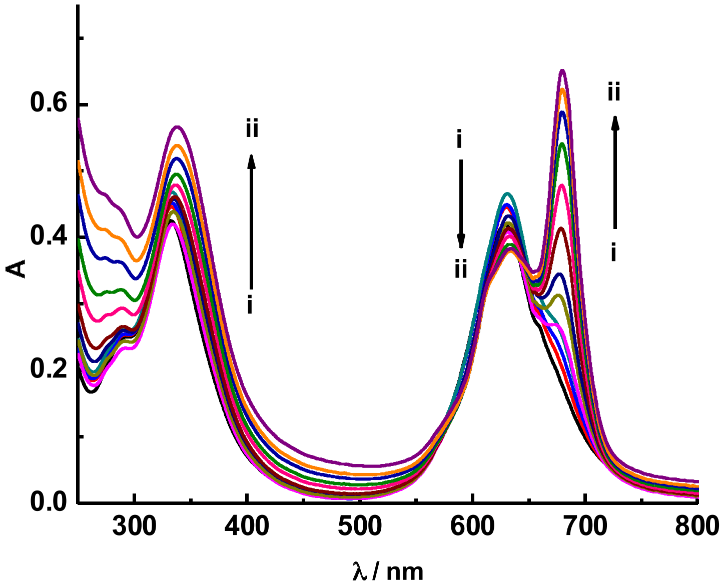

Figure 6.4. Representative absorption spectra of **2** (5 µM) in aqueous buffer solution at different concentrations of **1**. [**1**]/ mM= 1) 0.0, 2) 0.09, 3) 0.19, 4) 0.28, 5) 0.47, 6) 0.68, 7) 0.87, 8) 1.5, 9) 2.5, 10) 3.7, 11) 5.3, 12) 6.77, 13) 7.75 (in terms of CD units).

The Figure 6.4 shows that the absorption spectra of compound **2** undergo remarkable changes upon titration with different concentration of polymer. The Q band at 635 nm totally diminishes with the appearance of the new band at 680 nm (Figure 6.4). Moreover the Soret band also rises up with respect to the concentration of the polymer. This is in consequence with the disaggregation of compound **2** in presence of polymer.[30,31] This behavior is in line with the steady state fluorescence spectrum, which is shown below (Figure 6.5).

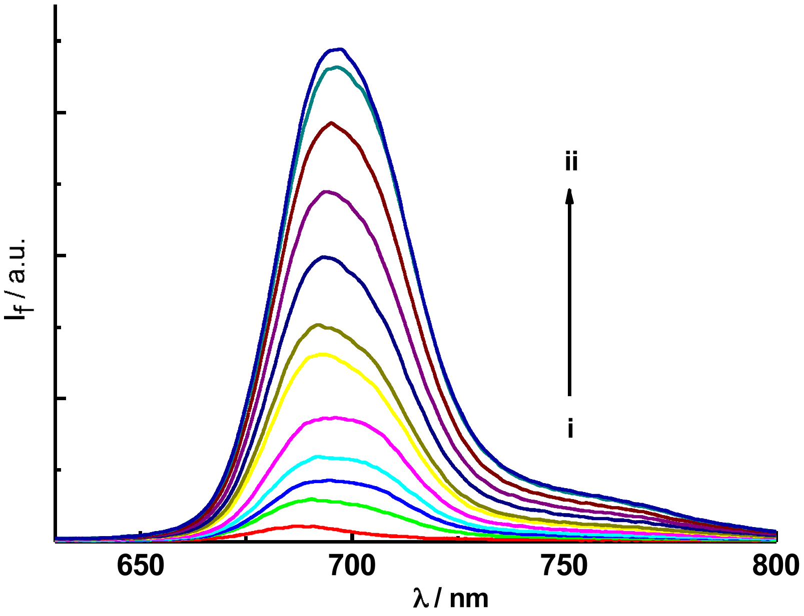

Figure 6.5. Representative steady state fluorescence spectra of **2** (5 μM) in aqueous buffer solution at different concentrations of **1**. [**1**]/ mM= 1) 0.0, 2) 0.09, 3) 0.19, 4) 0.28, 5) 0.47, 6) 0.68, 7) 1.5, 8) 2.5, 9) 3.7, 10) 5.3, 11) 6.77, 12) 7.75 (in terms of CD units), λ_{exc}= 575 nm (isosbestic point).

In aqueous polymeric solution, the compound **2** show the fluorescence spectra with the emission maximum at 691 nm with the concomitant red shift to 698 nm in presence of maximum concentration of **1**. The emission spectra undergo continuous enhancement on its fluorescence intensity upon addition of fixed polymer weight. The remarkable enhancement of fluorescence intensity of **2**, ca. 30 times higher than the solution with no polymer added, at saturated polymer concentration signify the effects of polymer **1** on the emissive properties of **2**. The same experiment was also performed in DMSO without adding the polymer, where all the photosensitizer exists in monomer[32] (Data not shown). The similarity in the emission profile of **2** in DMSO and at saturated polymer concentration refers the extended monomerization of the compound **2** in polymer. Mechanistically the compound **2** is able to interact with CD units, with the stoichiometry of 1:2 in terms of CD units, through the induced fit as the extended benzene ring can actively participate in inclusion process.[33,34] On the light of related studies of porphyrinoid structures, co-operative interaction induced by hydrophobic domain of folded polymer might enhance the inclusion phenomenon of **2** with **1**.[28]

Well-versed interaction of compound **2** with the polymer **1** was stimulating to understand the binding events of **2** with **1**. On this concern, we studied the quantitative binding calculation to understand the stability constant of former, which is displayed below.

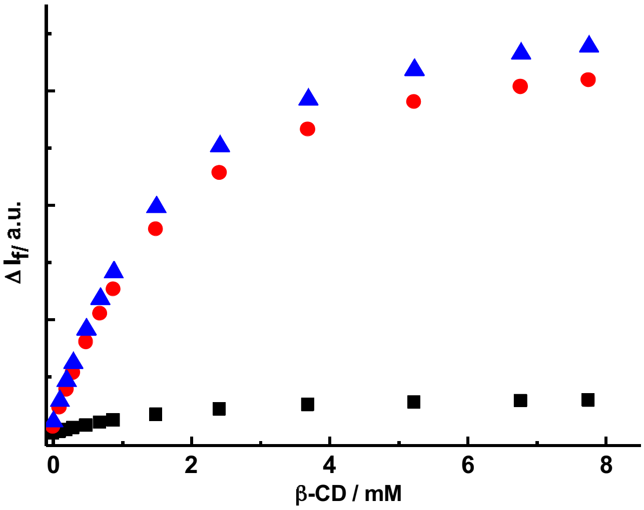

Figure 6.6. Calculated binding curves of **2** with different concentration of **1** (concentration in terms of CD units) using data obtained from fluorescence titration, (▲ 1:1 complex, ● 1:2 complex, ■ population of unbound aggregates).

Here the stability constant is calculated by considering the fluorescence titration experiment[35] as the absorption spectral changes does not give significant fitting values. Fluorescence changes of **2** upon interaction with various concentration of **1** (From 0 to 7.75 x 10^{-3} M, in terms of β-CD units) were taken as the experimental measures. The fluorescence spectrum was studied by a global analysis[36] while considering three emitters, 1) complex of **2** with **1** in 1:2 stoichiometry with respect to the CD units, 2) in 1:1 stoichiometry with respect to the CD units and 3) aggregate structures of **2**, over the wavelength range in between 600 to 800 nm (Figure 6.6). A good fitting model was observed by approximating complexation of the probe **2** with CD units in 1:2 and 1:1 stoichiometry with an association constant, Ka = 3 x 10^5 M^{-1} in case of 1:2 binding ratio and 1.5 x 10^4 in case of 1:1 ratio (Durbin-Watson factor is around 1.48 and relative error is 3.54 %).

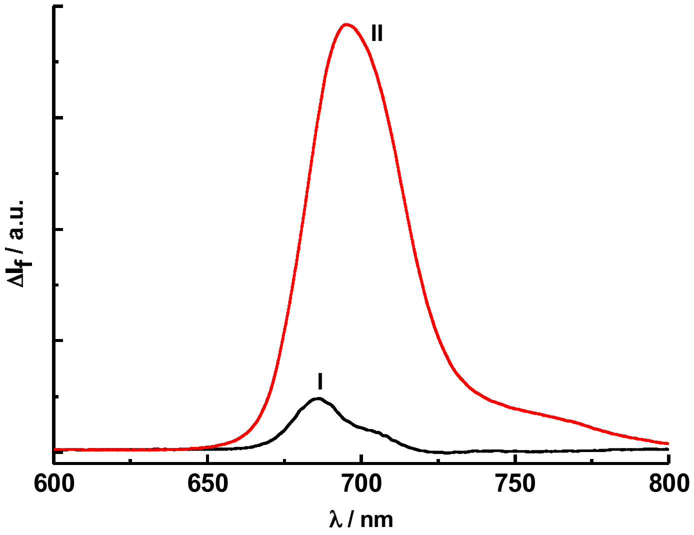

Figure 6.7. Calculated emission spectra of **2** upon interaction with **1**, I) Complex of **2** with **1**, II) Emission from the population of unbound aggregated structures.

Based on this global fitting calculation, the fluorescence titration spectrum was reconstructed by the optimization procedure based on singular value decomposition and non-linear regression modeling by the Levenberg–Marquardt method[37] (Figure 6.7). The exact resemblance of the simulated titration curve with experimental titration spectra, where the fluorophore undergoes exact bathochromic shift, ca. ~ 8 nm, and the enhancement in fluorescence intensity at the same order of magnitude, validate the binding calculations and propounds the concentration dependent physico-chemical characteristics of the photosensitizer **2**. The strong binding constant observed in case of 1:2 stoichiometry can be understood from the fact the tetrapods of benzene sulfonate appendage attached on the macrocyclic structure of **2** is free to interact with the CD units due to their favorable geometrical matching for induced fitting. Above all, this kind of interaction does not influence the inclusion of compound **3** in the native CD cavities as the matter of fact that polymer is interconnected with CD units and CD units are much high in number per molecular weight of the polymer, leaving a space to encompass the second probe.

Although the photosensitizer **2** entrapped nanoassembly is invariably fluorescent and enable the imaging features at the bio-sites, the key for the photodynamic action is the effective generation of triplet state and sensitization of the molecular oxygen.[38,39] In this regard we traced the transient absorption spectra of the **2** by laser flash photolysis (Figure 6.8). The transient band of aqueous polymeric dispersion of **2** shows characteristic positive band between 400 to 600 nm with the strong ground state bleaching at the soret band and Q band region of the absorption spectra in line to other related studies.[40,41] Interestingly, the transient band of **2** remains unchanged in presence of NO photodonor **3** while they are entangled together in bihromophoric assembly (Figure 6.8).

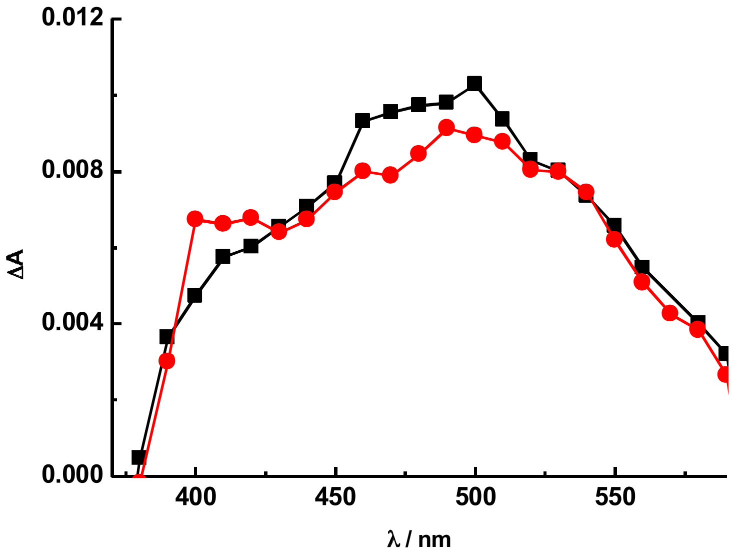

Figure 6.8. Transient absorption spectra observed upon 355 nm laser excitation of Ar-saturated solution of **2** loaded with **1** (■) and **2+3** (●), recorded 1 μs, after the laser pulse. Each point was obtained by signal average of 10 traces. E_{532} ~ 12 mJ/pulse, phosphate buffer (10 mM, pH 7.4), [**1**]= 12 μM, [**2**]= 5 μM, [**3**]= 40 μM, T= 25°C.

The efficient generation of transient species in the wavelength range of 400 to 600 nm is attributed to the photosensitization of the molecular oxygen and effective PDT actions. The similarity in the transient band of **2** in the presence and in the absence of **3** is justifiable by considering the fact that both solutions were optically matched and compound **2** does not afford any distortion on its orientational freedom from **3** in the bichromophoric assembly.[42]

Above all, the mono exponential kinetic decay of triplet state transient reveals absence any detrimental intermolecular quenching by the compound **3** (Figure 6.9). The long triplet state lifetime of polymer bound **2**, ca. 250 μs, well accounts the possibility of higher number of diffusional encounters with molecular oxygen for effective photodynamic actions.[32]

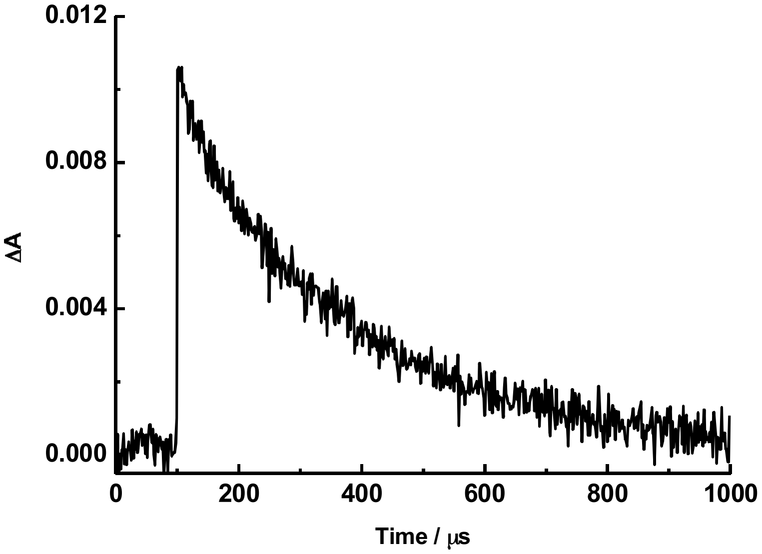

Figure 6.9. Kinetic decay trace of excited triplet state of **2** monitored at 530 nm. E_{532}~ 12 mJ/pulse. Phosphate buffer (10 mM, pH 7.4), [**1**] = 12 μM, [**2**] = 5 μM, [**3**] = 40 μM, T= 25°C.

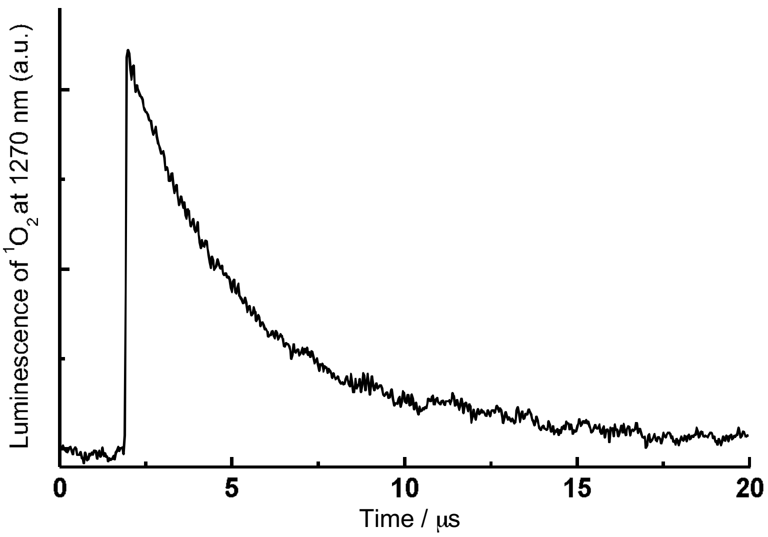

Figure 6.10. Kinetic trace of $^1O_2$ generated upon 355 nm laser excitation of the bichromophoric CD-based polymer NPs. Phosphate buffer (10 mM, pH 7.4), [**1**]= 12 μM, [**2**]= 5 μM, [**3**]= 40 μM, T= 25°C.

As the solutions are optically matched, the population of triplet state is the direct measure of triplet sate quantum yield, which in turn contribute significantly to the photosensitization actions of **2**. The majority of the compound **2** in aqueous buffer solution exist as aggregated structures and follows very fast decay pathway (in picosecond time scale[32]) which is undetectable with our instrumental setup and can be totally neglected as far as $^1O_2$ photosensitization is concerned. Finally the singlet oxygen generation has been analyzed by detecting the typical phosphorescence of $^1O_2$ at 1270 nm thanks to infrared luminescence technique (Figure 6.10).[43] The Figure 6.10 shows the unambiguous evidence of the generation of singlet oxygen sensitized by the photosensitizer **2**.

The bichrmophoric supramolecular assembly loaded with two chromogenic centers at the appropriate molar ratio has ben utilized to study the NO photorelease. In this regard, the former is irradiated with light of 400 nm and analyzed by the steady state absorption spectra (Figure 6.11). It can be seen that bleaching occurs in the corresponding absorption region of the NO photodonor (around 400 nm), whereas practically nothing changed on absorption peak representing compound **2** (absorption peaks at 635 and 680 nm). The exclusive photobleaching of NO photodonor in their absorption regime and no change in the absorption band of the photosensitizer upon NO photorelease assert the possibility of selective activation of either NO release or independent generation of $^1O_2$ from this nanosystem.

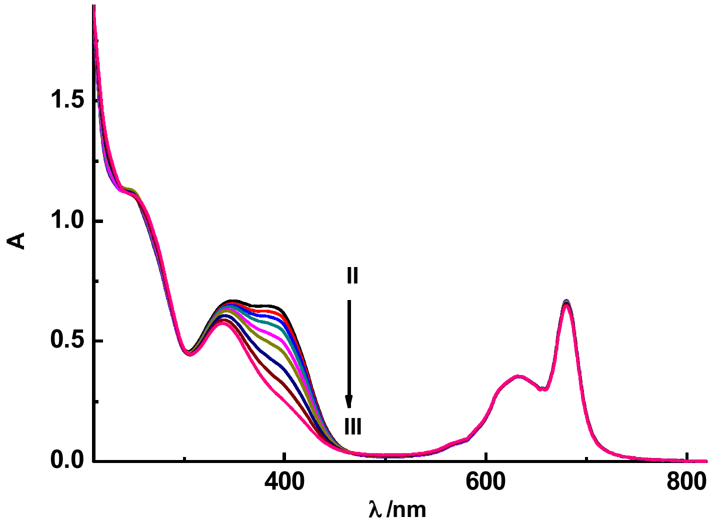

Figure 6.11. Absorption spectra of CD-based polymeric dispersion loaded with both **2** and **3** (**2**+**3**/**1**) at 25°C before (**II**) and after (**III**) 40 min of 400 nm light irradiation, (in phosphate buffer, pH 7.4, 10 mM, 25°C).

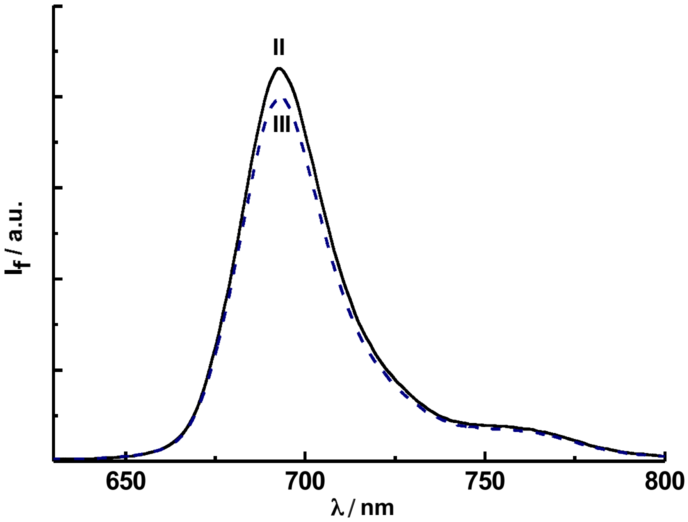

Figure 6.12. Fluorescence emission spectra of the bichromophoric supramolecular complex before (II) and after (III) photolysis (λ_{exc}= 575 nm).

It is worthy to point out that the photoirradiation and consequent NO photorelease does not effect emissive properties of the fluorophore **2**. In fact the fluorescence spectra of **2** in saturated solution of **1** was only little changed before and after the photoirradiation (II and III in Figure 6.12).

Though the photoirradiation experiment and absorption spectra reveals the qualitative evidence of NO photorelease, the most convenient way to demonstrate that the observed photochemical decomposition is related to the NO release from the bichromophoric nanoasssembly is the direct and real time measurement of this free radical. To this end, we have used an ultrasensitive NO electrode, which directly detects NO with nanomolar concentration resolution, by an amperometric technique.

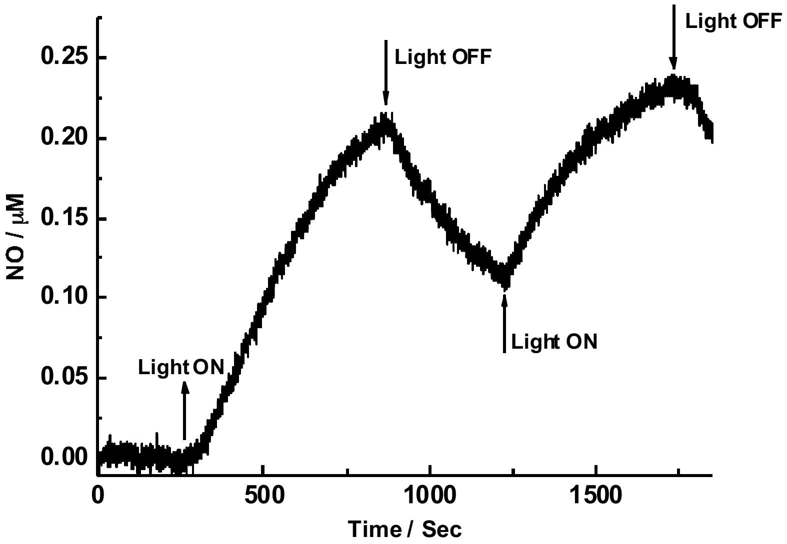

Figure 6.13. Amperogram of bichromophoric NPs (2+3/1) showing the release of NO upon 400 nm light irradiation in phosphate buffer (10 mM, pH 7.4), [1]= 12 μM, [2]= 5 μM, [3]= 40 μM, T= 25°C.

The result illustrated in Figure 6.13 provides unambiguous evidence that the bichromophoric nanoasssembly is stable in the dark but supply NO upon illumination when irradiated with 400 nm light. The release process is strictly dependent on the external light inputs, as confirmed by the linear NO photodelivery, which promptly stops as the light is turned off, and restarts as the illumination is turned on again. Furthermore, no NO release was detected when the excitation energy was longer than 450 nm, according to the negligible absorption of the NO photodonor unit at these wavelengths. Given that the photoproduct generated after NO release is not absorbing at the excitation wavelength,[44],[45] the photochemical reaction occurs almost quantitatively, generating NO concentrations up to the micromolar range, an important requisite for anticancer applications.[46,47]

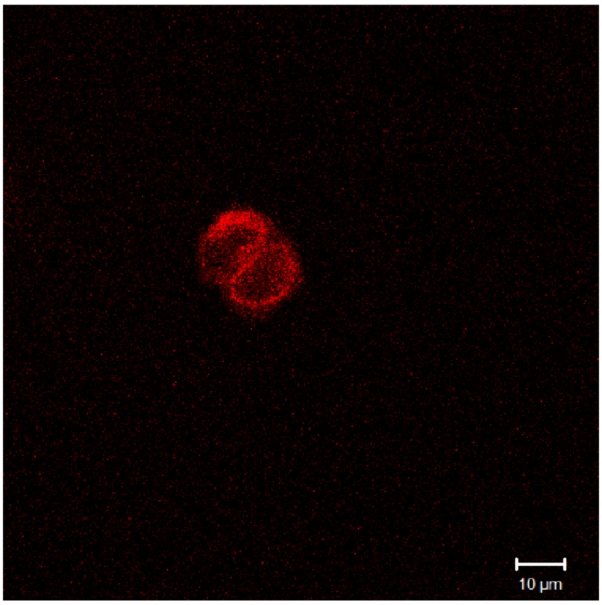

Figure 6.14. The two-photon fluorescence microscopy image of epidermal cancer cell lines (Model No. A431) incubated with the complex **2+3/1** (ca. 10 µM) in 10 mM phosphate buffer (pH 7.4). The assembly mapped at the excitation of 720 nm and the band pass filter at 577-700 nm.

Finally the fate of the bichromophoric ensemble was tracked in epidermal cancer cell lines by virtue of the emissive properties of compound **2** (Figure 6.14). In this regard the ensemble is incubated in cells for 5 hours and analyzed by two-photon microscopy. The amble red fluorescent emission, characteristic to the spectral features of compound **2**, from the cells explains the intake of the assembly in to the cytoplasm.

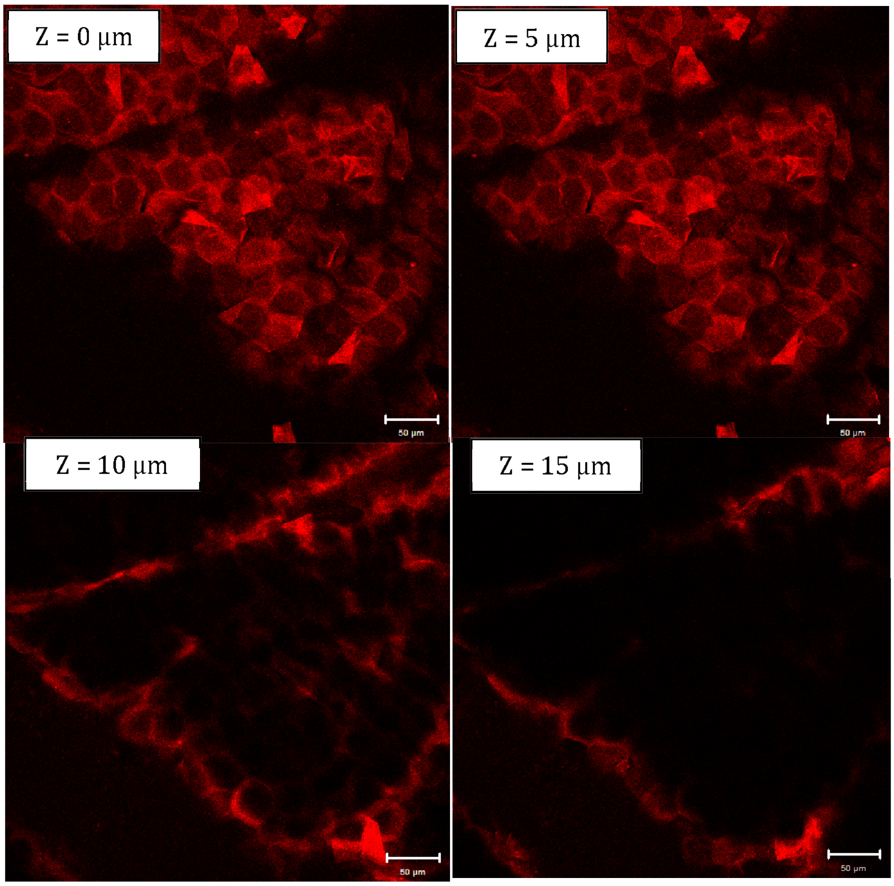

Figure 6.15. Penetration depth and distribution pattern of bichromophoric NPs in human *ex-vivo* skin sample after 24 h of incubation in the flow through diffusion chamber. Excitation wavelength 840 nm, Z- Zstack represents the depth of the sample.

Furthermore the same bichromphoric assembly is able to diffuse into the skin as shown in the picture (Figure 6.15). The figure represents the fluorescence distribution pattern of the bichromophoric NPs after 24 hours of application on skin detected with a help of TPM. The NPs could be detected at the depths of 10 µm within the skin and in the skin cracks and wrinkles at depths more than 25 µm.

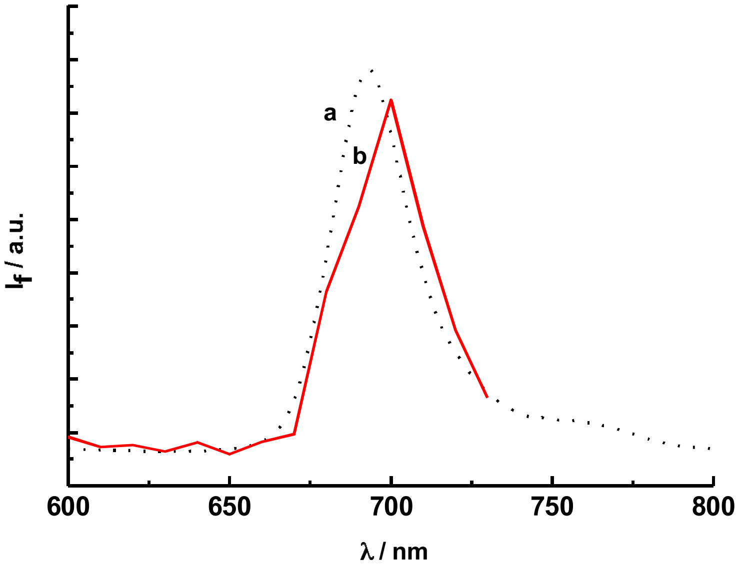

Figure 6.16. The emission spectra of the skin sample incubated with **2+3/1** for 24 hours in the flow through diffusion chamber registered with TPM equipment. Excitation wavelength was set to 840 nm, and emission registered at the range of 420-730 nm, with the unit of 10 nm.

Fluorescence distribution pattern also implies, that the penetration pathway of the ensemble is via extracellular space or cellular membranes. Characteristic shape of the cell typical to stratum corneum layer of epidermis was observed at the depth of 5 µm. All this findings proves the distribution of the ensemble in the cellular interphase. Finally the red fluorescence from the assembly has again confirmed by directly measuring the fluorescence emission spectra from the *ex-vivo* skin sample after 24 hour incubation with the conjugate mixture (Figure 6.16). As it can be observed in Figure 6.16, the emission spectra resembles the fluorescence spectra of compound **2**, with a maximum fluorescence intensity at 700 nm.

6.6 Conclusion

We have developed a supramolecular nanoassembly by formulating CD-based polymeric NPs and two independent photoactive centers namely a $^1O_2$ photosensitizer and NO releasing photodonor. The phthalocyanines are efficient fluorescent photosensitizer but prone to aggregation in aqueous phase. Here we laid out an active principle to disaggregate the former into its monomeric state in aqueous phase, somewhat similar in DMSO. The red fluorescence emission characteristics with the independent and distinctive spectral features of the phthalocyanine on comparison with the second probe, an NO photodonor, make this ensemble unique towards image-guided therapy. Furthermore, merging the novel therapeutic features of NO actions from the NO photodonor and $^1O_2$ from the phthalocyanine in single molecular scaffold would add up multimodal features to the anticancer therapy. The steady state and time-resolved spectral characteristics of both probe entrapped in the polymeric NPs attest independent photodynamic features of chromogenic moieties. The entire nanosystem is localized and studied in cell culture media and *in-vitro* results undoubtedly prove the suitability of the present system as a novel multimodal agent.

Finally we would like highlight some key features associated with present system for multimodal therapy. We incorporated the two probes in the same nanostructure without compromising their photodynamic features and both probe are distinctive in their spectral features. Convergence of dual therapeutic actions and imaging capabilities in single nanostructure make the present nanoensemble to stand out among contemporary molecular scaffolds intended for anticancer therapies.

6.7 References

1. F. H. Moser, A. L. Thomas, *The Phthalocyanines*, **Vol. I-II**, Eds.; CRC Press: Boca Raton, FL, 1983.
2. M. Emmelius, G. Pawlowski, H. Vollmann, *Angew. Chem. Int. Ed.*, 1989, **28**, 1445.
3. J. –D. Huang, S. Wang, P. –C. Lo, W. –P. Fong, W. –H. Kod, D. K. P. Ng, *New. J. Chem.*, 2004, **28**, 348.
4. R. Bonnett, *Chem. Soc. Rev.*, 1995, **24**, 19.
5. P. –C. Lo, J. –D. Huang, D. Y. Y. Cheng, E. Y. M. Chan, W. –P. Fong, W. –H. Ko, D. K. P. Ng, *Chem. Eur. J.*, 2004, **10**, 4831.
6. N. B. McKeown, *Phthalocyanine materials: Synthesis, Structure and Function*, **Vol. 6**, Cambridge University Press, 1998.
7. J. Metz, O. Schneider, M. Hanack, *Inorg. Chem.*, 1984, **23**, 1065.
8. S. G. Bown, C. J. Tralau, P. D. C. -Smith, D. Akdemir, T. J. Wieman, 1986, *Br. J. Cancer*, **54**, 43–52.
9. S. Wan, J. A. Parrish, R. R. Anderson, M. Madden, *Photochem. Photobiol.*, 1981, **34**, 679.
10. M. Triesscheijn, P. Baas, J. H. Schellens, F. A. Stewart, *Oncologist*, 2006, **11**, 1034.
11. S. C. H. Leung, P. –C. Lo, D. K. P. Ng, W. –K. Liu, K. –P. Fung, W. –P. Fong, *Br. J. Pharmacol*, 2008, **154**, 4–12.
12. C. C. Leznoff, A. B. P. Lever, *Phthalocyanines: Properties and Applications*; Eds.; VCH: New York, 1989.
13. W. J. Schutte, M. S. -Rehbach, J. H. Sluyters, *J. Phys. Chem.,* 1993, **97**, 6069.
14. A. Lyubimtseva, Z. Iqbala, G. Cruciusa, S. Syrbub, E. S. Taraymovich, T. Zieglera, M. Hanack, *J. Porphyrins Phthalocyanines,* 2011, **15**, 39-46.
15. A. W. Snow, In The Porphyrin Handbook-*Phthalocyanines: Properties and Materials,* **Vol. 17**, K. M. Kadish, K. M. Smith, R. Guilard, Eds.; Academic Press: New York, 2003; pp 129-176.
16. H. Ali, J. E. van Lier, *Chem. Rev.*, 1999, **99**, 2379-2450.

---

17. P. C. Martin, M. Gouterman, B. V. Pepich, G. E. Renzoni, D. C. Schindele, *Inorg. Chem.*, 1991, **30**, 3305.

18. P. -C. Lo, C. M. H. Chan, J. -Y. Liu, W. -P. Fong, D. K. P. Ng, *J. Med. Chem.*, 2007, **50**, 2100.

19. J. D. Spikes, J. E. van Lier, J. C. Bommer, *J. Photochem. Photobiol. A: Chem.*, 1995, **91**, 193.

20. D. K. Chatterjee, L. S. Fong, Y. Zhang, *Adv. Drug Deliv. Rev.*, 2008, **60**, 1627.

21. J. Li, W. Zhang, Z. Hu, X. –J. Jiang, T. Ngai, P. –C. Lo, W. Zhang, G. Chen, *Polym. Chem.*, 2013, DOI: 10.1039/C2PY20668D.

22. A. Harada, M. Kamachi, *Macromolecules*, 1990, **23**, 2821.

23. A. Harada, *Carbohydr. Polym.*, 1997, **34**, 183.

24. M. Othman, K. Bouchemal, P. Couvreur, R. Gref, *Int. J. Pharm.*, 2009, **379**, 218.

25. S. D. Mahammed, C. R. -Lefebvre, N. Razzouq, V. Rosilio, B. Gillet, P. Couvreur, C. Amiel, R. Gref, *J. Coll. Interfae Sci.*, 2007, **307**, 83–93.

26. H. Gampp, M. Maeder, C. J. Meyer, A. D. Zuberbühler, *Talanta*, 1985, **32**, 95-101.

27. H. Gampp, M. Maeder, C. J. Meyer, A. D. Zuberbühler, *Talanta*, 1985, **32**, 257.

28. D. Karl, M. Kadish, K. M. Smith, R. Guilard, In the Porphyrin Handbook, **Vol. 11-20**, *Phthalocyanines: Properties and Materials*, pp 168-170, 2003.

29. X. Leng, C. -F. Choi, H. –B. Luo, Y. –K. Cheng, D. K. P. Ng, *Org. Lett.*, 2007, **9**, 13, 2497-2500.

30. M. Morisue, S. Ueda, M. Kurasawa, M. Naito, Y. Kuroda, *J. Phys. Chem. A*, 2012, **116**, 5139–5144.

31. L. Howe, J. Z. Zhang, *J. Phys. Chem. A,* 1997, **101***,* 3207-3213.

32. A. Ogunsipe, J. –Y. Chenb, T. Nyokong, *New. J. Chem.*, 2004, **28**, 822–827.

33. J. W. Park, H. J. Song, *J. Phys. Chem.,* 1989, **93***,* 6454-6458.

34. A. Ruebner, Z. Yang, D. Leung, R. Breslow, *Proc. Natl. Acad. Sci. USA,* 1999, **96**, 26, 14692–14693.

35. N. Kandoth, S. D. Choudhury, T. Mukherjee, H. Pal, *Photochem. Photobiol. Sci.,* 2009, **8**, 82–90.

---

36. R. Anand, S. Ottani, F. Manoli, I. Manet, S. Monti, *RSC Advances*, 2012, **2**, 2346.

37. R. Anand, F. Manoli, I. Manet, S. D. -Mahammed, V. Agostoni, R. Gref, S. Monti, *Photochem. Photobiol. Sci.*, 2012, **11**, 1285.

38. R. Pandey, G. Zheng, In The Porphyrin Handbook, **Vol. 6,** Eds.; K. Kadish, K. M. Smith, R. Guilard, Academic Press, San Diego, 2000, pp. 157–230.

39. D. K. Chatterjee, L. S. Fong, Y. Zhang, *Adv. Drug Delivery Rev.*, 2008, **60**, 1627.

40. B. B. -Płuska, A. Jarota, K. Kurczewski, H. Abramczyk, *J. Mol. Struct.*, 2009, 924–926, 338–346.

41. S. M. T. Nunes, F. S. Sguilla, A. C. Tedesco, *Braz. J. Med. Biol. Res.*, 2004, **37**, 2.

42. D. B. -Smith, *Photochemistry: A Review of Chemical Literature*, **Vol. 25** (Specialist Periodical Reports), 1994, pp 39.

43. F. Wilkinson, W. P. Helman, A. B. Ross, *J. Phys. Chem. Ref. Data*, 1993, **22**, 113.

44 . S. Conoci, S. Petralia, S. Sortino, U.S. Pat. Appl. Publ., Appl. No. PCT/IT2006/000575, 2009, pp. 20.

45. E. B. Caruso, S. Petralia, S. Conoci, S. Giuffrida, S. Sortino, *J. Am. Chem. Soc.*, 2007, **129**, 480.

46. A. D. Ostrowski, P. C. Ford, *Dalton Trans.,* 2009, 10660.

47. E. V. Stevens, A. W. Carpenter, J. H. Shin, J. Liu, C. J. Der, M. H. Schoenfisch, *Mol. Pharmaceutics*, 2010, **7**, 775.

7 CD-based photoactivable nanoparticles with fluorescence imaging and bimodal therapy

7.1 Introduction

Identifying the molecule of interest is one of principal requirement in clinical diagnosis. [1] Employing the fluorescent imaging techniques to the clinical diagnosis is an appealing strategy as it offers inexpensive non-invasive live cell imaging with better contrast distinctive to cellular matrix. The strategy mostly evolved during last decade were mainly based on, i) the fluorescent tagging or labeling to an interior fluorescent molecule such as fluorescent proteins, ii) tagging the exogenous molecule with an inherent fluorescent moiety.[2]

Among several selective and sensitive fluorogenic labeling moieties, the nitrobenzofurazan (NBF) serves an important role as they are characterized by i) large fluorescence quantum yield, ii) long excitation and emission wavelength necessary to distinct the molecule of interest from cellular biomatrices and cellular autofluorescence,[3] iii) exact tunability on the fluorogenic property by the substitution on the aromatic ring.[4,5] Possibility of linking the fluorophore with therapeutically relevant moiety and consequent fluorescence imaging at the site of therapeutic actions in molecular level enable unprecedented directions to the imaging guided therapy.[6,7] On this route, we designed and developed a molecular conjugate where the NBF is covalently tethered to a NO releasing photodonor. Novel features associated with NBF and NO donor as imaging and therapeutically active species with the prompt light trigger may add remarkable avenues to the phototriggered imaging and anticancer therapy. The same logic of encompassing several photo-driven active moieties in a single multifunctional nanoarchitecture addressed to multimodal anticancer treatments is expected to avert nocuous side effects of conventional anticancer therapeutics.[8,9]

Based on the above-mentioned goal, the present work relies on a supramolecular polymeric nanoparticles where molecules of multiple functionalities *viz.*, a red fluorescent $^1O_2$ photosensitizer, NO photodonor and green fluorescent NBF based labeling agent are incorporated inside their supramolecular interiors.

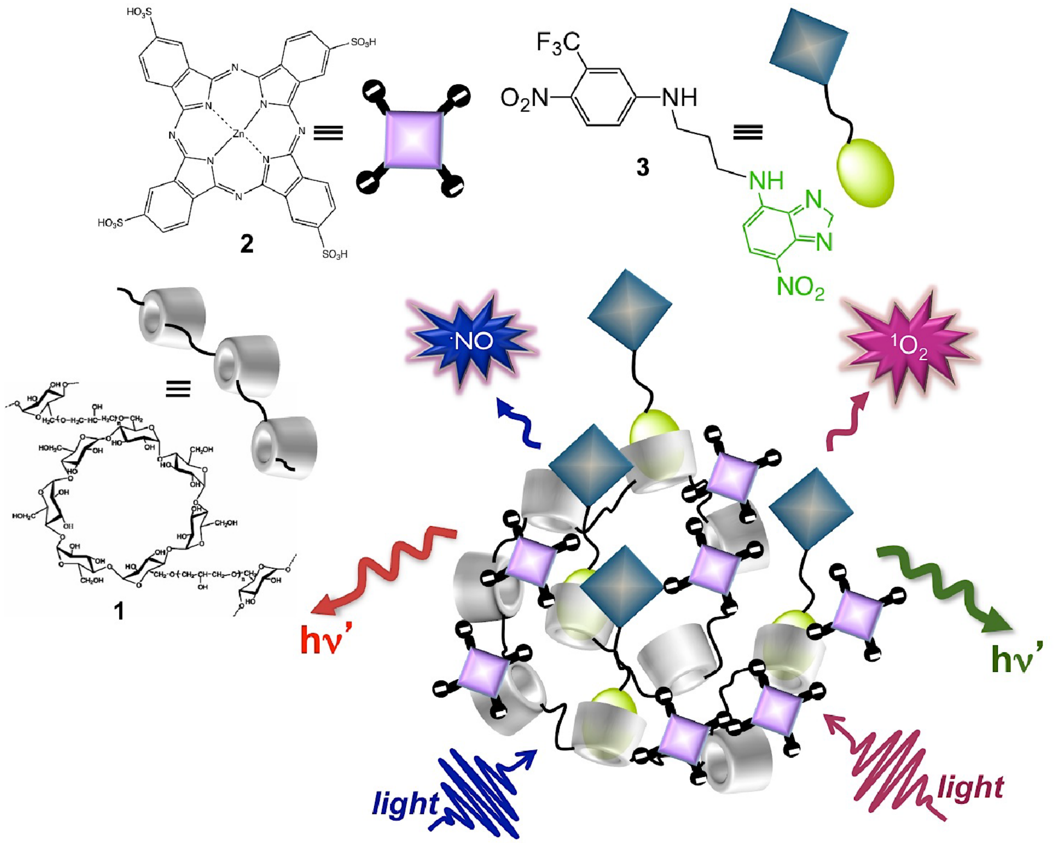

Scheme 7.1. Schematic representation of the multimodal photoaction from CD-based polymeric NPs. **1**) CD polymer, **2**) Zn phthalocyaninetetrasulfonate **3**) NBF attached NO photodonor.

The harmonious synchronization between photochemical and photodynamic features of each molecule, which has been achieved by the cutting edge design of the ensemble, allows the bimodal therapy accompanied by dual modal imaging. We demonstrate that such a complex internalizes in living cells, can be easily localized therein at two different imaging zone by optical microscopy techniques, exhibits a good biocompatibility in the dark, release both $^1O_2$ and NO independently under the exclusive control of visible light stimuli and, as result, induces an appreciable level of amplified photomortality in tumor cell lines. Here the photosensitizer **2** disaggregates and organizes themself inside the hydrophobic interiors of the CD-based polymer and in the native CD cavities through benzene sulfonate appendage[10] and the NO the photodonor **3** gets anchored on the CD NPs through the NBF appendage owing to the facile binding inclusion of the former with native CD pockets[11] (Scheme 7.1).

7.2 Experimental

7.2.1 Materials

A) CD-based polymer

The CD-based polymer (**1**) is obtained from Dr. Ruxandra Gref, Faculty of Pharmcay, CNRS, University of South-Paris, France, and used as such with out further purification.

B) Zinc Phthalocyaninetetrasulfonate

The macrocyclic Zinc phthalocyanineterasulfonate was directly purchased from Porphyrin Pdts. and used as such with out further purification.

All other reagents were of highest commercial grade available and used without further purification. All solvent used (from Carlo Erba) were analytical grade.

7.2.2 Synthesis of NBF- NO photodonor

4-(N-(aminopropyl)-3-(trifluoromethyl)-4-nitrobenzenamine)-7-nitrobenzofurazan (II) was synthesized in a two step synthesis as reported in Scheme 7.2. Syntheses were carried out under a low intensity level of visible light.

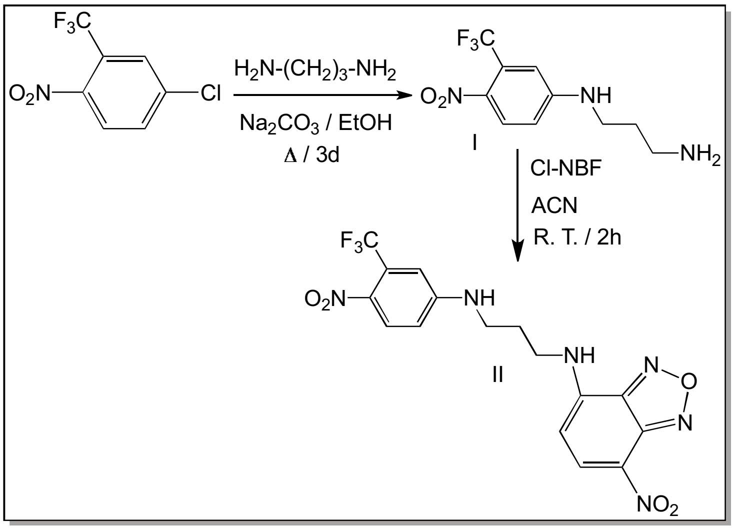

Scheme 7.2. Scheme showing the synthetic procedure of II.

The N-(aminopropyl)-3-(trifluoromethyl)-4-nitrobenzenamine **I** (200 mg, 0.8 mmol, 1 eq.) obtained as previously described[12] was solubilized in 10 mL of acetonitrile and the 4-chloro-7-nitrobenzofurazan (184 mg, 0.9 mmol, 1.1 eq.) in solution in 4 mL of acetonitrile was added to this solution. Although the starting compound was not fully converted, the reaction was stopped after 2 h of stirring at r.t. to avoid the formation of undesirable side products. The organic solution was concentrated under reduced pressure and purified by column chromatography over silica gel (chloroform:methanol, 99:1) to give **II** (yield 15 %, 50 mg) as a orange solid. ^{1}H-NMR CD_3CN: δ 2.07 (2H, qt, $^3J_{H\text{-}H}$= 6.5 Hz, $NHCH_2C\underline{H_2}CH_2NH$), 3.37 (2H, dt, $^3J_{H\text{-}H}$= 6.5 Hz, $C\underline{H_2}NHC_6H_3NO_2CF_3$), 3.64 (2H, m, $C\underline{H_2}$NH-NBF), 5.90 (1H, s broad, N$\underline{H}$ $C_6H_3NO_2CF_3$), 6.31 (1H, d, $^3J_{H\text{-}H}$ = 9.0 Hz, $C_{Ar}H$ (NBF)), 6.78 (1H, dd, $^3J_{H\text{-}H}$= 9.0 Hz, $^4J_{H\text{-}H}$= 2.5 Hz, $C_{Ar}H$), 6.99 (1H, d, $^4J_{H\text{-}H}$ = 2.5 Hz, $C_{Ar}H$), 7.44 (N$\underline{H}$(NBF),1H, s broad), 7.99 (1H, d, $^3J_{H\text{-}H}$ = 9.0 Hz, $C_{Ar}H$), 8.48 (1H, d, $^3J_{H\text{-}H}$ = 9.0 Hz, $C_{Ar}H$ (NBF).

^{13}C-NMR CD_3CN: δ 28, 41, 42, 99, 112, 113, 122, 130, 135, 138, 145, 154, With

^{1}H-NMR CD_3CN: δ 2.07 (2H, qt, $^3J_{H\text{-}H}$= 6.5 Hz, 9), 3.37 (2H, dt, $^3J_{H\text{-}H}$= 6.5 Hz, 10), 3.64 (2H, m, 8), 5.90 (1H, s broad, N$\underline{H}$ $C_6H_3NO_2CF_3$), 6.31 (1H, d, $^3J_{H\text{-}H}$= 9.0 Hz, 5), 6.78 (1H, dd, $^3J_{H\text{-}H}$= 9.0 Hz, $^4J_{H\text{-}H}$= 2.5 Hz, 16), 6.99 (1H, d, $^4J_{H\text{-}H}$= 2.5 Hz, 11), 7.44 (1H, s broad, N$\underline{H}$(NBF), 7.99 (1H, d, $^3J_{H\text{-}H}$= 9.0 Hz, 15), 8.48 (1H, d, $^3J_{H\text{-}H}$= 9.0 Hz, 6).

^{13}C-NMR CD_3CN: δ 28 (9), 41 (10), 42 (8), 99 (5), 112 (11), 113 (15), 122 (NBF), 130 (14), 135 (nitroaniline), 138 (6), 145 (NBF), 154 (11).

7.3 Instrumentation

UV/Vis. absorption and fluorescence spectra were recorded with a HP-8452 diode array spectrophotometer and Fluorolog-2 (Model, F-111) spectrofluorimeter respectively. Nanoparticle sizes were measured by a dynamic light scattering Horiba LS 550 apparatus equipped with a diode laser, working at the wavelength of 650 nm. Two-photon fluorescence images were recorded using LSM 710 NLO microscope (Carl Zeiss, Jena, Germany) equipped with mode-locked femtosecond pulsed *Mai Tai Deep See* laser. Microscope was equipped with a Plan-Apochromat 20x water immersion objective (NA 1.0) (Carl Zeiss, Jena, Germany). Laser light intensity at the sample, was approximately 15 mW. Fluorescence images were taken with a Biomed fluorescence microscope (Leitz, Wetzlar, Germany). Photolysis experiments were performed in a thermostated quartz cell (1 cm pathlength, 3 mL capacity) by using a Rayonet photochemical reactor equipped with 8 RPR lamps with an emission in the 380-480 nm range with a maximum at 420 nm in the presence of a 400 nm cut-off filter. The incident photon flux on quartz cuvettes was ca. 0.8 x 10^{15} quanta sec^{-1}.

Fluorescence imaging was performed on an inverted Nikon A1 laser scanning confocal fluorescence microscope equipped with a 405 nm pulsed/CW diode laser (Picoquant, Germany), a 488 nm CW Argon ion laser (Melles Griot) and a 640 nm CW red diode laser (Melles Griot). Confocal fluorescence imaging was carried out on the samples at 20°C. The 512x512 or 1024x1024 pixel images were collected using a Nikon PLAN APO VC 60 oil immersion objective with NA 1.40. With this imaging configuration, pixel side dimension ranged from 100 to 400 nm. Fluorescence was collected in several spectral windows. In front of the photomultiplier we used bandpass filters centered at 450 nm (50), 525 nm (50) and 700 nm (70). Spectral imaging has been performed using the Nikon A1 spectral detector consisting of a multi-anode photomultiplier with an array of 32 anodes. A wavelength range of 6 or 10 nm per anode has been applied.

7.3.1 Laser flash photolysis

The same instrumental setup used for the transient absorption spectra and transient decay kinetics in the previous experiment (Chapter 6) is also used here and all experimental procedure was followed as before.

7.3.2 NO detection

NO release was measured based on the protocol reported in Chapter 3.

7.4 Sample preparation

The methods of sample preparation were similar to Chapter 6. The cell culture experiments are detailed below.

7.4.1 Experiments with cells

A431 cells prepared for imaging studies was similar to that explained in Chapter 3. A375 human melanoma cell line was obtained from American Type Culture Collection (Rockville, MD, USA) and was maintained in Dulbecco's modified Eagle's medium (DMEM) containing 10 % fetal calf serum (FCS), 2.0 mM L-glutamine, 100 U/mL penicillin, 100 lg/mL streptomycin, and 25 lg/mL fungizone (Sigma–Aldrich, Italy), and incubated at 37°C and 5 % CO_2/ 95 % air. Cells from confluent cultures were detached using 0.25 % trypsin– 1 mM EDTA and seeded in complete DMEM medium.

For cell staining, the experimental cells were cultured in a 12 well culture dishes for 24 hours. The medium was removed and replaced with medium without phenol red containing the dispersion of **2** with for 12 hours. The cells were first washed with PBS, and then fixed with 4 % paraformaldehyde in PBS for 20 min. Cells after washing with PBS were incubated with 4-6-diamino-2-phenylindole (DAPI) (1:10,000; Invitrogen) for 10 min.

Cell proliferation was tested by MTT assay, based on the conversion by mitochondrial dehydrogenases of a substrate containing a tetrazolium ring into blue formazan, detectable spectrophotometrically. Briefly, cells were seeded at an initial density of 8×10^3 cells/microwell in flat-bottomed 200 µl microplates, incubated at 37°C in a humidified atmosphere containing 5 % CO_2 for 24 hours. After this time, some cells, as a control, were incubated in complete DMEM without phenol red. Some cells were incubated with complete DMEM without phenol red containing the polymer nanoparticles, 4 hours before the end of the treatment time, 20 µl of 0.5 % 3-(4,5-dimethyl-thiazol-2-yl)2,5-diphenyltetrazolium bromide in PBS were added to each microwell. After 4 h of incubation at 37°C, the supernatant was removed and replaced with 100 μl of DMSO. The optical density of each well sample was measured with a microplate spectrophotometer reader (Digital and Analog Systems, Rome, Italy) at 550 nm. The cell viability (%) was calculated according to the following equation:

$$\text{Cell Viability (\%)} = [A_{\text{Before}} - (A_{\text{After}} / A_{\text{Before}})] \times 100$$

where, A_{Before} and A_{After} are the absorbance values of the wells treated with samplesbefore and after irradiation respectively. The cell mortality (%) was the complement of cell viability.

7.5 Results and Discussion

The photosensitizer **2** is soluble in phosphate buffer with the propensity of strong aggregation; make them silent for the photodynamic actions (a in Figure 7.1).

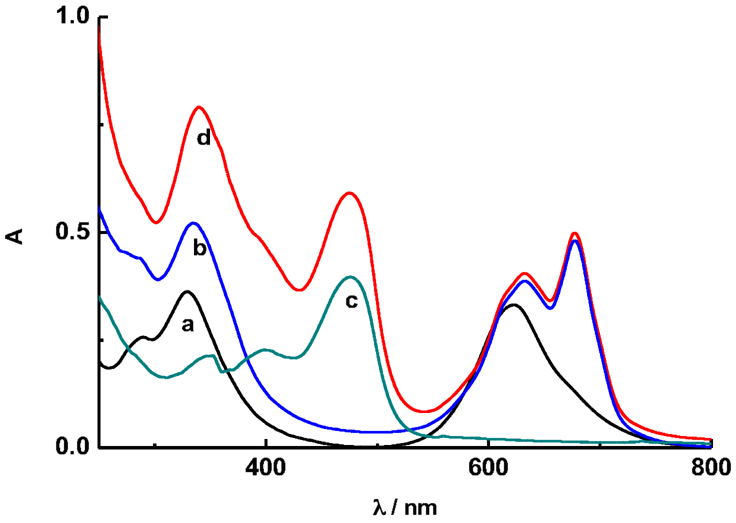

Figure 7.1. The steady state absorption spectra of **2** (in phosphate buffer, 10 mM, pH 7.4) in the absence (a) and in the presence (b) of **1**, **3** in the presence of **1** (c), bichromophoric mixture of **2** + **3** in the presence of **1** (d). [**1**]= 12 μM, [**2**]= 5 μM, [**3**]= 40 μM, T= 25°C, cell path length= 1 cm.

However compound **2** undergo clear disaggregation upon interaction with the CD-based polymer **1** with the appearance of new Q band at the 680 nm, which represent the monomeric form of **2**, along with feeble band at 635 nm representing the aggregated structure (b in Figure 7.1).[13] It is to be noted that monomeric form of the compound **2** is responsible for photosensitization actions as explained in the previous chapter. The conjugate compound **3** as such is not soluble in water but readily soluble in the aqueous dispersion of **1** as revealed from the appearance of absorption band with maximum peak position at 475 nm (c in Figure 7.1). In addition the absorption spectra shows a peak around 400 nm and small bands below 400 nm. All these bands signify the covalent conjugation of nitrobenzofurazan moiety with NO releasing nitroaniline chromophore as the latter absorb at 400 nm in polymer media. Whereas all the absorption features of both **2** and **3** is retained in the bichromophoric NPs as the absorption spectra shows main peaks at 680 nm and 475 nm, representing the disaggregated **2** and loaded **3** in the extended polymer networks. In addition spectra (d in Figure 7.1) is exactly overlapping with absorption peak position while only single chromophore get encompassed in **1**, validating the independent photochemical features and absence of any detrimental interaction between each probe at the ground state.

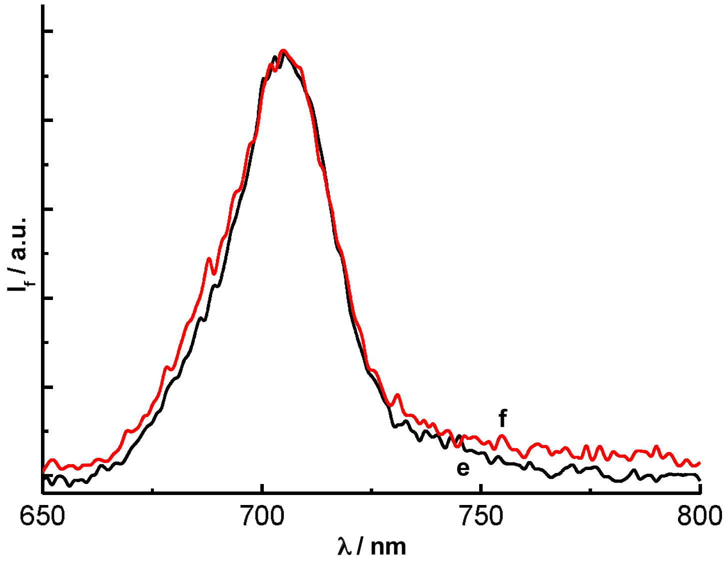

Figure 7.2. Fluorescence emission spectra (λ_{exc}= 575 nm) of **2/1** in the presence (e) and absence (f) of **3**.

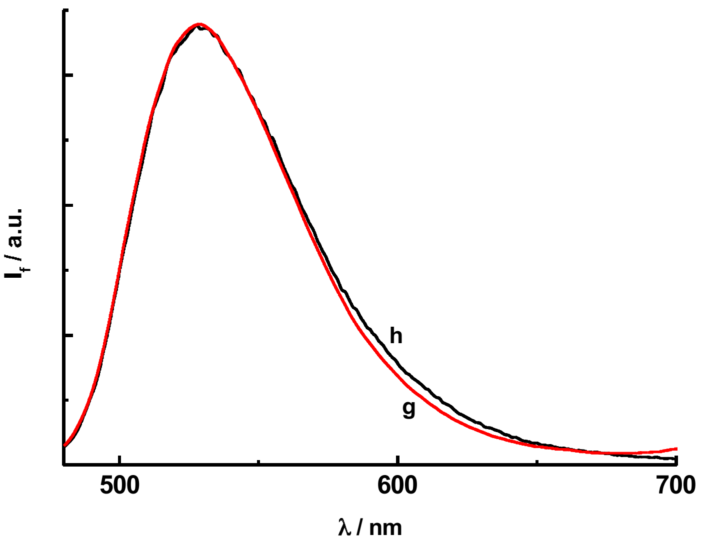

Figure 7.3. Fluorescence emission spectra (λ_{exc}= 470 nm) of **3/1** in the presence (g) and absence (h) of **2**.

The fluorescence spectrum of compound **2** shows emission maxima at 704 nm in polymer **1** and remains unaltered in the presence and in the absence of **3** (Figure 7.2). Whereas the compound **2** was very weakly fluorescent in phosphate buffer. The fluorescence enhancement upon interaction with **1** shows the disaggregated structures of compound **2** and its consequent radiative processes. At the same time, the compound **3** incorporated in **1** shows the emission with high quantum yield, characteristic to nitrobenzofurazan moiety, and demonstrate that the conjugation of latter with NO releasing nitroaniline chromophore does not impede its emissive property (Figure 7.3). In fact the fluorescent emission peak position of **3** is exactly retained in the bichromophoric ensemble ruling out any sort of interaction between **2** and **3** in the excited state. Moreover the excitation spectra of the compound **3** measured in presence of **2** in the polymeric NPs was exactly same as the steady state absorption spectra of **3** at the same environment (data is not included), asserting the lack of any quenching with **2** at the excited state.

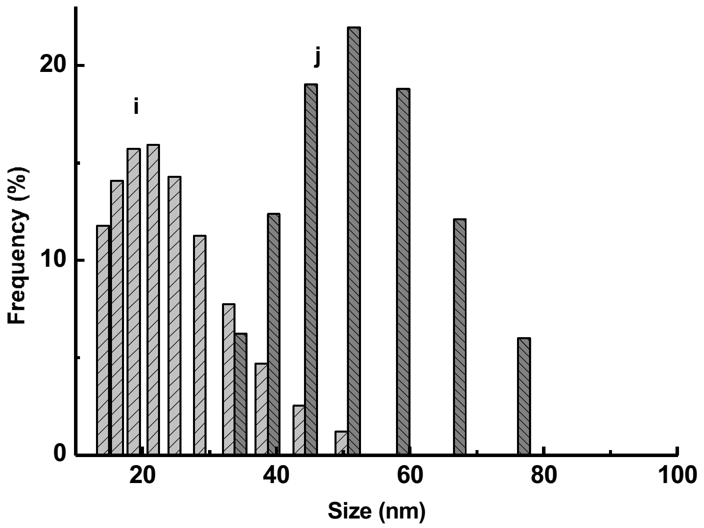

Figure 7.4. The size distribution polymeric NPs (in phosphate buffer, 10mM, pH 7.4) in the absence (i) and presence (j) of both **2** and **3**, obtained by DLS.

The hydrodynamic diameter of the ensemble that was measured by DLS instrument shows favorable nanometric size of the ensemble where the size of the polymeric NPs varies from 25 to 45 nm in the absence and in the presence of both **2** and **3** respectively (i and j in Figure 7.4).

The supramolecular ensemble incorporated with both **2** and **3** was simply irradiated with the light of 400 nm to understand the NO photoactions from the covalent conjugate **3** and traced by steady state absorption spectrum (Figure 7.5).

The absorption spectra show significant bleaching of the band below 430 nm where the nitroaniline chromophore of the covalent conjugate **3** absorbs.

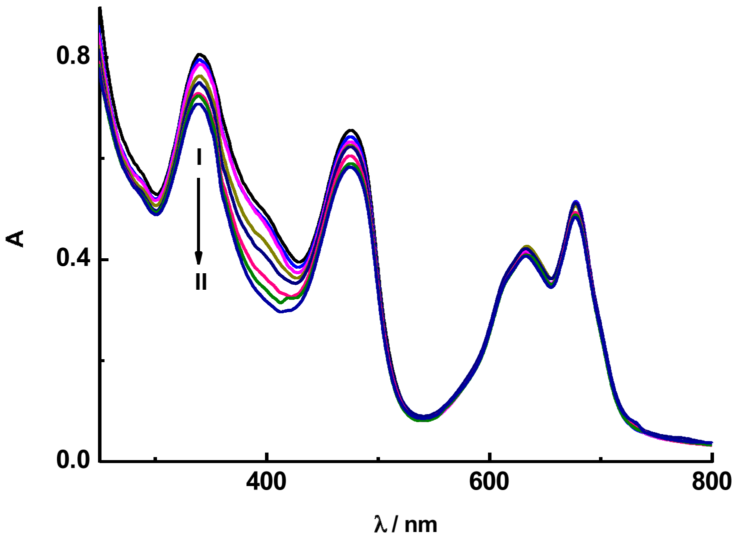

Figure 7.5. Absorption spectra of bichromophoric NPs (**2**+**3**/**1**) in phosphate buffer (10 mM, T= 25°C, pH 7.4) before (**I**) and after (**II**) 40 min of 400 nm light irradiation.

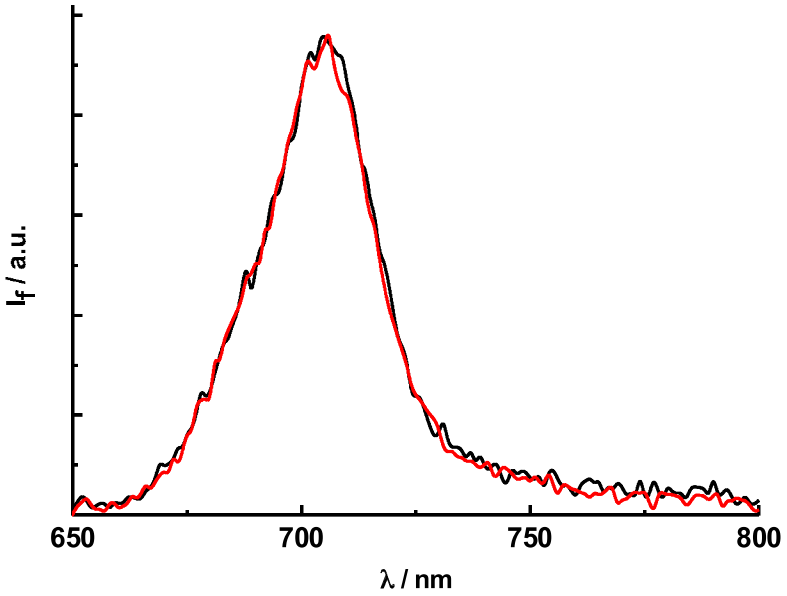

Figure 7.6. Fluorescence emission spectra of **2** in bichromophoric supramolecular complex before and after photolysis (λ_{exc}= 575 nm).

However the extend of photobleaching is in consistent with the irradiation of an optically matched solution of the same nitroaniline chromophore alone in the polymer,[14] pointing out the merge of both NO photoactions and fluorescence emission capabilities independently each other in the same covalent conjugate. It be observed from the absorption spectra that the compound **2** is not influenced by the photoirradiation and consequent bleaching of **3** albeit little variation in the peak position during the course of illumination (Figure 7.5). In addition the emission profile of **2** were also not affected by the course of photoirradiation (Figure 7.6). The little, beneficial increase over the fluorescence intensity of **3** after 30 minute photolysis (Figure 7.7) might be due to feeble uncaging effect of the fluorophore NBF from the nitroaniline and consequent changes in visco-elastic parameters of fluorophore moiety [15] or the much more organized orientation of the former with the photoproduct, phenol, in the CD networks.[16] Though the research in that direction was not studied in detail and presently out of current topic of discussion.

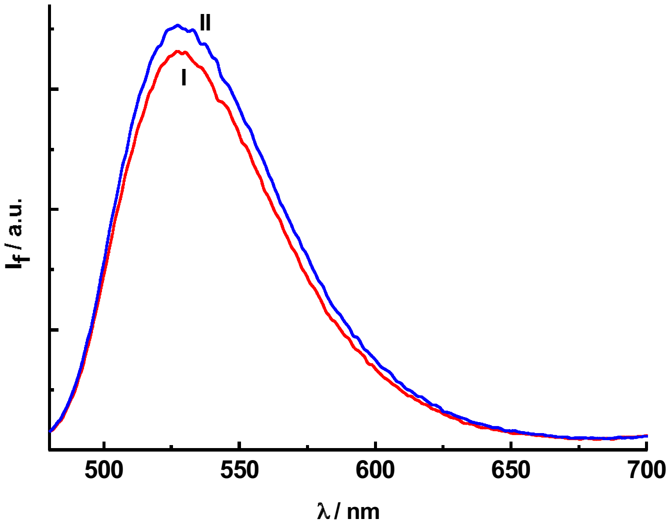

Figure 7.7. Fluorescence emission spectra of **3** in bichromophoric supramolecular complex before and after photolysis (λ_{exc}= 470 nm).

The photodynamic actions of photosensitizer **2** have been studied in detail to understand $^1O_2$ photosensitization. The laser flash photolysis experiment performed on the bichromophoric NPs reveals efficient generation of triplet transient characteristic to the compound **2** (see Chapter 6 for detailed disaggregation studies of compound **2**) Here the transient absorption is exactly proportional to the quantum yield of triplet state since the solutions of photosensitizer **2** in **1** and bichromophoric mixture of both **2** and **3** in **1** are optically matched at the excitation wavelength.[17] The slope of the spectra, that is plotted as respective transient triplet of compound **2** as a function of laser intensity (Figure 7.8), is the direct measure of triplet state quantum yield. The concurrent presence of **3** does not influence the transient triplet of **2** as revealed by the same value of slope of both solutions of **2** in the absence and in the presence of **3** (Figure 7.8).

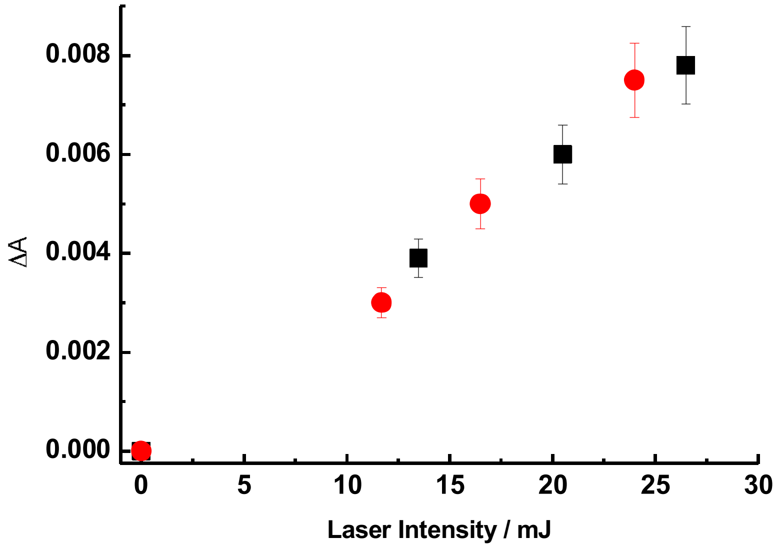

Figure 7.8. Laser intensity dependence of the absorbance changes, ΔA, taken 0.1 µs after 532 nm laser pulse excitation of **2** (5µM).

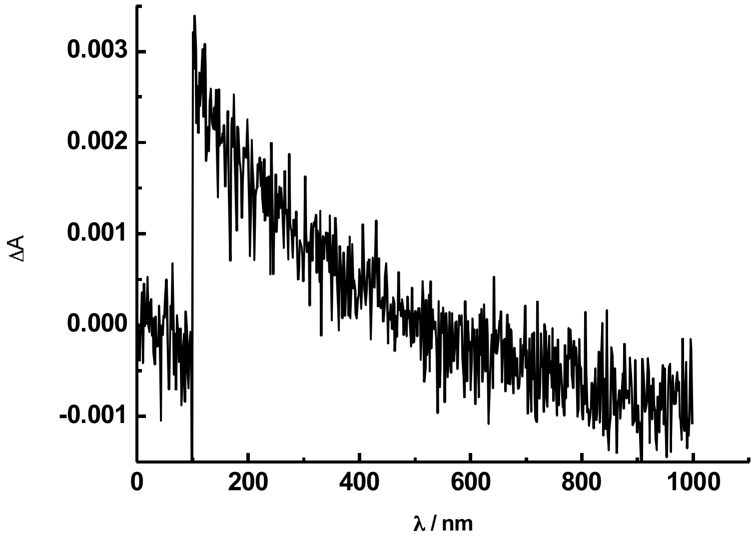

Figure 7.9. Kinetic decay trace of excited triplet state of **2** monitored at 500 nm. E_{532}~ 9.8 mJ/pulse. Phosphate buffer (10 mM, pH 7.4), [**1**] = 12 μM, [**2**] = 5 μM, [**3**] = 40 μM, T= 25°C.

The triplet transient of **2** measured by laser flash photolysis shows the kinetic decay in line to the finding of independent existence of triplet **2** (Figure 7.9). The single exponential decay curve illustrates the absence of any potential quenchers at excited triplet state of **2.**

The photostimulated NO release from the conjugate **3** was quantitatively analyzed by using an ultrasensitive NO electrode, which works on the principles of an amperometric technique and detect NO release at nanomolar resolution. The linear generation of amperogram upon illumination with light of 400 nm and totally mute in dark shows indubitable control over the NO release and dark stability of the entire system (Figure 7.10).

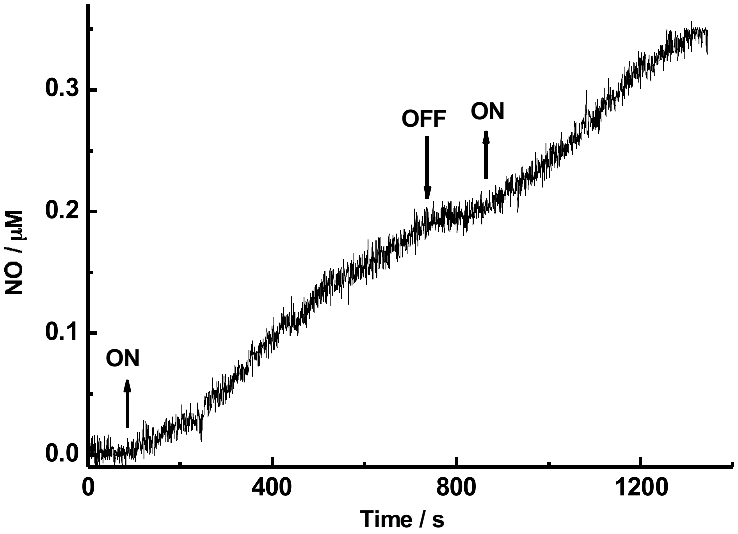

Figure 7.10. Amperogram of bichromophoric NPs (**2+3/1**) showing the release of NO upon illumination with the light of 400 nm through multiple ON-OFF switching in phosphate buffer (10 mM, pH 7.4), [**1**]= 12 µM, [**2**]= 5 µM, [**3**]= 40 µM, T= 25°C.

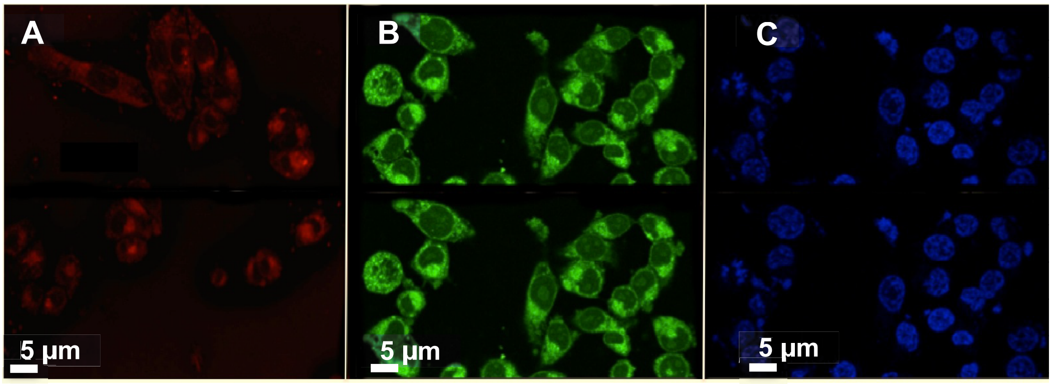

Figure 7.11. Fluorescence confocal imaging of A375 human melanoma cell line incubated with the complex **2+3/1** (*ca.* 10 µM) in 10 mM phosphate buffer (pH 7.4). The assembly mapped at the (A) excitation of 640 nm, detection through red channel and band pass filter centered at 700 nm (± 70 nm), (B) λ_{exc}= 405 nm, detection through the green channel and band pass filter centered at 525 (± 50 nm), (C) λ_{exc}= 405 nm detection through the blue channel and band pass filter centered at 400 nm (± 50 nm).

Suitability of the present system as double modal imaging and therapy agent at cellular environment stimulated us to do cell culture experiments to find their potency in tumor cells. Figure 7.11 shows the imaging of human melanoma cells after the incubation with bichromophoric ensemble for 4 hours at physiological pH and monitored by confocal microscopy techniques. The cell nucleus was stained with DAPY to understand the colocalization of the probe at the cell interiors (C in Figure 7.11). Here the intake of the entire NP ensemble was clearly visible from the significant amount fluorescence emission from two fluorphore, where compound **2** is emissive in red region (A in Figure 7.11) and the fluorophore **3** brightly emit green fluorescence (B in Figure 7.11). The emission profile of two fluorophore in the cells can be switch simply between each other just by changing the excitation wavelength or changing the filter, as both probes are co-entrapped in tandem with polymeric NPs. The emission profile signifies the localization of both probes at cytoplasmic level, though their mechanism of localization might be different and have not studied in details.

The same bichromophoric polymer suspension is imaged in the A431 epidermal tumor cells by two-photon microscopy (Figure 7.12). In fact, we observed higher two-photon excitation cross section in case of compound **3.** The fluorescent images are much more clear and shows that the compound **2** and **3** are clearly intake into the cell at the cytoplasm (A and B in Figure 7.12) and affirming the similar finding of confocal images. Though the co-localization each probe at the cell interior is not studied in detail.

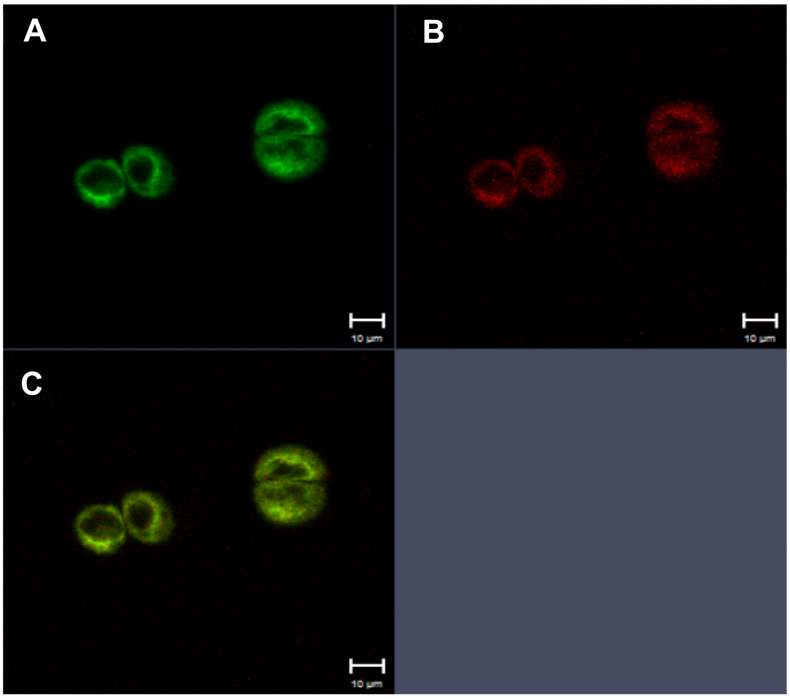

Figure 7.12. The two-photon fluorescence microscopy image of epidermal cancer cell lines (Model No. A431) incubated with the complex **2+3/1** (ca. 10 µM) in 10 mM phosphate buffer (pH 7.4). The assembly mapped at the excitation of 720 nm and the detection A) green channel; band pass filter at 526-618 nm, B) red channel; at the band pass filters of 634-700 nm, C) overlay of all images.

The significant fluorescence emission from the cellular suspension upon excitation of the both fluorescent probe leaves a space to detect their emission spectra in the cells. In this regard we traced the fluorescence emission spectra of the formulation in the cells as shown in Figure 7.13. It can be seen from the figure that the fluorphore **2** in cellular suspension emit with the peak maxima at 698 nm similar to that observed in buffer solution (c and d in Figure 7.14) where as the fluorophore **3** absorb at 560 nm followed by the red shift *ca*. 30 nm with respect to the buffer solution. This can be understand from possibilities of complex binding events between **3** and cellular matrix. In short, the spectrum of both **2** and **3** indubitably proves that red and green fluorescence, which is traced by the microscopy, is invariably generated from the probes incorporated in CD-based NPs.

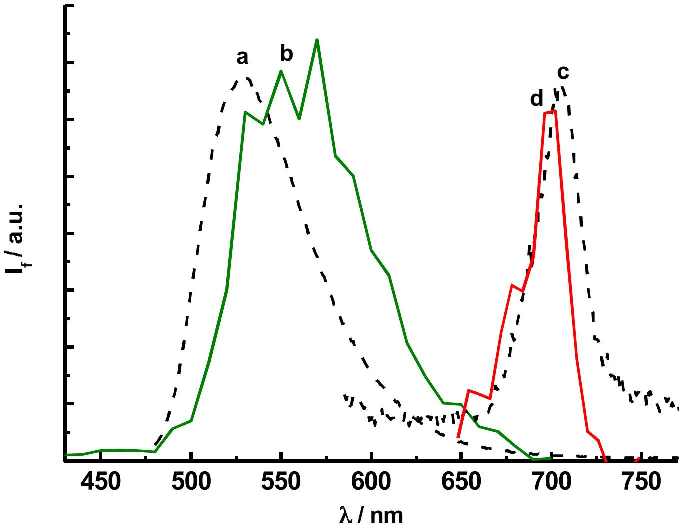

Figure 7.13. The emission spectra of the cell suspension incubated with the bichromophoric mixture **2**+**3**/**1**. The fluorescence emission of **2** in bichromophoric mixture, (a) in buffer solution, (b) in cellular suspension and fluorescence emission of **3** in in bichromophoric mixture (c) in buffer solution, (d) in cellular suspension. I) λ_{exc} =720 nm (two-photon excitation, b), λ_{em}= 420-700 nm, with the unit of 10 nm, II) λ_{exc}= 640 nm and λ_{em}= 400-725 with the cut-off filter at 405-488 nm and 650 nm.

Finally the bimodal therapeutic actions and tumor mortality induced by this multimodal ensemble have been analyzed in A375 human melanoma cancer cell lines and the light induced tumor mortality is displayed in the form of histograms (Figure 7.14). Three different formulations *viz.*, the supramolecular formulation of **2** in polymeric NPs **1**, conjugate **3** in **1** and bichromophoric assembly of both component **2** and **3** in polymeric NPs **1** (a, b, c in Figure 7.14 respectively) have been incubated in tumor cells for 5 hours and the mortality is measured by MTT assay.

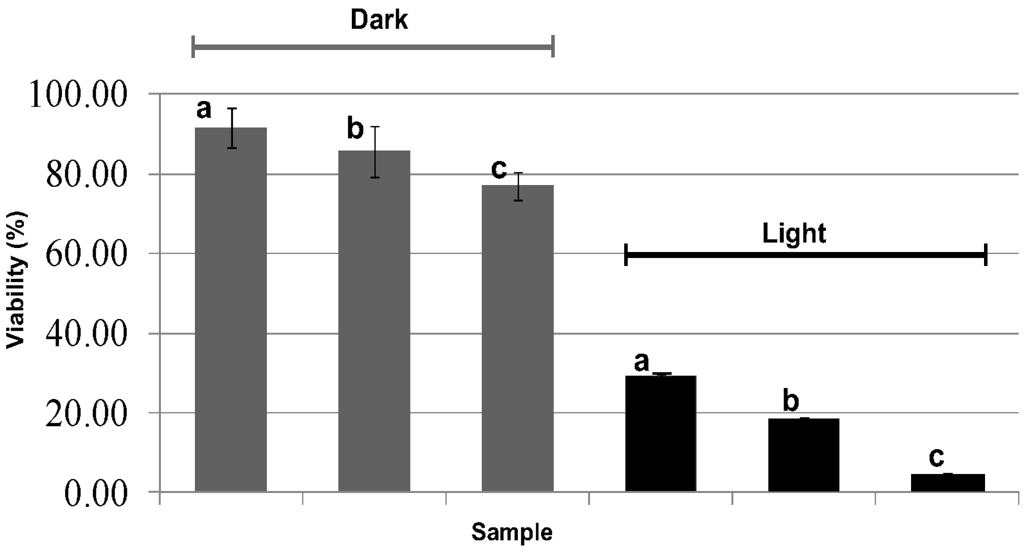

Figure 7.14. Dark and photoinduced mortality (λ_{exc}> 400 nm, t_{irr}= 30 min) of melanoma cells incubated with aqueous dispersions (PBS, pH 7.4, T= 25°C) of polymeric NPs incorporated with photoactive components, a) component **2** entangled in **1**, b) component **3** incorporated in **1**, c) both component **2** and **3** incorporated in **1**. [1]= 12 µM, [2]= 5 µm, [3]= 40 µm.

It is clear from Figure 7.14 that the formulations of CD NPs entrapped with the probe is stable in dark and able to induce good rate of mortality upon photoirradiation. The compound **2** loaded with **1** is attributed to 70 % mortality, whereas the compound **2** with **1** is able induce relatively higher mortality rate owing to multidirectional therapeutic action of NO than $^1O_2$. Remarkable level of mortality rate, more than 95 %, was observed in the case of formulation where both **2** and **3** are encompassed together in polymeric NPs **1**. The results of amplified mortality rate stems from the conjoint actions of both $^1O_2$ and NO released from the bichromophoric assembly.

7.6 Conclusion

A supramolecular nanoensemble incorporated with two different kinds of photoactive species is introduced in view of effective antitumor therapy and diagnosis. The rational design of the drug carrier, a CD-based polymeric nanoensemble, allows the organization and partition of the two probes, a $^1O_2$ photosensitizer and a NO photodonor, within their different regions. The steady state and time resolved spectroscopy characterization results undoubtedly prove the preservation of the photochemical and photodynamic feature of the each photoactive component while entangled alone or together in the CD-based polymeric NPs. Here the NO delivering moiety is covalently tethered to fluorescent molecule so as to trace the fate of NO actions and to have efficient incorporation in CD-based polymer. The direct and real time photorelease of NO from the NO photodonor proves that this strategy does not impede the NO releasing capabilities of the latter. The effective transient triplet generation from the photosensitizer, Zinc phthalocyaninetetrasulphonate, validates the possibility of dual modal actions of both $^1O_2$ and NO at the same bio-site. Finally the therapeutic feasibility of these bichromophoric nanoensemble is studied in human melanoma cells. The imaging of the cells by exploiting green and red fluorescence from both probes attests the localization of the entire ensemble at cytoplasm. The photoinduced mortality imparted by both probe when entangled alone or together in the polymeric NPs demonstrate the validity of the present system for the use in anticancer therapy. The amplified tumor mortality results from combined photoactions of both $^1O_2$ photosensitizer and NO photodonor and ability to locate the ensemble by dual mode fluorescene emission in green and red region, make this nanosytem a powerful arsenal for the antitumor therapy.

7.7 References

1. R. Weissleder, M. J. Pittet, *Nature*, 2008, **452**, 3, DOI:10.1038/nature06917.
2. Y. Li, Y. Yang, X. Guan, *Anal. Chem.*, 2012, **84**, 6877-6883.
3. J. Rohacova, M. L. Marín, A. M. –Romero, L. Diaz, J. –E. O'Connor, M. J. G. –Lechon, M. T. Donato, J. V. Castell, M. A. Miranda, *ChemMedChem*, 2009, **4**, 3, 466–472.
4. S. Uchiyama, K. Takehira, S. Kohtani, K. Imai, R. Nakagaki, S. Tobita, T. Santa, *Org. Biomol. Chem.*, 2003, **1**, 1067–1072.
5. B. Heyne, S. Ahmed, J. C. Scaiano, *Org. Biomol. Chem.*, 2008, **6**, 354–358.
6. T. Suzuki, T. Matsuzaki, H. Hagiwara, T. Aoki, K. Takata, *Acta Histochem. Cytochem.*, 2007, **40**, 5, 131–137.
7. Z. Ignatova, L. M. Gierasch, *Proc. Natl. Acad. Sci. USA*, 2004, **101**, 2, 523–528.
8. S. Jiang, M. K. Gnanasammandhan, Y. Zhang, *J. R. Soc. Interface,* 2010, **7**, 3.
9. J. Woodcock, J. P. Griffin, R. E. Behrman, *New Eng. J. of Med.*, 2011, **364**, 11, 985.
10. See the chapter 6 for the detailed study of binding interactions between Zinc phthalocyanine tetrasulphonate and CD-based polymer.
11. Z. Quan, Y. Song, A. Saulsberry, Y. Sheng, Y. –M. Liu, *J. Chromatogr. Sci.*, 2005, **43**, 121.
12. F. L. Callari, S. Sortino, *Chem. Commun.*, 2008, 1971-1973.
13. All the aggregation and disaggregation chemistry of Zinc phthalocyanine tetrasulphonate is well explained in Chapter 6.
14. E. Deniz, N. Kandoth, A. Fraix, V. Cardile, A. C. E. Graziano, D. L. Furno, R. Gref, F. M. Raymo, S. Sortino, *Chem. Eur. J.*, DOI: 10.1002/chem.201202845.
15. S. Mukherjee, A. Chattopadhyay, A. Samanta, T. Soujanya, *J. Phys. Chem.*, 1994, **98**, 2809-2812.
16. S. Sortino, G. Marconi, G. Condorelli, *Chem. Commun.*, 2001, 1226–1227.
17. S. Sortino, A. Mazzaglia, L. M- Scolaro, F. M. Merlo, V. Valveri, M. Teresa Sciortino, *Biomaterials*, 2006, **27**, 4256–4265.

8

CD-based nanoparticles for super-resolution imaging and therapy

8.1 Introduction

Optical microscopy techniques are well known for non-invasive biological imaging, but they are seriously limited on imaging the cellular environment at sub-micro level due to the abbe diffraction limit pertinent to any light based techniques.[1] The diffraction limit set all the flourophore, closer than 180 nm in focal volume, to be excited together and finally making the image blurred. In addition, these conventional microscopic techniques do not give in depth ideas of cell environment as most of the cell interior and cellular processes are at sub-micro level. Indeed, the imposition of diffraction limit is partly overcome by employing ultra fast laser optical techniques by arbitrarily locating the fluorophore at the single molecular level.[2,3] The advanced laser optical techniques could be avoided to evade the optical diffraction barrier by saturating the fluorophore through fluorescence ON/OFF switching mechanism. The reversible switching event open up a state where only one molecule gives the signal at the focal volume of sub-diffraction resolution and hence eliminate the possibility of all molecules getting excited at focal plane of incident light, which in turn results super-resolution imaging. [4,5] Here the photochromic molecules are more fascinating prospective towards reversible switching mechanism.

Photochromic molecules switch between two distinct states of different absorption spectra and they are inter-convertible each other by inducing with respective input such as electrochemical or thermal stimuli.[6] Recently our group, in collaboration with Prof. F. M. Raymo group at University of Miami, USA, has developed various kinds of the photochromic probe in which the fluorophore is logically integrated with the photochromic switching moiety with in the same molecular skeleton. This novel strategy enables emission of the fluorogenic moiety in synchronization with inter-conversion of the photochromic unit.[7,8] Specifically a fluorophore-photochrome dyad has been synthesized by incorporating coumarin and oxazine fragments within the same molecular skeleton (Figure 8.1). Here the conjugate of two moieties are inter-connected covalently with an alkenyl side chain. The fluorophore-photochromic dyad undergoes switching between nonfluorescent closed structure (**1a** in Figure 8.1) and open fluorescent structure (**1b** in Figure 8.1) in to hundreds of cycle with out any fatigue.[8] With the ongoing interest of having the photochromic switch to probe the biological environment, the present fluorophore-photochromic dyad was made soluble in the hydrophobic interior of polymeric micelles though they are not inherently aqueous soluble.[9,10] The resulting supramolecular assemblies can be dispersed in aqueous media and imaged with sub-diffraction resolution.

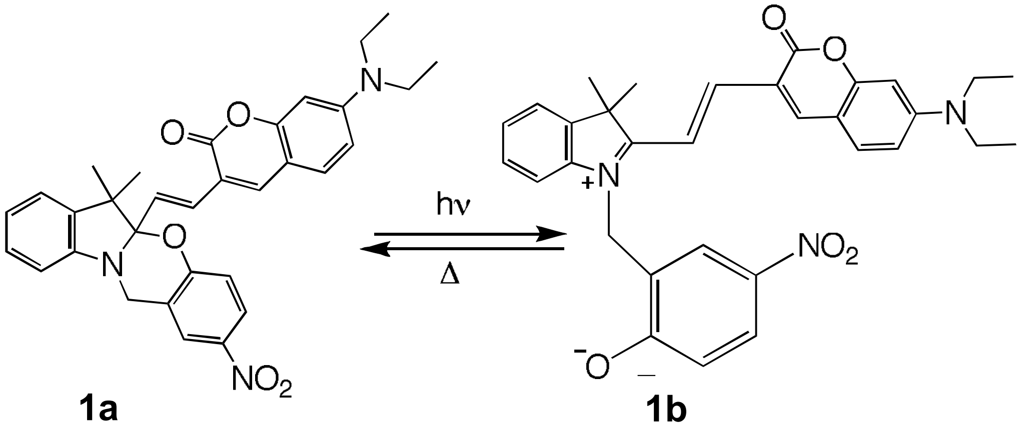

Figure 8.1. Photoinduced and reversible interconversion of closed (**1a**) and open structure (**1b**).

In fact, the micellar host protects the switchable guests from the aqueous environment and preserves their photochemical and photophysical properties, enabling the photoinduced activation of their fluorescence.

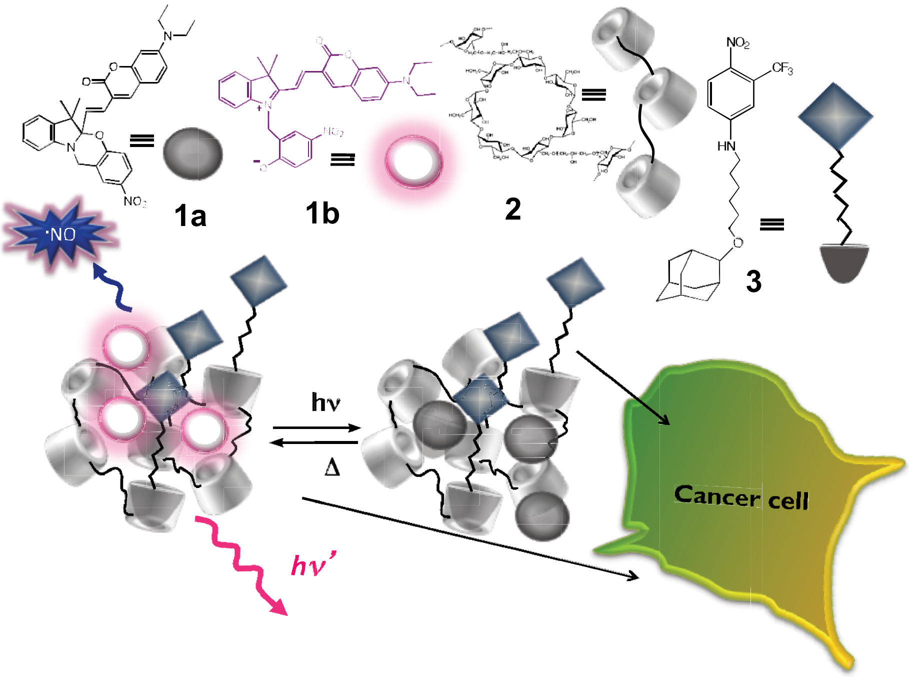

Scheme 8.1. The schematic representation of the design and construction of supramolecular assembly for simultaneous imaging and therapy.

The opportunity afforded by assembling NO releasing capacities with the probe that can dynamically detect the NO bio-site upon photoinduced activation of fluorescence at nanolevel open up a multidirectional perspective towards the anticancer treatments. On this context, the present effort is to make a supramolecular assembly by incorporating three dufferent units *viz.*, CD based polymeric NPs, the flouorophore-photochromic dyad and NO releasing photodonor (Scheme 8.1). Organizing two photoactive centers in the same supramolecular ensemble allows the simultaneous photoinduced fluorescence imaging in parallel to NO photoactions with matching light trigger.

8.2 Experimental

8.2.1. Materials and methods

Compounds **1a/b** was prepared according to literature procedures.[11, 12] The compound **3** is prepared as reported before in the previous chapters. All solvents used (from Carlo Erba) were analytical grade. Phosphate buffer saline (PBS 10 mM, pH 7.4) was prepared with biological grade reagents and all solutions were prepared with nanopure water (grade 18 MΩ).

8.3 Instrumentation

The spectroscopic and photochemical set up used for the steady state absorption and emission spectra are same as experimental part written in previous chapters.

8.3.1 Laser flash photolysis

All samples were excited with the third harmonic of Nd–YAG Continuum Surelite II–10 laser (355 nm, 6 ns FWHM), using quartz cells with a path length of 1.0 cm. The excited solutions were analyzed with a Luzchem Research mLFP–111 apparatus with an orthogonal pump–probe configuration. The probe source was a ceramic xenon lamp coupled to quartz fiber-optic cables. The laser pulse and the mLFP–111 system were synchronized by a Tektronix TDS 3032 digitizer, operating in pre-trigger mode. The signals from a compact Hamamatsu photomultiplier were initially captured by the digitizer and then transferred to a personal computer, controlled by Luzchem Research software operating in the National Instruments LabView 5.1 environment. The sample temperature was 295±2 K. The energy of the laser pulse was measured at each shot with a

SPHD25 Scientech pyroelectric meter. For fluorescence measurements, the laser was operated simultaneously at 355 and 532 nm.

8.4 Samples preparation

Compounds **1a** and **3** were dissolved in acetonitrile and slowly evaporated to form a thin film. These films were then hydrated with an aqueous solution of **3** in phosphate buffer at a pH of 7.4. The mixtures were stirred for 5 hours at 40°C and then the final solutions were left to equilibrate at room temperature.

8.4.1 Experiments with cells

A375 human melanoma cell line was obtained from American Type Culture Collection (Rockville, MD, USA) and was maintained in Dulbecco's modified Eagle's medium (DMEM) containing 10 % fetal calf serum (FCS), 2.0 mM L-glutamine, 100 U/mL penicillin, 100 lg/mL streptomycin, and 25 lg/mL fungizone (Sigma–Aldrich, Italy), and incubated at 37°C and 5 % CO_2/ 95 % air. Cells from confluent cultures were detached using 0.25 % trypsin– 1 mM EDTA and seeded in complete DMEM medium.

For cell staining, the experimental cells were cultured in a 12-well culture dishes for 24 hours. The medium was removed and replaced with medium without phenol red containing the dispersion of **2** for 12 hours. The cells were first washed with PBS, and then fixed with 4 % paraformaldehyde in PBS for 20 min. Cells after washing with PBS were incubated with 4-6-diamino-2-phenylindole (DAPI) (1:10,000; Invitrogen) for 10 min.

Cell proliferation was tested by MTT assay, based on the conversion by mitochondrial dehydrogenases of a substrate containing a tetrazolium ring into blue formazan, detectable spectrophotometrically. Briefly, cells were seeded at an initial density of 8×10^3 cells / microwell in flat-bottomed 200 µl microplates, incubated at 37 °C in a humidified atmosphere containing 5 % CO_2 for 24 hours.

After this time, some cells, as a control, were incubated in complete DMEM without phenol red. Some cells were incubated with complete DMEM without phenol red containing the polymer nanoparticles. 4 hours before the end of the treatment time, 20 μl of 0.5 % 3-(4,5-dimethyl-thiazol-2-yl)2,5-diphenyl-tetrazolium bromide in phosphate buffer were added to each microwell. After 4 h of incubation at 37°C, the supernatant was removed and replaced with 100 μl of DMSO. The optical density of each well sample was measured with a microplate spectrophotometer reader (Digital and Analog Systems, Rome, Italy) at 550 nm. The cell viability (%) was calculated according to the following equation:

$$\text{Cell Viability } (\%) = [A_{\text{Before}} - (A_{\text{After}} / A_{\text{Before}})] \times 100$$

Where, A_{Before} and A_{After} are the absorbance values of the wells treated with samples before and after irradiation respectively. The cell mortality (%) was the complement of cell viability.

8.5 Results and Discussion

The NO photodonor and fluorophore-photochromic dyad are only sparingly soluble in water and become readily soluble in CD based polymer **2** solution.[12,13] The supramolecular complex of **3**/**2** absorbs at 400 nm (b in Figure 8.2) and the complex **1a**/**2** have the characteristic absorption of peak position at 450 nm (a in Figure 8.2).

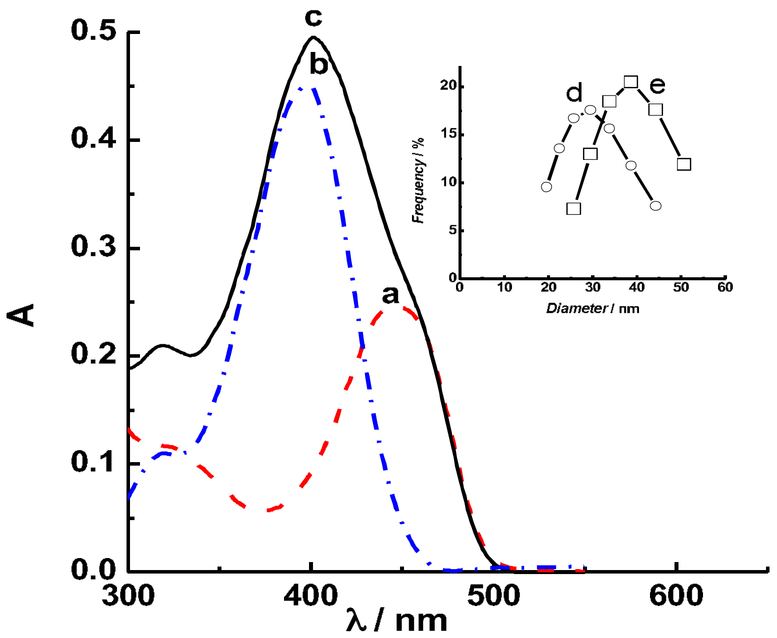

Figure 8.2. Absorption spectra of aqueous dispersions (PBS, pH 7.4, 25°C) of **2** in the presence ofcompound **1a** (**a**), **3** (**b**) and **1a** + **3** (**c**). The inset shows the hydrodynamic diameter for aqueous dispersions of **2** in the absence (**d**) and in the presence of both **1a** and **3** (**e**). [**1a**/**b**]= 8.5 μM, [**2**]= 6 mg mL^{-1}, [**3**]= 45 μM.

The characteristic absorption of both **1a** and **3** is remaining unchanged while they incorporates together in the CD based polymer assembly (**c** in Figure 8.2), revealing the preservation of their photochemical property at the ground state. This is not trivial in the photochemical studies as the undesirable events such as energy or electron transfer between two encompassed chromophores could be detrimental towards the final application.[14]

The dynamic light scattering measurement was used to analyze the hydrodynamic diameter of CD-based ensemble in the presence and absence of both guest and found to be less than 40 nm (Inset Figure 8.2), accounting the validity of using entire system at the biological environment.

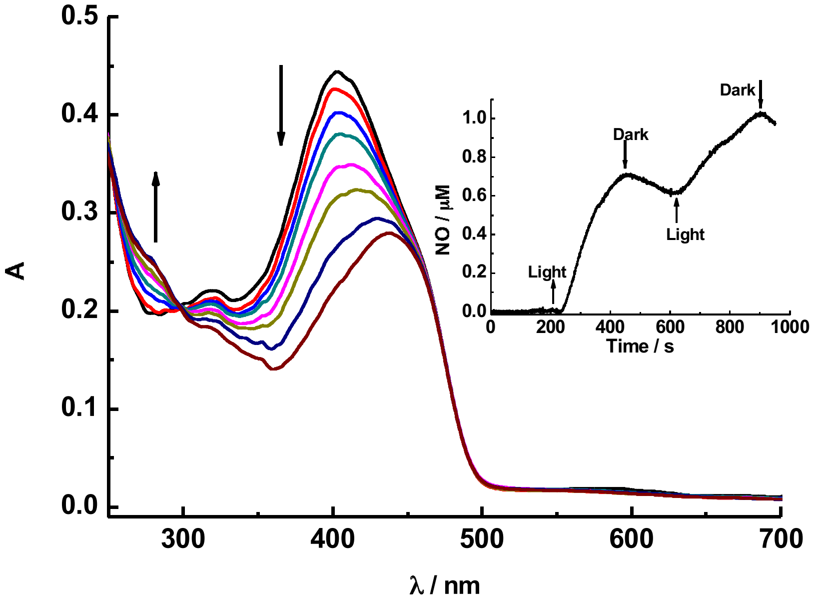

Figure 8.3. Absorption spectral changes observed upon irradiation of an aqueous dispersion (PBS 10 mM, pH 7.4, 25°C) of **2** in the presence of **1a** and **3** at 400 nm, from 0 min to 38 min (the arrows indicate the spectral evolution with irradiation time). The inset shows a representative NO release profile, observed upon alternate illumination periods, under identical experimental conditions as above. [**1a**/**b**]= 8 µM, [**2**]= 6 mg/mL, [**3**]= 40 µM.

The photoirradiation of the supramolecular ensemble of both **1a** and **3** with the respective light source of 400 nm results the bleaching of the characteristic absorption band of **3** followed by the decrease in absorbance (Figure 8.3). This in consequence with native NO photorelease from the nitroaniline chromophore upon matching light trigger.[15,16] The spectra reveals that the NO photorelease and respective bleaching do not influence on the photochemical features of **1a** as its absorption band remain unaffected during course of photoirradiation (Figure 8.3). The direct and real time measurement of NO gives the quantitative evidence of NO photorelease. In this regard, we used an ultra sensitive electrode that detects NO amperometrically at nanomolar resolution. The inset in Figure 8.3 gives the unambiguous evidence of real time NO release. The corresponding amperogram demonstrates that the supramolecular ensemble is ineffective to release NO in dark but promptly generate NO upon matching light inputs. Moreover all this processes solely depend on the photochemistry of nitroaniline chromophore.

Illumination of the very same dispersion with a pulsed laser operating at 355 nm induces the opening of the oxazine ring of **1a** within the duration of pulse (6 ns). This structural transformation brings the coumarin appendage in conjugation with the indolium cation of the photogenerated zwitterionic isomer **1b**. As a result, the band (a in Figure 8.4) for this extended chromophoric fragment appears in the visible region of the absorption spectrum recorded 0.1 μs after illumination. Simultaneous irradiation at 532 nm excites the photogenerated chromophore with concomitant fluorescence (b in Figure 8.4). Furthermore, no emission is observed if the sample is illuminated exclusively at 532 nm (c in Figure 8.4), demonstrating that the pulse at 355 nm is essential to open the oxazine ring and activate fluorescence.

The photogenerated isomer **1b** reverts spontaneously back to **1a** in microsecond timescale. Consistently, the absorbance of the extended 3*H*-indolium cation decays monoexponentially. Curve fitting of the resulting temporal absorbance profile (d in Figure 8.4) indicates the lifetime of **1b** to be *ca.* 0.3 μs. Thus, this particular system can be switched back and forth between its non-emissive state,

1a and fluorescent one **1b** simply by turning on and off a laser source operating at 355 nm.

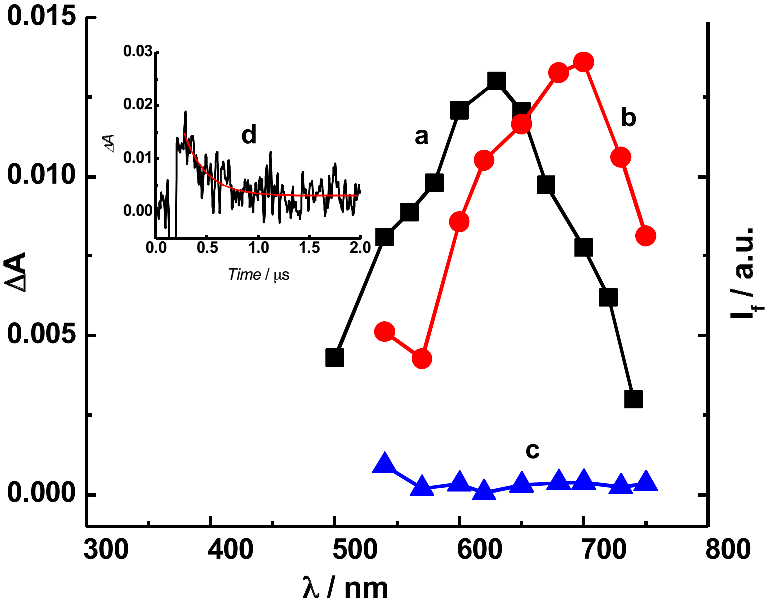

Figure 8.4. Transient absorption spectrum (**a**) of an aqueous dispersion (PBS, pH 7.4, 25°C) of **2** in the presence of **1a** and **3** recorded 0.1 μs after illumination at 355 nm with a pulsed laser (6 ns, 12 mJ/pulse) and the corresponding absorbance decay with related first-order fitting (**d**). Emission spectra of the same dispersion recorded upon illumination with a pulsed laser operating at 532 nm (6 ns, 10 mJ/pulse) with (**b**) and without (**c**) a simultaneous pulse at 355 nm (6 ns, 20 mJ/pulse). [**1a**/**b**]= 8 μM, [**2**]= 6 mg mL^{-1}, [**3**]= 40 μM.

In fact, the fluorescence of this fluorophore–photochromic dyad can be modulated for multiple cycles (Figure 8.5) under the influence of a pair of lasers operating at 355 and 532 nm.

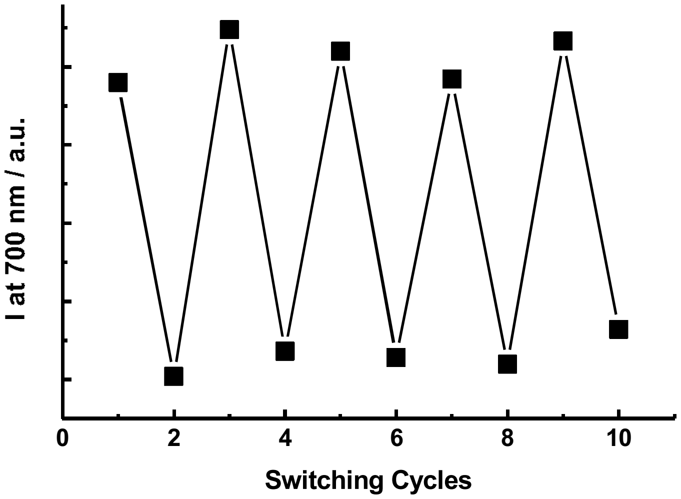

Figure 8.5. Evolution of the emission intensity recorded upon excitation at 532 nm while turning on and off the activating source at 355 nm.

In addition, the steady state absorption spectra (a and b in Figure 8.6) recorded before and after 500 cycles are essentially identical, demonstrating that this switchable system tolerates prolonged illumination without significant degradation. Thus, the presence of the nitric oxide photodonor **3** within the host NPs does not affect the photochemistry of **1a** and the photophysics of **1b**. In fact, the transient absorption and emission spectra of an aqueous dispersion of **1a** and **2**, as well as the reisomerization kinetics of **1b** in the absence of **3** are virtually identical to those recorded in the presence of this species.

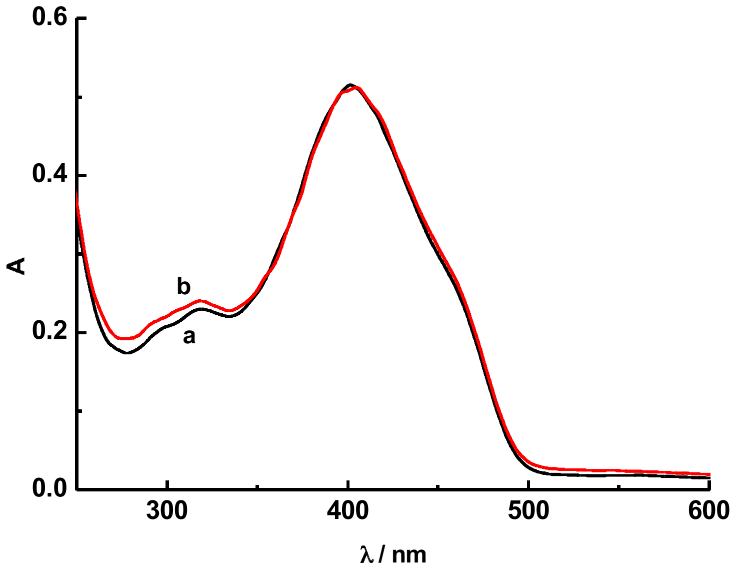

Figure 8.6. Absorption spectra of an aqueous dispersion (PBS, pH 7.4, 25°C) of **2** in the presence of **1a** and **3** recorded before (**a**) and after (**b**) 500 laser pulses at 355 nm (6 ns, 12 mJ/pulse). [**1a/b**]= 8 μM, [**2**]= 6 mg mL^{-1}, [**3**]= 40 μM.

The suitability of the supramolecular construct as a biocompatible vehicle with imaging and phototherapeutic capacities was demonstrated with biological experiments performed by using human melanoma cell lines. In order to assess if **1a** and its photogenerated isomer **1b** are localized in the cell compartment, the cell lines were incubated at pH 7.4 with an aqueous dispersion of **2** in the presence of **1a** and **3** previously left at pH of 6.8 for 10 min. Under these pH conditions a fraction of **1a** is thermally converted into the protonated form of the isomer **1b**.[9] These two species emit at *ca.* 500 nm and *ca.* 650 nm respectively. Therefore they can be identified in cells under steady state illumination conditions by their typical green and red fluorescence respectively.

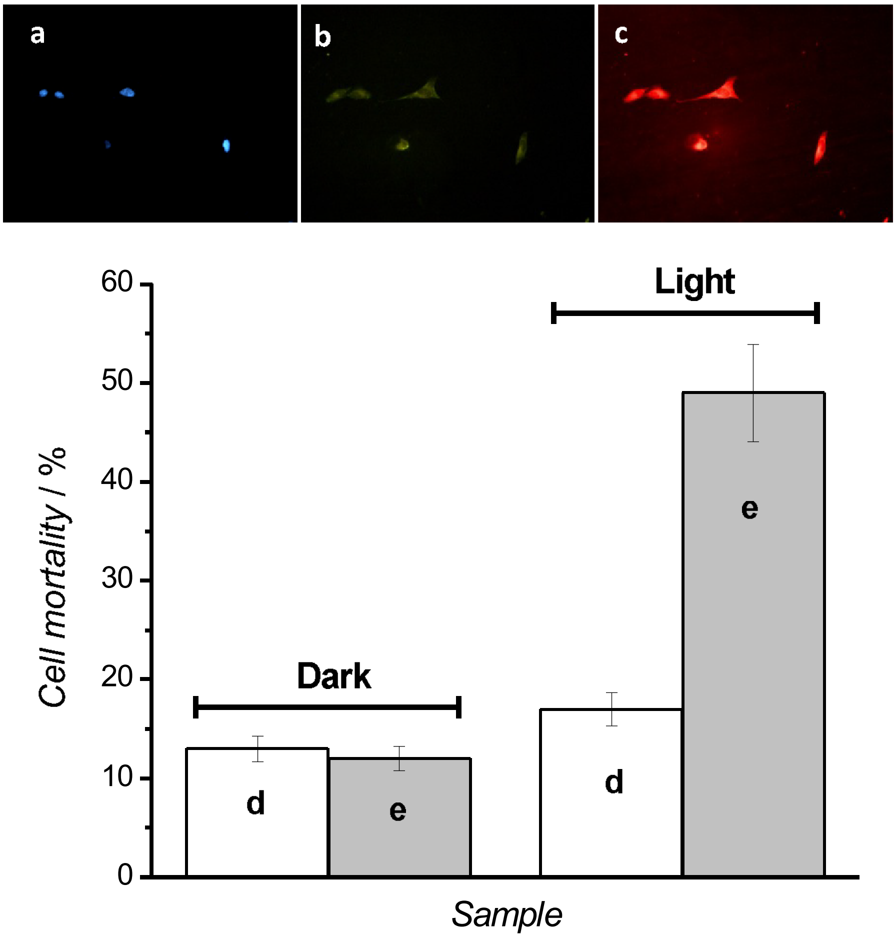

Figure 8.6. Fluorescence images of melanoma cells, pretreated with DAPI, incubated for 12 hours at pH of 7.4 with an aqueous dispersion of **2** in the presence of **1a** and **3** left at a pH of 6.8 for 10 min before incubation, and collected with blue (**a**), green (**a**) and red (**b**) emission filters. Dark and photoinduced mortality (λ_{exc} > 400 nm, t_{irr} = 30 min) of melanoma cells incubated with aqueous dispersions (PBS, pH 7.4, 25°C) of **2** in the presence of **1a** (8 μM) without (**d**) and with (**e**) **3**. [**1a**/**b**]= 8 μM, [**2**]= 6 mg mL^{-1}, [**3**]= 40 μM.

The incubation of living cells, pretreated with the nuclear stain DAPI, results the internalization of the polymer nanoparticles. The corresponding fluorescence images show the emission of DAPI in the nucleus (a in Figure 8.6) and those of the assemblies of 2 (b and c in Figure 8.6), which localize their cargo mainly at cytoplasmic level. Cell mortality experiments were performed by incubating the melanoma cells with **2** loaded with **1a** in the absence and in the presence of **3**, and the samples were either kept in the dark or irradiated with visible light for 30 min. The results reported in Figure 8.6 show that both samples exhibit a low level of cytotoxicity in the dark. In contrast, considerable cell mortality is observed under light excitation in the presence of **3** (e in Figure 8.6), as a result of the photogeneration of the cytotoxic nitric oxide radical. Accordingly, negligible change in cell mortality with respect to the basal level is observed with irradiation in the absence of **3**, under otherwise identical conditions. Thus, the fluorophore–photochrome dyad **1a** has no significant cytotoxicity under illumination, while the nitric oxide photodonor **3** encourages cell mortality.

8.6 Conclusion

Our results demonstrate that two distinct photoresponsive guests can be encapsulated within the hydrophobic interior of micellar assemblies of a cyclodextrin-based polymer. The two entrapped species can be operated independently under the exclusive control of light inputs, as proven by the excellent preservation of their photochemical and photophysical properties. One of them permits the reversible photoswitching of fluorescence on a microsecond timescale and for multiple cycles with no sign of degradation. The other enables the release of nitric oxide under illumination. Furthermore, the macromolecular host can cross the membrane of melanoma cells and transport its photoresponsive cargo in the cytoplasm. The fluorescence of one component enables the visualization of the labeled cells and the release of nitric oxide from the other induces their mortality. We would like to highlight that in contrast to non-photoresponsive compounds, the preservation of the photobehavior of independent components after their assembling is not a "trivial result". In most cases, the response to light of single or multiple photoactive units located in a confined space can be in fact considerably influenced, in both nature and efficiency, by the occurrence of competitive photoprocesses (*i.e.*, photoinduced energy and/or electron transfer, hydrogen abstraction, nonradiative deactivation, *etc.*), which preclude the final goal.[17,18] Thus, our operating principles for the assembly of biocompatible supramolecular constructs can evolve into the realization of a valuable photoresponsive and multifunctional nanoparticles for biomedical applications.

8.7 References

1. E. Abbe, *Arch. Mikrosk. Anat.*, **9**, 1873, 413.
2. T. A. Klar, S. Jakobs, M. Dyba, A. Egner, S. W. Hell, *Proc. Natl Acad. Sci. USA*, **97**, 2000, 8206
3. R. Kasper, B. Harke, C. Forthmann, P. Tinnefeld, S. W. Hell, M. Sauer, *small*, **6**, 2010, 13, 1379.
4. S. W. Hell, *Nature Biotechnol.*, **21**, 11, 2003.
5. S. W. Hell, *Physics Letters A*, **326**, 2004, 140.
6. R. Pardo, M. Zayat, D. Levy, *Chem. Soc. Rev.,* **40**, 2011, 672.
7. E. Deniz, M. Tomasulo, J. Cusido, S. Sortino, F. M. Raymo, *Langmuir*, 2011, **27**, 11773.
8. E. Deniz, S. Sortino, F. M. Raymo, *J. Phys. Chem. Lett.* 2010, **1**, 3506.
9. E. Deniz, M. Tomasulo, J. Cusido, I. Yildiz, M. Petriella, M. L. Bossi, S. Sortino, F. M. Raymo, *J. Phys. Chem. C,* 2012, **116**, 6058.
10. J. Cusido, M. Battal, E. Deniz, I. Yildiz, S. Sortino, F. M. Raymo, *Chem. Eur. J.*, 2012, **18**, DOI:10.1002/chem.201201184.
11. E. Deniz, S. Sortino, F. M. Raymo, *J. Phys. Chem. Lett.,* 2010, **1**, 3506.
12. N. Kandoth, E. Vittorino, M. T. Sciortino, T. Parisi, I. Colao, A. Mazzaglia, S. Sortino, *Chem. Eur. J.,* 2012, **18**, 1684.
13. J. Cusido, M. Battal, E. Deniz, I. Yildiz, S. Sortino, F. M. Raymo, *Chem. Eur. J.*, 2012, **18**, 33, 10399.
14. P. Bortolus, S. Monti, *Adv. Photochem.*, 1996, **21**,1996, 1.
15. E. B. Caruso, S. Petralia, S. Conoci, S. Giuffrida, S. Sortino, *J. Am. Chem. Soc.*, 2007, **129**, 480.
16. S. Conoci, S. Petralia and S. Sortino, U.S. Pat. Appl. Publ., Appl. No. PCT/IT2006/000575, 2009, pp. 20.
17. V. Ramamurthy, *Photochemistry in Organized and Constrained Media*, VCH, New York, 1991.

18. S. Monti, S. Sortino, *Chem. Soc. Rev.*, 2002, **31**, 287.

9 CD-based photocage for NO release and fluorescence reporting

9.1 Introduction

Limitation of conveying optimum concentration of therapeutically active species at the desired bio-targets draw major downfall to conventional drug delivery strategies. The active drug, once delivered *in situ* in the body is scattered at the complex cellular environment and all the control over the release of species get lost, which in turn end up simply on increasing the toxicity of the drug at undesired sites.[1] Though the quest for continuous improvement over the conventional delivery methods unraveled unprecedented opportunities to track down the dose and site of therapeutic actions quantitatively.[2,3,4] Here the light can play an immense role on regulating the dose and distribution of therapeutically active species upon tagging with a photoresponsive moiety. The concept of "photocaging" the bioactive molecule with a photolabile moiety through a covalent conjugation outline a simple strategy with major implication on releasing higher localized concentration of therapeutic payload at the tumor site.[5,6,7] Here the photolabile group renders the covalent conjugate passive over its therapeutic action. Though the suitable light trigger irreversibly cleaves the conjugate and knock out the therapeutic species into its active form. In principle the light can control the biological activity of released species by multiple on-off switching events, which ensure sustained and controlled release of active species.[2]

On the basis of above-mentioned parameters, prospective of linking therapeutically relevant NO releasing molecule with a photoclevable group is more desirable to achieve site directed NO release.[8] The information on the kinetic profile of the NO action at the desired bio-site and real time mapping of the site were NO mediated cellular process is said to occur give more idea on therapy accompanied by the clinical diagnosis. This has been achieved by interconnecting a fluorescent label with NO releasing moiety. The comprehensive idea on the dose of NO delivered at the site could be understand from variations in the fluorescence signal of the respective label.

Though certain parameters need to be addressed for the strategy of photocaging to be feasible for cellular experiments such as efficient thermal stability, neat photochemistry, adequate absorption at wavelength longer than 300 nm, satisfactory aqueous solubility and generation of nontoxic and nonabsorbing photoproducts.[9] On this concern, we have designed and synthesized nitroaniline based photocage in which two chromophore; NO photodonor and anthracene moiety integrated on the same molecular skeleton (Scheme 9.1).

Photocaging the NO donor with a fluorescent label, anthracene, is more favourable since the latter is good candidate for the present design as i) a fluorophore of high quantum yield[10] and the ability to transfer excited singlet energy to the NO donor, ii) satisfactory two-photon cross section allowing the imaging with the non-invasive light in far red region,[11] iii) ability to intercalate at the DNA proximity because of planar geometry. In addition, the secondary amino group connected between each chromophore is expected to bind with opposite charge of DNA. Finally the bichromophoric conjugate is expected to photorelease NO at the DNA proximity and amplifies the NO release via energy transfer from anthracene moiety.[12] Since both chromophore are attached at the same equivalent on the conjugate skeleton, the fluorescence emitted from the anthracene moiety is exactly proportional to the dose of NO delivered to the DNA proximity, addressing the challenge of quantification of delivered species at the cellular environment. Inspired from the previous work of our group,[13] present effort relies on a supramolecular complex in which antharcene NO donor is incorporated in the hydrophobic cavities of CD based polymer (Scheme 9.1).

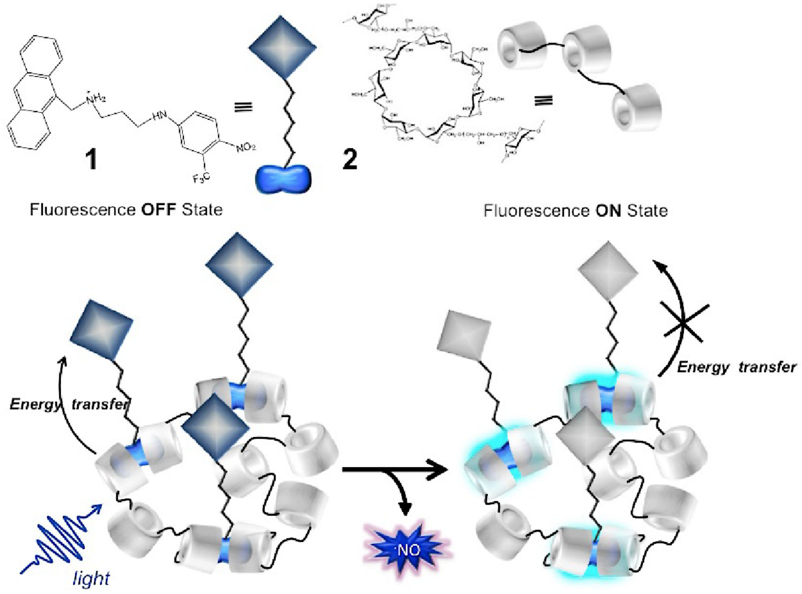

Scheme 9.1. The principle of fluorescence on-off switching by the supramolecular complex of anthracene-NO donor with CD based polymer.

Assembling the dual function conjugate in CD cavities of the polymer imparts enhanced aqueous solubility of entire ensemble and efficient NO photorelease at micromolar level as high concentration of NO photodonor incorporates in the CD network and the latter is expected to target the bio-site with high concentration of NO. Since the NO release mechanism from NO photodonor is driven by the photoconversion of the nitroaniline moiety to the phenoxy radical, the presence of secondary hydroxyl group on the CD rim increase the rate of proton abstraction[14] and consequently the rate of NO photorelease is expected to be higher in CD based polymer than in mere solvent phase. Furthermore, as the polymer is interconnected with normal β-CD units, number of CD units should be high enough for the effective encapsulation with the hydrophobic anthracene moiety making the orientation of nitroaniline chromophore towards the aqueous phase, one of the main criterion need to be fulfilled for efficient NO photorelease process.[14] From the geometrical constrains, it could be speculated that the binding of CD cavities with conjugate should be with antharcene moiety and the aromatic planar ring of anthracene could be encapsulated inside hydrophobic pockets of CD with the stoichiometry of 1:2 respectively. Above all, the conjugate is at the fluorescence 'OFF' state upon excitation as the energy transfer occurs from antharcence moiety to the NO donor and gets change in to fluorescence 'ON' state once all the NO is knocked out from the nitroaniline chromophore.[13] This lead to a *release and reporting* system for the on-site NO based therapy (Scheme 9.1).

9.2 Experimental

9.2.1 Materials and methods

The same CD-based polymer explained in previous chapters has been used here. All other photochemical experimental methods are similar to previous chapters.

9.2.2 Synthesis and characterization

The conjugate **1** is synthesized as per the protocol, which is reported before[13]. Phosphate buffer (10 mM, pH 7.4) was prepared with biological grade reagents, and all solutions were prepared with nanopure water (grade 18 mW). All other solvents used were analytical grade. All the spectroscopic characterizations were done exactly same as in the previous cases (see the experimental part in Chapter 3).

9.2.3 Cellular experiments

A431 epidermal carcinoma cells were used to study cell mortality and imaging. Firstly the cells were seeded into 96 well plates at the concentration of 10^4 cells per well. After that, the cell media was changed by the compounds and incubated for 4 hours. The cell colony was irradiated after the incubation. Photoirradiation was performed with a LED lamp array with the spectral peak position at 405 nm. Irradiation time was 39 minutes (15 J/cm^2). The compound was substituted immediately after the irradiation with cell media and incubation was allowed for 24 hours. The MTT assay has been performed to evaluate the cell viability. All the supernatant of MTT/media is removed and all the cells are killed by DMSO/HCl (0.6 mL of 0.01 M HCl in 50 mL of 100 % DMSO). The cells were incubated for 30-60 minutes. Next, the cells are killed with DMSO/HCl (0.6 mL of 0.01 M HCl in 50 mL of 100 % DMSO) to dissolve the purple formazan crystals that are produced in the mitochondria of the living cells. The 96 well plate was taken for reading the absorption with spectrophotometer. The plate was taken to the spectrophotometer to read the absorption of formazan. The OD data represents the viability of the cells after treatment.

9.2.4 Cell preparation for the imaging studies

2x10^5 of A431 cells were seeded on the glass bottom of 3 cm diamter petridish 24 hours prior to experiment. The medium was substituted with the solution of complex **1/2** in PBS (10 mM) and diluted 3 times, 4 hours prior to imaging. The experimental solution was removed before imaging and cells are gently rinsed with PBS. Afterwards, 2 mL of protein free MEM medium was added to the cell culture to keep cells alive and allow imaging with water imersion objective.

9.2.5 Two-photon imaging

Two-photon fluorescence spectra were recorded using LSM 710 NLO microscope (Carl Zeiss, Jena, Germany) equipped with mode-locked femtosecond pulsed *Mai Tai Deep See* laser. Excitation wavelength was set to 700 nm and laser power was set to 130 mW. Fluorescence intensity was evaluated by analyzing two photon images and comparing mean gray value of region of interest (ROI).

Two-photon fluorescence images were obtained using the same equipment described above. Microscope was equipped with a Plan-Apochromat 20 x water immersion objective (NA 1.0) (Carl Zeiss, Jena, Germany). Frame size of the images of suspension that were used for spectral analysis were 512x512 pixels that corresponds to 425x425 µm. Images were acquired with a pixel dwell time of 1.58 µs. Frame size of the images of cells that were used for spectral analysis were 680x680 pixels that corresponds to 85x85 µm. Images were acquired with a pixel dwell time of 1.92 µs. Image processing was performed with Carl Zeiss ZEN 2011Black and Blue versions.

9.3 Results and Discussion

The conjugate **1** is only sparingly soluble in water whereas clearly soluble in CD based aqueous dispersion as evident from the Figure 9.1.

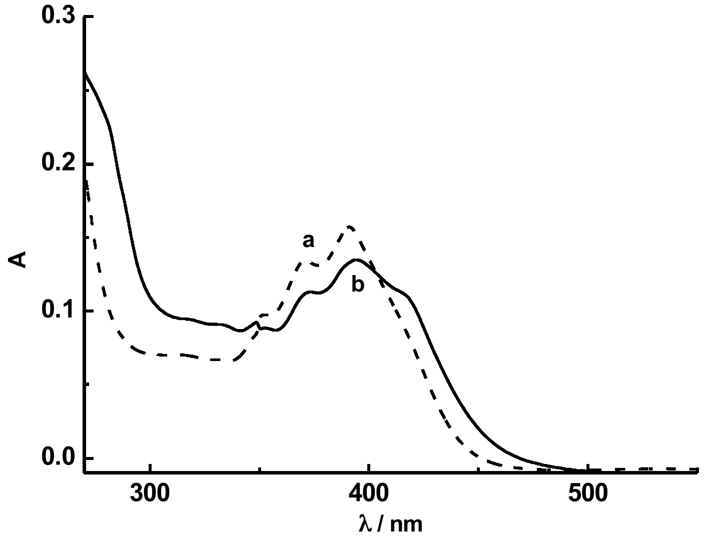

Figure 9.1. Absorption spectra of **1** (ca.10 μM) in the absence (i) and in presence of **2** (ii) in phosphate buffer (10 mM, pH 7.4) at 25°C. [**1**]= 10 μm, [**2**]= 8 mg/mL.

The spectra integrates the distinctive absorption features of antharacene moeity below 500 nm and an intense absorption at longer wavelengths extending beyond 450 nm, due to the contribution of the nitroaniline moiety.

It is clear from the spectra that the maximum peak position of **1** undergoes bathochromic shift of *ca.* 5 nm. This is in correspondence with the well accounted solubility of **1** in aqueous polymeric dispersion. The absence of any significant changes on the absorption spectra of **1** demonstrates preservation of its photochemical features and the respective shift is attributed by the orientation of the nitroaniline moiety towards aqueous pool. The distinctive band of nitroaniline moiety of **1**/**2** in polymeric suspension prompted us to study the NO release profile. Figure 9.2 shows the absorption spectrum of nanoensemble during the course of photoillumination with the light of λ_{exc}= 420 nm, for 40 minutes. It can be seen that the characteristic absorption band of nitroalinine moiety centered at 400 nm undergo photobleaching followed by the increase of UV band less than 300 nm. The respective photobleaching undergoes characteristic hypsochromic shift (*ca.* 7 nm) towards absorption regime of anthracene.

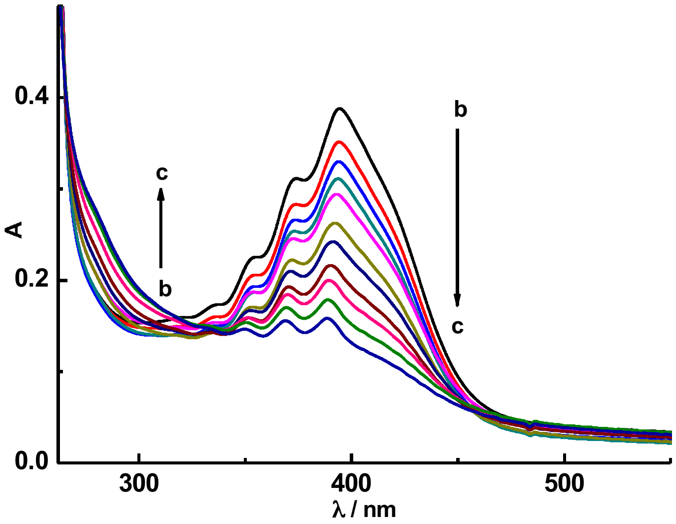

Figure 9.2. Absorption spectral changes observed upon 420 nm light irradiation (40 min) of the complex **1**/**2** in phosphate buffer (10 mM, pH 7.4, 25°C). The photobleaching of **1** from (b) 0 to (c) 40 minutes. [**1**]= 10 μM, [**2**]= 8 mg/mL.

The photobleaching of the absorption spectra is in direct consequence with the NO release from the nitroaniline chromophore of **1.** The mechanism of NO photorelease from the chromophore is well explained in the previous sections.

The photobleaching of NO donor **1** results the formation of phenol as the photoproduct, which in turn absorbs at near UV region and results the increase of the band below 350 nm. In addition blue shift of the spectra towards antharcene side well account the fact that nitroaniline part continuously undergoes photobleaching and contribution of antharcence moiety increase on the spectra of **1** upon photoirradiation.

The steady state emission spectra measured during the interval of photoirradiation shows the revival of the emissive property of the anthracene as shown in the Figure 9.3.

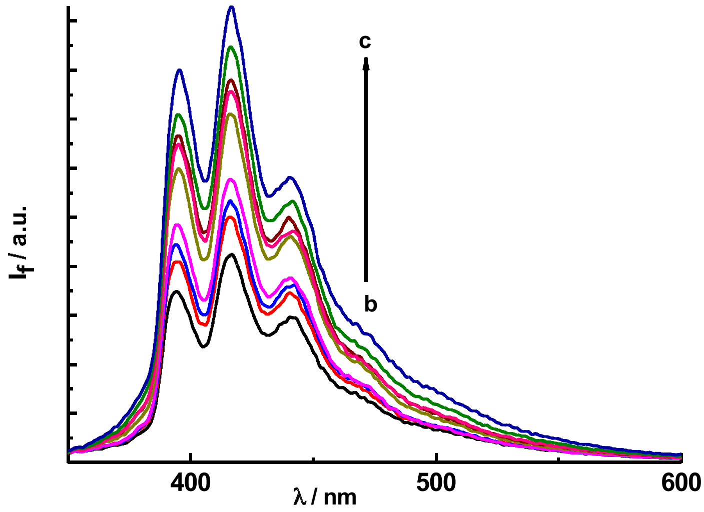

Figure 9.3. Normalized steady state emission spectra of **1**/**2** upon photoirradiation (λ_{ex}= 335 nm) in buffer solution (10 mM, pH 7.4) at 25°C. [**1**]= 10μM, [**2**]= 8 mg/mL.

The fluorescence of the anthracene in photocage is practically low since the photoinduced energy transfer is highly favored from excited singlet state of antharcene to the low lying singlet of nitroaniline moiety. As the nitroaniline moiety undergo photoconversion in to phenoxy radical upon irradiation, the energy transfer process is no longer feasible since the low lying excited singlet state of the latter is 1 eV above than the excited singlet of the fluorophore, making the entire energy transfer thermodynamically endergonic. [15] The enhancement of fluorescence from a certain level of OFF state to the ON state validates the logic of using the present conjugate as a fluorescence reporter at cell environment.

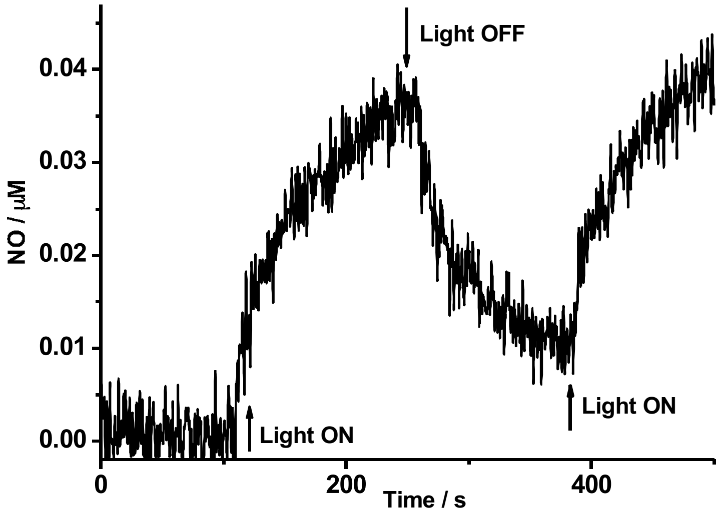

Figure 9.3. Amperogram of complex (**1**/**2**) showing the release of NO upon illumination with the light of 400 nm in phosphate buffer (10 mM, pH 7.4), [**1**]= 10 μM, [**2**]= 8 mg/mL, T= 25°C.

The bleaching of the absorption band and consequent NO release was precisely tracked quantitatively by an amperometric technique. The method is similar to that explained in previous chapters. The ultrasensitive NO electrode directly detects the NO release in nanomolar level and the corresponding amperogram unanimously proves the release of NO upon illumination with light of 400 nm and total dark stability of the ensemble (Figure 9.3).

Logical designing and novel properties of conjugate **1** stimulated us to study their feasibility for ON-OFF reporting and cell mortality at the biological interface. In this regard, we incubated the ensemble in epidermal carcinoma cells and mapped the mixture after photoirraidation with the light of 420 nm. The multi-photon imaging shows the significant fluorescence emission from the cytoplasm where the nanoensemble is located (Figure 9.4).

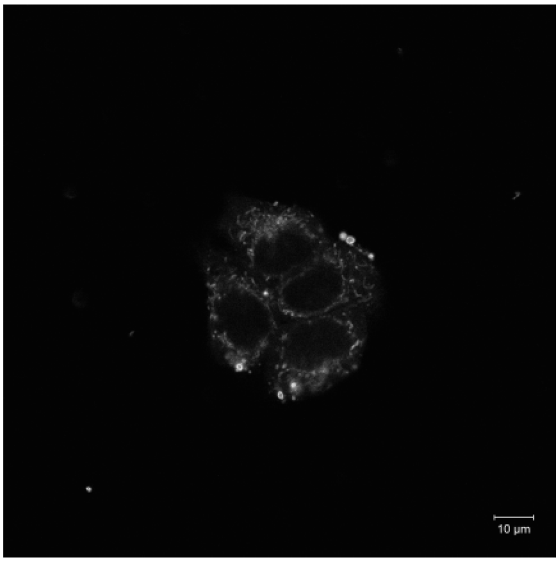

Figure 9.4 TPM image of a cluster of A431 cells incubated with **1**/**2**. Excitation wavelength 700 nm, emission collected in the range 390-600 nm. [**1**]= 40 µM, [**2**]= 8 mg/mL.

As the photocage as such is non-emissive, the substantial fluorescence from the cellular cytoplasm demonstrate the ‘decaging’ of the conjugate **1** upon NO photorelease and revival of the fluorescence from anthracene moiety (Scheme 9.1).

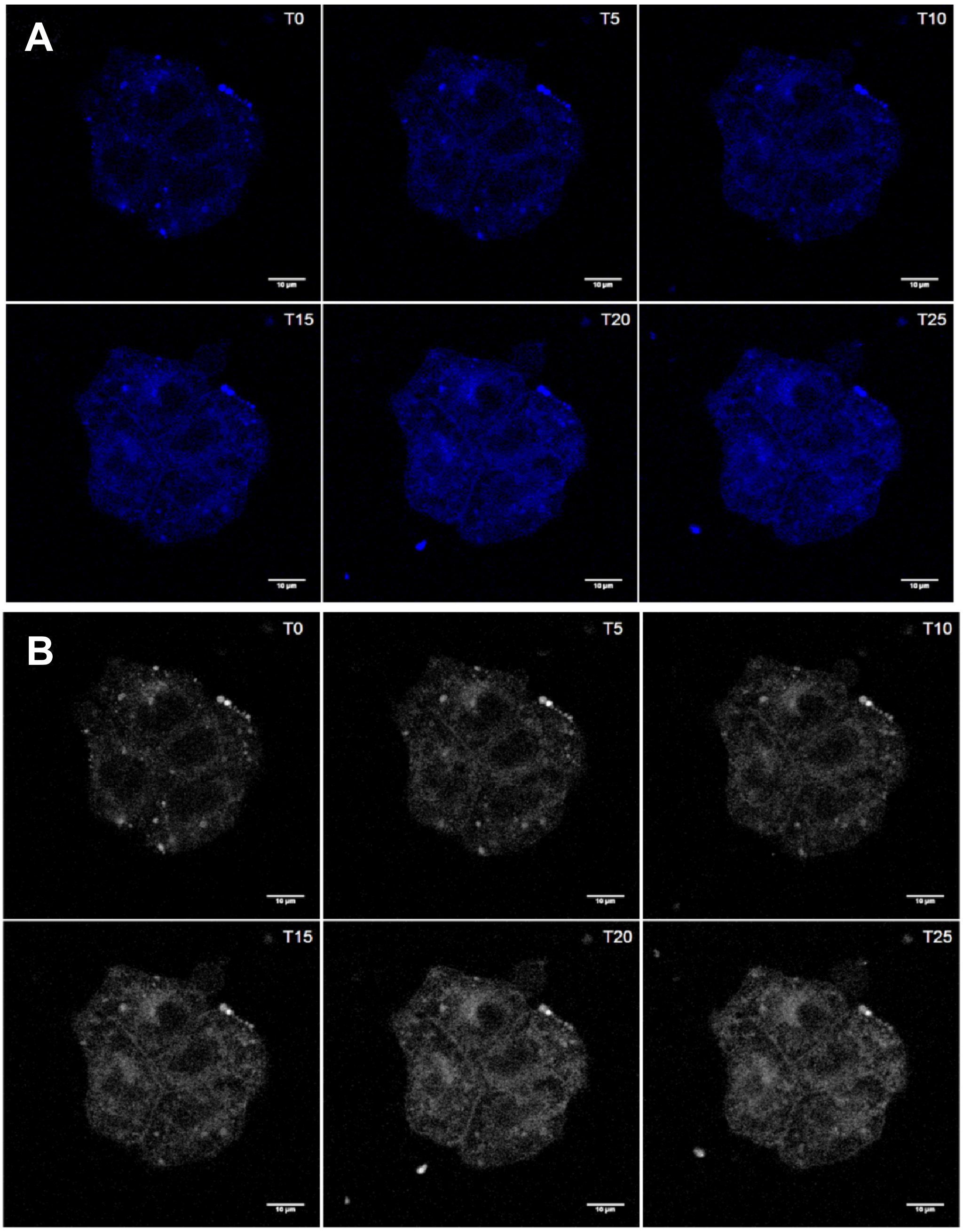

Figure 9.5. TPM images of a cluster of A431 cells incubated with **1**/**2** acquired at different exposure times after irradiation with white light of the microscope (12 V, 100 W, 80 % of maximum power) halogen-lamp for t= 0, 5, 10, 15, 20 and 25 min. λ_{exc}= 700 nm, λ_{em} 420-530 nm. A) blue color scale, B) grey scale. [**1**]= 40 µM, [**2**]= 8 mg/mL.

The results demonstrate the ON-OFF switching behavior of **1** since the conjugate undergo a transition from fluorescence OFF state to fluorescence ON state upon NO photorelease. In addition fluorescent images of cells, incubated with **1/2**, taken at definite time interval of photoirradiation simply show the increase of the fluorescence brightness with the irradiation time (Figure 9.5). Further, the close inspection of the image reveals the transition of the fluorescence into the nuclei; a possible reasoning is the rupture of nuclear envelope and facile intercalation of anthracene moiety with DNA.[12] In addition the protonated amino group (in physiological conditions) of the conjugate can interact electrovalently with the anionic phosphate backbone of DNA nucleotide.

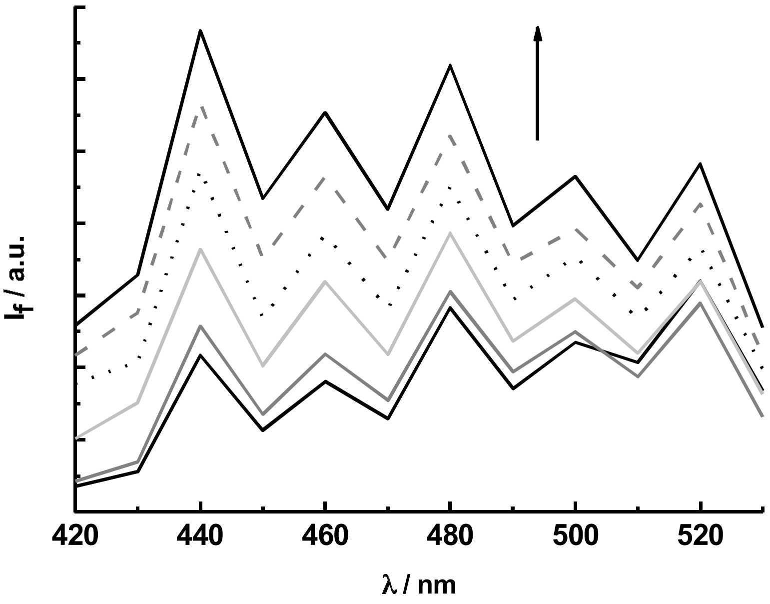

Figure 9.6. Fluorescence emission spectra acquired from the A431 cells incubated with **1/2** after irradiation with white light of the microscope halogen lamp for t = 0, 5, 10, 15, 20 and 25 min. λ_{exc}= 700 nm, the emission recorded in the range 420–530 nm using the spectral detector in the TPM.

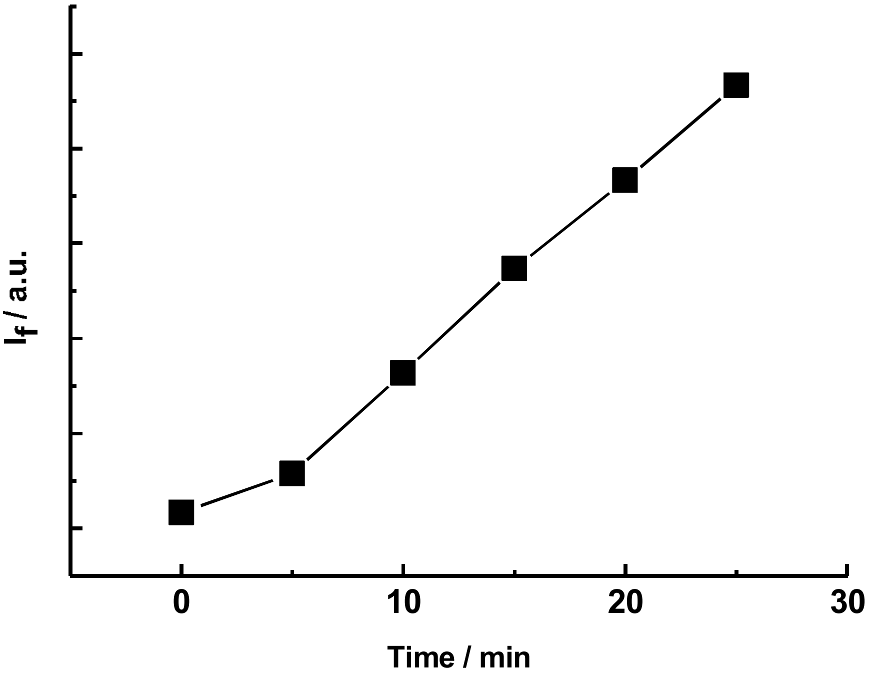

Figure 9.6. Variation of fluorescence intensity of cell suspension incubated with **1/2** at 440 nm as a function of irradiation time.

To note, these emission characteristics of anthracene acts as reporter of NO photorelease since the emission intensity is exactly equivalent to the NO release. The same fluorescence intensity profile of **1/2** in the cellular suspension is measured directly by emission spectroscopy (Figure 9.6) and shows the evolution of the fluorescence in cells as observed in aqueous polymeric suspension. Above all, the linear generation of the fluorescence with the irradiation time clearly augment the idea of having a light activated release and reporting system for NO based anticancer therapy.

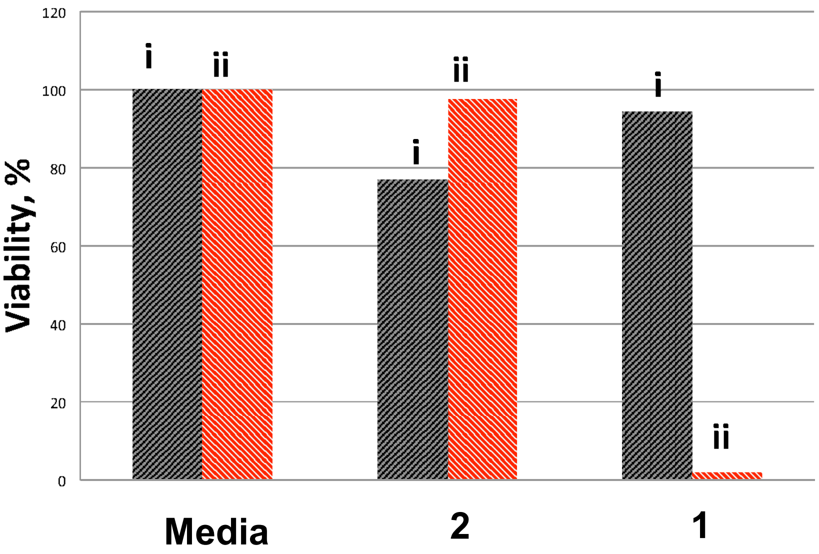

Figure 9.7. Dark (i) and photoinduced (ii) mortality of A431 cancer cells incubated with the compound **1**/**2** and supramolecular assembly. [**1**]= 3 μM, [**2**]/ CD units= 1 mM.

Finally, the therapeutic impact of the present system is verified in tumor cells by studying their tumor mortalities. Figure 9.7 shows the viability of the epidermal cancer cell lines in the presence and absence of light irradiation at 420 nm. Significantly low level of mortality observed in case of **2** demonstrates that the CD based polymer is biocompatible and conveys the conjugate **1** into the cell in great yield than used alone. Remarkable level of cell mortality (*ca.* 99 %) was observed in case of supramolecular assemblies, confirms undisputed action of NO as an antitumoral agent and attesting the idea that the mortality is solely depend on the interaction of NO photodonor with matching light trigger.

9.4 Conclusion

The innate limitations of drug delivery strategies are lack of spatio-temporal control over the delivery agents. Precise understanding and continuous modulation over the spatial distribution and temporal control of the active species at bio-sites is the key to avert the drug delivery inadequacies.

Serious efforts have been taken in the present chapter to address this issue by designing a NO releasing photocage, where a fluorescent label, anthracene, is covalently bound to nitroaniline based NO releasing moiety. The CD based polymer dispersion of this conjugate conveys a great amount payload to the desired bio-site with high quantum efficiency of NO release. The quantitative control of the NO delivery could be accomplished by recording the fluorescence emission from the anthracene moiety that acts as a reporter of NO concentration. The revival of the fluorescence emission from the anthracene upon uncaging the conjugate evokes an ON/OFF release and report system, overruling some limitations of current therapeutic delivery methods. Convergence of many suitable features such as remarkable level of photoinduced cell mortality, ability to excite the fluorophore with multiphoton together with their aqueous solubility, biocompatibility and membrane permeability adds innumerable therapeutic prospective to these smart nanomaterials.

9.5 References

1. H. –M. Lee, D. R. Larson, D. S. Lawrence, *ACS Chem. Biol.*, 2009, **4**, 6, 409.
2. S. Sortino, *J. Mater. Chem.*, 2012, **22**, 301.
3. J. P. Pellois, M. E. Hahn, T. W. Muir, *J. Am. Chem. Soc.*, 2004, **126**, 7170.
4. G. Mayer, A. Heckel, *Angew. Chem. Int. Ed.*, 2006, **45**, 4900.
5. J. H. Kaplan, B. Forbush, J. F. Hoffman, *Biochemistry*, 1978, **17**, 10, 1929.
6. N. -C. Fan, F. –Y. Cheng, J. –an A. Ho, C. –S. Yeh, *Angew. Chem. Int. Ed.*, 2012, **51**, 8806 –8810.
7. G. C. E. -Davies, *Nat. Methods*, 2007, **4**, 619.
8. J. P. Pellois, M. E. Hahn, T. W. Muir, *J. Am. Chem. Soc.*, 2004, **126**, 7170.
9. A. P. Pelliccioli, J. Wirz, *Photochem. Photobiol. Sci.*, 2002, **1**, 441.
10. W. R. Dawson, M. W. Windsor, *J. Phys. Chem.*, **72**, 1968, 3251.
11. X. Li, X. Zhang, W. Li, Y. Wang, T. Liu, B. Zhang, W. Yang, *J. Mater. Chem.*, 2011, **21**, 3916.
12. F. L. Callari, S. Sortino, *Chem. Commun.*, 2008, 1971.

13 E. Vittorino, M. T. Sciortino, G. Siracusano, S. Sortino, *ChemMedChem,* 2011, **6**, 1551.

14. S. Sortino, G. Marconi, G. Condorelli, *Chem. Commun.*, 2001, 1226.
15. M. Montalti, A. Credi, L. Prodi, M. T. Gandolfi, *Handbook of Photochemistry (3rd ed.)*, CRC Press, Boca Raton, 2006.

SECTION IV

Photoactivable polymeric nanogels

" In the field of observation, Chance favours only the prepared mind",
-Louis Pasteur

10

NO photoreleasing hydrogel with antimicrobial actions

10.1 Introduction

The drug delivery systems based on polymeric nanoassemblies is appears to transform the landscape of the current pharmaceutical industries,[1,2] The polymeric nanocarriers offer tremendous possibilities to modulate its physicochemical characteristics through simple methods so as to adapt the vulnerable drug therapeutics and convey the latter with precise spatio-temporal control to the specific target.[3] The polymeric nanocarriers are featured with several kinds of microdomains where they can potentially link to the respective molecules of hydrophilic or hydrophobic nature. Though the expansive field of polymeric drug delivery systems is emerged as promising alternative, the processing and design often demands large complexity with potentially toxic interconnectors to enable specific functionalities to the polymer core[4] and often they are limited to nocuous burst release of therapeutic payload. However the intricate associative behavior of the polymeric systems can be effectively exploited to modulate supramolecular self-assembling process with other molecular scaffolds. Specifically the CD based polymers can be effectively interlocked with the hydrophobically modified dextran grafted onto alkyl chains.[5] The 'lock and key' bridging of these two water-soluble polymers enable supramolecular nanoassemblies or nanogel of size ranges between 100-200 nm together with various entrapment features.[6,7]

The above-mentioned parameters are logically exploited for fostering an active strategy to decimate microbial infections as they emerged recently as one of the most daunting task to treat with. Actually, the evolution of bacterial resistance to the multitude of current antibiotics poses a serious concern over the clinical treatments.[8] Very short endurance of antimicrobial agents in the bacterial colonies attributed by the fast emergence of multiple drug resistance make the scenario more acute.[9] Here NO plays an important role on filling the shortcoming of current antibiotics addressed to antimicrobial actions.[10,11] The NO is a 'killer application' as it is able to induce multiple level of nitrosative and oxidative stress at the antibiotic resistant bacterial colonies, which impair vital cellular functions towards irreversible cellular damage.[11] The NO is superior to the conventional antibiotics as the former mediate with cellular functions in omnidirectional pathway leaving narrow window for bacterial resistance. Though the eradication efficacy of NO largely depend on the manner and the dose in which the NO is delivered to the microbial site. On wake of these multilevel constrains of delivering the NO to the desired site, we have encompassed NO photodonor with in the container of CD based supramolecular nanogel. The novel multiple features associated with the present ensemble make them stand out among related approaches as they i) form superior sticky gel structures to adhere on any topological space, ii) have well integrity of entire assembly with no sign of leaching of NO donor from the ensemble, 3) facilitate fast release kinetics of NO directly to the microbial site. Here the nanogel obtained by mixing equimolar concentration of two polymers are well explored by Dr. Ruxandra Gref group, University Paris-Sud, Paris, France.[12,13,14,15] The exploitation of the same as novel antibacterial agent is first art of design for photoactivated bactericidal action. Similar to the strategy explored in the previous chapter (Chapter 6), adamantane terminated NO photodonor (**1**) is incorporated in CD-based polymer networks where the adamantane appendage encapsulate inside the hydrophobic CD pockets (Scheme 10.1).

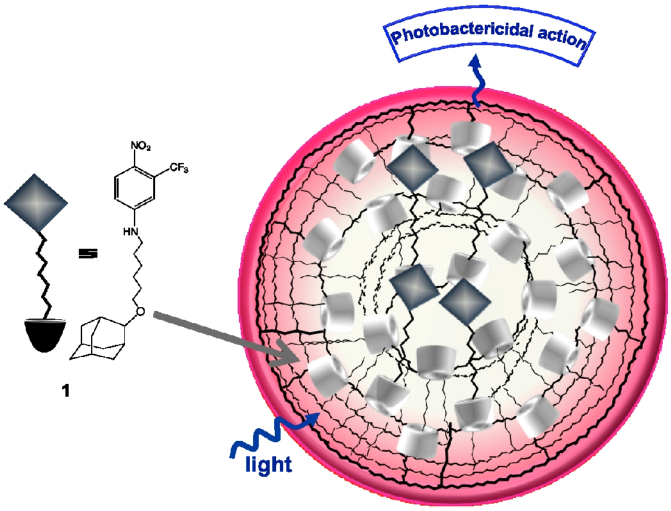

Scheme 10.1. Pictorial representation of NO photodonor **1** entangled with CD-based polymeric nanogel.

The loaded CD polymer is continuously entangled with the second polymer of dextran grafted with hydrophobic alkyl chain to form solid gel structure. Actually the method comprise just mixing of two polymers. The gel like rheological properties of the carrier is expected to facilitate the enhanced NO release since rate of photoisomerization of the nitroaniline moiety is much more favored in semi-solid topological environment.[16] The loaded gel is able to release NO upon illumination with light as indubitably proved by the significant rate of cell mortality of antibiotic resistant bacterial colonies.

10.2 Experimental

10.2.1 Materials

The components to prepare the nanogel carrier; β–CD based polymer and dextran modified with hydrophobic alkyl chains were obtained from Dr. Ruxandra Gref, University of Paris-Sud, Paris, France as the part of ITN- Marie Curie Program, Cyclon and used as such with out any further purification. The Myoglobin (Mb) is used to understand the NO complexation and is directly purchased from Sigma-Aldrich, (Myoglobin, from equine heart, Product No. M1882). The reagents 5-bromo-4-chloro-3-indolyl-β-D-galactopyranoside (X-Gal) and isopropyl-β-D-thiogalactoside (IPTG) were used for studying the viability of bacterial colonies and taken as received from Invitrogen, USA.

All other reagents were of highest commercial grade available and used without further purification. All solvent used (from Carlo Erba) were analytical grade.

10.2.1 Synthesis of tailored NO photodonor

The protocol followed to synthesize the NO photodonor is exactly same as synthetic procedure reported before (Chapter 3).

10.3 Instrumentation

UV/Vis absorption and fluorescence spectra were recorded with a Beckman DU-650 spectrophotometer. Photolysis experiments were performed in a thermostated quartz cell (1 cm pathlength, 3 mL capacity) by using a Rayonet photochemical reactor equipped with 8 RPR lamps with an emission in the 380-480 nm ranges with a maximum at 420 nm in the presence of a 400 nm cut-on filter. The incident photon flux on quartz cuvettes was ca. 0.8×10^{15} quanta sec^{-1}.

10.3.1 NO detection

NO release was measured based on the protocol reported in previous chapters.

10.4 Sample preparation

10.4.1 Photochemical experiments

The compound **1** is dissolved in acetonitrile and slowly evaporated to form a dry film, dissolved in aqueous dispersion of CD based polymer. The former is polymerized with second polymer of dextran modified alkyl chains non-covalently. Both polymer components are stirred overnight, mixed each other to obtain the gel phase, and finally equilibrated. The supernatant is removed out and directly used for the experiments.

10.4.2 NO photodelivery to myoglobin

A) Preparation of phosphate buffer solution

50 mM phosphate buffer solution of pH 6.8 was prepared by mixing 0.2096 g of NaH_2PO_4. $2H_2O$ and 0.16415 g of anhydrous Na_2HPO_4 to 25 mL H_2O and making the volume in a 100 mL standard flask.

B) Preparation of myoglobin stock solution

5 mg equine skeletal muscle Mb was dissolved in 5 mL of the above buffer solution.

C) Binding of photoreleased NO with myoglobin

Steady state absorption spectra were obtained by taking the phosphate buffer solution as the reference. 150 µL of Mb stock solution was diluted up to 2 mL buffer solution. The absorption spectrum shows the peak at 409 nm (Soret band). The absorption spectrum of reduced Mb at 434 nm was obtained by addition of excess sodium dithionate on the same cuvette (constant weight of sodium dithionate was added into the above solution to obtain the final concentration of 10 mM). This solution was poured into the nanogel phase in an eppendorf to get a two-phase of gel and supernatant. The latter is irradiated by Rayonet photochemical reactor equipped with 8 RPR lamps with an emission in the 380-480 nm range and the absorption spectra was plotted at different time interval of photoirradiation.

10.4.3 Antibacterial experiments

The gel loaded with NO photodonor was formed on the wall of the quartz cuvette (1×1×4 cm). 3 mL of bacterial suspension (30,000 CFU/mL) of *Escherichia coli* DH5α (Invitrogen, USA) containing plasmid pGEM11Z (Promega) was then placed into the cuvette and irradiated (0-10 min) by the stabilized Xe lamp (500 W, Newport) equipped with cut-on filter $\lambda > 400$ nm, Laser Components). During the irradiation, gradually, an inoculum (50 μl) was took away from the irradiated cuvette (3 times for each irradiation time) and placed on the sterile agar plate enriched by 50 μl X-gal (20 mg/mL in DMF) and 50 μl IPTG (23 mg/mL in H_2O). The plates were then incubated 20 hours in the dark at 37^0C to allow individual bacteria to grow and form visible blue-green colonies. Blue-green color of the colonies was due to an indolyl dye produced from X-gal substrate (5-bromo-4-chloro-3-indolyl-β-D galactopyranoside) by the bacterial β-galactosidase with assistance of IPTG inducer. Finally, the number of the colonies was calculated for each irradiation time.

10.5 Results and Discussion

The compound **1** is loaded with the aqueous polymeric NPs as similar to the procedure followed previously. The loaded polymeric NPs simply interact with the dextran modified alkyl chain to form the gel structures.

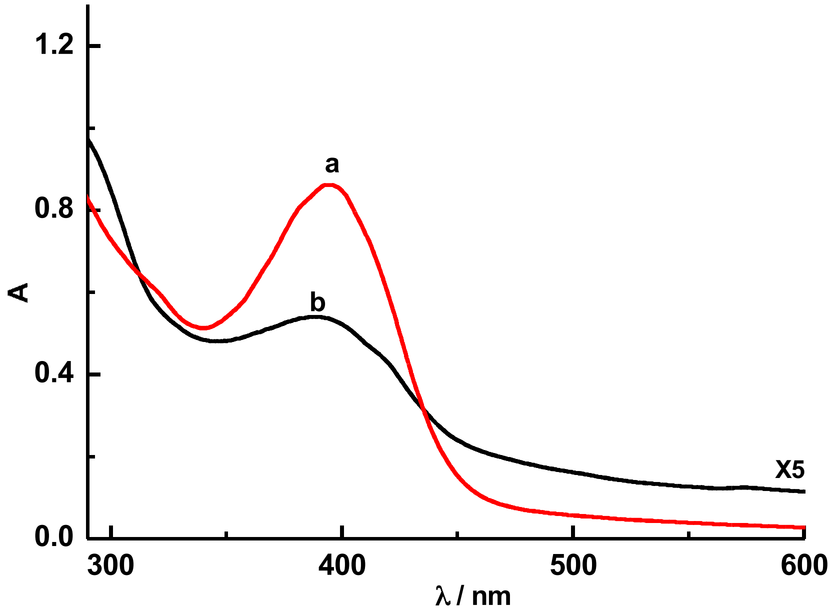

Figure 10.1. Steady state absorption spectrum of **1** loaded in, (a) CD based polymer, (b) in polymeric hydrogel (ca. 5 μM, spectra is multiplied by the factor 5 for the sake of comparison).

The steady state absorption spectrum measured by pasting the gel on cuvette wall demonstrates the absorption features of the compound **1** (b in Figure 10.1). The spectra shows the absorption of compound **1** incorporated in gel structure with the peak maxima around 400 nm similar to the absorption when the compound **1** incorporate only in the polymer (a in Figure 10.1), albeit the percentage of the loading was lower. The scattering of the compound **1** (b in Figure 10.1) was higher as compared to the polymer alone pertinent to the measurement of steady state absorption on solid gel structures. In addition the significant amount of gel get lost while processing very sticky gel phase. It is worth pointing out that absorption spectrum was remaining intact for a week and no leaching of the compound **1** from the gel was observed. In fact, we analyzed whether the probe **2** is oozing out into the supernatant and spectrum of the supernatant was pretty transparent, demonstrating the validity of the present system with regard to the similar systems seriously limited by the premature release of enclosed probe.[17,18] All these findings refer to the possibility of having a gel structure able to release NO continuously upon matching light inputs.

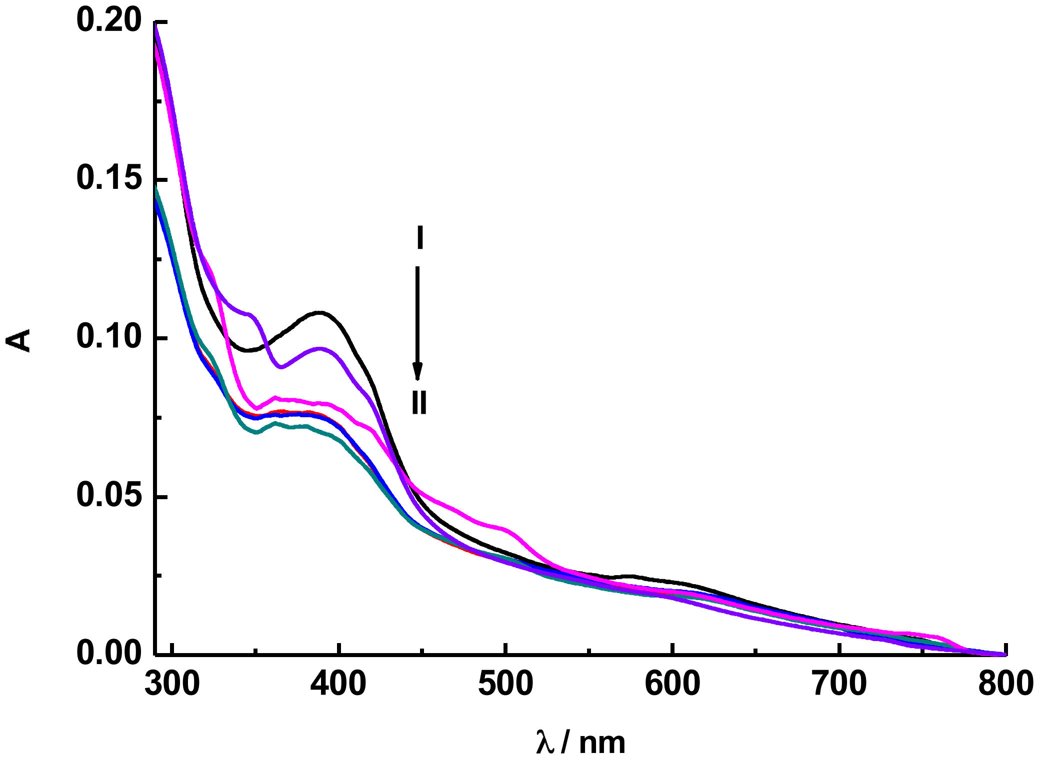

Figure 10.2. Steady state absorption spectra of **1** loaded in hydrogel (I) before and (II) after exposure to light of 420 nm.

The photolytic pathway of NO photodonor loaded with nanogel is analyzed by illuminating the latter with the light of 420 nm and absorption spectra measured at definite interval of photoirradiation shows the bleaching of absorption band of compound **1** (Figure 10.2). Here the gel is pasted on the cuvette wall and exposed to the photoreactor. The characteristics absorption peak position of compound **1** at 400 nm is found to decrease upon irradiation followed by the small rise of band below 350 nm. The previous studies on NO photodonor demonstrate that this behavior is an exact consequence of the NO release profile from the nitroaniline moiety.[19,20,21] However in the present case, the probe is locked inside the network of solid gel container, thanks to the adamantane appendage and only NO gas is diffuse out of the gel. Unperturbed direct diffusion of NO from the gel well suits to the aim of having direct convey of NO to the bio-targets.

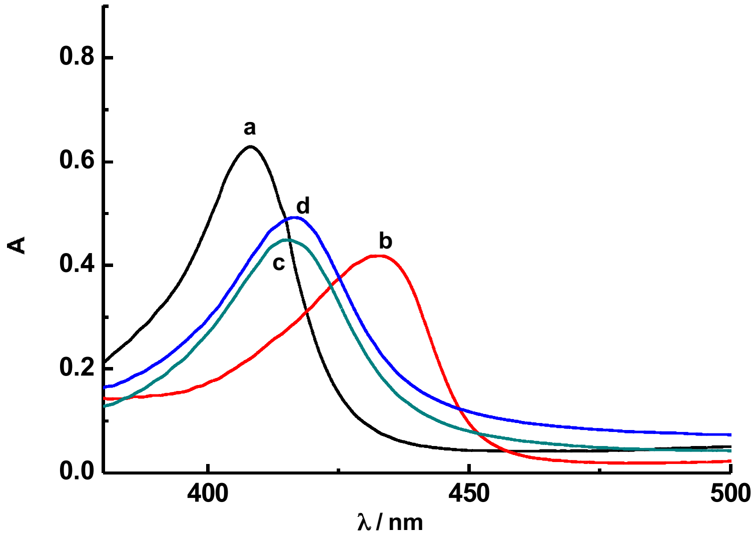

Figure 10.3. The steady state absorption spectrum showing the formation of Mb-NO complex upon photoillumination. Oxidized Mb (a), reduced Mb (b), transfer of photoreleased NO to reduced Mb and formation of Mb-NO complex (c and d) upon exposure to the light of 420 nm.

The sustained photorelease and direct diffusion of NO from the nanogel matrix to the desired target was first verified by exploiting the fervent complexation features of the NO with myoglobin.[22,23,24] The complexation dynamics is tracked by steady state absorption spectrum (Figure 10.3). The Mb shows the absorption spectra with the peak position at 409 nm and 434 nm while in reduced state (a and b respectively in Figure 10.3). The central Fe (III) metal ion readily reduce to Fe (II) with the appropriate reducing agent and Fe (II) ion is characterized by its innate propensity of complexation with NO.[25] The absorption spectra measured at different interval of irradiation shows the transition of absorption peak from the 434 nm of reduced Mb to the 420 nm representing the soret band of Mb-NO complex (c and d in Figure 10.3). In addition, the assumption of NO diffusion and consequent formation of Mb-NO complex is in agreement with diffusivity parameters of NO gas as the latter diffuse to 40-200 μM in cellular environment with the average lifetime between 1-500.[26,27]

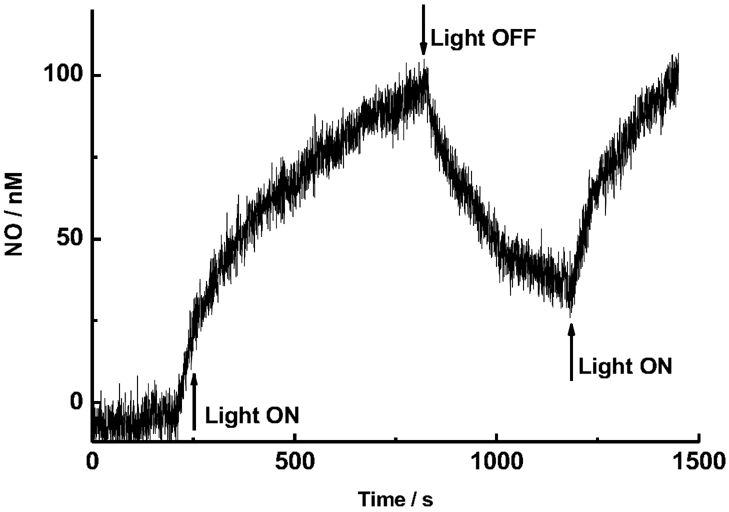

Figure 10.4. Amperogram showing NO photorelease of **1** loaded with hydrogel through multiple on-off switching with the light of 420 nm.

The quantitative evidence of NO release from the gel matrix is obtained by monitoring NO relase in a direct and real-time manner. To this end, we used an ultrasensitive NO electrode, which detects NO release in nanomolar level. Practically the NO electrode is immersed into the supernatant of water where the gel loaded with NO photodnor **1** is kept at the bottom. The electrode can directly sense the NO once it diffuses into the water supernatant. The linear generation of the amperogram which promptly stops when the light is turned off and resume the generation upon illumination proves the undisputed photorelease of NO and its diffusion to the supernatant.

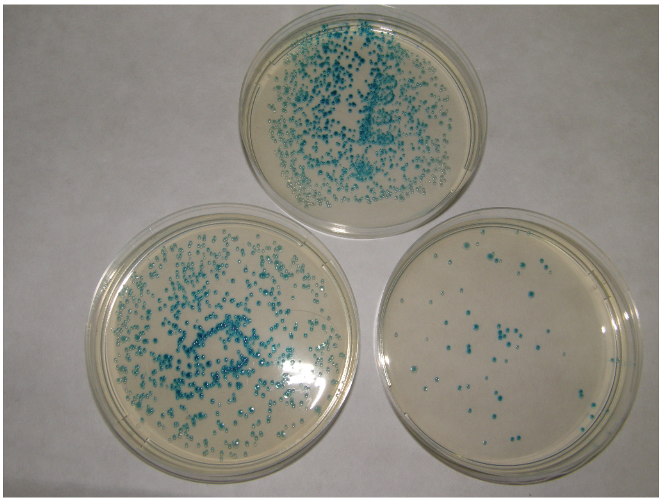

Figure 10.5. Agar plate with X-Gal and IPTG inoculated with 50 μl of bacterial suspension *E. Coli* DH5α (*ca.* 30000 CFU/mL) before (upper plate) and after the irradiation (10 minutes, 500 W Xe lamp, cut- on filter λ > 400 nm) in the cuvette with (bottom right) and without (bottom left) of NO-gel on the wall of the irradiated cuvette.

Stimulating results of photochemical studies of compound **1** in nanogel prompted us to study its bactericidal actions. The antibacterial properties of NO-photodonor **1** loaded with nanogel were demonstrated on the *E. Coli* DH5α strain with the pGEM11Z plasmid (see Experimental part).

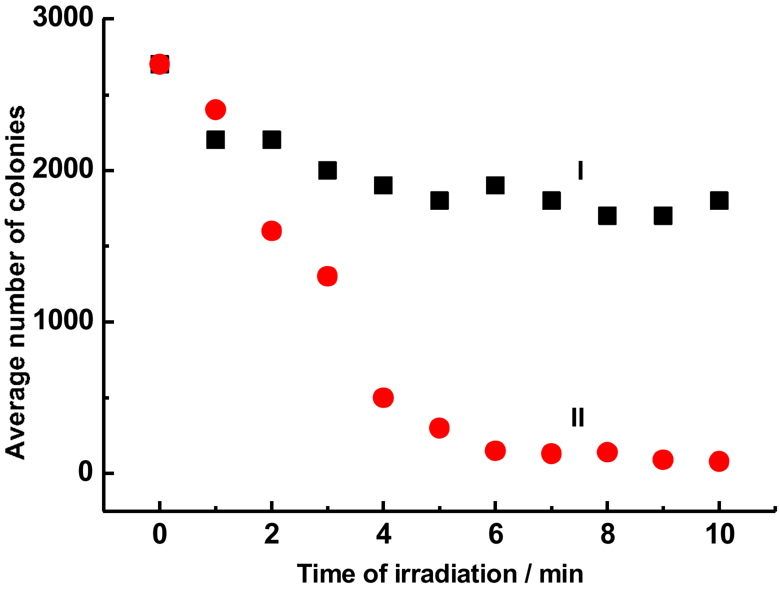

Figure 10.6. Photobactericidal effect of hydrogel loaded with **1** in *E. Coli* DH5α. Decreasing average number of CFU of *E. Coli*, DH5α during the time of irradiation (500 W Xe lamp, cut-on filter λ > 400 nm) of the inoculum in the absence (I) and presence (II) of NO-gel on the wall of the irradiated cuvette.

Figure 10.5 displays samples of agar plates with X-gal and IPTG that were inoculated with *E. coli*, after cleaving the X-gal substrate into an indolyl dye. Significant decrease in number of colonies (CFU) was observed after irradiation of a bacterial inoculum by visible light in the presence of NO photodonor, in contrast to controls (in the absence of NO-photodonor **1** and/or the light). Whereas, Figure 10.6 illustrates the progressive decreasing of CFU during the time of irradiation and the control shows no effects on CFU.

10.6 Conclusion

Here the attempt was to design an active formula to contain the antibiotic resistant bacterial colonies on the context where the efforts of developing new antibiotics haplessly ceased by the pharmaceutical companies. We outlined a proof of concept by exploiting the tremendous possibilities hatched out by the repertoire of NO actions. The NO releasing photodonor is logically incorporated in the polymer based nanogel matrix by exploiting the novel features spanning from synthetic chemistry to supramolecular self-assembling. The NO photodonor is particularly stable in the gel matrix with no sign of premature leaching or burst release of the drug payload as the former could be detrimental to the therapeutic action.[18,28] To note, the probe is remain entrapped through out its course of action and did not require any coating or shell to prevent the leaching, thanks to the novel designing of the carrier. The dark stable nanogel is able to release NO directly and efficiently to the bacterial target on demand with the prompt trigger of visible light in 400-450 nm region. This NO release profile and consequent diffusion is confirmed by the facile complexation of NO with myoglobin. However the real-time quantitative detection of NO after the photoillumination demonstrates the release and diffusion of NO in nanomolar level, an optimum concentration for antimicrobial actions.[29] Finally all these photochemical revelations are unanimously proved in antibiotic resistant *E. Coli* DH5α bacterial strains. The mortality rate, *ca.* 95 % of the bacterial colony within 6 minutes of photoirradiation definitely proves the suitability of the system towards efficient bactericidal action.

However, lot of attention need to be required to finely tackle the cross resistance imparted by rapidly disguising bacterial traits. One of the strategies is to attack the vital cellular functions of the microbes in multiple ways so as to give no chance to acquire drug resistance. On these ground, the exploitation of multimodal therapy to address this requirement could be viable for the multimodal bactericidal action. In fact the next chapter is devoted on these perspective.

10.7 References

1. K. E. Uhrich, S. M. Cannizzaro, R. S. Langer, K. M. Shakesheff, *Chem. Rev.*, 1999, **99**, 3181-3198.

2. O. C. Farokhzad, R. Langer, *ACS Nano*, 2009, **3**, 1, 16–20.

3. S. E. Gratton, S. S. Williams, M. E. Napier, P. D. Pohlhaus, Z. Zhou, K. B. Wiles, B. W. Maynor, C. Shen, T. Olafsen, E. T. Samulski, J. M. Desimone, *Acc. Chem. Res.*, 2008, **41**, 1685–1695.

4. S. D. -Mahammed, P. Couvreur, R. Gref, *Int. J. Pharm.*, 2007, **332**, 185–191.

5. R. Gref, C. Amiel, K. Molinard, S. D- Mahammed, B. Sébille, B. Gillet, J- C. Beloeil, C. Ringard, V. Rosilio, J. Poupaert, P. Couvreur, *J. Control. Release*, 2006, **111**, 316–324.

6. K. Bouchemal, P. Couvreur, S. D- Mahammed, J. Poupaert, R. Gref, *J. Therm. Anal. Calorim.*, 2009, **98**, 57–64.

7. S. D- Mahammed, P. Couvreur, K. Bouchemal, M. Cheron, G. Lebas, C. Amiel, R. Gref, *Biomacromolecules*, 2009, **10**, 547–554.

8. A. Coates, Y. Hu, R. Bax, C. Page, *Nat. Rev. Drug Discov.*, 2002, **1**, 895.

9. K. Page, M. Wilson, I. P. Parkin, *J. Mater. Chem.*, 2009, **19**, 3819–3831.

10. A. W. Carpenter, M. H. Schoenfisch, *Chem. Soc. Rev.*, 2012, **41**, 3742–3752.

11. C. Chen, Y- Q. Shi, J. Song, Q- S. Qi, L. Gu, P. G. Wang, *Biol. Pharm. Bull.*, 2006, **29**, 6, 1239—1241.

12. E. Battistini, E. Gianolio, R. Gref, P. Couvreur, S. Fuzerova, M. Othman, S. Aime, B. Badet, P. Durand, *Chem. Eur. J.*, 2008, **14**, 4551–4561.

13. S. D- Mahammed, S. A. Agnihotri, K. Bouchemal, S. Klçters, P. Couvreur, R. Gref, *Curr. Nanosci.*, 2010, **6**, 654–665.

14. S. D- Mahammed, J. L. Grossiord, T. Bergua, C. Amiel, P. Couvreur, R. Gref, *J. Biomed. Mater. Res. Part A*, 2008, **86A**, 3, 736–748.

15. M. Othman, K. Bouchemal, P. Couvreur, R. Gref, *Int. J. of Pharm.*, 2009, **379**, 218.

16. S. Sortino, G. Marconi, G. Condorelli, *Chem. Commun.*, 2001, 1226.

---

17. T. R. Hoare, D. S. Kohane, *Polymer*, 2008, **49**, 1993, 2007.
18. X. Huang, C. S. Brazel, *J. Control. Release*, 2001, **73**, 121–136.
19. N. Kandoth, E. Vittorino, M. T. Sciortino, T. Parisi, I. Colao, A. Mazzaglia, S. Sortino, *Chem. Eur. J.*, 2012, **18**, 1684–1690.
20. E. Deniz, N. Kandoth, A. Fraix, V. Cardile, A. C. E. Graziano, D. L. Furno, R. Gref, F. M. Raymo, S. Sortino, *Chem. Eur. J.*, DOI: http://dx.doi.org/10.1002/chem.201202845.
21. N. Kandoth, M. Malanga, A. Fraix, L. Jicsinszky, E. Fenyvesi, T. Parisi, I. Colao, M. T. Sciortino, S. Sortino, *Chem. Asian J.*, DOI:10.1002/asia.201200640
22. G. M. Halpenny, M. M. Olmstead, P. K. Mascharak, *Inorg. Chem.*, 2007, **46**, 6601.
23. U. Flögel, A. Fago, T. Rassaf, *J. Exp. Biol.*, 2010, **213**, 2726-2733.
24. K. Tsuchiya, M. Yoshizumi, H. Houchi, R. P. Mason, *J. Biol. Chem.*, 2000, **275**, 3, 1551–1556.
25. P. C. Ford, J. Bourassa, K. Miranda, B. Lee, I. Lorkovic, S. Boggs, S. Kudo, L. Laverman, *Coord. Chem. Rev.,* 1998, **171**, 185-202.
26. S. Sortino, *Chem. Soc. Rev.*, 2010, **39**, 2903–2913.
27. M. Feelisch, J. S. Stamler, Editors. *Nitric Oxide Research*; John Wiley and Sons: Chichester, U.K., 1996.
28. J. Wanga, B. M. Wanga, S. P. Schwendeman, *J. Control. Release*, 2002, **82**, 289.
29. P. N. Coneski, M. H. Schoenfisch, *Chem. Soc. Rev.*, 2012, **41**, 3753–3758.

11 CD-based hydrogel with bimodal bactericide action

11.1 Introduction

Recently the nanostructured metal particles have garnered an upsurge of interest in fascinating avenues of biomedical science. The metal nanoparticles are featured by their uniqueness over other related materials for instance, the intriguing surface properties, versatile synthetic building blocks, novel probe for biomedical imaging and therapy.[1,2] Among this silver nanoparticles (AgNPs) serves a significant role especially in antimicrobial actions, as they are capable to image and dictate the therapeutic fate at the disease site.[3,4,5] One can see the novel features of AgNPs as an antimicrobial agent, explained in Chapter 1. Here the intention is to exploit the antimicrobial features of the AgNPs while encompassed in the nanocarrier. Since certain parameters such as size, shape and surface morphology of NPs often determine their therapeutic efficacy and hence unique synthetic methodology to develop these nanostructures is the key to achieve AgNPs as a therapeutic arsenal.[6,7] In this direction, the research group reported a facile green synthetic protocol for the preparation of water soluble uncapped AgNPs in the nanometer regime.[8]

On relying on aforementioned aspects, we developed a supramolecular system where AgNPs are entrapped inside extended CD networks, designed in view of bactericidal actions. Actually the findings explained in the previous chapter leave a space where the photostimulated NO toxicities can merge with potential bacterial cytotoxicity offered by AgNPs. The multimodal approach of this kind is expected to have increased impact and implications on more virulent bacterial strains. Based on the rational design of the gel nanostructure explained in the previous chapter, herein we demonstrate a multimodal nanogel structure in which two probe *viz.*, a NO photodonor and AgNPs are rationally organized at their interior.

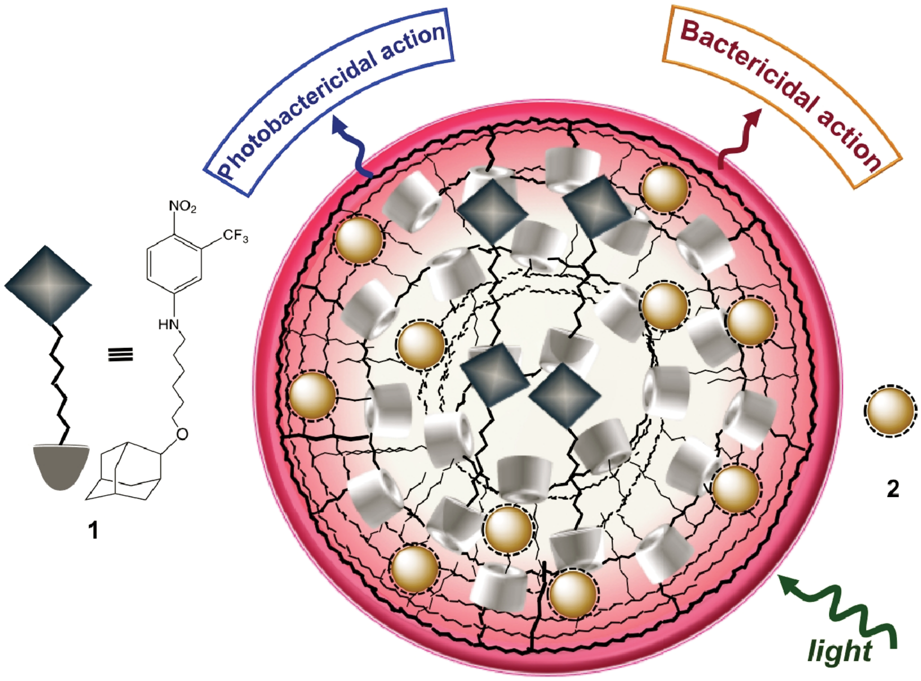

Scheme 11.1. Pictorial representation of bimodal entrapment of both NO photodonor (**1**) and AgNPs (**2**).

The adamantane terminated NO photodonor is found to incorporate in apolar CD cavities while the AgNPs organize at the folded polymer matrix randomly (Scheme 11.1). The combined and amplified effects of innate antibacterial actions bestowed by the AgNPs and NO cytotoxicity from the NO photodonor is expected to have direct consequence at microbial onsets. In addition the imaging capabilities owing to the SPR characteristics of AgNPs enable to track down the ensemble in cells.

11.2 Experimental

11.2.1 Materials

The components to prepare the nanogel carrier; CD-based polymer and dextran modified with hydrophobic alkyl chains were obtained from Dr. Ruxandra Gref, University of Paris-Sud, Paris, France, as the part of CYCLON community, ITN-Marie Curie Program and used as such with out any further purification. The 2,4-pentandionate silver (I) complex, Ag(acac), reagent grade provided by Aldrich, was used without further purification.

All other reagents were of highest commercial grade available and used without further purification. All solvent used (from Carlo Erba) were analytical grade.

11.2.2 Synthesis

A) Tailored NO photodonor

The protocol followed to synthesize the NO photodonor is exactly same as synthetic procedure reported before (Chapter 3).

B) Silver nanoparticles

AgNPs was synthesized from Ag(acac) based on the protocol already reported.[8]

11.3 Instrumentation

The spectroscopic and photochemical set up used for the steady state absorption is same as experimental part written in the previous chapters. Nanoparticle sizes were measured by a dynamic light scattering, Horiba LS 550 apparatus equipped with a diode laser with a wavelength of 650 nm.

11.4 Samples preparation

11.4.1 Photochemical experiments

The aqueous solution of AgNPs is titrated by adding fixed weights CD-based polymer. The compound **1** is slowly evaporated in acetonitrile and dissolved with AgNPs loaded polymer solution. The nanogel is prepared by constant stirring and mixing of the former solution with the second polymer of dextran modified alkyl chain. Supernatant is removed, equilibrated for 15 minutes and directly taken for the experiments.

11.5 Results and Discussion

We studied the interaction of both NO photodonor **1** AgNPs **2** in the CD based polymer networks *en route* to understand their probing in gel ensemble. The AgNPs **2** were spontaneously formed in water upon decomposition of the complex Ag(acac) and the negatively charged uncapped AgNPs readily interact with CD-based polymer.

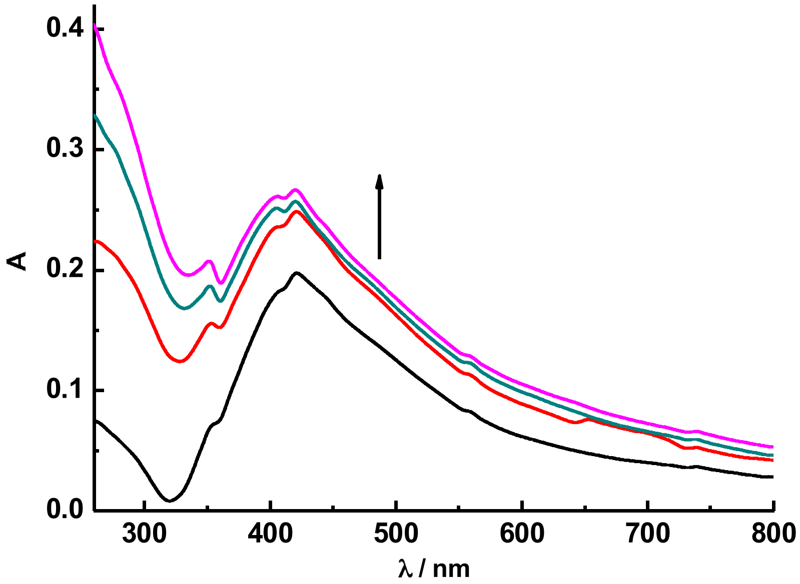

Figure 11.1. Steady state absorption spectrum of **2** upon titration with different concentration of CD-based polymer (Concentration/ CD units= 0 mM, 0.82 mM, 4 mM, 7.5 mM respectively).

The results prompted us to do the titration of **2** with definite concentrations of the polymer. The steady state absorption spectrum shows the increase in the plasmon absorption band of **2** at 420 nm upon adding constant weight of polymer (Figure 11.1). This increase in the absorption and extinction coefficient of the **2** stems from the binding of negatively charged hydrophobic particles at the interior of polymer networks. Whereas the binding of **2** with CD polymer does not influence the interaction of latter with compound **1** and the CD units are remain free to host the adamantane appendage of compound **1**.

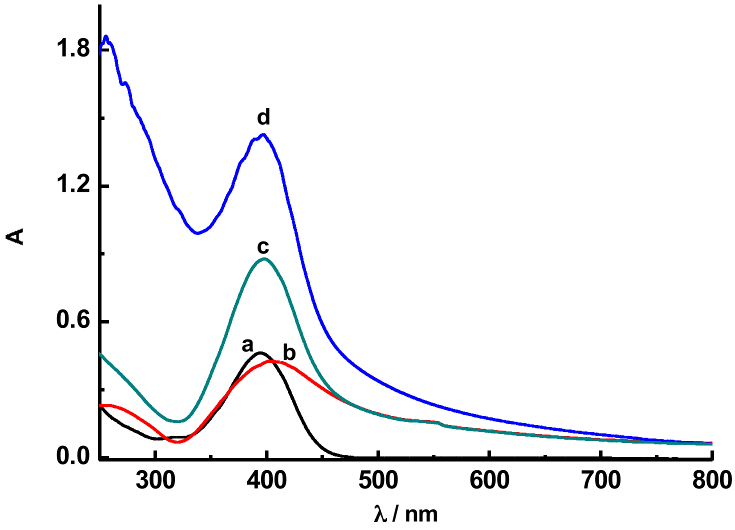

Figure 11.2. Steady state absorption spectra of CD-based polymeric dispersion of (a) **1** (ca. 40 μM), (b) 2 (40 nM), (c) arithmetic addition of a and b, (d) both 1 and 2 together.

As revealed by the absorption spectra (Figure 11.2), the polymeric dispersion of compound **1** shows absorption spectra with peak maxima at 400 nm similar to the behavior observed in previous cases (a in Figure 11.2). In addition, the absorption spectra of compound **1** in polymer was unaffected by the joint incorporation of the component **2**. In fact arithmetic addition of individual absorption of both probe in the polymer suspension were same as the absorption peak of the ensemble at which both probe entrapped together (c and d in Figure 11.2), ruling out any interactions between each probe at the ground state. Independent behavior of both probe are of pivotal importance to achieve independent bimodal photoactions. Interestingly, all these components entangled in the polymeric network remains under nanometer regime as revealed from the measurement of their hydrodynamic radius by dynamic light scattering (Figure 11.3).

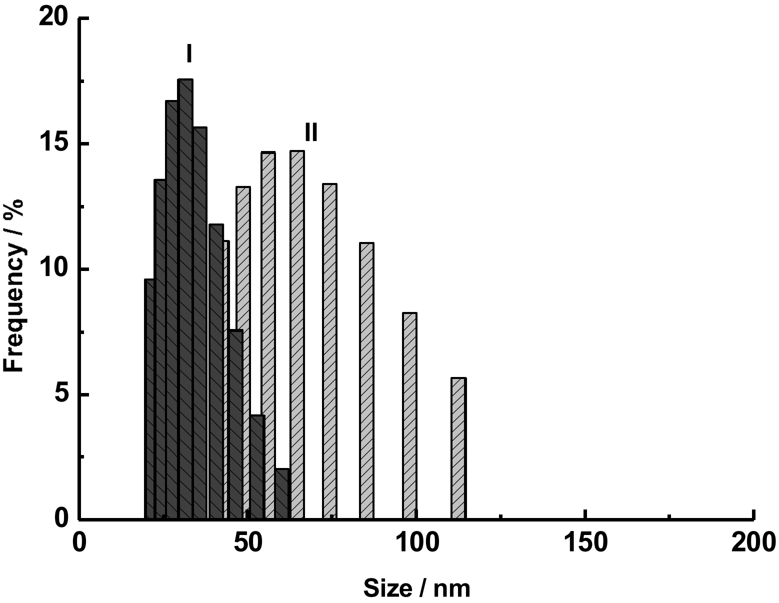

Figure 11.3. The hydrodynamic diameter of CD-based polymeric dispersion, (I) in the absence and (II) in the presence of both **1** and **2**.

The results keep us to understand the NO photoactions of the polymeric ensemble loaded with both component **1** and **2**. In this regard we illuminated the ensemble with light of 400 nm and measured the absorption spectra at definite time intervals. The absorption spectrum shows the bleaching of the absorption band at 400 nm followed by the increase at 410 nm (Figure 11.4).

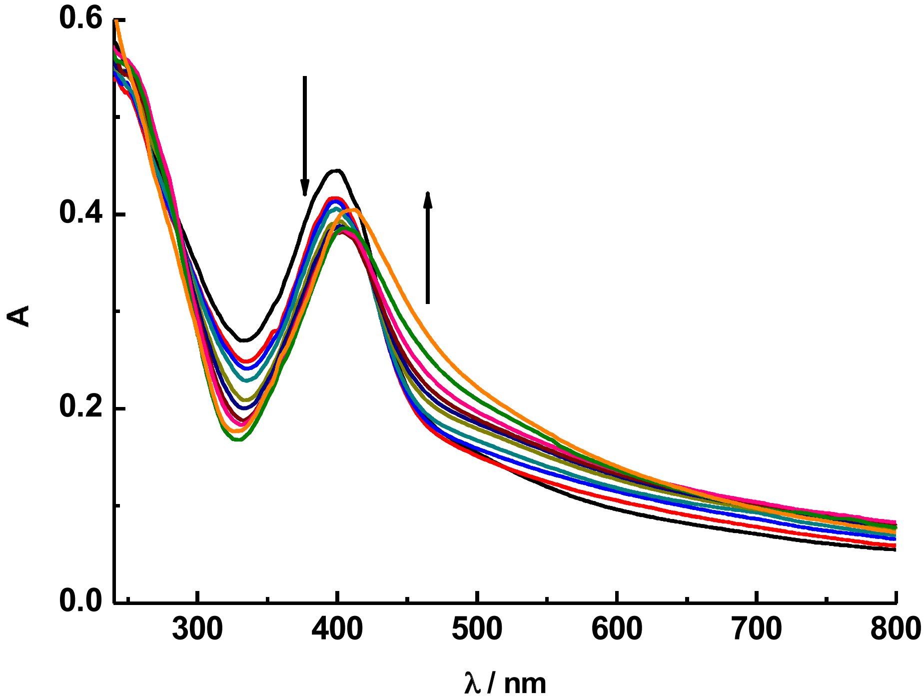

Figure 11.4. Variation in the absorption spectra of CD-based polymeric dispersion of both **1** and **2** upon 45 minutes exposure to the light of 400 nm.

From the absorption spectra, it can be asserted that the NO is releasing out upon illumination with 400 nm light and results the bleaching of absorption band characteristic to the nitroaniline moiety anchored in constrained environment.[9,10] This exhibits in the increase of the band below 300 nm upon illumination (Figure 11.4). Moreover it can be seen that the main peak of spectrum undergoes red shift *ca*. 10 nm, on the course of irradiation and can be reasoned that nitroaniline looses all its chemical characteristics upon NO release leaving the solution mainly with AgNPs. To note, we photolysed only 50 % of NO photodonor and further irradiation may shift the spectra towards the characteristic absorption of AgNPs alone. The results unanimously prove that the illumination does not influence the chemical features of component **2**.

Finally the ensemble loaded with both component **1** and **2** is made into gel structure upon entangling with dextran-modified polymer. The absorption spectra of the gel encompassed with both component look similar to the solution phase of polymeric analogue (Figure 11.5).

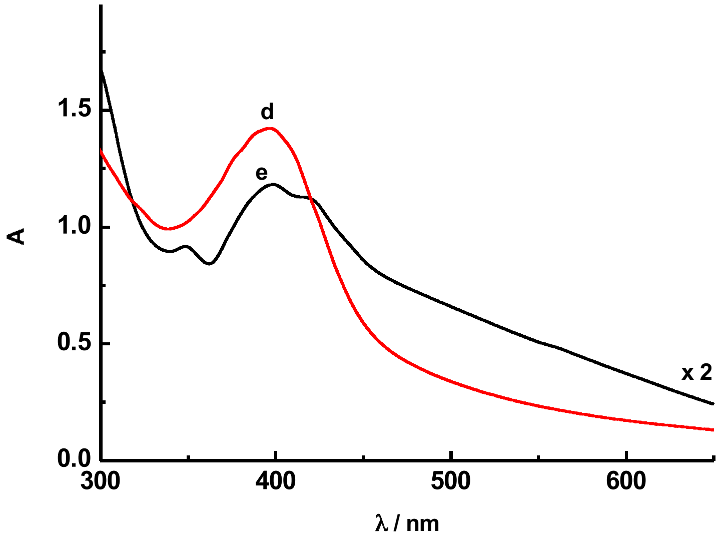

Figure 11.5. Steady state absorption spectrum of both **1** and **2** loaded in, (d) aqueous CD-based polymer, (e) nanogel.

Note that the scattering is very high in the case of gel loaded with both probe (e in Figure 11.5). This can be ascribed to surface features and consequent aggregation profile of AgNPs once encompassed in the semi-solid gel phase. It is well known that the metal NPs are liable to aggregation and its surface features closely dependent on the environment and composition of the particle surface.[11,12,13]

Finally we studied the photolytic pathway of the gel nanostructure loaded with both probe upon illumination with the light of 400 nm. In this case we pasted gel on the cuvette wall end exposed on the light source. The photobleaching of absorption spectra in the similar fashion to that observed in the solution phase demonstrate the NO photorelease from the gel structure (Figure 11.6).

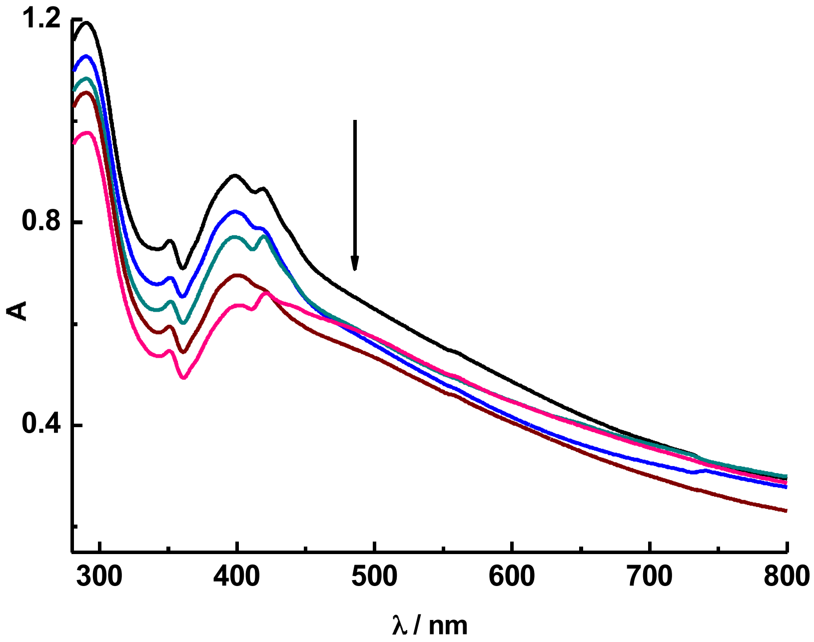

Figure 11.6. Variation in the steady state absorption spectra of both **1** and **2** loaded in CD-based polymeric nanogel upon 25 minutes exposure to the light of 400 nm.

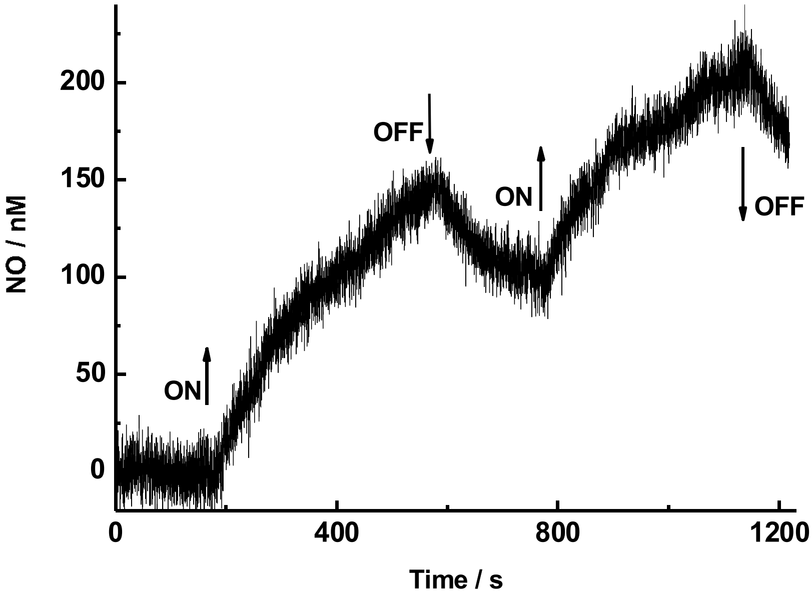

Figure 11.7. Amperogram showing the NO photorelease from the nanogel loaded with both **1** and **2** upon on-off switching of light at 420 nm

The NO photorelease and respective diffusion of NO gas is measured quantitatively by using a NO electrode in nanomolar level similar to the previous experiments. The set up was same to that used in the previous chapter. The thin cuvette wall pasted with gel is immersed in water and NO electrode is directed in to the water supernatant. The electrode directly detects diffused NO from the cuvette wall upon photoirradiation. The corresponding amperogram confirms the NO release upon illumination with light and the system is totally stable in dark as the amperogram follow a negative slope in dark state (Figure 11.7).

11.6 Conclusion

An active functional nanomaterial based on a gel nanostructure have been introduced and explained in view of bimodal antibacterial actions. The gel nanostructure is loaded with two probe *viz.*, a NO releasing photodonor and silver nanoparticles through innovative non-covalent assembling techniques. The merge of well known inherent antibacterial actions of silver nanoparticles with the NO based cytotoxicity is expected to address advanced bacterial resistance in an amplified manner. However the photochemical and photodynamic behavior of two probes loaded in same carrier has to be independent to attain amplified bactericidal actions. The spectroscopic results show that two probe entangled in the gel nanostructure have no intermolecular interactions and behave independently on their course of actions.

We outlined an active proof of principle to achieve double killing of antibiotic resistant bacterial colonies through rational chemical routes. However it is important to say some of the limitations of the current ensemble for the effective antibacterial actions. Actually we evaluated the effectiveness of the bimodal gel ensemble in antibiotic resistant bacterial colonies. The results show that some of the chemical parameters need to be scrutinized for the amplified antibacterial actions (data not shown). The AgNPs assembled in semi-solid gel structure is in aggregated state, which has profound negative impact on its bactericidal properties.[14,15] Some protocol has to be implemented to keep the AgNPs in disaggregated state while entangled in the gel structure. The gel structure is liable to leaching of the probe with time (data not shown), but capping or conjugating the probe with some agents is expected averts the leaching. The research to fix above-mentioned issues is under continuous exploration.

11.7 References

1. X. Huang, P. K. Jain, I. H. El-Sayed, M. A. El-Sayed, *Nanomedicine*, 2007, **2**, 681.

2. P. D. Nallathamby, X. –H. N. Xu, *Nanoscale*, 2010, **2**, 942–952.

3. K. Page, M. Wilson, I. P. Parkin, *J. Mater. Chem.*, 2009, **19**, 3819–3831.

4. R. Bryaskova, D. Pencheva, M. Kyulavska, D. Bozukova, A. Debuigne, C. Detrembleur, *J. Colloid Interface Sci.*, 2010, **344**, 424.

5. V. K. Sharma, R. A. Yngard, Y. Lin, *Adv. Colloid Interface Sci.*, 2009, **145**, 83.

6. M. Rai, A. Yadav, A. Gade, *Biotechnol. Adv.*, 2009, **27**, 76–83.

7. J. J. Mock, M. Barbica, D. R. Smith, D. A. Schultz, S. Schultz, *J. Chem. Phys.*, 2002, **116**, 15.

8. S. Giuffrida, G. Ventimiglia, S. Sortino, *Chem. Commun.*, 2009, 4055–4057.

9. S. Sortino, G. Marconi, G. Condorelli, *Chem. Commun.*, 2001, 1226.

10. E. Deniz, N. Kandoth, A. Fraix, V. Cardile, A. C. E. Graziano D. L. Furno, R. Gref, F. M. Raymo, S. Sortino, *Chem. Eur. J.*, DOI: http://dx.doi.org/10.1002/chem.201202845.

11. L. Kvitek, A. Panacek, J. Soukupova, M. Kolar, R. Vecerova, R. Prucek, M. Holecova, R. Zboril, *J. Phys. Chem. C,* 2008, **112**, 5825-5834.

12. X. Li, J. J. Lenhart, *Environ. Sci. Technol.*, 2012, **46**, 5378-5386.

13. R. P. Bagwe, K. C. Khilar, *Langmuir*, 2000, **16**, 905-910.

14. S. Shrivastava, T. Bera, A. Roy, G. Singh, P. Ramachandrarao, D. Dash, *Nanotechnology,* 2007, **18**, 9.

15. J. G. Teeguarden, P. M. Hinderliter, G. Orr, B. D. Thrall, J. G. Pounds, *Toxicological Science,* 2007, **95**, 300.

12

CD based hydrogel for multimodal imaging and therapy

12.1 Introduction

Some of intriguing features, among various *ad-hoc* modified gel nanostructure described in the previous chapters, are exploited here to assemble a nanocarrier ensemble with the double imaging and double therapy actions intended for antitumor therapy. Tailoring two probes; fluorescent labeled NO photoreleasing moiety and fluorescent photosensitizer in the single nanocarrier, and finally forming the gel nanostructure of the same is said to have imperative implications for topological applications and *in-vivo* injections to the tumor sites. Here the idea is to merge the prospective of components that is explained in Chapter 7 and to assemble those probes in gel nanostructure (explained in Chapters 10 and 11). The gel carrier is formed with the interlocking between CD-based polymer and dextran modified with hydrophobic alkyl chain. Since the number of CD units are high enough and only some part of the CD cavity is occupied for the interlinking with dextran polymer, majority of the CD units are free to host both fluorophore labeled NO photodonor and phtotsensitizer. The ability to release out both $^1O_2$ and NO with prompt light source and imaging capabilities in red and green region in the single carrier structure make the present ensemble an appealing strategy for the onsite antitumor therapy.

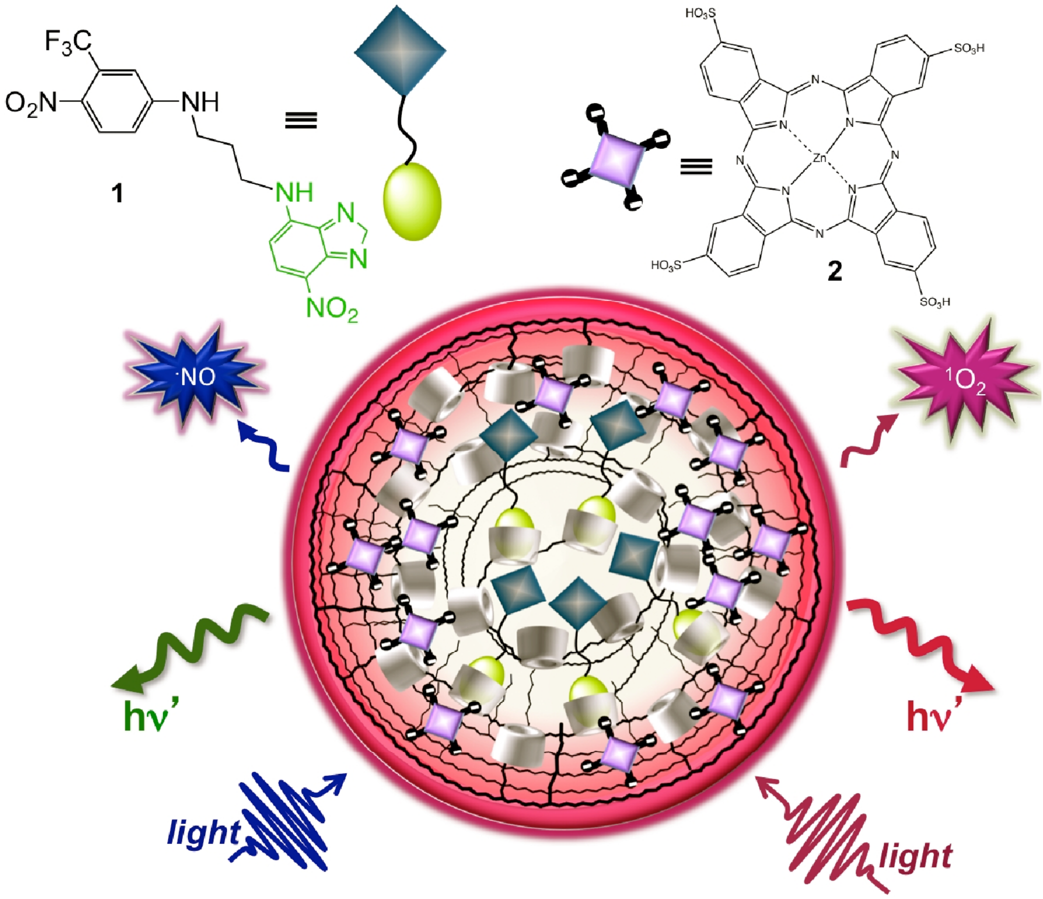

Scheme 12.1. Pictorial representation of multimodal gel ensemble loaded with both NBF attached NO photodonor (**1**) and Zinc phthalocyaninetetrasulfonate (**2**).

In line to the above mentioned goals, we designed a system in which NBF labeled NO photodonor (**1**) and Zinc phthalocyanine tetrasulphonate (**2**) is incorporated jointly in CD-based polymer and made into a gel nanostructure by entangling with second polymer of dextran modified hydrophobic alkyl chain (Scheme 12.1).

12.2 Experimental

12.2.1 Materials

The probes **1** and **2** are same as Chapter 7. The CD-based polymer and dextran modified with alkyl chain is obtained from Dr. Ruxandra Gref, Faculty of Pharmcay, CNRS, University of South-Paris, France, and used as such with out further purification. All other reagents were of highest commercial grade available and used without further purification. All solvent used (from Carlo Erba) were analytical grade.

12.3 Instrumentation

All the instrumental methods are same as Chapter 11.

12.4 Sample preparation

The method of preparing the gel is same as reported in Chapter 10. Both probe were loaded with CD-based polymer and finally polymerized with dextran modified alkyl chains.

12.5 Results and Discussion

On the way to achieve the gel ensemble loaded with two probes, both components **1** and **2** are incorporated in CD-based polymer and made in to the gel phase with the second unit of dextran polymer. The steady state absorption spectra shows that both components incorporated in gel retain their photochemical features. The compound **1** shows the absorption with peak maxima at 400 and 475 nm, while the component **2** at 635 and 680 nm as similar to the observation in case of CD-based polymer solution (a and b in Figure 12.1).

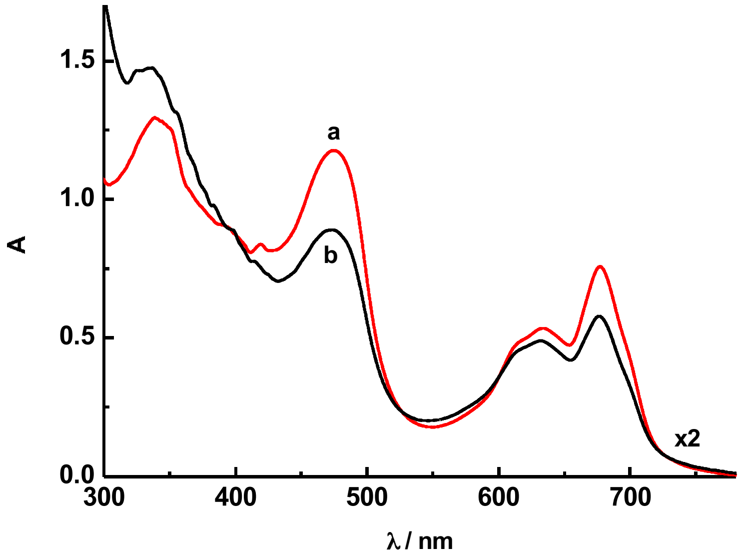

Figure 12.1. Comparison between the absorption spectra of both **1** and **2** loaded (a) in aqueous CD-based polymer, and (b) CD-based polymeric nanogel (multiplied by the factor 2 for comparison), [**1**]= 6 μM, [2]= 100 μM.

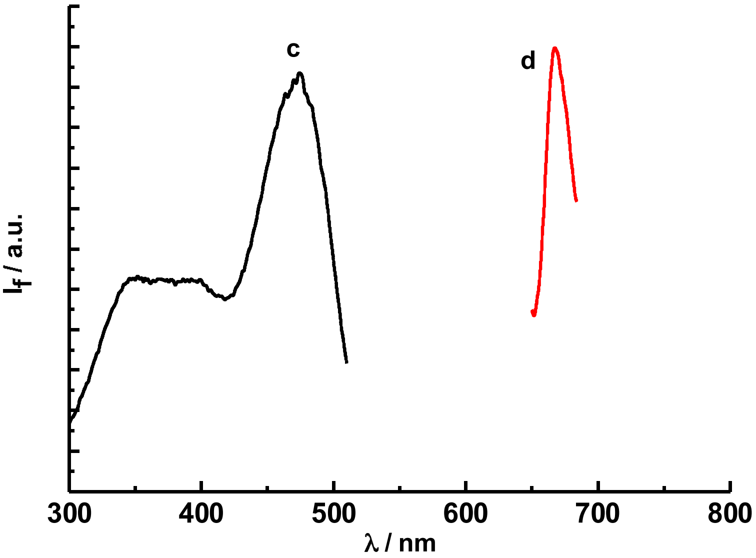

Figure 12.2. Excitation spectra of CD-based polymeric nanogel loaded with both **1** and **2**, λ_{exc}= 510 nm (c) and 700 nm (d), [**1**]= 6 μM, [2]= 100 μM.

Majority of the compound **2** does exist in disaggregated state upon incorporation in gel structure and have pivotal consequences as far as the photosensitization actions are concerned.[1,2]

The excitation spectrum measured by exciting the gel ensemble in the respective absorption region of both porbes also confirms the preservation of indpenedent photodynamic actions of both probes. The figure show the excitation spectrum of both **1** and **2** (c and d in Figure 12.2), which is resemble to its ground state absorption spectrum and validate the absence of any intra/intermolecular quenching events at the excited singlet state of both component.

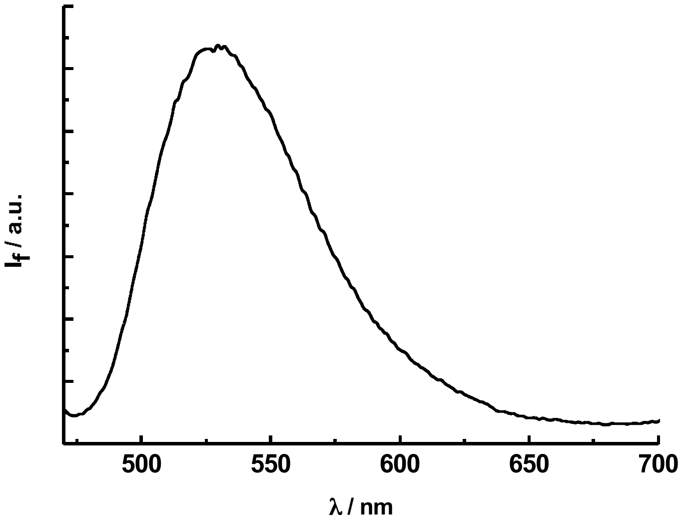

Figure 12.3. Steady state fluorescence emission spectra of CD-based polymeric nanogel loaded with both **1** and **2** (λ_{exc}= 460 nm, compound **1**).

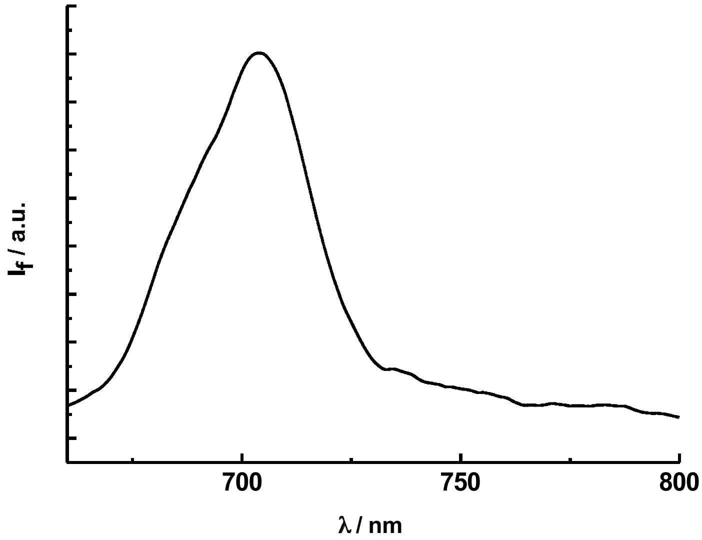

Figure 12.4. Steady state fluorescence emission spectra of CD-based polymeric nanogel loaded with both **1** and **2** (λ_{exc}= 650 nm, compound **2**).

The observation of independent photobehaviour of both **1** and **2** is further confirmed by tracking down their fluorescence emissive properties. Figure 12.3 and 12.4 reveal the amble fluorescence emission from compound **1** and **2** of bichromophoric gel ensemble with the peak position exactly matching while they entangled in CD based polymer solution (see Chapter 7 for detailed understanding). The results refer to the possibility of the present system to image the bio-sites both at red and green region simply by changing the wavelength of filter.

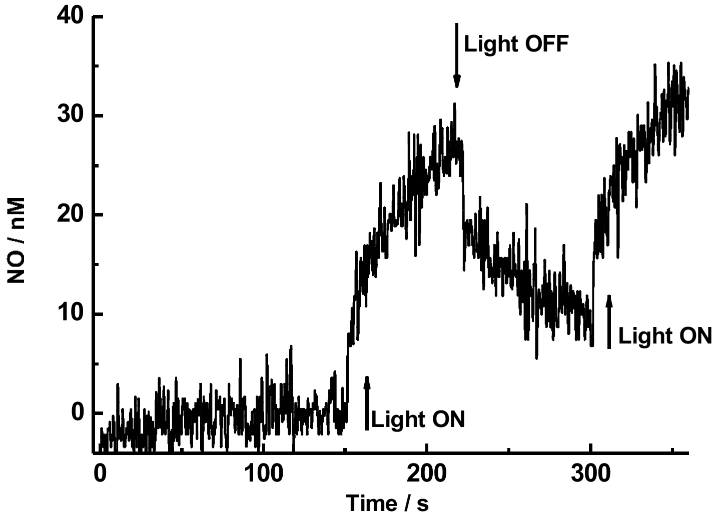

Figure 12.5. Ameprogram showing the real time NO photorelease from the nanogel loaded with both **1** and **2**.

Finally the suitability of the present system as NO releaseing scaffold has been verified by the real time monitoring of NO photorelease. To this end we used a NO electrode, which detects NO releae in nanmolar level by an amperometric technique. The practical set up was exactly same to that used in capter 11 and 12. The linear generation of amperogram that stops when light is turned off and resume again with prompt light undoubtedly prove the controlled release of NO in nanomolar level.

12.6 Conclusion

In line to the methodology explained in Chapter 7, we demonstrated the possibility of having a multimodal gel ensemble with bimodal emission and dual modal therapy. This has been achieved by logical formulation of different units, 1) green fluorophore attached to NO photodonor and 2) red fluorescent $^1O_2$ photosensitizer. Possibility to achieve green and red fluorescence along with NO photoaction and $^1O_2$ photosensitization in same supramolecular container and finally the capability to inject *in-vivo* or adhere to any topological surface impart a great prospective towards multimodal anticancer/ antimicrobial actions.

12.7 References

1 *Phthalocyanines: Properties and Applications*; Leznoff, C. C., Lever, A. B. P., Eds.; VCH: New York, 1989.

2 W. J. Schutte, S. M. -Rehbach, J. H. Sluyters, *J. Phys. Chem*., 1993, **97**, 6069.

General remarks

The logic behind this thesis was to synchronize several inter-disciplinary concepts, ranging from material engineering to medicine, to build up multifunctional photoactive nanoparticles. They are developed in view of addressing current therapeutic challenges related to biomedical application.

With these objectives in mind, we tried to integrate several photoactive molecules in nanocarriers. In someway they work as independent units while entangled in the same ensemble and in some other way as dependent communicating units. Light is an immense tool and handle to regulate the functional behavior of all the systems explained here, as it can exclusively tune the functionalities of molecules in photodependent or photoindependent pathway.

We are perfectly aware that functional ensembles introduced here need to be studied further to be into the therapeutic field. Some of the systems are closed to real world applications and some are just the proof of principle. However some of the facile features of the ensemble such as perfect spatio-temporal control over the release of active therapeutic species, good biocompatibility, capabilities of cell penetration etc. strongly encourage us to make it happen in real world applications of *in-vivo* treatments. The fundamental understanding of molecular photochemistry and its effective exploitation to design the nanomaterial is the key to achieve this goal and the present effort was to disclose and unleash the innumerable possibilities where the molecular photochemistry can strongly mediate.

Acknowledgement

I feel immense pleasure to be here on this page to appreciate the people who really contributed in enriching my scientific and nonscientific life here at Catania and abroad. Now many images of the people simply turning around in my mind and I am totally unsure whether I can express my deep gratitude in mere words writing here. However write down here, some of the most prominent figures who influenced my research life.

First and foremost I express my deep thanks to my research supervisor Prof. Salvatore Sortino for giving me the opportunity to work in his lab, empowering me to stand up here with the research finding of this thesis, patience and confidence he had on me. His uncompromised dedication, passion and dynamism towards science greatly influenced me for creative thinking and designing my research. The experience was like listening music and I was lucky to have such a strong guidance, which definitely makes an impact on my future research career.

I specially thank Prof. Guido De Guidi and Prof. S. Giuffrida for all the moral and scientific support. They were approachable all the time for scientific assistance. I would like to acknowledge Dr. A. Mazzaglia, U. Messina, Italy for some of the nanomaterials and facilitating my short stay at his lab, Dr. M. T. Sciortino, Tizziana, Ivana, U. Messina for the biological experiments of chapter 3 and 5, Prof. V. Cardile, Adriana, Debora for the help in biological experiments of Chapter 7 and 8.

Great appreciation goes to the CYCLON network, ITN Marie Curie Program. The network community was instrumental in making this entire research would happen in reality. Many groups in the network actively collaborated in the thesis. Grateful to Dr. R. Gref, CNRS, U. Paris-Sud, France, for "feeding" me with enough polymer materials; Dr. S. Monti, U. Bologna, Italy, for the valuable tips and binding studies inserted in Chapter 6; Dr. É. Fenyvesi for all kinds of materials obtained from CycloLAb, Hungary. Deeply appreciate the efforts of Prof. Marica B. Ericson and her group for setting up a wonderful and friendly environment in the lab during my secondment period at U. Gothenburg, Sweden. Greatly appreciate the help of Dr. C. Halldin and Dr. M. Smedh for the imaging studies at CCI, U. Gothenburg, Sweden. I acknowledge Prof. F. M.

Raymo and Dr. E. Deniz, U. Miami, USA, for the fluorophore-photochromic molecules.

I am grateful to my research coordinator Prof. G. Mussumara for the constant mentoring and advices regarding my PhD and greatly indebted to research officer Sabrina for clearing my all bureaucratic liabilities of the PhD program.

I am very proud and consider myself very fortunate to be the part of Dr. H. Pal group and as a student of Dr. S. D. Choudhury at BARC, Mumbai, India, where I could sharpen my knowledge in basic photochemistry. Palda was one of the great teachers I ever met and thank many other teachers I had in my university life.

Apart from supervisors and big bosses, the great moment came with my colleagues are greatly acknowledged. Elisa for giving assistance in synthesis and other lab and extra lab activities, Alfio for the understanding instrument 'language' and cherishing friendship, Giusi for the nice friendship and humility, Aurore for the collaboration in synthesis and doing the work swiftly. I really appreciate your serious efforts of proof reading of this thesis. I thank all my 25th cycle PhD colleagues for the nice friendship during my PhD period. I am grateful to Fabio, advfactory, Catania for the design and printing of this thesis. Special thanks to the security men for permitting me to stay at the lab during off time!

This page would not be completed with out remembering my CYCLON community colleagues. My 'synthesis man' Milo, in whom I found great friendship and matching interest in all activities. The 'great' Vladimir for running endless nights in the biology lab at Gothenburg. I greatly memorize the cheerful moments with Yilun, Maria, Valentina, Linda, Ricardo, Violeta, Ahmet, Zoltan and sharing ideas with my local friend, Resmi in my local language! I am sure that those magnificent moments will be with me as all time memories. Acknowledge my Master friends Shibin, Sooraj and Anju.

Take this opportunity to acknowledge my long list of local friends in Catania especially my roommate Alberto, Ahmed etc. for the nice friendship and many others for 'corridor relationship' and '*ciao-ciao*' relationship.

Last not least, I am deeply indebted to my family, my sisters in particular, and they were always behind me on catalyzing my future and guiding me all the time.